Droplet Microfluidics for Continuous Chemical Monitoring

Gareth William Harry Evans

First Supervisor

Dr Xize Niu

Faculty of Engineering and Physical Sciences

Second Supervisor

Dr David Voegeli

Faculty of Health Sciences

Faculty of Engineering and Physical Sciences

University of Southampton

Southampton, UK

Abstract

In a variety of fields such as disease diagnostics, clinical monitoring, drug development and environmental science, there is a need to continuously measure chemical and biomolecule concentrations over long periods. Continuous monitoring of chemicals has proven to be particularly challenging even for the current state-of-the-art electrochemical sensors, which can suffer from surface degradation and measurement drift. The gold standard “bulk” assay techniques require large sample volume and laborious professional time, making them unsuitable for many continuous monitoring applications.

This has led research attention to microfluidics (the study and manipulation of microlitres to picolitres volumes of fluid in microchannels 1-1000 μm in diameter), which can carry out biochemical analysis consuming less sample and reagent and providing higher throughput.

Microfluidics has seen several successful applications including the development of "Micro Total Analysis Systems" (μTAS) or “lab-on-a-chip” devices, which carry out all the necessary steps for chemical analysis of a sample and have been exploited for a wide variety of processes. Indeed, many modern point-of-care tools also incorporate some element of microfluidics, notably lateral flow devices (e.g. glucose testing for diabetics and home pregnancy tests).

This thesis focuses on a subset of microfluidics called droplet microfluidics. While standard “continuous flow” microfluidics handle fluids in a single phase (mostly aqueous phase) under laminar flow regimes, droplet microfluidics is based around the production of many individual and separate chemical reactors in an immiscible carrier fluid. Droplet microfluidics greatly improves the possible temporal resolution and throughput of assay and analysis by eliminating Taylor dispersion and band broadening exhibited by continuous flow microfluidics. Surface contamination is avoided as droplets never come into contact with the channel wall. Chaotic advection within the droplets greatly improves mixing of sample and reagent and reduces reaction time. These properties of droplet microfluidics make it particularly suitable for the task of *in-situ* monitoring requiring high temporal resolutions and low volumes of reagent and sample consumption per measurement.

Currently, most droplet microfluidic systems are still “chip-in-a-lab”, requiring bulky and extensive supporting equipment such as microscopes, external pumps and valves. This thesis addresses the challenges of taking droplet microfluidics from a useful laboratory tool to field applications. With a focus on robust droplet generation and miniaturisation of the fluidics suitable for portable/wearable applications.

Droplet generation is most commonly achieved by introducing aqueous and oil phases into a T-junction or a flow focusing channel geometry. This method produces droplets that are sensitive to changes in flow conditions and fluid composition. Here I present a new novel form of droplet generation utilising pulsed flows. This pulsed droplet generation regime is robust and invariant to both flow conditions and fluid composition. This method offers controllable droplet dynamics, with droplet volume and composition solely determined by pulsation volumes, which are defined by the design of a peristaltic micropump.

Importantly, sequences of droplets with controlled composition can be hardcoded into the pump, allowing chemical operations such as titrations and dilutions to be easily designed into the system, as well as including *in-situ* standards etc. for the calibration of droplet microfluidic sensors and accomplishing more complicated assay procedures in a droplet format.

In this thesis, I showcase two prototype platforms, which utilise this pulsed droplet generation regime coupled with in-line spectrophotometer flow cell. The platform contains a compact and low power 3D-printed peristaltic micropump, capable of continuously collecting samples, generating droplets close to the sampling site and with short stabilisation time. This has allowed for the first ever system capable of continuous *in-situ* sampling and real-time chemical measurement using droplet microfluidics as well as the integration of complex multiple step assays into a portable droplet platform.

One application of this platform technology is the *in-situ* monitoring of water chemistry in rivers, lakes and oceans based on this novel approach. This prototype device has been tailored for the measurement of nitrite and nitrate, two of the most important macronutrients in natural water that are important for determining the health of aquatic ecosystems and studying biogeochemical changes. Traditional manual sampling and laboratory analysis is logistically challenging and costly, *in-situ* measurement using small and low power analytical devices removes the need for sample transport, allowing for larger and more temporally detailed data collection. All previously reported state-of-the-art *in-situ* microfluidic analysers have been based on continuous (single-phase) microfluidics. Shifting to a droplet-flow regime results in great improvement in temporal resolution, fluid and power economy.

Furthermore, as an example application in healthcare, I present a prototype device capable of producing ‘trains’ of droplets. The device is tailored to carry out a multiple step competitive heterogeneous assay for continuous measurement of cortisol when coupled with other custom tools. Cortisol is a stress related steroid hormone, its concentration in the body varies rapidly and abnormal changes are associated with a variety of disease states. The ability of continuous and *in-situ* monitoring of its concentration, rather than the current single snapshot measurement, opens the door to trend-related diagnostics and treatment.

Acknowledgements

First, I would like to thank my supervisor Dr Xize Niu for his expert advice, encouragement and support throughout my research, without which, the production of this work would not have been possible.

I would also like to thank my second supervisor Dr David Voegeli for his support, advice and encouragement in throughout my research.

Thank you to all my collaborators (named throughout). Special thanks to Dr Adrian Nightingale for all the training mentorship and support he has provided throughout my PhD, to Dr Sammer-ul Hassan for his support in using the multi-point detector, Dr Sharon Coleman for support on lab based work. Thank you to Wahida T. Bhuiyan for continued collaboration. Thank you to my industrial collaborators particularly Brett Warren from SWS (SouthWestSensor Ltd) on automation of magnetic trapping and Dr Susan Pang from LGC group (London Government Chemists ltd). Thank you to the technicians in the ECS workshop for their support in manufacturing various devices and equipment during my PhD. I would also like to thank all members of the electro-mechanical research group for their support and encouragement.

Thank you to EPSRC for funding my research and for their continued support through the EPSRC doctoral prize award.

Finally, I would like to thank my family and friends for their continued support throughout my studies.

Research activities and achievements

List of Publications

Part of this work has been or will be reported in the following publications or conference presentations:

Conference Presentations

Peer Reviewed International Conference Presentations:

1. C.H.A.D.: Continuous Heterogeneous Assays in Droplets for the measurement of cortisol. Gareth Evans, Wahida Bhuiyan, Sammer-Ul Hassan, Brett Warren, Sharon Coleman and Xize Niu. Oral Presentation Microtas 2018, Kaohsiung
2. Gas-mediated crosstalk in droplet flow - characterisation and correction. Adrian M. Nightingale, Sammer-ul Hassan, Gareth W.H. Evans, Sharon Coleman and Xize Niu. Oral Presentation Microtas 2018, Kaohsiung
3. Generation of “droplet trains” for continuous and multiple sample or multiple step assays in droplet microfluidics. Gareth W.H. Evans, Adrian M. Nightingale, Sammer-Ul Hassan and Xize Niu. Poster presentation, Microtas 2017, Savannah.
4. A drop in the ocean: monitoring of water chemistry using droplet microfluidics. Gareth W.H. Evans, Adrian M. Nightingale, Sammer-Ul Hassan, and Xize Niu. Poster presentation, Microtas 2017, Savannah.
5. Wearable Droplet-Based Microfluidic Sensor Device for Continuous Sampling and Real-Time Analysis. Sammer-ul Hassan, Adrian M. Nightingale, Yu Zhang, Gareth Evans, Martyn G. Boutelle, Xize Niu,. Oral presentation, Microtas 2016, Dublin.
6. Generation of droplet sequences with pre-specified compositions using a “hardcoded” peristaltic micropump. Adrian M. Nightingale, Gareth W. H. Evans, Sammer-ul Hassan, Byung-Jae Kim and Xize Niu. Poster presentation, Microtas 2016, Dublin.
7. Robust droplet generation and sampling with micro-peristaltic pump and antiphase pulsed flows. Gareth W. H. Evans, Adrian M. Nightingale, Sammer-ul Hassan, Byung-Jae Kim and Xize Niu., Poster presentation, Microtas 2016, Dublin.

National Conference Presentations:

1. 'Droplet microfluidics for continuous chemical sensing of cortisol' Gareth Evans, Wahida Bhuiyan, Sammer-Ul Hassan, Brett Warren Sharon Coleman and Xize Niu Oral Presentation, BioMedEng18, Imperial College London
2. Droplet microfluidics for *in-situ* chemical sensing - Adrian Nightingale, Gareth Evans, James Zhu, Brett Warren, Kyriacos Makris, Sammer-ul Hassan, Hywel Morgan, Matthew Mowlem and Xize Niu poster presentation Challenger Conference 2018
3. Droplet Microfluidics for continuous chemical sensing of Cortisol - Gareth W. H. Evans, Wahida T. Bhuiyan, Sammer-ul Hassan and Xize Niu Poster presentation, Royal Society of Chemistry Microfluidics for Analytical Chemistry Conference 2018 The National Oceanography Centre Southampton UK.

Other conference presentations

1. Droplet microfluidics for continuous chemical monitoring - Gareth W. H. Evans, Dr David Voegeli and Xize Niu, Oral presentation delivered at The Postgraduate Conference in Engineering Sciences, 2016, Southampton, UK

Peer Reviewed Publications

1. Droplets in the wild: field-deployable droplet microfluidics for *in-situ* analysis of natural waters Adrian M. Nightingale, Gareth W. H. Evans, Sammer-ul Hassan and Xize Niu. In preparation

2. Droplet Microfluidics for continuous chemical sensing of Cortisol - Gareth W. H. Evans, Wahida T. Bhuiyan, Sammer-ul Hassan, Susan Pang and Xize Niu. In preparation

3. Nitrate measurement in droplet flow: gas-mediated crosstalk and correction Adrian M. Nightingale, Sammer-ul Hassan, Gareth W. H. Evans, Sharon Coleman, and Xize Niu DOI: 10.1039/C8LC00092A (Paper) Lab on a Chip, 2018,18, 1903-1913

4. Phased peristaltic micropumping for continuous sampling and hardcoded droplet generation. Gareth W. H. Evans, Adrian M. Nightingale, Peixiang Xu, Byung Jae Kim, Sammer-ul Hassan and Xize Niu DOI: 10.1039/C6LC01479H (Paper) Lab on a Chip, 2017, 17, 1149-1157

Awards and grants

1. EPSRC doctoral prize award - A grant targeted at the top 10-15% of EPSRC-funded students supporting students who have recently received support for their PhD studies from EPSRC in the form of fees and/ or stipend to increase the impact of the PhD in terms of publications, Knowledge Transfer (KT) and outreach, and to help and encourage the very best students to move into research careers.

2. MicroTAS 2016 - CBMS Travel Grant student travel grant from the Chemical and Biological Microsystems Society (CBMS) to attend the 20th International Conference on Miniaturized Systems for Chemistry and Life Sciences (MicroTAS 2016) in Dublin Ireland.

Declaration of authorship

I, Gareth Evans, declare that this thesis and the work presented in it are my own and has been generated by me as the result of my own original research.

Droplet Microfluidics for Continuous Chemical Monitoring

I confirm that:

1. This work was done wholly or mainly while in candidature for a research degree at this University;
2. Where any part of this thesis has previously been submitted for a degree or any other qualification at this University or any other institution, this has been clearly stated;
3. Where I have consulted the published work of others, this is always clearly attributed;
4. Where I have quoted from the work of others, the source is always given. With the exception of such quotations, this thesis is entirely my own work;
5. I have acknowledged all main sources of help;
6. Where the thesis is based on work done by myself jointly with others, I have made clear exactly what was done by others and what I have contributed myself;

Signed: .....
Date: .....

Table of Contents

List of Figures

List of Tables

Nomenclature

POC	Point-of-Care
µTAS	Micro Total Analysis Systems
MEMS	Micro-Electro-Mechanical Systems
Ca	Capillary numbers
γ	Interfacial tension
Q	Volumetric flow rate
μ	Viscosity
U	Flow velocity
G	Axial elongation rate from the flow-focusing nozzle
a_0	Droplet radius for flow focusing geometry
Δz	Axial distance between the end of the inlet channel for the dispersed phase and the focusing orifice
w_{or}	Width of the focusing orifice
w_o	Width of the inlet channel for the continuous phase
r_{crit}	Critical thread radius
L_b	Droplet length
ϕ	Flow ratio
W	Channel width
V	Droplet volume
EWOD	Electro-wetting on di-electrics
DEP	Dielectrophoresis
PDMS	Polydimethylsiloxane
SDOD	Steady Drop on Demand
POCT	Point-of-Care Testing
No	Nitric oxide
O_2	Oxygen

H_2O_2	Hydrogen peroxide
SDs	Spreading depolarization waves
ELISA	Enzyme linked immunosorbent assays
CL	Chemiluminescence
DNA	Deoxyribonucleic acid
PCR	Polymerase chain reaction
CSF	Cerebro-Spinal Fluid
DNNF	Dynamic no-net-flux
V	Voltage
PTFE	Polytetrafluoroethylene
ID	Droplet Identity
fps	Frames per second
RSD	Relative standard deviation
DGR	Droplet Generation Rate
V_0	Initial reaction rate
[S]	Concentration of the substrate
V_{max}	maximum possible reaction rate (where [S] is in large excess)
K_m	Michaelis constant representing the value of [S] at which $V_0 = ½V_{max}$
n	Number of features in the peristaltic micropump rotorhead
PFPE-PEG	Perfluoropolyether- Polyethylene glycol

List of Equations

Peclet number

$$Pe_L = \frac{advective\ transport\ rate}{mass\ diffusion\ rate} = Re_L Sc = \frac{u}{D/L} \quad (1)$$

Capillary number in Cross/co-flow geometry

$$Ca = \frac{\mu_O U}{\gamma} \quad (2)$$

Capillary number in Flow focusing geometry

$$Ca = \frac{\mu_O G a_0}{\gamma} \quad (3)$$

Mean velocity component

$$U = \frac{Q_o}{wh} \quad (4)$$

Axial elongation rate in flow focusing geometries

$$G = \frac{Q_o}{h\Delta z}\left(\frac{1}{w_{or}} - \frac{1}{2w_o}\right) \quad (4)$$

Droplet radius in flow focusing geometries

$$a_o = \frac{w_i}{2} \quad (5)$$

Critical thread radius

$$r_{crit} = \frac{hw}{2(w+h)} \quad (6)$$

Droplet length in squeezing

$$\frac{L_b}{W} = A_1 + A_2\varphi \quad (7)$$

van Steijn droplet volume

$$\frac{V}{hw^2} = \frac{V_{fill}}{hw^2} + \alpha\varphi \quad (8)$$

Weber number

$$We = \frac{\rho U 2 a_0}{\gamma} \quad (9)$$

Hagen–Poiseuille equation	$\Delta P = \frac{8\mu LQ}{\pi r^4}$	(10)
Beer Lambert Law	$A = \log_{10}\frac{I_0}{I} = \varepsilon lc$	(11)
Total flow rate	$Q = nVf$	(12)
Volume pumped per feature space	$V = ksA$	(13)
Combined flow rate equation	$Q = nksAf$	(14)
Trinder assay	$\text{glucose} + H_2O + O_2 \xrightarrow{\text{glucose oxidase}} \text{gluconic acid} + H_2O_2$ $2H_2O_2 + \text{4-AAP} + \text{TOPS} \xrightarrow{\text{peroxidase}} \text{quinoneimine} + 4H_2O$	(15)
Michaelis-Menten	$V_0 = \frac{V_{max}[S]}{K_m + [S]}$	(16)
Gas mediated cross talk correction equation	$A_{a,corrected} = \left(\frac{1+\alpha}{1-\alpha^2}\right)(A_a - \alpha A_b)$	(17)

Chapter 1 Introduction and background

In this chapter, I introduce the motivation for my work and the challenges of continuous monitoring. I present a comprehensive overview of the literature pertaining to current state of the art droplet microfluidics and biosensors that use “wet chemical assays”. Special consideration is paid to droplet generation techniques to explain why the current techniques are poorly suited for field deployment.

1.0 The challenge of continuous monitoring

In a variety fields such as disease diagnostics, clinical monitoring, drug development, and environmental science, there is a need to monitor chemical and biomolecule concentrations continuously over long periods of time often with high temporal resolution. This has proven particularly difficult with accurate lab-based systems, too large for field deployment and others not sufficiently accurate for analysis and often suffering from signal drift. Over the past 40 some years, there has also been a huge technological push to develop tools for point-of-care testing (POCT) (St John and Price 2014). POCT aids clinicians in making more rapid decisions regarding patient care, while reducing professional time and resources spent on testing, and allows for quick responses especially to pandemic or rapidly progressing diseases. Less progress however has been made on point-of-care monitoring which unlike point-of-care testing requires good performance over long periods of time, hence devices used in single measurement diagnostics and other applications are not always suitable for monitoring.

1.1 Aims and objectives

The primary aim of this thesis is the development of a droplet microfluidics-based platform technology suitable for continuous use and which can be tailored to applications in clinical and environmental monitoring applications. This could form the basis of a portable/wearable chemical sensor capable of continuous and on-line/in-situ measurement of biomolecule/drug concentrations directly from body/tissue fluids. This device has also been tailored for application in field deployments for environmental monitoring over long periods with a small overall footprint and power consumption as well as high temporal resolution and in-situ calibration, thereby providing considerable improvements over previously reported systems.

This thesis tackles many of the challenges of these types of measurement caused by small volumes of samples, complex fluid mixtures, real-time assay, and sensitive detection of less abundant molecules. This platform could be tailored to aid in the study of drug metabolism and allow the development of new ‘smart’ therapies that use biochemical marker levels to guide treatment in real time at the point of care (POC).

To this end the main objectives addressed in this thesis are:

1. The creation of a fully integrated micro pump for robust sample collection and droplet generation.
2. Development of this micropump and specialised droplet generation strategy into a more holistic liquid handling system.
3. The integration of this tool with novel portable detection methods, assays and sampling into a continuous monitoring device.
4. The application of this device to the in-situ continuous and long-term monitoring of molecules of interest for environmental monitoring.
5. The integration of more complex assays such as ELISA into this platform suitable for the in-situ continuous monitoring of biomolecules in a clinical setting.

1.2 Point-of-care medical testing

Current technologies in clinical diagnostics generally fall into two categories: the automation and consolidation of processes in centralised labs (Bock 2000), and the decentralization of these tests to the point-of-care (St-Louis 2000, Junker, Schlebusch et al. 2010). While centralisation may reduce cost and assay time with specialised facilities, point-of-care testing (POCT) offers further reduced cost and professional time requirements.

There are several lab-based and point-of-care (POC) tests for biochemical analysis of biological fluids. Most commonly urine and blood are analysed by standard lab-based spectroscopy or chromatography techniques or POC lateral flow immunoassay. The most common POC tests for biochemical analysis are lateral flow assay strips and immunosensors including: blood glucose meters commonly used by diabetics and rapid diagnostic tests for a variety of applications. When using lateral flow immunoassay test strips, a finger prick sample of blood is placed on the sample pad and wicks through the nitrocellulose membrane. As the sample moves through the strip, steps of the assay take place; resulting in a coloured complex of the antibody, marker and sample anchored to the test line. A colour change of the test line caused by this complex indicates the presence of the target analyte. A control line is also included where a colour change occurs as the sample passes the line to indicate that flow has occurred if there is no colour change in the test line (indicating a negative result).

1.2.1 Point-of-care medical monitoring

Many of the tools used in point-of-care testing of biochemical markers are unsuitable for monitoring purposes offering only single point measurement, requiring too large a sample size for higher sampling rates. Currently in the medical field the most common and successful point-of-care (POC) monitoring tools are small electrical devices such as heart rate monitors. A lot of research has gone into the development of miniaturised platforms for mature technologies such as bio-electrical signal analysis (Electrocardiograms etc.)(Patel, Park et al. 2012) and temperature monitoring (Latré, Braem et al. 2011), portable ultrasound devices and other small devices such as pulse oximeters.

For measuring biochemistry, technologies such as microfluidics have played a key role in developing POC diagnostics. Tools such as lateral flow assay strips have revolutionised our ability to diagnose and care for patients from the clinic or home, with assays testing for a biomarkers. These tests offer many advantages over lab-based tests such as reduced sample and reagent consumption and the combination of many steps into a single device making them easy to use. While these systems are very successful for diagnosis where only a single reading is required, they are not sufficient for many POC monitoring applications. POC monitoring often requires high temporal resolution of measurements, to monitor the concentration of fast changing biomarkers (such as metabolites). POC monitoring of biomarkers such as metabolites and hormones would provide physicians and treatment teams with a continuous readout of the patient's biochemical marker levels. Timely information on these biomarker levels as well as trends and rate of biomarker change over longer periods would allow clinicians to make better informed decisions. Studies on real-time online monitoring of glucose levels in traumatic brain injury (TBI) (Rogers and Boutelle 2013) and diabetes (Yoo and Lee 2010) patients have shown

that continuous and rapid monitoring of key analytes could play critical roles in clinical decision-making.

A number of medical device companies including Abbott and Medtronic have spent years developing devices for the continuous monitoring of glucose without the requirement for repeated finger pricks (Mader, Weinhandl et al. 2010). All of these devices employ electrochemical sensors and sample from subcutaneous adipose tissue, either directly or with a microdialysis harvesting approach (Ricci, Moscone et al. 2008). The Abbott Glucose Free Style Navigator is one of the most popular, incorporating a disposable sensor delivery unit and radio frequency (RF) transmitter directly connected to the sensor (Weinstein, Schwartz et al. 2007). The RF transmitter delivers the measured glucose level wirelessly to a display. This device has been shown effective in identifying cases of hypoglycaemia (<70 mg dL^{-1}) and hyperglycaemia (>240 mg dL^{-1}) in diabetic patients with high accuracy (96% and 99.7% respectively).

The success of such devices has led to interest in wearable monitoring devices for biochemical markers aimed at the commercial market, with many sponsored initiatives promoting novel wearable systems. Companies including Google LLC. and Apple inc. have also announced projects aiming to integrate chemical (particularly glucose) sensors into devices (Matzeu, Florea et al. 2015).

1.2.2 Under-served clinical areas

There are many clinical care situations, which require fast results and would benefit from automated long-term monitoring without the need for large amounts of professional time. This include surgical and post-surgical monitoring, monitoring of myocardial infarction and stroke patients, monitoring of patients in critical condition during transit and in coma state. In particular those with traumatic brain injuries (TBI) of which there are estimated at 500,000 new cases each year in the United States alone and over 300,000 in the United Kingdom (Yates, Williams et al. 2006), with many resulting in significant and long term disabilities. Approximately 40% of TBI patients will survive the “primary injury” but deteriorate days after the initial injury due to secondary injury (Narayan 2002). Several factors may cause secondary injuries, but recent evidence has highlighted that more traditional prognostic factors can only explain 30% of variability in TBI cases. Spreading depolarization waves (SDs) however have been highlighted as an independent and strong indicator of poor patient outcome (Strong, Fabricius et al. 2002, Hartings, Bullock et al. 2011). Repolarisations required after the spontaneous and frequent spreading depolarization waves which often occur in TBI patients cause a high-energy demand and a rapid decrease the tissue’s local glucose concentration. It has been shown that persistently low extracellular glucose correlates with increased lactate/pyruvate ratio and carries a poor prognosis with oxidative brain metabolism also playing a central role (Xu, McArthur et al. 2010).

Currently there is no adequate method of monitoring these patients’ levels of vital biochemical markers such as glucose, lactate and pyruvate with the required accuracy and temporal resolution. While there are lab assays and some less accurate portable devices primarily for glucose monitoring commonly used by diabetics today, these require relatively large sample and reagent volumes, 2μl for top market glucose meters and as much as 5ml for lab testing which is more accurate, this is not

suitable for the monitoring needs of those patients with TBI. The temporal resolution is also poor due to this large sample volume. Direct electrochemical sensing may seem like a good candidate technology for these applications due to its small size, ease of use, etc. however, it is unsuitable for a number of reasons. Electrochemical sensors cannot be used for long periods due to short durability of sensing strips, loss of electrode materials and degradation of enzymes as well as the impact of biofilm formation. Their need for frequent recalibration also makes them not ideal for long-term use. Electrochemical sensors also suffer from interference from other sample components, and electrical interference from equipment in the operating theatre or recovery bed adding to their unsuitability (Huang, Leduc et al. 2012).

Recent years have seen investigation of microdialysis and microfluidic based sensors (Rogers, Feuerstein et al. 2013, Gowers, Curto et al. 2015) as a possible platform to monitor dynamic neurometabolic events. However, many of these systems suffer from poor temporal resolution limited by Taylor dispersion (explained in section 1.4) and low accuracy compared with benchmark lab equipment. Droplet microfluidics has the potential to revolutionise point-of-care monitoring of patients when coupled with other technologies such as micro-dialysis, biochemical assays and small-scale sensors (optical or in some cases electrochemical). This approach offers many benefits over other methods such as high temporal resolution, small sample size, and suitability for long-term automated usage.

1.2.3 Cortisol as a biomarker

One of the biomarkers focused on in this thesis (explored in chapter 6) is the steroid hormone cortisol. The endocrine and nervous systems influence the body's homeostasis by regulating hormones. Hormonal balance relies on a feedback system that secretes a variety of hormones from the hypothalamus, pituitary gland and the adrenal glands known as the HPA axis as shown in Fig. 1. The adrenal gland located above the kidneys secretes three classes of hormones, glucocorticoids, mineralocorticoids and androgenic steroids (Kaushik, Vasudev et al. 2014). Glucocorticoids such as cortisol (produced by multiple catalysed oxidations of cholesterol) function to increase glucose production for energy and metabolic needs.

Free cholesterol is metabolised to produce cortisol controlled by the HPA axis shown in Fig. 1. Cortisol release is regulated by adrenocorticotropic hormone (ACTH) produced by the pituitary gland. However, the pituitary gland secretes only small amounts of ACTH without stimulation. Corticotropin releasing hormone secreted by the hypothalamus, induces release of ACTH by the pituitary gland. Cortisol also acts on both the hypothalamus and pituitary gland as an inhibitory feedback mechanism stabilizing cortisol plasma under normal conditions (Dobson and Smith 2000, De Kloet 2005, Kaushik, Vasudev et al. 2014).

Cortisol has a relatively small molecular weight (362.46 g/mol) and has a strong affinity to bind to lipids leading it to be found in a variety of body fluids (Lee et al., 2015). Cortisol plays an important role in homeostasis of the cardiovascular, immune, renal, skeletal and endocrine system (De Kloet 2005, Levine, Zagoory-Sharon et al. 2007, Gatti, Antonelli et al. 2009, Kaushik, Vasudev et al. 2014). It acts on other hormones instigating hepatic gluconeogenesis, affects myocardial-cells and blood

pressure, and plays a role in regulating the central nervous system (Mahla, Tiesenhausen et al. 2000, Christensen, Johannesen et al. 2004). One of the biggest factors in systemic cortisol variation is psychological/emotional stress hence cortisol is popularly called a “stress-hormone” (Holsboer and Ising 2010).

Like many hormones in the body, cortisol has a circadian rhythm, varying over a 24-hour period mediated by changes in metabolic activity. Under normal, non-stress conditions, glucocorticoid levels peak in the early morning (30 minutes after awakening), are at half of morning levels by late afternoon, and are negligible by midnight (Corbalán-Tutau, Madrid et al. 2014). Other than this day–night cycle, controllable factors such as eating patterns and physical activity can also affect cortisol levels in the body.

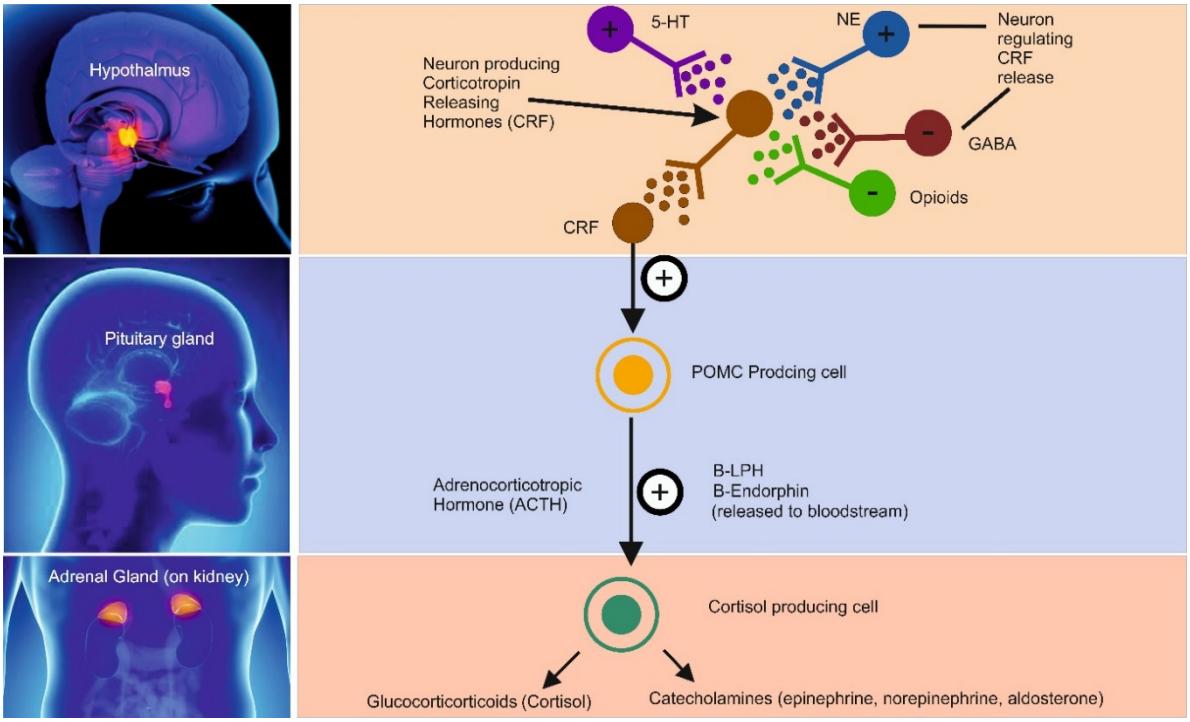

Figure 1 Hypothalamus-Pituitary-Adrenal (HPA) axis (Adapted from(Smith and Vale 2006)) Cholesterol is metabolised by this process through a variety of hormones including cortisol

Under conditions of stress, HPA axis function can be altered. Stress normally acts on the hypothalamus and ongoing stress may cause continuous stimulation of the hypothalamic pituitary function, by overriding the inhibitory action of cortisol. Stress may even eliminate the cyclic nature of cortisol causing them to remain elevated throughout the day (Sachar, Hellman et al. 1973, Kirschbaum and Hellhammer 1994). Moderate homeostatic alterations in the HPA axis are beneficial for the physiological and the psychological development of the human body (Dettling, Gunnar et al. 1999). Abnormal increases in cortisol inhibits inflammation, depresses immune system, increases fatty and amino acid levels in blood and it has been related to chronic fatigue syndrome , fibromyalgia, and many autoimmune disorders. Excessive cortisol levels contribute to the development of Cushing’s disease (symptoms: obesity, fatigue and bone fragility) (McEwen 2002) while low levels of cortisol lead to Addison’s disease (symptoms: weight loss, fatigue, and darkening of skinfolds and scars) (Edwards,

Galley et al. 1974). Cortisol is also an important biomarker indicating body condition and training effects in elite athletes. In order to monitor the immediate fluctuations in cortisol level above a baseline, analysis of cortisol containing body fluids must be rapid and accurate (Barron, Noakes et al. 1985, Banfi, Marinelli et al. 1993, HARTE and EIFERT 1995). In recent years, there has been a wide array of approaches in the attempt to develop wearable detection analytical devices to quantify stress to gain useful information for timely diagnostics and treatment, with particular focus on post-traumatic stress disorder (PTSD) (Delahanty, Raimonde et al. 2000, Yehuda, Halligan et al. 2001, Yehuda, Halligan et al. 2002, Levine, Zagoory-Sharon et al. 2007, Gatti, Antonelli et al. 2009).

1.2.4 Sample sources for cortisol measurement

Traditionally, blood or urine samples have been used to detect cortisol response, but many other options have opened up by new advances in sensing and sampling technologies. Regular estimation of free biologically active cortisol is required for accurate diagnosis and treatment of cortisol-related conditions.

Blood sampling is one of the oldest forms of bio-fluid sampling due to the large quantities of analytes present. Typically, blood samples are drawn at morning and evening. Cortisol in blood normally varies between 25 mg/dL (9AM) to 2 mg/dL (midnight), however <10% of it is in the biologically active state with the rest bound to globulin (Vining, McGinley et al. 1983) and serum albumin. Assays for measuring cortisol in blood typically measure total cortisol (bound & free) with the active fraction, called the Cortisol Free Index (CFI) calculated using Coolen's method (le Roux, Chapman et al. 2003). Blood is not an ideal sampling fluid. Sterile equipment is required to combat the possibility of infection and special storage protocols due to biohazard and the instability of cortisol in blood at room temperature. Cortisol levels in blood can be affected by a variety of factors such as patient anxiety during venepuncture (Levine, Zagoory-Sharon et al. 2007) and estrogen-containing medications (Kirschbaum, Pirke et al. 1995).

Free cortisol can be found in urine and is typically measured in the 24hr urinary free cortisol (UFC) test with a normal range 10–100µg released over 24 hours (only the biologically active free cortisol is found in urine). Large variations in cortisol in urine can be used to diagnose adrenal function abnormalities and a wide variety of assays have been reported in the literature (Brossaud, Ducint et al. 2012). While the 24hr UFC test is painless and non-invasive, it does suffer from some issues of convenience for the patient and reliable collection and storage. Patients are required to carry a special urine collection container all day or remain confined to a location for the 24-hr period and containers require refrigeration from collection until testing. Several factors can also affect urinary free cortisol including: blood in urine (le Roux, Chapman et al. 2003), pregnancy and medication such as diuretics. These factors make UFC unsuitable for real-time detection at point-of-care.

Saliva has also gained attention as a bio-fluid for analysis and detection of cortisol concentrations with infusion studies demonstrating that cortisol released in the blood stream reaches saliva in as few as five minutes (Ryoji 1981, Vining, McGinley et al. 1983). Salivary cortisol levels are representative of unbound cortisol plasma levels (Teruhisa, Ryoji et al. 1981, VanBruggen, Hackney et al. 2011), with

capillary exchange and other intracellular mechanisms at the salivary ducts filtering out corticosteroid-binding globulin and albumin bound cortisol. Sample collection from saliva is relatively non-invasive and causes little to no discomfort (Van Caenegem, Wierckx et al. 2011). Since only free cortisol is present in saliva, the concentration of cortisol is much lower than that of blood nominally between 0.5 mg/dL to 0.05 mg/dL during the diurnal cycle and hence requires assays with high sensitivity and low detection limits. Issues during sample collection and storage (cortisol is unstable at room temperature) may also lead to errors in measurement, oral lessons may lead to elevated levels of cortisol due to the presence of cortisol in blood. Nevertheless, salivary cortisol assays have been reported in the literature characterizing the circadian rhythm (Price, Close et al. 1983), Cushing's syndrome (Raff, Raff et al. 1998), Addison's disease (Løvås, Thorsen et al. 2006), adrenal abnormalities (Ambrosi, Peverelli et al. 1995), and stress related disorders (Carpenter, Shattuck et al. 2011).

Sweat analysis has been used for diagnoses of drug abuse and conditions such as cystic fibrosis. Cortisol in sweat has been shown to range between 141.7ng/mL (daytime) to 8.16ng/mL (Russell, Koren et al. 2012). While little is known about cortisol in sweat and there are possible drawbacks in sample volume variations between patients and environment. Sweat patches can be used as an effective non-invasive tool to collect sweat (Prunty, Andrews et al. 2004), a microfluidic sweat collection cloth has been proposed with collection and analysis carried out in an integrated device (Xing, Jiang et al. 2013). Cortisol can also be measured in hair follicles (Gao, Xie et al. 2010, Russell, Koren et al. 2012) however, the need for repeated sampling and rate at which cortisol enters the follicle makes this unsuitable for long term monitoring.

Interstitial fluid (ISF) is similar in composition to blood plasma with small to moderate sized molecules (e.g. glucose, lactate, and cortisol) in similar concentrations thus, periodic calibration using blood samples is not required. ISF cortisol levels have been found to be 3–4 times larger than that in saliva. Metabolites and proteins move through ISF as they move from capillaries to cells. While ISF is present just below the skin, obtaining it for detection of target biomarkers can require an invasive approach due to the low permeability of the epidermal keratinized layer (the stratum corneum) which blocks permeation of fluid through the skin. Many approaches have been reported in the literature to obtain ISF including minimally invasive, painless approaches. Low-energy lasers have been used to create micropores (diameter approx. equal to human hair) in the stratum corneum and ISF drawn through these pores by vacuum pressure (reported rate 10 mL/h, sampling 3ml every six hours) (Venugopal, Feuvrel et al. 2008). This approach has been shown coupled with electrochemical detection (Venugopal, Arya et al. 2011). The sample volumes used in the presented study limits its suitability for high temporal resolution monitoring at the point-of-care, but perhaps this may be improved upon in the future. Microneedles have also been used to harvest ISF (Mukerjee, Collins et al. 2004, Prausnitz 2004, Wang, Cornwell et al. 2005, El-Laboudi, Oliver et al. 2013) and may find good application in wearable systems when continuous low sampling rates are required however there are some concerns regarding biocompatibility and biodegradation of the microneedles, infection and other sterility issues. Microdialysis has also been shown to be a viable method of extracting interstitial fluids (ISF) and other fluid samples. Here fluid with a similar ionic composition to the tissue is pumped through the probe, small molecules pass through the membrane by passive diffusion and the fluid containing these particles continue downstream to the outlet keeping the concentration gradient constant as

described in section 1.10.2. Generally, the semi-permeable membranes used in microdialysis do not allow large molecules or cells to pass though removing some possible need for pre-processing of samples. Possible issues with microdialysis include its low temporal resolution but this can be circumvented by coupling with droplet microfluidics (Petit-Pierre, Bertsch et al. 2016).

1.2.5 Current state-of-the-art measurement of cortisol

Monitoring of patient cortisol can provide information that can assist clinicians in better diagnosis and treatment of a wide variety of conditions. However, current monitoring procedures are a cumbersome process which often require the patient to be admitted for the time of the study and take up a lot of clinicians time (Czeisler, Moore Ede et al. 1976). Large sample volumes (compared to microfluidics) (Giavarina and Lippi 2017), of blood/saliva/urine are collected at specified time intervals and shipped to a diagnostic lab (Brezina, Haberl et al. 2011). Sample collection/storage procedures may introduce additional error especially in the pre-analytical stage (Wallin, Söderberg et al. 2008, Plebani and Lippi 2010, Bhat, Tiwari et al. 2012, Plebani, Sciacovelli et al. 2014). Some patients may collect their own samples and this further increases the possibility of error in collection. In the typical case, turn around for results is 8-10 days and still may not provide a true representation of cortisol levels in a normal or true stressed state. Even if analysis were carried out at the bedside using conventional assay procedures, this would take up to several hours for a single sample. Hence, there has been wide research interest in the development of new point-of-care methods for measurement and monitoring of cortisol in recent years. This has included: electrochemical immunosensors and a variety of single use assays with compact analysis tools (Kaushik, Vasudev et al. 2014). As with all point-of-care systems sensors for cortisol monitoring need to be small, disposable, sterile, low power, provide fast results and sampling rates while remaining cost effective (Ahn, Jin-Woo et al. 2004, Soper, Brown et al. 2006, Wang 2006).

Electrochemical sensor technology has been suggested as a possible tool for the detection of cortisol at the point-of-care with a variety of approaches taken in the literature. Antibodies immobilised on micro fabricated electrodes (Sun, Ramgir et al. 2008) have been used to detect cortisol in saliva (detection limit cortisol 0.27 ng/mL, incubation time 10 min). Self-assembled monolayer (SAM) modified interdigitated μ-electrodes (IDμEs) have also been used to detect cortisol in ISF harvested by means of vacuum pressure and micropores (linear response 0.36 pg/mL-36 ng/mL) (Venugopal, Arya et al. 2011). Immunosensors which utilise single-walled carbon nanotubes (SWCNTs) (Tlili, Myung et al. 2011) have been demonstrated with increased sensitivity and further lower detection limits. However, there are limitations to electrochemical immunosensors suitability for POC use including: susceptibility to signal drift (especially over long term use (Bertocci, Huet et al. 2002)) and a low shelf-life due to the environmental factors. While different encapsulation strategies and antibody choices have been suggested to combat this susceptibility to environmental factors (temperature fluctuations, humidity, change in pH, exposure to light) these are not yet common practice (Kaushik, Vasudev et al. 2014).

A variety of assay and sensing technologies have been implemented for monitoring cortisol (Gatti, Antonelli et al. 2009, Kaushik, Vasudev et al. 2014). Chromatographic techniques have been

traditionally used to detect cortisol, however issues relating to assay formation, system complexity, and multi-step extraction/purification limits its application in the field. As explained in section 1.9.6 high degree of selectivity and specificity of antigen–antibody binding makes immunoassays the gold standard technique for the detection, and measurement (concentration) of an analyte of interest. Radioisotopes (Ryoji 1981), fluorescent tags (Kobayashi, Amitani et al. 1979) and electro-chemiluminescent tags have all been used to great effect with chemiluminescence offering much promise (Kaushik, Vasudev et al. 2014). However, many of these lab based assays are not suitable for point-of-care use requiring pre-treatment steps, large expensive analysis equipment, and long assay times (several hours). If these assays are to be applied to continuous monitoring at the point-of-care, sampling rate and throughput will need to be greatly increased. This will provide an accurate picture of short-term events and long-term trends present in the circadian rhythms of analytes such as cortisol (this is explored in Chapter 6).

1.3 Environmental Monitoring

Medicine is not the only area that would benefit from effective monitoring of chemistry with a high degree of temporal and spatial resolution. To characterise the state of aquatic ecosystems, contextual measurements of physical properties must be gathered in concert with measurements of biology and chemistry. With the right technological approach, it should even be possible to monitor markers of disease in waterways. This is important both for monitoring the health of the environment and also ensuring the health of people who use this water for drinking and farming.

1.3.1 Biogeochemistry

Monitoring how chemical species are distributed in oceans, lakes and rivers (natural waters) is fundamental for the study of the biogeochemical cycles that drive important global processes such as biological productivity. To fully characterise the state of these aquatic ecosystems a wide variety of chemical species must be measured. Nutrients such as nitrate, phosphate and silicate should be quantified in concert with trace metals (e.g. dissolved iron and manganese), dissolved gases (e.g. oxygen and methane) and carbonate system parameters such as pH, dissolved inorganic carbon, total alkalinity and pCO2 (partial pressure of CO2) (Flynn 2001, Moore, Doney et al. 2001, Moore, Doney et al. 2004, Dutkiewicz, Follows et al. 2005, Yool, Popova et al. 2013).

Traditional manual sampling, where water is collected, preserved and transported for lab analysis (Brügmann and Kremling 2007) does not offer sufficient resolution and is often simply not practical. Samples are often transported long distances, for analysis using standard laboratory methods such as colorimetry, fluorescence or atomic absorption spectroscopy and may degrade in transit. *In-situ* measurement reduces the risk of sample degradation, contamination and, removes transportation logistics. If *in-situ* monitoring devices can be deployed on a mobile platform such as a submersible vehicle, a spatially detailed map of chemical composition can also be generated. There have been several published reports on *in-situ* chemical sensors based on microfluidic systems deployed on remotely operated vehicles (ROVs) (Le Bris, Sarradin et al. 2000, Vuillemin, Le Roux et al. 2009, Provin,

Fukuba et al. 2013) and automated underwater vehicles (AUVs) (Chin, Coale et al. 1994, Statham, Connelly et al. 2003, Statham, Connelly et al. 2005). Some chemical parameters such as pH (Martz, Connery et al. 2010, Takeshita, Martz et al. 2014), oxygen (Revsbech 1989, Klimant, Meyer et al. 1995), pCO_2 (Neurauter, Klimant et al. 2000) and nitrate (Finch, Hydes et al. 1998, Johnson and Coletti 2002, Johnson, Coletti et al. 2006, Johnson, Riser et al. 2010) have been monitored with solid state sensors. However, many chemical species cannot be measured with sufficient accuracy or dynamic range in natural waters.

This has led to the use of *in-situ* liquid analysers to monitor chemistry. These typically draw a sample from the environment, chemically treat it, measure the response and then expel the waste. However, operational lifetime of such sensors in the field has so far been limited by requirements for large stores of reagents and power consumption. Microfluidics systems offer greatly reduced sample and reagent volumes per measurement and also reduce energy expended on pumping. These have been applied as *in-situ* analytical devices with much higher measurement frequency and uninterrupted continuous measurement even in remote locations. Analysing water samples on site greatly reduces sample degradation or risk of contamination, with no requirement for sample preservation and transport. Devices may even be deployed on mobile platforms to generate detailed maps of chemical composition of waterways. These *in-situ* microfluidics based chemical sensors recently generated a great deal of interest as they have a unique and important role to play in environmental measurement and monitoring (Nightingale, Beaton et al. 2015).

This is further explored in Chapter 5 where alongside academic colleagues I have developed a first of its kind droplet microfluidics platform, incorporating *in-situ* calibration of sensors and begun testing of nitrate and nitrite levels in a local estuary. Estuarine levels of these compounds vary with the tide and are relevant to the overall health of the surrounding ecosystem. This work has been further taken forward by SouthWestSensors Ltd.

1.3.2 Public health

While in developed countries clean drinking water is mass-produced and often taken for granted, in many places around the globe there have been outbreaks of waterborne diseases in the last decade. Recently there has been effort to detect chemicals and bacteria which cause disease using *in-situ* sensors. For example a group have deployed a network of “artificial mussels” to detect and study eight heavy metals in waterways across Bangladesh (Kibria, Hossain et al. 2016). During this study, they identified seven metal pollution “hot spots”, five of which were located in the Buriganga River, close to the capital Dhaka. Untreated industrial discharge, agriculture and fish farming effluents and ship breaking activities have all been highlighted as possible causes. Metal pollution has significant impact on water quality, aquatic biodiversity, food contamination/food security due to bioaccumulation of metals in crops and seafood. Microfluidic systems may also be applied to detect levels of waterborne bacterial pathogens such as Cryptosporidium and Escherichia coli, and discriminate between infectious and non-pathogenic species. These bacteria have even caused outbreaks of disease in developed nations such as the United States from contaminated drinking water (Neumann, Smith et al. 2005, Leitch and He 2011, Shirley, Moonah et al. 2012).

The widespread use of *in-situ* sensors will hopefully allow for the development of large scale sensor networks, both for modelling natural processes, and monitoring of rivers and coastal waters for pathogens and anthropogenic pollution (Hart and Martinez 2006).

1.4 Microfluidics

As mentioned in previous sections, many modern biochemistry measuring tools incorporate some element of microfluidics, a technology first developed in the 1980s (Whitesides 2006). Microfluidics is the study and manipulation of small volumes of fluid (microlitres to picoliters) in microchannels 1-1000 μm in diameter. At this scale the properties that dominate liquids change with the relative effect of the force produced by gravity at microscale dimensions greatly reduced, with surface tension and capillary forces dominating. Therefore, microfluidics is typically characterized by low Reynolds numbers (<1)and laminar flow regimes and leads to many advantages when applied to biochemical assay development; the advantage of rapid and predictable heat and mass transfer; reduced reagent use and waste generation when compared to 'bulk lab procedures'. Microfluidics ability to create small chemical reactors has seen a number of successful areas of applications including the development of "Micro Total Analysis Systems" (μTAS) or "lab-on-a-chip" devices (Dittrich, Tachikawa et al. 2006) which automate and include all necessary steps for the chemical analysis of a sample and have been exploited for a wide variety of processes in cell biology, nanoparticle manufacture, analytical chemistry and others(Li Jeon, Baskaran et al. 2002, Lucchetta, Munson et al. 2006) (Squires and Quake 2005).

Microfluidics has been talked about for a long time as a technology which would revolutionise the way biomedical research is carried out with a chorus of researchers adulating its many favourable properties (Sackmann, Fulton et al. 2014). However, while there is a great deal of research published in engineering journals regarding microfluidics this is not translating to proportional uptake in other areas such as biology and medical research. Approaches such as lateral flow assay strips have been integrated into common use extremely well however, others have not. This may be largely due to the difficulties in using some of these large lab-based platforms with complex liquid handling procedures requiring large pumps and control systems as well as sample and reagent volumes required and fabrication/running costs. Hence, this will be an important design consideration for the coming point-of-care monitoring platforms. The development of simple and easy to use field deployable platforms features heavily in this thesis as it is vitally important for this technology to have the maximum possible impact.

1.4.1 Pumps for *in-situ* microfluidic analysis

Micropumps are a crucial component of any microfluidic micro total analysis system (μTAS) and hence have been an area of much research interest for many years with key criteria being size, power consumption and robust delivery of flow. The first MEMS micropumps were developed in the 1980s by Jan Smits and Harald Van Lintel; these drove fluid through piezoelectrics (Yang, Yang et al. 1995,

Lintel, M. Van De Pol et al. 2018). Since then a wide variety of micropumps have been developed. In general external-power driven pumps are the most common type used in microfluidics, such as syringe pumps, rotary pumps, peristaltic pumps, piezoelectric micropumps. These rely on off-chip power to automate sample flow and may use mechanical parts to displace fluids. Other pumping strategies include those which rely on surface tension, hydrostatic-pressure, gas diffusion etc. as well as which impart energy to the fluids without moving parts utilising acoustics, electro-osmosis, magnetohydrodynamic or electrokinetic effects.

Figure 2a shows an example of a syringe pump (open source design (Wijnen, Hunt et al. 2014)), the most widely used type of pump for microfluidics in the literature. Syringe pumps make use of pressure driven flow and have been utilised for a variety of lab processes providing reliable pumping up to several hundred bars of pressure.

However, there are many drawbacks to using syringe pumps particularly for point-of-care applications or for long-term deployment in remote locations. Many syringe pumps may be required to pump all necessary fluids for analysis increasing overall size and cost. Generally syringe pumps are slow to stabilise if the flow rate is changed , have a limited total volume before needing refilled (Neff, Fischer et al. 2001) and may suffer from unpredictable oscillations (especially at low flow rates) due to issues with motors used to drive the pump, gear problems such as misalignment, and plungers dragging on syringe housing.

Some systems have been created to combat the problems faced by syringe pumps Fig. 2b shows an example which makes use of a stepper motor, screw thread and check valves to provide a push pull pump with longer running time and more stable performance than other instrumentations (Nightingale et al., 2015). Some manufacturers now sell specialised syringe pumps especially for microfluidic applications, along with a variety of flow control, stabilisation tools and automated refill tools but these can be prohibitively expensive and also increase the size of the platform further. While syringe pumps do face issues, which make them less suitable for portable and other applications they have been used to great effect for a variety of microfluidic in lab applications.

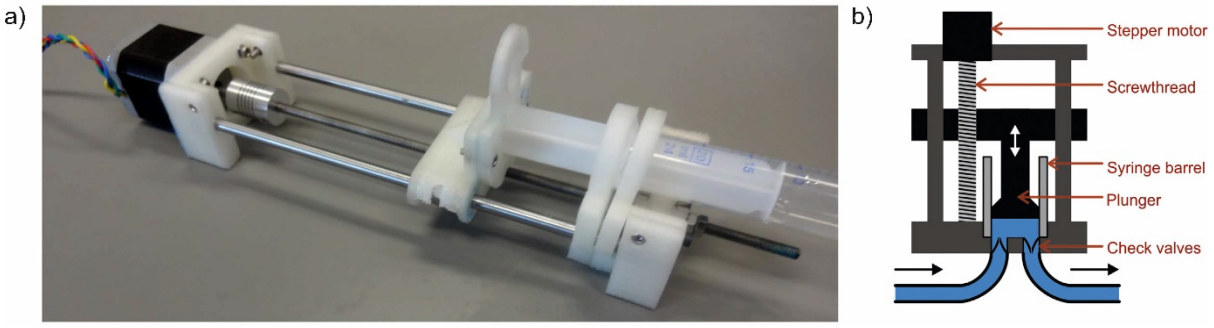

Figure 2 *Syringe pumps for microfluidic analysis a) Example of an open-source syringe pump apparatus (Wijnen, Hunt et al. 2014) b) Example schematic of a syringe pump system for in-situ monitoring including check valves (Nightingale, Beaton et al. 2015).*

Pumping via the process of osmosis has been suggested as a possible low power pumping alternative. Osmosis pumps consume no electrical power during routine sampling and so may be particularly

suitable for long stationary deployments in remote locations, where power longevity is critical (Chapin, Jannasch et al. 2002). Osmotic pumps operate by osmotic pressure difference between low and high-salinity reservoirs within the sensor to passively drive very slow flows typically around a single Litre/hour (Jannasch, Johnson et al. 1994, Chapin, Jannasch et al. 2002, Jannasch, Wheat et al. 2004). However, mechanically driven pumps are still required for administering blank and standard solutions during calibration. Osmotic pumping also suffers from other key drawbacks: flow rates drift over time, and cannot be arbitrarily set by the user with calibrations taking approx. six hours due to low flow rates (Chapin, Jannasch et al. 2002). Rapid temperature and pressure changes also cause significant flow rate variation (Jannasch, Johnson et al. 1994), and even reversal of flow. As a result, reports of osmotically pumped sensors have been rarely reported in the literature (Jannasch, Johnson et al. 1994, Chapin, Jannasch et al. 2002).

Another low-power pumping solution first proposed by Weeks et al. in 1996 (Weeks and Johnson 1996) and has since been widely used (Thouron, Vuillemin et al. 2003, Chapin, Caffrey et al. 2004, Okamura, Hatanaka et al. 2004, Plant, Johnson et al. 2009, Meyer, Prien et al. 2012) are solenoid pumps. These operate using an electromechanically actuated linear piston and a pair of check valves, propelling a fluid forward as a series of discrete pulses (Weeks and Johnson 1996, Thouron, Vuillemin et al. 2003, Plant, Johnson et al. 2009)). Solenoid pumps offer particularly low power consumption ~0.5 W. However, they typically cannont handle large back pressure of the fluidic system and flow rates are often subject to drift. Peristaltic pumping which I have chosen to use in all further chapters have been used for many years in microfluidic and other applications. All peristaltic pumps induce fluid flow by the displacement of elastic-walled channels with fluid essentially transported through continuously moving valves as seen in Fig. 3a. Peristaltic micropumps comprising a small number of discrete actuators (typically three placed along the fluid channel) (Yong, Shin et al. 2013) have been shown in the literature, however fabrication and control are an issue. Pumps which more resemble the larger peristaltic pumps utilising a rotorhead with rollers, and tubing have also been shown with much promise.

There are many advantages to peristaltic pumping particularly for point-of-care medical applications and others such as environmental applications. Fluid does not come into contact with the main parts of the pump reducing the risk of contamination and the tubing pumplines can be easily replaced (Klespitz and Kovács 2014). Peristaltic pumps are also self-priming requiring no additional fill pump etc. further decreasing concerns with contamination. Peristaltic pumps are cheap and easy to fabricate and can be made such that the overall platform size is relatively small when compared to others which include large control structures, etc. However, possible issues which may limit its application include its strong pulsations and possible drift in flow rates with changing plasticity and elasticity of tubing due to temperature changes, etc. (Le Bris, Sarradin et al. 2000).

An interesting example of a peristaltic pump is the screw driven variety. Figure 3b&c shows one developed by (Wonsei and Toshiro 2010) featuring a disposable pumping head with eight fluid channels and reusable parts. A shaft rotating inside the pumping channel unit has a spirally arranged projection resembling a corkscrew on the surface which deforms and closes the channels. When the

shaft rotates, the pinched locations in the channels move according to the direction of rotation, squeezing out the fluid.

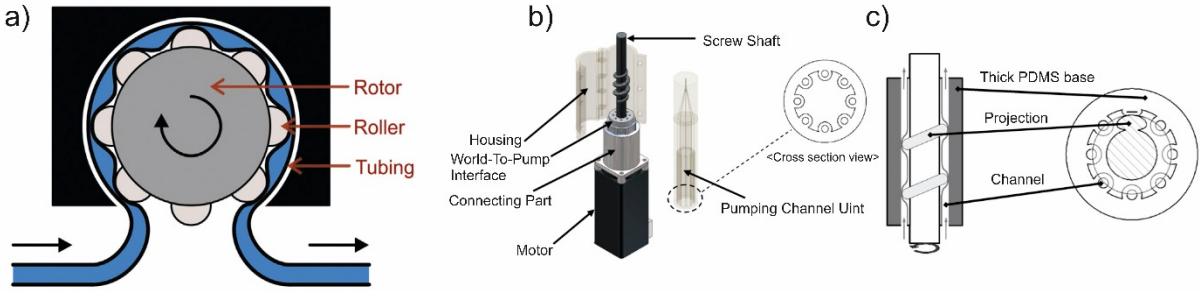

Figure 3 *Peristaltic pumps for microfluidic analysis a) Example schematic of a peristaltic pump (Nightingale, Beaton et al. 2015) b&c) Schematic views of screw driven peristaltic pump (Wonsei and Toshiro 2010).*

An important concern for field deployed *in-situ* sensors is that unless the sensor is deployed close to a suitable exterior power source, it will to some extent rely on a finite reserve of electrical power. Many components will affect energy consumption including any light sources for sensors, but the pump is the main power consumer in any flow system. One of the main limitations of flow-based sensors is Taylor dispersion as described in Fig. 4, an effect caused by viscous drag at channel walls which effectively smears chemical composition down the length of the channel (Nightingale and de Mello 2010). This results in optimum temporal resolution in the order of minutes, which is not sufficient for many applications in both the clinical monitoring and environmental science fields. One possible method to address this is multiplexed stop-flow (MSF) architectures (Ogilvie, Sieben et al. 2011). In MSF systems long delay channels which are used to allow samples and reagents time to mix are removed, instead solutions are left to diffusively mix under no flow. This is repeated in multiple parallel measurement channels in order to increase measurement frequency, with solutions continuously pumped into each measurement channel in turn. While MSF can reduce the effect of taylor dispersion, it can be completely removed and sampling frequency dramatically increased by shifting flow regime from continuous phase to droplet flow (Song, Chen et al. 2006, Nightingale and deMello 2013) i.e. droplet microfluidics.

1.5 Droplet Microfluidics

Droplet microfluidics is a technology used to manipulate discrete sub-microliter volumes of fluids in two immiscible phases under low Reynolds numbers (<1), laminar flow regimes offering many attributes which make it particularly suitable for high-throughput analytical testing. Droplets were first applied as a tool for biological analysis in the 1600s by Antonie van Leeuwenhoek, observing algae and flagellates held inside water droplets under an early microscope (Dobell and Leeuwenhoek 1932). Research into droplet microfluidics as we think of it today, confined within microchannels, began in the late 1990s/early 2000s (Thorsen, Roberts et al. 2001, Dreyfus, Tabeling et al. 2003, Whitesides 2006). This approach to droplet microfluidics inherits many of its beneficial characteristics from precursor technologies such as Micro-Electro-Mechanical Systems (MEMS), molecular analysis and continuous phase microfluidics (first developed in the 1980's). This includes low cost and high-speed

manufacturing techniques (when scaled up to industrial levels), short times for analysis, fast heat exchange, favourable fluid dynamics (laminar flow), small sample size and reagent usage and small device footprint compared to other 'bulk chemistry' devices (McDonald, Duffy et al. 2000, Whitesides 2001, Wang, Liu et al. 2015, Yazdi, Popma et al. 2016). Droplet microfluidics has emerged as a powerful engineering tool for bio-chemical assay and analysis using small sample volumes with high analytical throughput. Droplet microfluidics has seen successful application to fields such as: cell biology (particularly single cell (El-Ali, Sorger et al. 2006) or particle analysis (Craighead 2006)), high-throughput low volume polymerase chain reaction (PCR) (Zhu, Jenkins et al. 2012), organic synthesis (deMello 2006) and the manufacture of nanomaterials (Weibel and Whitesides 2006), and has many favourable characteristics for the application of continuous monitoring.

In recent years there have been a variety of multiphase system approaches which may be referred to as droplet microfluidics. For the sake of this thesis we will define droplet microfluidics as droplets of liquids sometimes called 'plugs' contained within a continuous immiscible liquid phase in a confined channel of size 1-1000µm in diameter. Some other approaches not covered in detail here are: droplets in large channels/bulk systems (Stone 1990, Stone 1994) gas droplets or 'slugs' and digital microfluidics where droplets on planar surfaces rather than contained within microchannels are manipulated by electro-wetting or other means (Abdelgawad and Wheeler 2009, Choi, Ng et al. 2012).

Droplet microfluidics offers many benefits over other technologies, due to its ability to produce many individual and separate chemical reactors suitable for multiplexed and repeated analysis. The discrete volume of droplets can be matched to the desired entity size from a few femtolitres to hundreds of nanolitres minimizing sample size and reagent usage. One of the favourable qualities of droplet microfluidics for carrying out chemical assays is the particularly fast mixing of chemicals best described by the peclet number. A dimensionless term the peclet number is one of the most relevant metrics for transport of chemical species described in equation 1. The Péclet number is defined as the ratio of the rate of advection of a physical quantity by the flow to the rate of diffusion (matter or heat) of the same quantity driven by an appropriate gradient. This can also be described as the product of the Reynolds number, which describes the flow regime, and the Schmidt number, which is used to characterize fluid flows in which there are simultaneous momentum and mass diffusion convection processes Where: *u* is the flow velocity, *L* is a characteristic linear dimension, (travelled length of the fluid; hydraulic diameter etc.), *D* is the mass diffusivity [m^2/s]. (Rapp 2017)

Peclet number
$$Pe_L = \frac{advective\ transport\ rate}{mass\ diffusion\ rate} = Re_L Sc = \frac{u}{D/L} \quad (1)$$

As shown in Fig.4a, increased mixing in flowing droplets is caused by the two vortices in the droplet which are the result of the carrier phase moving over the surface of the droplet. The increased chaotic advection produced by these vortices results in a particularly high Peclet number. When travelling through a serpentine channel these vortices fold over each other to further increase mixing (further explained in section 1.9.1). This chaotic mixing leads to increased mass transfer within each droplet and accurate control of reactions. This chaotic advection is not present in the relatively slow diffusion dependent mixing seen in continuous phase microfluidics as shown in Fig. 4a.

Droplet microfluidics also does not suffer from Taylor dispersion. As shown in Fig. 4b Taylor dispersion is an effect of shear flow resulting in a parabolic flow profile and increasing the diffusivity of a species, by 'smearing' the concentration distribution in the direction of the flow. While taylor dispersion does increasing mixing by diffusion by increasing the size of the interface between the two liquids, the elimination of Taylor dispersion reduces the risk of sample dilution and increases temporal resolution of time resolved measurements, giving it great potential for continuous monitoring. As droplets are completely confined, they can also be stored if desired for other analysis later (Chen, Li et al. 2007, Bai, He et al. 2010).

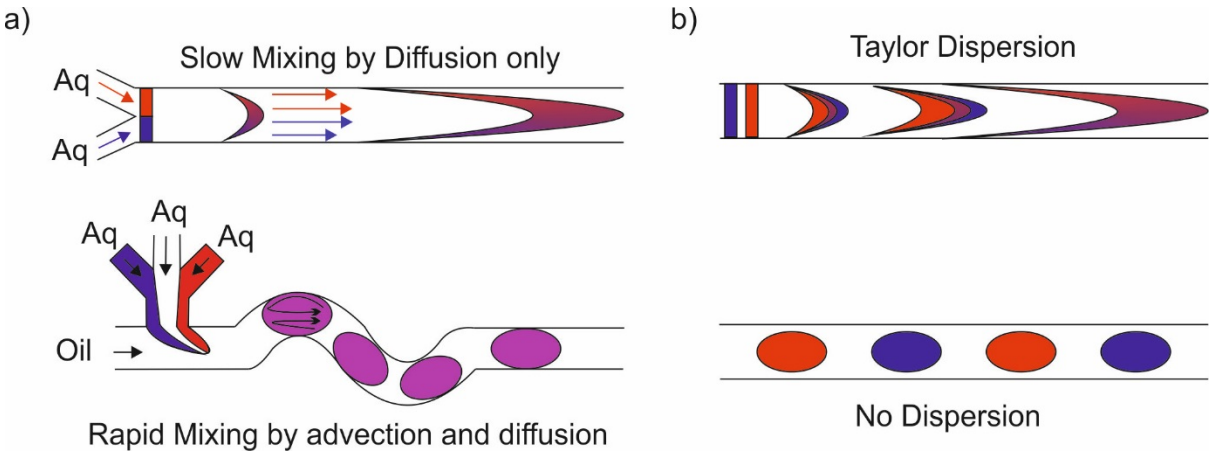

Figure 4 *Comparison of a two input continuous microfluidics (top) with droplet microfluidics format (bottom) adapted from (Huebner et al., 2008) a) Schematic demonstration of droplet microfluidics rapid mixing the increased chaotic advection compared to diffusion dominant mixing in continuous flow b) Schematic demonstration of Taylor dispersion in continuous flow and the lack of this 'smearing' on the channel wall in droplet flow which leads to higher temporal resolution possibilities.*

1.6 Droplet generation and manipulation

Robust droplet generation is the most important part of any droplet microfluidic system. The ideal droplet used for analytical or many other purposes should have a defined volume with a variance below 5%, definable contents, and surface tension with the carrier fluid. This requires a fine control of droplet size, contents and morphology with narrow monodisperse size distributions being a necessity for most applications. Fine control of these parameters reduces the compound error in analysis. Hence, there has been much academic research into various mechanisms of droplet generation, as well as manipulation for splitting/fission, merging/fusion, mixing, sorting etc. Droplet generation and manipulation tools can be divided into two main categories "passive" and "active", which will be explained in this chapter.

1.6.1 Choice of carrier phase

Droplet microfluidics makes use of two immiscible phases with, both water-in-oil and oil-in-water droplets possible by careful design of the system. The phase that has a lower interfacial tension with the channel wall will wet the channel and become the continuous phase, the other becoming the dispersed or droplet phase. In water-in-oil systems fabricated in PDMS it is common to pre-treat the channel with a hydrophobic agent (such as aquapel) to ensure the oil phase wets the channel. The choice of carrier phase can have a great effect on droplet generation as it will affect the capillary

number and therefore droplet generation (see section 1.6.2) by the interfacial tension (γ) between the two phases and the wetting of the microchannel walls by the carrier phase.

Many liquids have been used for the carrier phase in droplet microfluidic systems including silicone oil, mineral oils and fluorinated oils. Fluorinated oils such as FC-40 attract wider attention because of their non-reactivity with extremely stable bonds between its carbon and fluorine atoms, super hydrophobicity, weak intermolecular forces, high density and oxygen dissolvability (Gruner, Riechers et al. 2015). These properties help with stability of the droplets to avoid coalescence and help ensure there is adequate oxygenation as required for a wide variety of chemical processes and in the case of single cell analysis, to ensure cells remain alive.

1.6.1.2 Surfactants

The carrier phase may also be "spiked" with a surfactant in order to stabilize the fluid-fluid interfaces of the droplets. Surfactants are a class of compounds known as amphiphilic molecules; these reduce the surface tension between the oil and water phases due to their structure which for example may consist of a hydrophilic head and lipophilic tails which drive the molecules towards the interface between water and oil layers as shown in Fig. 5a adapted from (Song et al., 2006). This helps stabilize droplet generation and creates a layer on the liquid/liquid interface to prevent coalescence or leakage of molecules from the droplets after generation (Holt, Payne et al. 2010, Baret 2012, Seemann, Brinkmann et al. 2012).

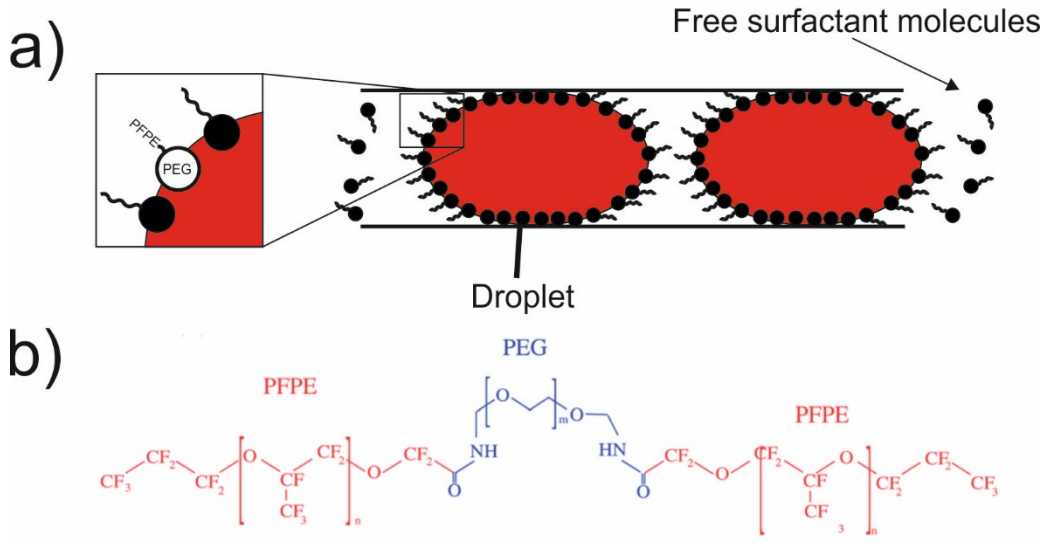

Figure 5 *a) Operation of example surfactant (polyethyleneglycol (PEG) head with perfluorinated polyethers (PFPE) tail) in droplet microfluidics (adapted from (Song, Chen et al. 2006) b) Tripolymer PEG-PFPE Surfactant (Brosseau, Vrignon et al. 2014).*

Although it is normally assumed that interfacial tension is constant but typically, this is only true in systems where no surfactant is present or at very high concentrations of surfactant. Due to the

importance of creating a stable droplet population which will not merge unless desired, the carrier phase chosen for future experiments in this report includes a surfactant shown in Fig. 5b a tri-block copolymer of hydrophilic PEG and two PFPE tails (Brosseau, Vrignon et al. 2014) produced in a method similar to (Chokkalingam, Tel et al. 2013) suspended in fluorinated FC-40 oil. When suspended in oil with droplets the PFPE-PEG molecules arrange themselves on the surface with the hydrophilic heads pointed in towards the droplet and the hydrophobic tails on the outside as shown in Fig. 5a inset. This surfactant was chosen and is commonly used in the literature due to its effectiveness in stabilising droplets and in particular its biocompatibility, not shared by others such as ionic surfactants which may damage cells and their contents (Wagner, Thiele et al. 2016).

1.6.2 Passive droplet generation

The most common approach to droplet generation often called “passive” generation, achieved by pumping two or more immiscible fluids into a junction at constant flow rates. A variety of dimensionless numbers can be used to characterise microfluidic systems. One of the most important among these for droplet microfluidics is the capillary number. The capillary number is a dimensionless parameter which represents a comparison of the viscous and interfacial forces present in a droplet system. The capillary number can be used to determine how a droplet will break up from the incursion site of the dispersed phase. The capillary number essentially indicates the length of a coaxial flow period in the system between the dispersed and carrier phases.

The capillary number can be determined experimentally and due to its effect on droplet breakup will also affect droplet volume, contents and spacing. The capillary number is determined by the equation 2 or 3 (depending on channel geometry) and is affected by volumetric flow rate of the fluids (Q), interfacial tension between them (γ), viscosity of the fluids (μ) and channel geometry. The subscript o is representative of outer (carrier) fluids, in this case the fluorous oil. In the literature three primary breakup regimes have been identified, described in section 1.6.2.2 and droplet volume can be calculated for experiments by equation in these breakup regimes (Anna 2016):

Capillary number in Cross/co-flow geometry $$Ca = \frac{\mu_O U}{\gamma} \quad (2)$$

Capillary number in Flow focusing geometry $$Ca = \frac{\mu_O G a_0}{\gamma} \quad (3)$$

The capillary number is defined differently depending on channel geometry. Common droplet generation geometries are shown in Fig. 6. Equation 2 for cross-flow or co-flow geometries relies on flow velocity (U) and equation 3 for flow focusing geometries is in terms of axial elongation rate from the flow-focusing nozzle (G) and droplet radius (a_0) defined by equation 6 and 7 respectively.

1.6.2.1 Geometries for passive droplet generation

Passive droplet generation has been achieved with a number of microchannel geometries as shown in Fig. 6 (Collins, Neild et al. 2015) these include: Co-flow Fig. 6a using parallel/concentric channels,

Cross-flow Fig. 6b exemplified by the T-Junction geometry which uses perpendicular channels (Garstecki, Fuerstman et al. 2006) and Flow focusing Fig. 6c (Garstecki, Gitlin et al. 2004) geometries.

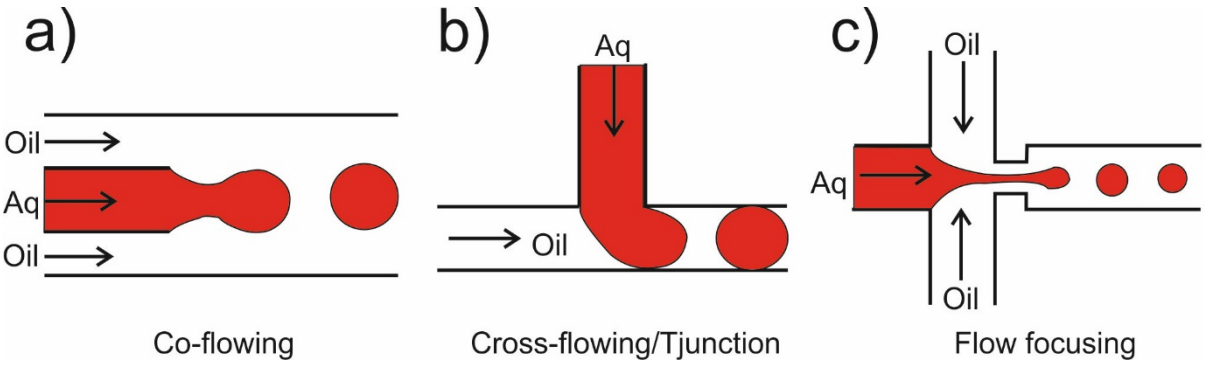

Figure 6 *Common droplet generation geometries (Collins et al., 2015) a) Concentric co-flowing geometry b) T-junction cross-flowing geometry and c) Flow focusing geometry.*

The capillary number (which is relevant to measurable droplet generation parameters) in both parallel/co-flowing geometries (Fig. 6a) and perpendicular/T-Junction (Fig. 6b) is given by equation 2 and the mean velocity component (*U*) is given by equation 4. Where Q_o is the flow rate of the carrier fluid, *w* is the width of the downstream channel and *h* its depth (De Menech 2006, Christopher, Noharuddin et al. 2008, Glawdel and Ren 2012).

Mean velocity component

$$U = \frac{Q_o}{wh} \tag{4}$$

The cross flow/T-Junction geometry is a very commonly used geometry for droplet generation (Thorsen, Roberts et al. 2001, Nisisako, Torii et al. 2002, Xu, Li et al. 2006). For this geometry, the droplet phase is injected into a channel perpendicular to the continuous phase already flowing in the main channel. Shear forces generated by the carrier phase stretch the interface between the fluids until a droplet breaks off by one of three mechanisms described in section 1.6.2.2. This geometry may have multiple inlets for either phase joined in a Y-shaped channel before the T-Junction and is most commonly used for larger droplets (100 - 1000μm).

Flow focusing geometries are typically used for smaller droplets in the order of 1 – 100 μm (Tan, Cristini et al. 2006). A common flow focusing geometry is shown in Fig. 6c although others have been used all are based upon forcing the droplet and carrier phase through a narrowing in the channel (Anna, Bontoux et al. 2003, Tan, Cristini et al. 2006, Yobas, Martens et al. 2006, Zhou, Yue et al. 2006, Woodward, Cosgrove et al. 2007). This design relies on the shear force of two streams of carrier fluid "pinching" the dispersed phase as they are forced through a narrow channel. In contrast to the co-flow or cross flow, the capillary number for flow focusing is not given by the mean velocity (*U*) of the outer fluid, instead it is a function of the droplet radius (a_0) and axial elongation rate from the flow-focusing nozzle (*G*) given by equation 5:

Axial elongation rate in flow focusing geometries

$$G = \frac{Q_o}{h\Delta z}\left(\frac{1}{w_{or}} - \frac{1}{2w_o}\right) \tag{5}$$

Where Δz is the axial distance between the end of the inlet channel for the dispersed phase and the focusing orifice of width w_{or} and w_o the width of the inlet channel for the continuous phase (Lee, Walker et al. 2009). Droplet radius is given by the half width of the dispersed phase channel, as shown in equation 6:

Droplet radius in flow focusing geometries

$$a_o = \frac{w_i}{2} \tag{6}$$

1.6.2.2 Mechanisms for passive droplet breakup

Mechanisms for droplet breakup in microchannels have been studied by experiment and simulation and are similar for many geometries but differ greatly from those seen in larger channels (Stone 1994, Eggers and Villermaux 2008). In microchannels strong confinement is the major controlling factor critical to the breakup of the fluid interface (Janssen, Meijer et al. 2012) contrary to early models (Dollet, van Hoeve et al. 2008), although viscous stresses and inertia still have an effect. The 3-dimensional nature of flow while previously ignored (Wong, Radke et al. 1995, Wong H 1995) also plays an important role in breakup particularly gutter flow in non-circular channels (van Steijn, Kleijn et al. 2009) and study of 3D flows has led to improved methods of estimating droplet size (Musterd, van Steijn et al. 2015). Droplet breakup in microchannels is usually categorised as one of three regimes: “squeezing”, “dripping” or “jetting” with capillary number predicting the breakup regime (Garstecki, Gitlin et al. 2004, Garstecki, Stone et al. 2005, Garstecki, Fuerstman et al. 2006, Utada, Fernandez-Nieves et al. 2007).

At very low capillary numbers (Ca < 0.01), when the confining effects of the microchannel wall is far greater than the viscosity forces acted upon the outer carrier liquid, droplets are generated by a “squeezing” regime shown in Fig. 7 (van Steijn, Kleijn et al. 2010).

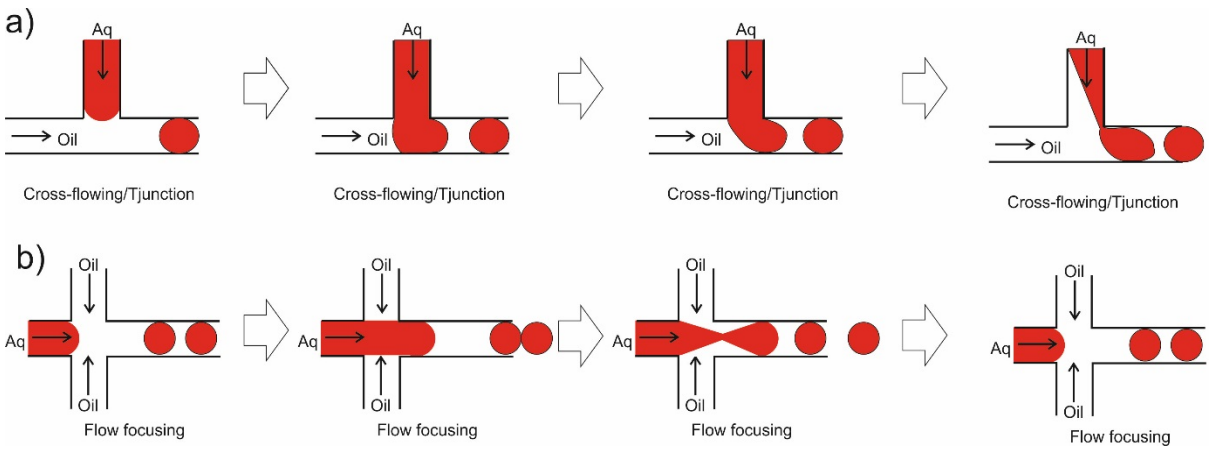

Figure 7 *Squeezing regime of droplet generation a) In cross flow/T-junction geometry (van Steijn et al., 2010) droplet breakup close to leading edge b) In flow focusing geometry droplet breakup close to the junction (Both of these structures have particularly short co-flow periods due to low capillary number in this regime).*

First, the dispersed phase is injected into the microchannel obstructing the flow of the carrier phase until the flow of the continuous phase and the tension between the liquids stretches the interface between them in a quasi-static fashion until a critical thread radius (r_{crit}) when the neck collapses. This

point is determined by geometry and can be expressed by equation 7 (van Steijn, Kleijn et al. 2009). At this pinch-off point, a pressure gradient causes a shift in the gutter region flow causing rapid neck collapse (Funfschilling, Debas et al. 2009, van Steijn, Kleijn et al. 2009).

Critical thread radius

$$r_{crit} = \frac{hw}{2(w+h)} \tag{7}$$

This has been shown in both cross flow (Garstecki, Fuerstman et al. 2006) and flow-focusing geometries (Garstecki, Gitlin et al. 2004). The droplet length L_b is expected to be linearly proportional to the flow ratio φ and the channel width W following equation 8

Droplet length in squeezing

$$\frac{L_b}{W} = A_1 + A_2\varphi \tag{8}$$

A_1 and A_2 are representative of coefficient's which must be fitted and vary with the T-Junction's or pinch-off region (inflow focusing devices) cross sectional geometry. This equation is derived from experiments measuring the local pressure in the fluid by laplace pressure sensors and is the same for both T-junction (Abate, Mary et al. 2012) and flow-focusing (Romero and Abate 2012) geometries. Overall downstream pressure remains relatively constant while changes in upstream pressure of each phase increase and decrease out of phase during droplet generation.

Van Steijn *et al.* later summarised previous observations of velocity and pressure in the squeezing breakup regime into one simple expression equation 9 (closed-form model). This is consistent with previous equations but also integrating the role of geometry and 3D flow which can be used to predict droplet volume (V) for given conditions. (van Steijn, Kleijn et al. 2010).

Van Steijn droplet volume

$$\frac{V}{hw^2} = \frac{V_{fill}}{hw^2} + \alpha\varphi \tag{9}$$

V_{fill} is a function solely of the geometry of the T-junction, and α depends on geometry and the fraction of flow allowed to leak through the corner gutters.

At larger capillary numbers (*Ca* > 0.1), the fluid interface is not broken up as easily and co-flowing streams emerge. This causes the formation of a "thread" whose radius is dependent on the flow rate ratio. The thread is broken up downstream, by either a narrowing resulting in dripping or a widening resulting in jetting depending on the capillary number of the outer fluid and the weber number (see equation 10) of the inner fluid. These regimes are shown in Fig. 8.

Weber number

$$We = \frac{\rho U 2 a_0}{\gamma} \tag{10}$$

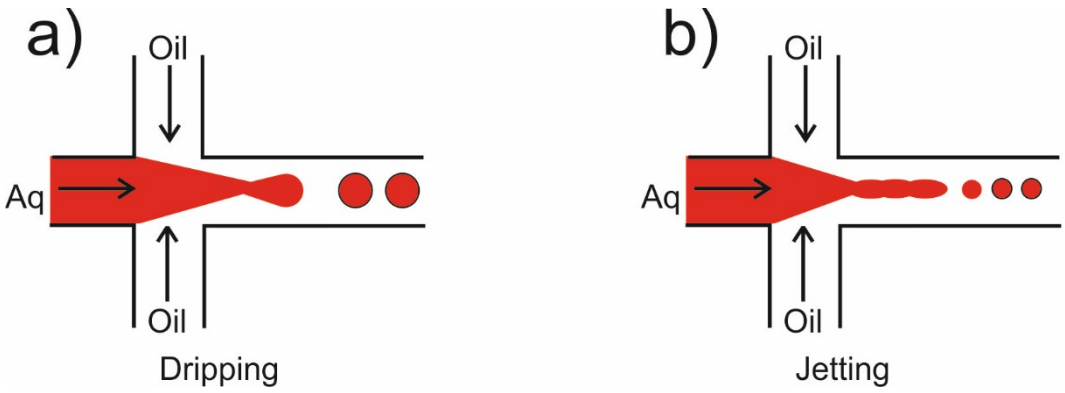

Figure 8 *Droplet breakup regimes at capillary numbers>0.01 a) Dripping and b) jetting regimes of droplet generation in a flow focusing geometry (Collins et al., 2015) displaying long periods of co-flow with breakup far from the junction due to high capillary number.*

Droplet size in dripping and jetting regimes is typically smaller than squeezing. There does not seem to be a reliable model to determine droplet size in passive breakup, so this may be best determined by experiment. However, droplet size is heavily influenced by the breakup location of the fluid thread, with conditions for breakup determined by flow rate ratio, thread radius and channel depth (Humphry, Ajdari et al. 2009, Janssen, Meijer et al. 2012)

Dripping occurs when viscous and capillary forces dominate and is caused by a narrowing of the thread at a stationary breakup location as shown in Fig. 8a. Using very high viscous forces dripping regime-based devices have been shown to produce droplets with 1-30µm diameter (Marín, Campo-Cortés et al. 2009, Gordillo, Sevilla et al. 2013).

Jetting occurs when the thread widens, and the instability is progressed along the thread as shown in Fig. 8b (Utada, Fernandez-Nieves et al. 2007, Utada, Fernandez-Nieves et al. 2008). This generally produces less uniform droplets than dripping. Jetting occurs when inertia and capillary forces dominate and breakup occurs downstream from the nozzle at a position that depends on geometry, flow rates, and fluid properties (Cubaud and Mason 2008).

While passive droplet generation is very useful in the lab, it is generally unsuitable for use in POC environments, as this droplet formation process follows a non-linear trend and droplet size changes with flow rate and fluidic properties such as sample viscosity and interfacial tension. Additionally, these systems normally require priming and a ‘ramping up’ period for the system to come up to a steady pressure and flow rate.

1.7.3 Active droplet generation

One of the major drawbacks of passive droplet generation is the slow response seen when changes are to be made to flow rate due to “ramping up” time caused by the “fluidic resistance and capacitance”. Droplet size in passive systems is altered by flow rates and liquid properties and so these must be set in advanced. Various “active” droplet generation approaches have been developed aiming to achieve robust droplet generation and manipulation capable of responding quickly to variations in

flow conditions. These active approaches rely on external energy applied locally to the droplet formation and many rely on changing one or more parameters relating to the capillary number.

The viscosity (μ) can be tuned by local heating by a number of instrumentation strategies including: microheaters and lasers have been used to modulate droplet generation and manipulate droplets (Nguyen, Ting et al. 2007, Stan, Tang et al. 2009, Park, Wu et al. 2011). The flow velocity (U) has been controlled by a variety of microvalves either to change flow speed or to alter local channel dimensions. The interfacial tension (γ) between the fluid and the channel wall may be tuned by thermal or electro-hydrodynamic methods. Active droplet generation techniques can be categorized by the method of control with thermal, electrical and mechanical being common examples.

1.7.3.1 Thermal control droplet generation

A variety of instrumentations have been implemented for the active generation of droplets by thermal control, including microheaters and locally applied lasers. These all work on the same principles of altering the viscosity and interfacial tension, and thereby the capillary number which affects droplet generation.

Figure 9a and Fig. 9b shows an early thermal control instrumentation developed by the Nguyen group, where a coupled microheater and temperature sensor are used to modify droplet size in a flow-focusing device (Nguyen, Ting et al. 2007, Tan, Murshed et al. 2008) with pressure driven fluids. The droplet size increases with temperature as shown in Fig. 9b. The flow induced by thermal gradient also known as the Marangoni effect has also been exploited as a droplet generation tool (Stan, Tang et al. 2009) as shown in Fig. 9c. This same effect has been shown in devices using pulsed focused laser for local heating seen in Fig. 9d (Park, Wu et al. 2011).

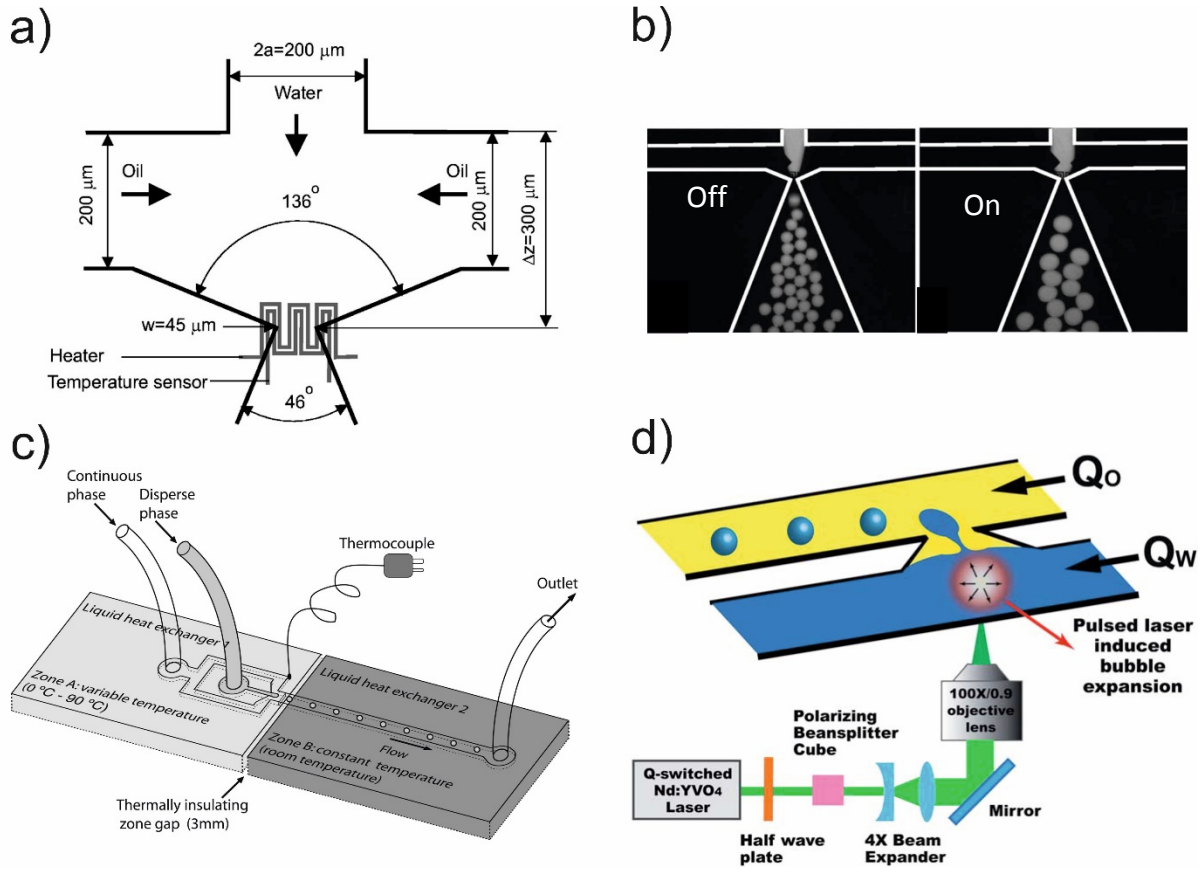

Figure 9 *Active droplet generation methods via thermal control. a) Schematic of a microheater droplet generation tuning device (Nguyen et al., 2007) b) Output of droplet generation tuning device demonstrating increased droplet radius with increased temperature a) (Nguyen et al., 2007). c) Thermal gradient droplet generation device. (Stan et al., 2009) d) Pulsed laser based droplet generation device. (Park et al., 2011).*

While thermal control does offer a certain degree of control for droplet generation, instrumentation size and power consumption are a concern for point-of-care applications as well as, the effect of temperature change on biological samples and reactions.

1.7.3.2 Electrohydrodynamic control droplet generation

Interfacial tensions can also be changed by the presence of free charge at the interface between the droplet and a solid surface. Devices may employ electro-wetting on di-electrics (EWOD) shown in Fig. 10a (Pit, Duits et al. 2015) similar to the most common method of digital microfluidics or electrophoretic effects such as di-electrophoresis Fig. 10b (Jones 2002, Zeng and Korsmeyer 2004, Pit, Duits et al. 2015). Electrowetting refers to the wetting force, which arises from the application of an electric field to a solid electrode in contact with a droplet. The interfacial shear flow produced by electrowetting has been used to generate, move, split and merge droplets (Lee and Kim 2000). However, there are concerns relating to direct contact with electrodes including electrolysis seen at higher voltages. Insulating layers have been used to reduce this risk but with increased power consumption (Moon, Cho et al. 2002). Continuous electrowetting generates a non-uniform interfacial

tension at the two-fluid interface similar to the Marangoni effect. Dielectrophoresis (DEP) based devices make use of non-uniform electric fields to exert electromechanical forces on electrically neutral particles as shown in Fig. 10b. Devices that make use of DEP have been shown to be capable of generating nanolitre droplets (Pit, Duits et al. 2015).

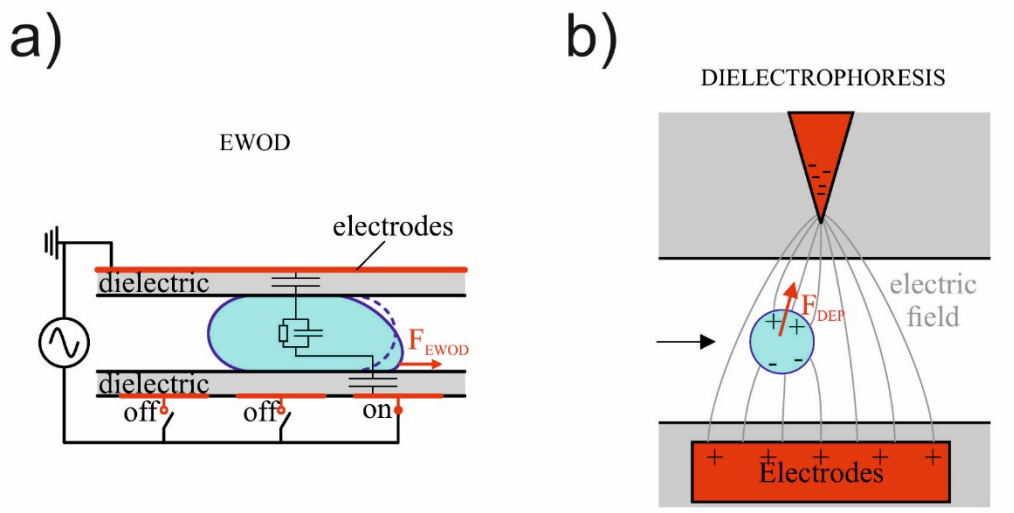

Figure 10 *a) Schematic of the principle of electrowetting on dielectric (EWOD) where electrodes in the direction of desired flow are switched on in sequence causing increased wetting leading to flow (FEWOD) b) Schematic of the principle of dielectrophoresis with non-uniform electric field exerting electromechanical force on electrically neutral particle leading to flow (Pit et al., 2015).*

Electrohydrodynamic control of droplet generation does offer a good degree of robustness and programmability for droplet generation, however with expense of complicated circuitry. Surface contamination could also mitigate the effectiveness of EWOD control.

1.7.3.3 Mechanical control droplet generation

A variety of mechanically controlled droplet generation devices have been demonstrated which use alternative generation regimes to passive methods. Flow characteristics can be by tuned by changing channel geometry by mechanical actuation. Lin et al have shown this by a membrane valve/T-junction, which generates droplets by controlling the flow of the aqueous phase into a continuous oil phase only opening the valve when droplets are to be generated (Lin and Y.C. 2008). A similar device capable of parallel generation of a number of droplets of various composition has also been shown by (Zeng, Li et al. 2009) as shown in Fig. 11a and Fig. 11b. In this case, a negative pressure gradient drives fluid and individually controlled pneumatic valves 'chop' the droplet phase as it enters the main channel. Passive droplet generation regimes may also be altered by changing channel dimensions. One instrumentation by (Lee, Lin et al. 2009) made use of mechanical 'pincer' valves. As shown in Fig. 11c-f the more the valve is occluded the smaller the droplets produced. Similar manipulation of flow has also been established with an adjustable orifice plate (Wang and Lee 2013) which was also used for generation of Steady Drop on Demand (SDOD) by control of the instantaneous flow rate of the

dispersed phase. Leung et al also showed programmable droplet generation with similar principles using a series of embedded microvalves (Leung, Zahn et al. 2012). Piezoelectric valves commonly used in inkjet printers have also been shown to be capable of supplying fixed volumes for on-demand droplet generation (Xu and Attinger 2008). However, control mechanisms and back pressure due to small orifices can be an issue.

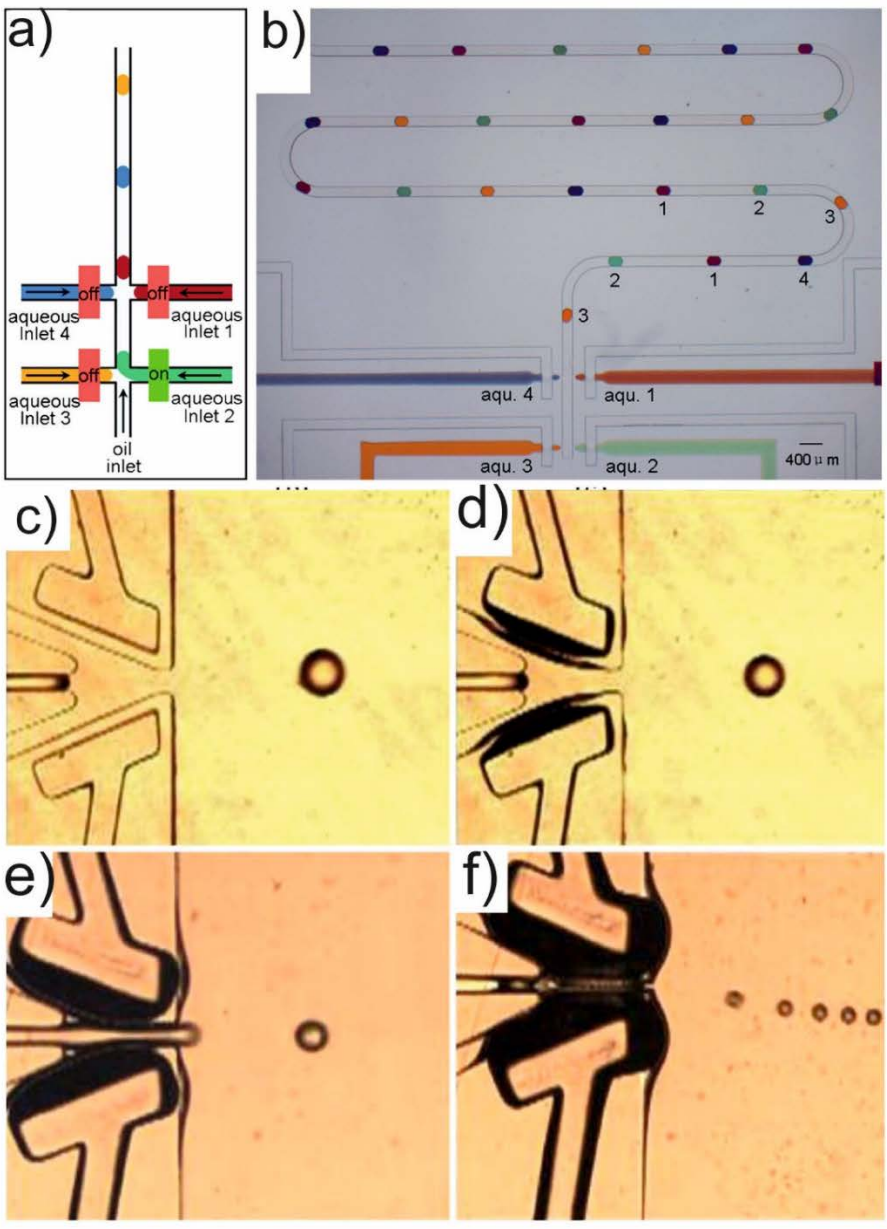

Figure 11 *a) Schematic of microvalve based droplet generation device capable of producing droplet trains based on hydraulically actuated valves at each T-Junction. (Zeng et al., 2009) b) Droplet trains with four coloured ink solutions produced by the device shown in a) (Zeng et al., 2009) c-f) Tunable droplet generation device with moving-wall structures demonstrating the reduction in droplet size as the channel dimensions are reduced by the 'pincer' valve. (Lee et al., 2009a).*

The main limitations of these previously reported mechanical techniques are in control methods and in the size of off chip structures used such as pressure pumps and large structures not suitable for field use.

1.7.3.4 Acoustic control droplet generation

Surface acoustic waves and other acoustofluidic tools have also been implemented as methods of controlling droplet generation by interference of the interface between the two phases. Schmid and Franke reported in 2014 a method for modulation of droplet size using surface acoustic waves (SAW) in a T-junction with a low capillary number, producing droplets by the squeezing regime (Schmid and Franke 2014). They quantitatively explored the effect of actuation of the continuous phase by SAW far away from the T-junction on droplet size, volume, and frequency in a simple system. Fig. 12a shows that the increasing power of the SAW (up to 200mW tested) generates a volume force on the liquid in the propagation direction of the wave forming a pressure gradient and effectively increasing the pressure from the continuous phase at the T-junction, reducing the size of the generated droplets and also increasing the droplet frequency. Collins et al. reported an altered T-junction geometry featuring a SAW device where the waves produced were focused at the orifice shown in Fig. 12b (Collins, Alan et al. 2013). Here they show that droplets are formed by application of SAW to the interface between the oil and water phases. The applied SAW energy deforms the interface resulting in the aqueous phase extending into the oil phase producing droplets after breakoff caused by the syringe pump driven flow on the continuous phase.

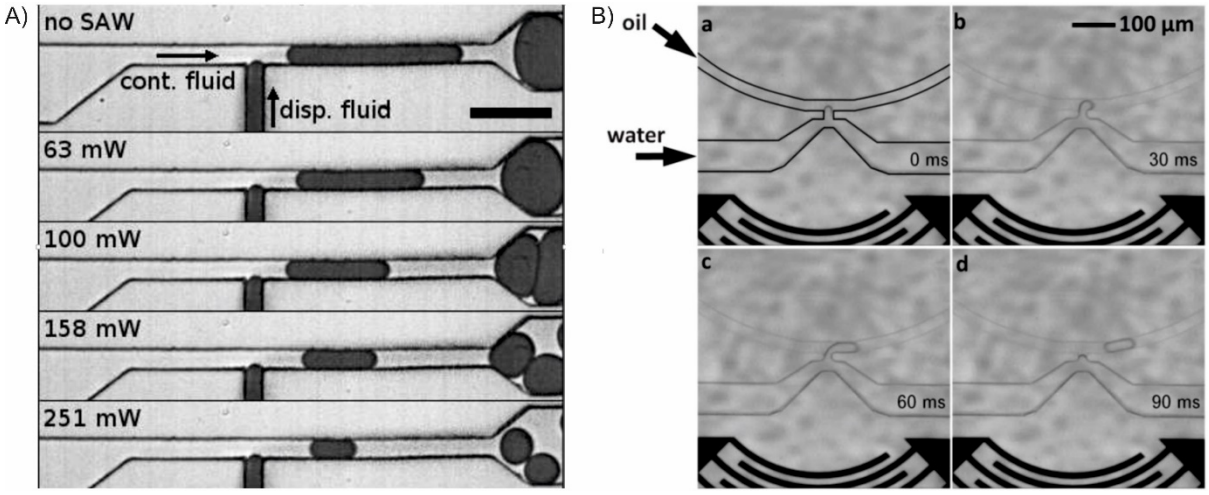

Figure 12 *Acoustic control of droplet generation a) The effect of surface acoustic waves on droplet generation in a microfluidic T-Junction (Schmid and Franke 2014) b) Droplet generation by direct application of surface acoustic waves deforming the interface between water and oil flows (Collins, Alan et al. 2013).*

Acoustic control of droplet generation does offer a programmability for droplet generation, however with expensive instrumentation, as well as considerable power consumption and fabrication requirements, make this method unsuitable for widespread field and point-of-care use.

1.7.3.5 Volumetric control droplet generation

Volumetric control droplet generation relies on the filling and emptying of chambers of defined volume. The volume of droplets generated is defined solely by the dimensions of the chamber. Droplet generation by volumetric control has been demonstrated with robotic samplers coupled with conventional pumps (Gielen, van Vliet et al. 2013), however this instrumentation is too large for point-of-care applications. The Ismagilov group have demonstrated a device called 'slipchip' which makes use of predefined wells in a planar chip, which filled with the droplet phase and then introduced to the carrier by sliding over the channel (Du, Li et al. 2009). A valve based chamber pump developed by Yong et al for volumetric control droplet generation is shown in Fig. 13a & Fig.13b; here the droplet volume is reliant on the chamber volume (Yong, Shin et al. 2013). Chen et al. presented another method of volumetric control of droplet size incorporating pressure driven flow and pneumatic 'choppers' which defined the droplet length (Chen and Lee 2006). After a co-axial flow is established, the choppers compress the channel (as the chopper releases the channel the continuous phase enters) droplet size is defined by spacing between the 'choppers' as shown in Fig. 13c-e. Generation frequency is limited by the speed at which the chopper can be actuated. There is also a possible increase in the variance of droplet size, generated upstream as downstream valves may chop droplets again. (Thakur, Zhang et al. 2015) demonstrated a peristaltic pump-based approach to droplet generation with membrane valves externally actuated. Although this approach required external control and a relatively large instrumentation, not well suited to point-of-care.

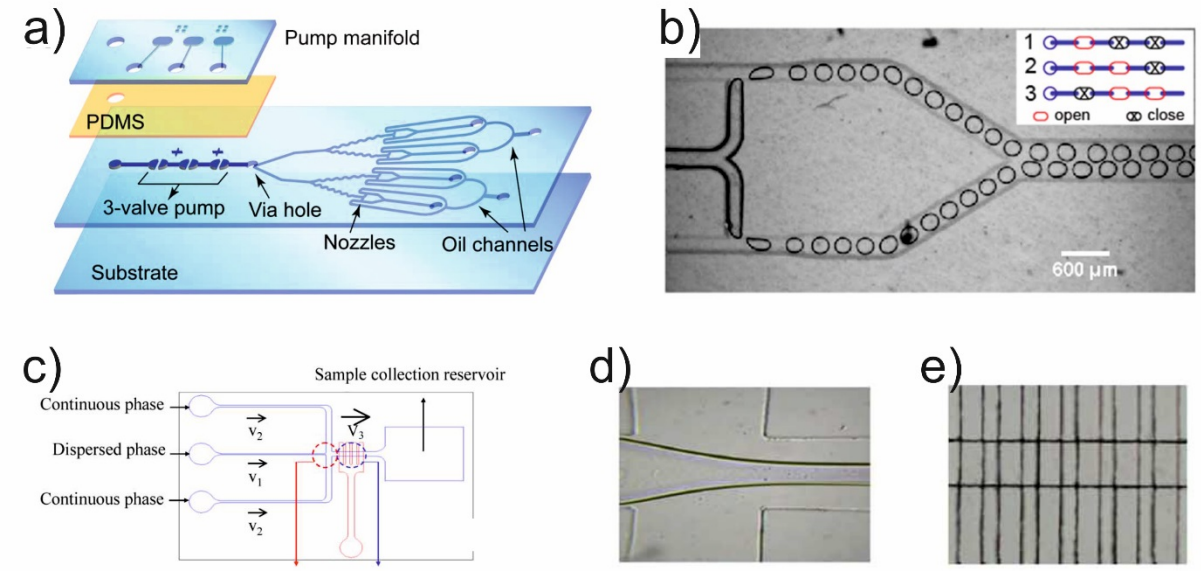

Figure 13 *Droplet generation by volumetric control a) Schematic of PDMS valve based chamber pump (Yong, Shin et al. 2013). b) Operation of chamber pump generating droplet pairs at one of four sets of twin T-Junctions by sequential opening and closing of the three valves causing peristalsis (Yong, Shin et al. 2013) c-e) Schematic and operation of pneumatic 'chopper' droplet generator. As the two phases are pumped into the flow-focusing nozzle, a coaxial 'thread' is formed d). Then chopped by the device as seen in e) (Chen and Lee, 2006).*

Volumetric control methods circumvent the nonlinearity implicit to passive co-flow strategies by avoiding the dynamic competition between viscous and capillary forces. When compared to other active strategies for droplet generation, these methods produce higher compressive/shear forces,

which may cause issue with some particularly sensitive applications. However, they are made desirable due to the simplicity of their operation, linearity and promise of low power systems based on actuation of mechanical structures that makes them suitable for point-of-care devices. Many of the volumetric control devices previously described suffer issues of scaling and functionality.

In the following chapters, another volumetric control method of pulsed droplet generation is described in detail that addresses these issues. Peristaltic pumping was used offering low power and pulsatile nature which is not usually thought of as good in droplet generation, but the novel method described in the following chapters developed uses this to its advantage (Nightingale, Evans et al. 2017). This method is well suited to continuous monitoring, as it is small, low power and due to its push-pull nature requires no separate sample loading.

1.8 Droplet manipulation

Droplet manipulation encompasses several tools or operational units for splitting, merging, mixing and dilution. Droplet manipulation takes advantage of the same properties of multiphase flows as droplet generation and may be both active and passive in nature.

1.8.1 Droplet splitting

Droplet splitting/fission is one of the many vital tools/operations in the development of droplet microfluidics as a tool for assays. Droplet splitting increases the system's ability to multiplex and replicate measurements. In addition, by making smaller and smaller droplets, a system may increase analytical throughput. This is crucially important for droplet based polymerase chain reaction (PCR) or single cell studies where millions or more similar droplets are required (Furuberg, Mielnik et al. 2008). Many methods of splitting droplets have been described. Earlier papers described how splitting may be accomplished by a simple bifurcation geometry as shown in Fig. 14, where splitting will occur so long as this droplet is 'plug like' with a length larger than the diameter of the microchannel (Link, Anna et al. 2004).

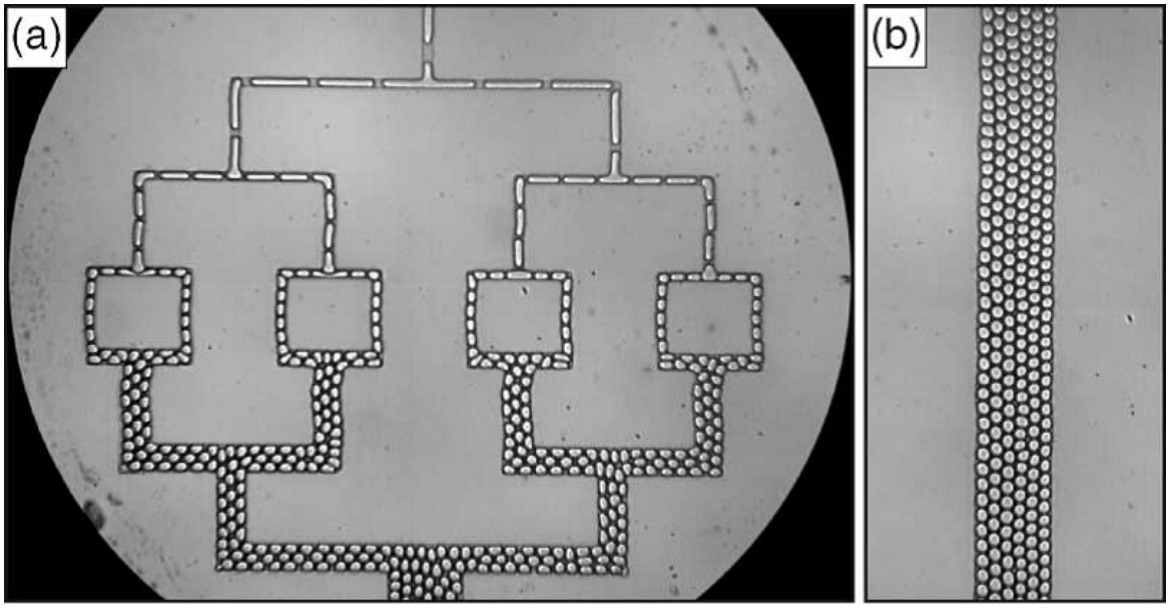

Figure 14 *Passive droplet splitting by T-Junction geometries a) Sequential passive droplet breakup. (b) Resultant droplet flow downstream of a). (Link et al., 2004)*

Link et al demonstrated that droplets split evenly with even fluidic resistance in the bifurcated channels. Splitting can then also be tuned by altering channel geometry particularly length which is proportional to fluidic resistance as can be described by the Hagen–Poiseuille equation (equation 11) (Link et al., 2004).

Hagen–Poiseuille equation for circular channel

$$\Delta P = \frac{8\mu L Q}{\pi r^4} \quad (11)$$

The Hagen–Poiseuille equation shows the effect of microchannel length (L), radius (r), viscosity (μ) and volumetric flow rate (Q) of the fluid on pressure loss (ΔP) in each channel (assuming laminar flow regime of an incompressible Newtonian fluid). Building on this technology Adamson et al split a parent droplet into as many as 16 daughter droplets of nanolitre volume (Adamson, Mustafi et al. 2006). Another design proposed by (Link, Anna et al. 2004) induced droplet fission by a large pillar in the centre of the microchannel, with daughter droplet size ratio tuned by the position of this post. While passive methods can split droplets reliably, with the ratio of splitting set by geometry, they generally lack flexibility. Hence, several active methods employing electric fields, heat and lasers to split droplets in a controlled and programmable fashion have been investigated. However, this functionality comes at the cost of increased complexity of manufacturing, the same bifurcating channel as previously described, with an added electric field has been used to induce droplet splitting by charge with increased throughput; although the use of electrical fields may limit the possible sample this system can be used with(Link, Grasland-Mongrain et al. 2006). Local heating is another method of tuning the droplet splitting from focused laser (Baroud, Delville et al. 2007) or micro heater (Nguyen, Ting et al. 2007) to modulate breakup. Here, by default droplets split symmetrically but local heating decreases surface tension for one channel and so produces a programmable asymmetrical split. This can also be used to force the whole droplet into a single channel with increased laser power (Baroud, Robert de

Saint Vincent et al. 2007). EWOD has also been used to split droplets (Cho, Moon et al. 2003, Fan, Hsieh et al. 2009) applying electrical potentials at specific points. Another similar heating grid method has also been shown which is similar to EWOD configuration while relying on thermocapillary actuation (Darhuber, Valentino et al. 2010) rather than electrowetting.

1.8.2 Droplet merging

As with the splitting of droplets, merging droplets is a critical tool in the creation of certain assays allowing the combination of reagents at specific time points in a controlled fashion or the conversion of droplets into a continuous stream as may be required for analysis (Fidalgo, Whyte et al. 2008). For coalescence to occur the continuous phase between the droplets must be drained to bring them into close contact and this contact must be held for a critical minimum amount of time. Merging occurs when the surface tension at the interface between the water and oil phases fluctuates and destabilises the interface. A set of equations for predicting coalescence have been provided by (Bibette, Calderon et al. 1999). Droplets that have not been stabilised by a surfactant readily coalesce and this has been used by some groups to facilitate one to one merging regimes (Mazutis, Baret et al. 2009). However, adding surfactants to the system, as is common practice in droplet microfluidics to increase interfacial tension will decrease the likelihood of coalescence, affecting the throughput and efficiency of these devices, key to the systems performance. Contamination (or unwanted material transfer) and preservation of the viability of biological materials are also concerns in many forms of droplet merging.

A number of approaches both passive and active have been taken to cause merging of droplets with high throughput and efficiency; the simplest passive method is a widening of the channel (Tan, Fisher et al. 2004, Hung, Choi et al. 2006, Liu, Ding et al. 2007). Building on the concept of droplet trapping (Niu, Gulati et al. 2008) developed a geometry which included a set of two tapering pillars in the centre shown in Fig. 15.

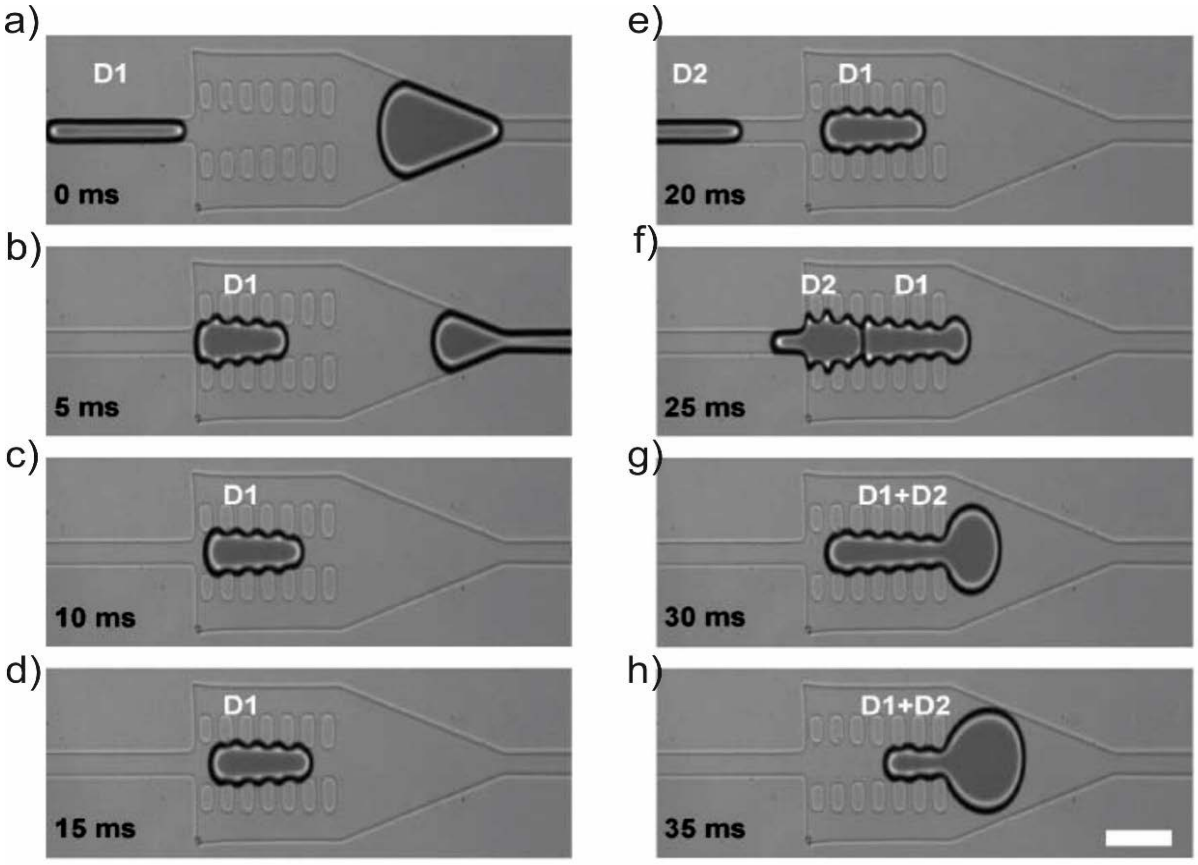

Figure 15 *Sequence of images demonstrating passive merging of two adjacent droplets (D1&D2) in tapered pillar containing chamber. a)-d) D1 enters chamber and is trapped by pillars while the continuous phase passes through. e)-g) D2 enters the chamber. The continuous phase is drained as it passes around the pillars and the 2 droplets are merged h) The merged droplet exits the chamber pushed forward by the continuous phase now blocked from the entrance to the chamber (Niu et al., 2008).*

As a droplet enters the expansion, the pillars slow down the droplet and the continuous phase drains around them. With this design, a droplet can be held indefinitely until a second droplet merges with it, and by tuning the design multiple droplets can be fused. This system is particularly robust, able to function with non-uniform inter droplet spacing and droplet velocities. Another method which has been used to merge droplets uses a membrane valve to trap droplets (when closed) instead of interfacial tension (Lin and Su 2008). Systems for merging have also been designed which exploit the decrease in droplet speed with increasing size or viscosity (Jin, Kim et al. 2010). Droplet merging has also been accomplished with a hydrophilic patch in the microchannel slowing droplet movement. The number of droplets to be merged can be tuned by the flow rate, which affects the viscous drag force on the trapped droplets (Fidalgo, Abell et al. 2007). This approach may be applied to any geometry, although there is an unavoidable contamination risk between droplets. Several active methods have also been demonstrated for droplet merging generally these methods generally offer a higher throughput and are based upon the same principles as active droplet generation. However, these methods are more complex in their fabrication and operation than passive methods and again biological compatibility is a concern. Programmable merging has been demonstrated by local heating,

driven by an Argon ion laser, destabilising the liquid interface by disturbing surface tension (Baroud, Robert de Saint Vincent et al. 2007). This approach allows for trapping of multiple droplets to be merged and the risk of contamination is minimal as the droplets may remain at a safe distance from the channel walls. However, due to the laser control it is only capable of relatively low throughput. Electrohydrodynamic based merging has also been demonstrated (Wang, Yang et al. 2009). Designs include the use of platinum wires generating an electrophoretic force positioned inside a microchannel where two perpendicular droplet streams meet, merging droplets at the tip of the wire. This principle has been coupled with optical tweezers to align and merge several droplets (Tan and Takeuchi 2006). Electrical methods offer very fast fusion rates, with fusion rates as high as 100 fusions per second being demonstrated (Zagnoni and Cooper 2009) although the high voltage can cause degradation of some samples. With much lower energy the incompatibility with biological samples becomes less of a risk although fusion rates also decrease (Priest, Herminghaus et al. 2006). As a technique for the coalescence of droplets electro wetting offers fine control over droplet movement but contamination is a concern due to contact with the electrode (Schwartz, Vykoukal et al. 2004).

1.8.3 Droplet injection

Another approach to adding reagents in droplets separate from droplet fusion, is the injection of reagents into an already formed droplet (Li, Boedicker et al. 2007) via a series of smaller perpendicular channels. This approach accomplishes the same as droplet fusion without the requirement to generate as many droplet populations. Here contamination is a major concern and so systems have been designed with several small hydrophilic injection channels such as those shown in Fig. 16 (Li, Boedicker et al. 2007); these minimize diffusion and hence reduce contamination. This design reduces the complexity of temporal synchronicity as droplets pass many channels, although offers less control over the specific amount of reagent added to the droplet than the merging of droplets. It is also possible to inject reagents into droplets by electric field. Similar to the passive method a series of perpendicular microchannels inject reagent while an electric field destabilise the droplet interface. Using this method researchers have also demonstrated selective addition of reagents at a rate of 10000 droplets per second(Abate, Hung et al. 2010).

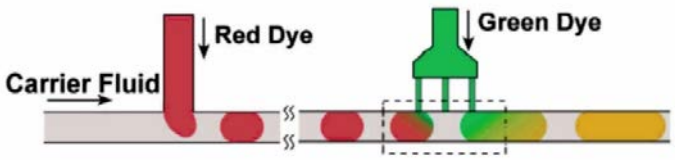

Figure 16 *Schematic of platform for injection of reagents into preformed droplets using multiple pico-injectors with no cross contamination (Li, Boedicker et al. 2007)*

1.8.4 Droplet sorting

Droplet sorting is obviously very important for a number of applications. The simplest sorting method is passive side sorting by simple bifurcating channels of differing sizes (Tan, Fisher et al. 2004, Tan and Lee 2005), which is useful for the removal of smaller undesirable satellite droplets (although made

obsolete by a robust droplet generation system). Hydrodynamic sorting has been shown to be capable of sorting droplets with cells from those without, as the presence of the cell changes the surface tension between the droplet and the carrier fluid. This has many applications including the separation of cells for study from whole blood (Huh, Bahng et al. 2007, Chabert and Viovy 2008). Just as dielectrophoresis can be used to split droplets, it is possible to sort droplets by the application of an electric field (Ahn, Kerbage et al. 2006). This method allows for a high degree of programmability and selectivity and devices have been demonstrated that can sort droplets based on markers in droplets and cells contained within droplets (Baret, Miller et al. 2009). Similar devices based on thermocapillary action have also been described (Baroud, Delville et al. 2007, Nguyen, Ting et al. 2007).

1.8.5 Droplet dilution

Dilution is an important tool for applications such as studying enzyme kinetics, and has been shown in droplets. While simply generating droplets with a range of reactant concentrations is possible, specialist tools have been made for the generation of dilution series. One example shown in Fig. 17 operates by the merging, mixing and splitting of droplets passively using hydrodynamic forces (Niu, Gielen et al. 2011). A nanolitre-sized sample droplet of defined concentration is trapped within a microfluidic chamber and diluted by a series of smaller buffer droplets generating a sequence of droplets. This defines a digital concentration gradient as each of the small droplets injected dilutes the larger droplet. Another method of creating droplet dilution series is described in chapter 2 and 3.

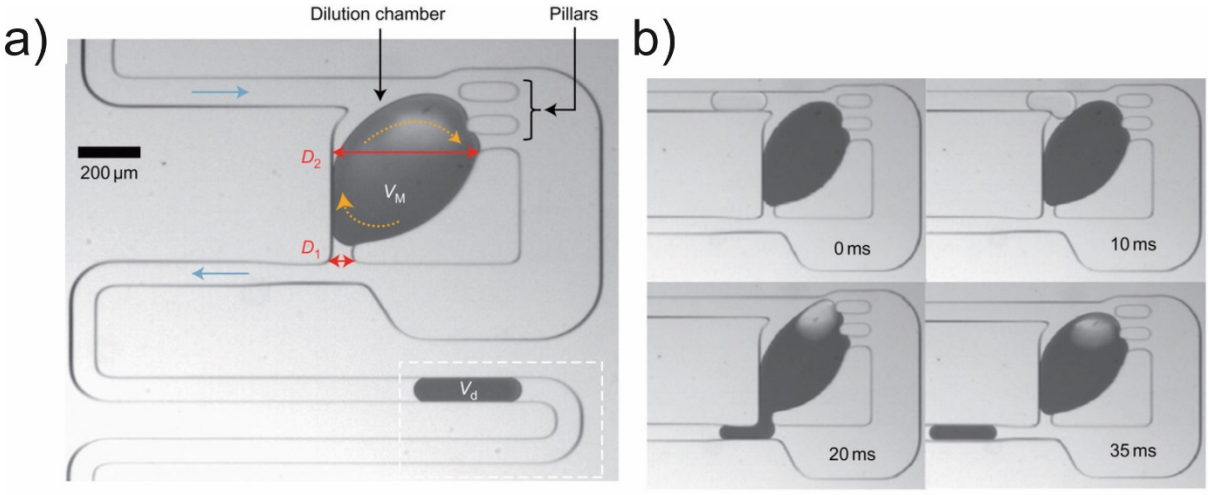

Figure 17 *a) Design of droplet dilution series generating device with large mother droplet of size defined by D_2 of stock solution of high concentration trapped in chamber by pillar structures that allow the continuous phase to pass around them. b) Operation of a) generating a dilution series by sequential addition of dilutant droplets to the mother droplet. As dilutant droplets merge with the mother droplet, daughter droplets of size defined by D_1 exit the chamber with progressively lower concentration of the stock solution (Niu et al., 2011)*

1.9 Assays in microfluidics

As previously stated, chemical/biological assays are one of the main applications for microfluidics. Assays performed in droplet microfluidics are generally very similar to those performed in bulk lab procedure. Droplet microfluidics offers many advantages as detailed in section 1.5 especially compartmentalisation of assays into many individual and separate chemical reactors, suitable for multiplexed and repeated analysis with products of reactions also confined in droplets. This effectively increases the concentration of rare molecules, thereby increasing detection sensitivity. The fast and predictable chaotic mixing and the high surface to volume ratio (which results in fast heat exchange) exhibited by droplet microfluidics also decreases time taken to reach detection thresholds. When compared with more traditional methods of compartmentalisation, such as well plates, droplet microfluidics can provide high throughput for assays capable of processing ~10^8 samples per day (Guo, Rotem et al. 2012). The use of an oil carrier phase prevents undesirable interactions between the assay and the solid surface of the channel wall and allows assays to be substituted without tedious washing to prevent cross contamination. However, the high surface-to-volume ratio means that the oil/water interface must be stable and inert to avoid contamination of the assay. Other possible complexities with droplet microfluidics include the difficulty of creating heterogeneous assays with multiple washing steps, although some solutions have been devised (Ferraro, Champ et al. 2016), further discussed in section 1.9.7 and chapter 7.

1.9.1 Controlling reactions in droplets

Reactions in microfluidics and in particular droplet microfluidics are generally much quicker than that of bulk materials. One of the main advantages of assays in droplets over bulk assays is their fast and predicable reaction kinetics due to chaotic mixing, low volumes and fast heat transfer. This means reaction times, can be predicted and controlled and reaction kinetics can be directly observed (Song and Ismagilov 2003). Increased flow rates cause increased mixing as the double recirculating flow (caused by the oil moving over the interface) within droplets is affected by shear forces (Song, Tice et al. 2003). Structures may also be added to the microchannel to aid in mixing. Surface striations on the channel walls increase mixing by enhancing the asymmetry of shear forces (Liau, Karnik et al. 2005). Winding serpentine channels accelerate mixing by stretching and folding the droplet contents. This perturbs the double vortices which facilitate advection in the droplet and shortens the distance over which diffusion must take place as shown in Fig. 18 (Wang, Wang et al. 2015).

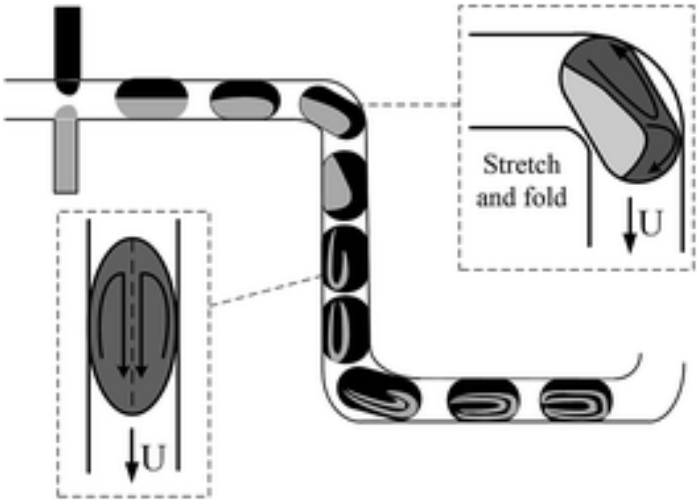

Figure 18 *Mixing in droplets showing stretching and folding as droplet turns corners in a channel (U = flow rate) (Wang, Wang et al. 2015)*

Mixing has also been shown to be increased by active methods such as pulsing lasers, which locally heat the fluid increasing flow towards the heat source. However, this has limited application due to possible interference with the sample and low throughput (María Luisa, Hans Olav et al. 2009).

Additionally, some reactions require heating and possibly longer mixing times (taking minutes not seconds). Droplet PCR, one of the key applications of droplet microfluidics in the literature makes use of the fast heat transfer in droplets and simple heating elements with the fluidics laid over them and heat cycling controlled by the flow rate of the liquid (Boybay, Jiao et al. 2013, Hayes and Dalton 2015). Many other methods have also been explored for heating in microfluidics and droplets including many different metal heating element structures, lasers and beads which are excited with electromagnetism (Song, Chen et al. 2006).

1.9.2 Quantifying assays in droplets

While qualitative assays may rely on a simple colour change or other indication as to whether the target is present or not, quantitative and functional assays however, require transduction to relate the reaction output to a quantity of analyte and relay this information. The first immunoassay from (Yalow and Berson 1960) made use of a radioisotope marker and detector and some assays still use this method today although these are unsuitable for widespread POC use. Electrochemical immunosensors are commonly used for field applications. These use transduction by electron exchange during the binding process of the analyte to an antibody immobilised on an electrode. Electrochemical sensors have been combined with microfluidics (Wang 2002). However they typically suffer from fouling and signal drift over long term use (Bertocci, Huet et al. 2002). Additionally, combining droplet microfluidics with electrochemical sensors can be difficult due to hydrodynamic issues with droplet breakage as well as surface contamination.

Droplet based assay systems also require some method to quantify the contents of the droplet. In the lab many techniques require the use of bulky equipment such as microscopes and powerful fast

cameras (Zhu and Fang 2013). However, some analytical techniques have been adapted for use in droplet systems including optical and electrochemical methods. Miniaturised optical immunosensors are particularly suitable to be integrated with droplet microfluidics for field applications. Not contacting the droplet directly. They reduce opportunity for fouling even over long-term usage and can be implemented simply at low power.

Colorimetry is one of the most popular optical methods for quantitative assays and for *in-situ* analysis (Grasshoff and Johannsen 1974, Han, Li et al. 2013) due to its low cost and ease of use. An analyte-specific reagent reacts with the target analyte to give a coloured product, allowing us to quantify analytes via absorption spectroscopy in a spectrophotometer. A beam of light of intensity I_0 is focused through the sample and after a portion of light is absorbed by the assay, the intensity I can then be measured and used to calculate absorbance by equation 12. The concentration of the analyte is then quantified by the Beer Lambert law. Which states that absorbance (A) is directly proportional to the molar absorption coefficient ε and concentration of analyte (c) with constant solution pathlength (l) and wavelength of measurement light used.

Beer Lambert Law

$$A = \log_{10}\frac{I_0}{I} = \varepsilon l c \tag{12}$$

Colourimetry has also been shown to be suitable for accurate quantitative analysis in microfluidics with many assays for many important analytes (Ellerbee, Phillips et al. 2009, Sieben, Floquet et al. 2010, Rushworth, Jones et al. 2015). Microfluidic colorimetry has been applied in *in-situ* analysers utilising small, cheap and easily sourced components. Offering robust analytical performance and limits of detection typically in the order of 10 nM (Chin, Johnson et al. 1992, Beaton, Sieben et al. 2011, Meyer, Prien et al. 2012)

There are of course a variety of other methods for probing the contents of droplets such as fluorescence assays, which can also be measured by spectrophotometry. These may be preferable for some analytes due to their non-destructive nature and extremely high sensitivity however, they are generally more expensive and require better storage (separated from light etc.) than the colourimetric markers. Chemiluminescence (CL) markers have also been used in immunoassays replacing colorimetric markers (Shi, Xu et al. 2009). In these assays target concentration is indicated by the intensity of light emitted produced by the reaction. These have been shown to exhibit high sensitivity and a wide linear range while offering simple operation and the possibility of automation.

While microscopes and a variety of analysers can be used in the lab, field systems require smaller and low power methods to "probe" the droplet contents such as miniaturised spectrophotometers (Hassan, Nightingale et al. 2016) . Also the time taken for colorimetric assays to develop the full colour (up to an hour in some cases) creates challenges for clinical and field applications and means end-point quantification may be unsuitable (Mamoru and Kazuyuki 1977). Methods have been developed to determine concentration of the analyte in colorimetric droplet assays quickly such as the Michaelis-Menten method where the initial rate of colour development is used to determine analyte concentration. (Srinivasan, Pamula et al. 2004) demonstrated this method on a planar droplet microfluidic chip. Similar systems have also been developed using an optical microscope to follow

colour development of assays in droplets over time, study the effect of enzyme concentrations, generate Michaelis-Menten kinetics, and quantify the effect of an inhibitor on enzyme activity (Fradet, Bayer et al. 2015). It has also been shown by (Gielen, van Vliet et al. 2013) that it is possible to monitor enzymatic reactions by oscillating the assay-droplets back-and-forth through an absorption flow cell consisting of LED and photodiode with a path length of 200 µm. These methods are able to follow the colour development in detail and obtain accurate reaction rates, however, the throughput is still low when compared to the potential high throughput analysis that droplet-based microfluidics can offer (thousands of droplets can be produced per second in a single T-junction (Gu, Duits et al. 2011)).

Recently the Niu group demonstrated a method of measuring the kinetic response of an immunoreaction in a droplet-based system by multi point colorimetric detection with greatly improved analytical throughput (Hassan, Nightingale et al. 2016). The system shown in Fig. 19 consists of multiple sets of LEDs and photodiodes arranged in a flow cell measuring light intensity through PTFE tubing. Hassan et al. demonstrated in this system their developed method which relies on the flow rate of droplets through the flow cells to determine the time points used as the input for a calibration based on the Michealis-Menten equation and tested the method using glucose assay.

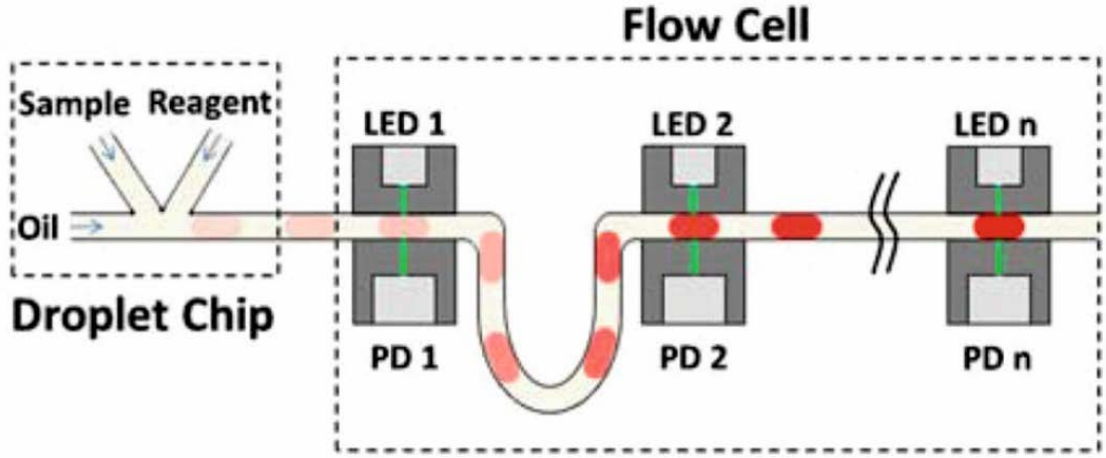

Figure 19 *Schematic of multipoint colorimetric droplet detector adapted from (Hassan et al., 2016) used throughout thesis*

1.9.3 Droplet microfluidics for compound screening

For many applications such as drug discovery, screening of pathogens and genetic elements, it is common practice to use microtitre plates to screen libraries of thousands of variants, which can be very time consuming. The use of droplet microfluidics for these compound screens allows for increased multiplexing and increases the relative concentration of cellular, genetic elements or low concentration compounds of interest allowing for increased throughput and sensitivity (Guo, Rotem et al. 2012). Droplet microfluidics can aid in detection of pathogen species which would infect at high concentrations but take a long time to detect in low concentrations (Maaroufi, Heymans et al. 2003) with an increase relative concentration in droplets. When bulk samples contain a mix of genetic elements, sufficient dilution before encapsulation in droplets allows each droplet to contain only one

element with the unique genetic sequence offering a 'barcoding'. These droplet based genetic screens have many applications in diagnostics allowing the fast identification of pathogens, and biological research including: directed evolution (Petrounia and Arnold 2000) and the study of combinations of different forms of genes (haplotyping) (Fan, Wang et al. 2011). For droplet libraries barcoding with fluorophores or other markers may be used to mark droplets, these may be read in real-time but distinguishable fluorophore combinations are limited by the optical setup in use (Han, Gao et al. 2001).

1.9.4 Single cell assays

Cell growth assays are frequently performed for biological and pharmacological screening, as cell growth is a useful indicator of the effect of conditions on target cells. Cell density is often used to quantify cell growth limited by the density detection threshold (the lowest volume in which cells can be detected). An advantage of carrying out these assays in droplets is the large reduction in the volume of media in which cells are grown. This increases the density of the cell population with a single cell in a 10 μm diameter droplet equivalent to a billion cells in a 1 mL making it possible to detect a single cell in a small droplet (Brehm-Stecher and Johnson 2004, Koster, Angile et al. 2008). This decreases the minimum number of cells the system can detect.

Single cell assays may be applied to diagnostics where a sample suspected of containing a pathogen must be cultured until the population density is large enough for detection (Maaroufi, Heymans et al. 2003). Monitoring single-cell growth in droplets can also allow for the detection of unusual growth rates (Balaban, Merrin et al. 2004, Lecault, VanInsberghe et al. 2011). As the cell population is separated so no cell type may dominate the population this could improve understanding of emerging antibiotic resistance and viral epidemics. The changes from a flask environment to a droplet environment do however need to be accounted for (Clausell-Tormos, Lieber et al. 2008, Koster, Angile et al. 2008) with carrier phases etc. chosen carefully. Beads may also be included in droplets as solid substrates for cell growth. Single cell droplet assays are useful for a number of biological assay applications including screening for bacterial persistence (Balaban, Merrin et al. 2004). Virus plaque assays where infections of single cells can be detected even at rates which would not be detected by traditional plaque assays (Guo, Rotem et al. 2012). Condition screening may be used to generate a library of antibodies used in a wide range of diagnostics and therapeutics by designed molecular domains of antibody-secreting B rather than the traditional means using mice (Yokoyama, Christensen et al. 2001, Carter 2006). Droplet microfluidics may also be used for the development of enzyme and protein variants by directed evolution (Kaur and Sharma 2006) screening for desired properties such as: increased specificity, catalytic efficiency or solubility.

1.9.5 Droplet PCR

Polymerase chain reaction (PCR) is used for wide-ranging applications particularly medical diagnostics. PCR produces many copies of a DNA template making it easier to detect small quantities of molecules or cells and increase signal-to-noise ratio by decreasing the relative quantity of inhibitors (Baker 2010, Schroeder, Gonzalez-Perez et al. 2013). Careful and specialized sample preparation is necessary to

eliminate extraneous DNA and minimize noise (Rueckert and Morgan 2007, Woyke, Sczyrba et al. 2011). In droplet PCR after compartmentalization, DNA of interest can by amplified for detection (Dressman, Yan et al. 2003, Zeng, Novak et al. 2010). This helps with detection of small quantities of abnormal DNA in body samples such as bacterial DNA and the DNA of tumour cells (Pantel, Brakenhoff et al. 2008) with competition and biases eliminated as each cell's DNA is confined within its own droplet. Droplet based single cell PCR may also be applied to metagenomics studies (Ottesen, Hong et al. 2006, Tadmor, Ottesen et al. 2011). Analysing sequences of DNA from mixed microbial populations and their effect on the whole population (Sleator, Shortall et al. 2008) has application in medicine, such as analysing samples from the human gut (Gill, Pop et al. 2006, Turnbaugh and Gordon 2008, Sommer, Dantas et al. 2009) as well as environmental applications from soil, sewage and wastewater. The use of droplets for encapsulation of single cells makes it possible to study cells individually while traditional methods only allow the study of the population as a whole. Droplet PCR also simplifies the overall computational challenge of these studies (Miller, Koren et al. 2010). Encapsulation of single cells means that PCR can be performed on the entire genome of a single cell (even parts of the genome relatively distant from each other) as all DNA in the droplet originates from the cell. After encapsulation of a single biological entity, cell or virus has been performed, targeted PCR of this entity within a droplet can be used to amplify a desired gene. After sorting for droplets containing the PCR products, these droplets may be subjected to whole genome sequencing using conventional bulk methods. This would be impossible for rare genetic variants without the use of droplets.

1.9.6 Immunoassays and microfluidics

Currently immunoassays such as ELISA first demonstrated by (Engvall and Perlmann 1971) are considered the gold standard for many biochemical tests across a wide array of applications (Lequin 2005). All immunoassays take advantage of the highly selective nature of immune interactions and couple this with some marker to indicate the presence of the desired analyte.

Since the 1980s there have been developed many automated analyser units based on immunoassays. However, these are not without their disadvantages including: analysis time up to several hours (Ng, Choi et al. 2012) using a large quantity of sample and reagents, resulting in high running costs. In addition, the liquid handling systems in the analysers are bulky, usually due to their expensive robotic instrument setup. Microfluidics and droplet microfluidics can dramatically decrease analysis time, quantity of samples and reagent required and size of the overall system.

The most common assays carried out in microfluidics and droplet microfluidics are single step homogenous assays. An antibody/marker and sample analyte are freely distributed in solution to form complexes (taking advantage of the chaotic mixing in droplets). Once mixed, sample concentration can be quantified by changes in the marker (Song and Ismagilov 2003, Song, Tice et al. 2003, Song, Chen et al. 2006).

1.9.7 Multiple step immunoassays in microfluidics

Many of the more accurate assays available require multiple reaction steps, this can be accomplished by merging droplets, dosing droplets (Song, Chen et al. 2006) or by heterogeneous methods. Typically, in heterogeneous assays selective antibodies are immobilised on a solid substrate, and liquid components of the assay are 'washed' over them. This is commonly carried out in the lab using microwell plates and other systems, but has not seen widespread uptake in droplet microfluidics. Some microfluidic lateral flow heterogeneous immunoassays do exist, mostly for qualitative detection of biomarkers such as those used for home pregnancy detection (Bock 2000).

One of the most promising methods of performing heterogeneous assays in microfluidics utilises magnetic beads as a solid substrate to pass through washes contained in droplets. The movement of magnetic particles in microfluidic systems has been shown to be predictable and controllable (Gijs 2004, Pamme 2006). Peyman et al have demonstrated a device shown in Fig. 20 capable of performing heterogeneous, multiple step immunoassays by passing magnetic beads through parallel laminar streams. Here a single magnet causes movement of beads between streams timed such that the washes and each step of the reaction take place at the desired rate, as controlled by the fluid flow (Peyman, Iles et al. 2008, Peyman, Iles et al. 2009). As proof of principle, a streptavidin/biotin binding assay was used. Streptavidin coated magnetic particles move through a reaction chamber, across parallel streams of reagents and buffers, performing all reaction steps in one motion, over a period of less than a minute. Similar devices have been used for the detection of C-reactive protein with a significant improvement to the time taken when compared to the lab process (Phurimsak, Tarn et al. 2014). This device has also been used for applications in cell biology such as creating so called "cyborg cells" (Tarn, Fakhrullin et al. 2013).

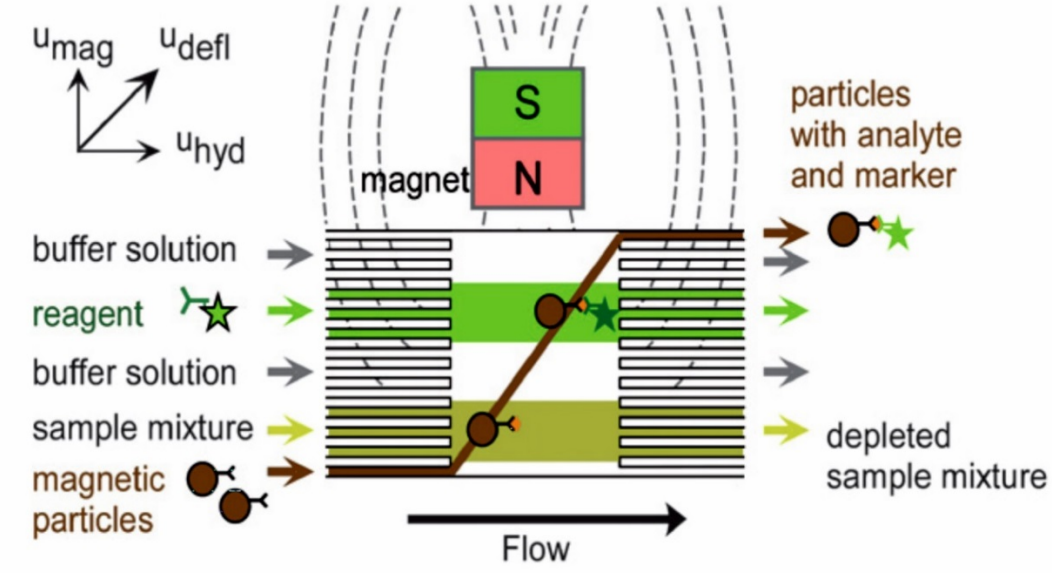

Figure 20 *Microfluidic continuous flow reactor where heterogeneous assays are carried out on magnetic particles as they move through several different laminar reagent streams (Peyman, Iles et al. 2009).*

1.9.8 Multiple step immunoassays in droplets

Similar methods to those used in continuous flow have been shown in droplet microfluidics by (Gu, Zhang et al. 2011) to produce a droplet based washing module for magnetic particle-based assays. Here, droplets were generated on demand from a series of reagents and buffers, then pumped through a chamber over an external permanent magnet. The magnetic particles were trapped by the magnet and effectively dragged between each of the droplets containing the assay components. This was demonstrated by a DNA purification assay performed at single cell level. An alternative and more complex geometry with a ladder like channel network was later demonstrated by (Lee, Xu et al. 2014) performing a streptavidin/biotin assay. Ferraro et al. have demonstrated a system which utilised electromagnets to manipulate magnetic beads (Ferraro, Lin et al. 2015) moving them between droplets in flow. The electromagnetic "tweezer" approach they use (shown in Fig. 21) offers greater versatility than permanent magnets and shows great promise for carrying out a variety of heterogeneous assays in droplets. To demonstrate the capabilities of their system, Ferraro et al demonstrated RNA purification, reverse transcription and amplification in droplets clinically validating the method by determination of their HER2 expression in a group of breast cancer samples (Ferraro, Champ et al. 2016). However, this system and others like it while demonstrating excellent functionality as lab instruments, are not suited for POC use due to their size (benchtop) and complicated controls of syringe pumps, valves etc.. In chapter 6, I detail the development of a similar approach to carry out heterogeneous assays in droplets using a small-automated electromagnetic trap and novel fluidics.

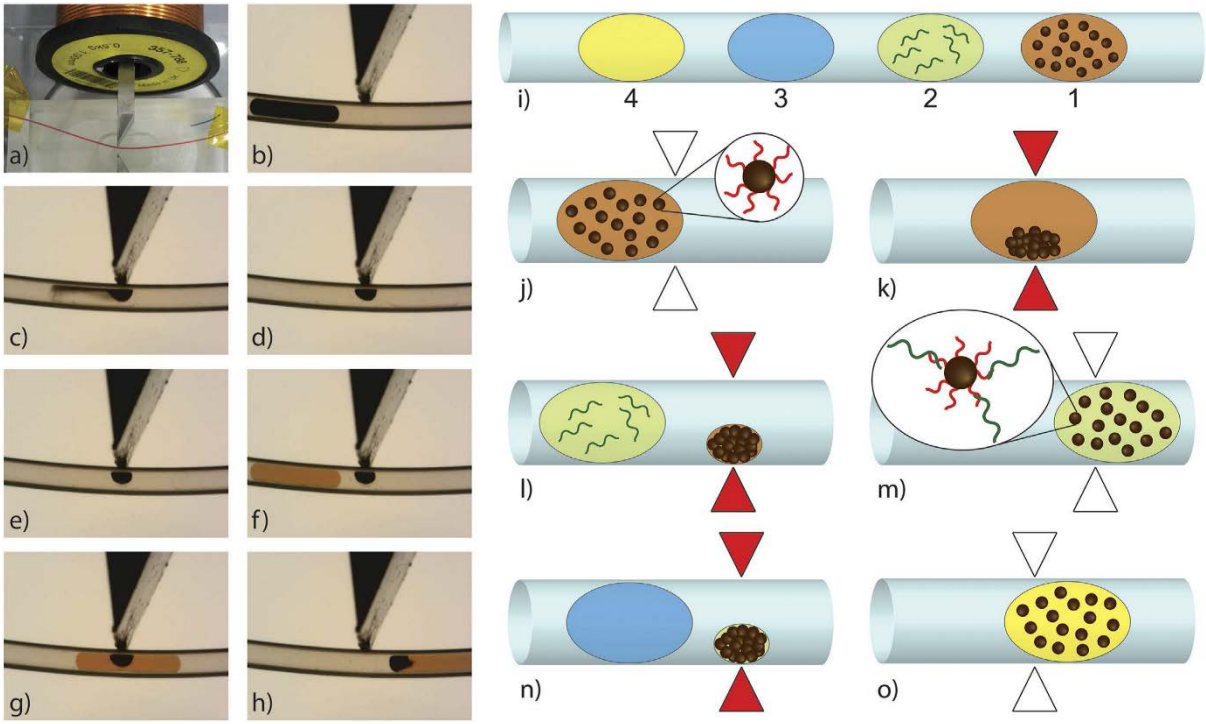

Figure 21 *Magnetic tweezer technology and experimental workflow a) Image of magnetic tweezers with capillary (highlighted by red liquid) b)–h) Sequence of images showing extraction and redispersion of magnetic beads in droplets. b-c) droplet containing magnetic beads passes the magnetic tweezers where the beads are captured. d-e) passing through the continuous phase. f-g) Until they pass into the next droplet h) and the magnetic field removed to allow the beads to remain inside the droplet. i) Scheme of a typical droplet train for the RT-qPCR analysis: 1) oligo-dT magnetic beads, 2) total RNA sample, 3)*

washing buffer and 4) RT-PCR mix. j)–o) Workflow of passing beads through during heterogeneous assay triangles represent the magnetic tweezers (red=on) (Ferraro et al., 2016).

1.10 Microfluidic to world interface

Sample collection and preparation are crucial for any continuous monitoring system including point-of-care monitoring and environmental monitoring. The complexity of sample collection and preparation depends on the sample type as well as the chosen detection method. Often cells, particulates and a wide range of interferrents need to be removed from the sample before analysis.

1.10.1 Biological fluids for minimally invasive monitoring

Many biological fluids have been highlighted as sources of biochemical data, the most common being blood, urine and saliva. In some applications particularly sport (Morgan, Patterson et al. 2004), pathologies such as cystic fibrosis (Rosenstein and Cutting 1998) and diabetes (Talary, Dewarrat et al. 2007), sweat has been employed as a source of biochemical analytes including metabolites, ions and ammonia (Timmer, Olthuis et al. 2005). Devices have also been produced which monitor breath vapour due to its non-invasive nature. The most common breath vapour sensors are portable electrochemical alcohol breath analysers used by police officers (Paixão and Bertotti 2004). Breath sensors have also been used to monitor NO and O_2 (Hunter, Xu et al. 2011, Pantalei, Zampetti et al. 2013) in asthmatic patients and others, and for the detection of ammonia related to some infections (Hibbard and Killard 2011). Saliva has also been utilised as a source of biochemical markers for detection of drugs (Ghimenti, Lomonaco et al. 2011), Gastro oesophageal Reflux Disease (GERD) events (Bouchoucha, Callais et al. 1997)and to non-invasively monitor conditions in the mouth, which may be related to processes around the body (Mitchell, Lowe et al. 2009). Likewise, tears have been suggested as a possible source of biochemical markers particularly glucose with the hope of producing non-invasive monitoring devices. Although current electrochemical based devices have been tested showing a number of issues and further research would be required before electrochemical detection of glucose in tears may be implemented for POC monitoring (Baca, Finegold et al. 2007, Zhang, Hodge et al. 2011, O'Donnell and Efron 2012).

Interstitial fluid is the fluid medium between cells where diffusion takes place between the tissue and capillaries which feed it nutrients and has been highlighted as a powerful source of data for a variety of applications. Leading to the creation of devices for the measurement of cholesterol, H_2O_2, pH, glucose and lactate variations in interstitial fluid (Windmiller, Zhou et al. 2011, Miller, Skoog et al. 2012). Interstitial fluid has many similarities with blood (the most well understood source of biochemical analytes). For example, measurements from sub-cutaneous implanted devices shows good correlation of glucose in interstitial fluid with blood glucose levels(Nielsen, Djurhuus et al. 2005, Mader, Weinhandl et al. 2010). However, the time delay between blood and interstitial fluid concentrations must be accounted for (Keenan, Mastrototaro et al. 2009).

There are a number of devices on market, which use direct sampling and microdialysis coupled with an electrochemical sensor to monitor interstitial fluid glucose levels (Matzeu, Florea et al. 2015). Sensitivity and lifetime are generally an issue particularly at hypoglycaemic and hyperglycaemic levels (Mader, Weinhandl et al. 2010). Though some strategies have been developed to increase device lifetime such as incorporating protective membranes (Piechotta, Albers et al. 2005), with some promising early results. Some non-invasive techniques have also been demonstrated for measurement of glucose in interstitial fluid. However, these still require intense research with early devices being recalled from the market (Tierney, Tamada et al. 2001, Li, Yu et al. 2007). Simple/passive systems for microfluidic sample collection have been shown, such as those that use capillary driven flow (Martinez, Phillips et al. 2010, Osborn, Lutz et al. 2010) and vacuum driven flow (Hosokawa, Sato et al. 2004, Dimov, Basabe-Desmonts et al. 2011) although often further preparation and processing of the sample must be completed before any detection/analysis.

1.10.2 Microfluidics and sampling technologies integration

Many bodily fluids are complex mixtures including blood, interstitial fluid and urine. These can pose a variety of difficulties for detection: they may contain large particles, exhibit non-Newtonian properties (such as the shear thinning of blood) resulting in changing fluid dynamics and they may contain a number of interferrents that may give false positive or false negative results. This can make qualitative measurement difficult and quantitative measurement near impossible without pre-treatment.

It will likely be desirable to filter out many of the constituents and add anti-coagulants or other chemicals before detection for these types of samples. Whole blood is one of the most commonly used bodily fluids in point-of-care testing and many microfluidic approaches have been investigated for the separation of blood components employing: whole blood fractionation, centrifugal microfluidic separation, sedimentation, plug-assisted separation, hydrodynamic separation, microfiltration and many other tools (Cui, Rhee et al. 2015).

Systems have been designed which increase the temporal resolution of droplet systems further, such as the chemistrode shown in Fig. 22 as developed by (Chen, Du et al. 2008). This platform delivers a ‘stimulus plug’ of nanolitre volume to an aqueous sample or hydrophilic surface while the surrounding fluorocarbon carrier fluid remains in contact with the hydrophobic wall of the chemistrode. After diffusion of the sample into the stimulus fluid the plugs reform and are delivered to other components, which carry out functions such as splitting, dosing with reagents and sensing.

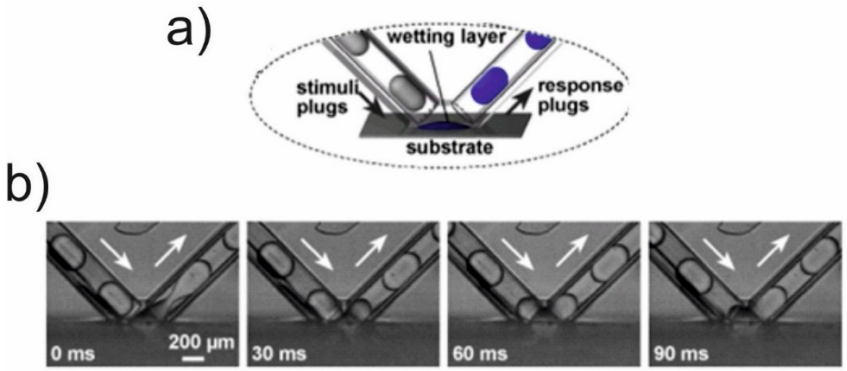

Figure 22 *Chemistrode: A droplet-based microfluidic device for stimulation and recording of substrates on a surface a) Schematic of the chemistrode brought into contact with a hydrophilic substrate. b) Time-lapse bright-field images (side view) of an incoming stimulus plug merging with the wetting layer above a hydrophilic glass surface and the formation of a response plug as the fluid exits the wetting layer(Chen, Du et al. 2008).*

Microdialysis was first employed as a research tool in the early 1960s to study tissue biochemistry of rodent brains. Microdialysis probes such as the schematic example shown in Fig. 23 are minimally invasive *in-situ* sampling tools, which mimic the function of blood capillaries. The probe contains a shaft comprised of a semi-permeable membrane connected to tubing inlet/outlet (Ramanathan, Nelson et al. 2015). Fluid with a similar ionic composition to the tissue is pumped through the probe. Small molecules pass through the membrane by passive diffusion and the fluid containing these particles continues downstream to the outlet keeping the concentration gradient constant (Hersini, Melgaard et al. 2014). The solution containing the molecules of interest (dialysate) is then pumped to some analysis system. These probes may also be used to deliver small molecules to the tissue by perfusion (Hersini, Melgaard et al. 2014).

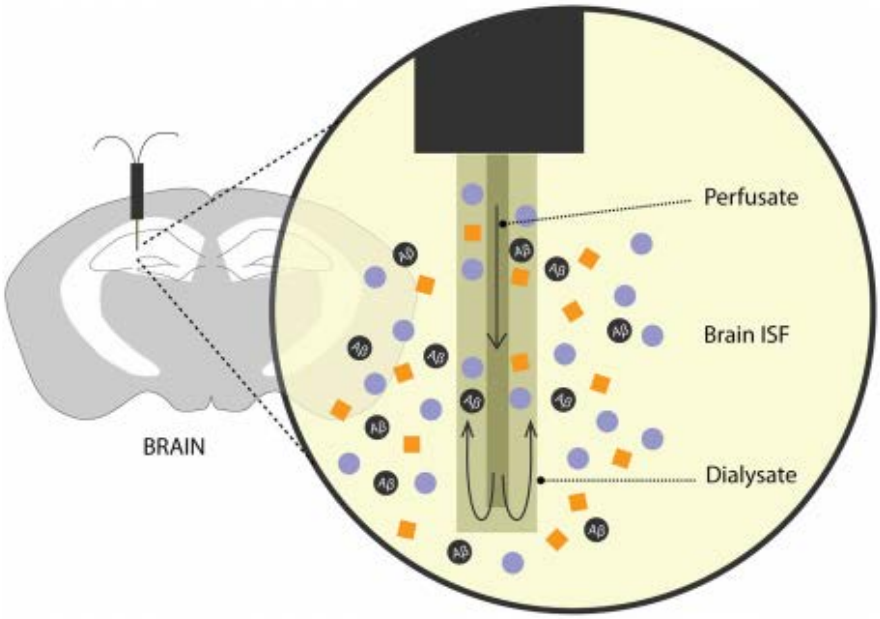

Figure 23 *Principle of microdialysis - A microdialysis probe is implanted into a tissue (e.g. brain tissue) via an introducer needle. Solutes (here represented by Aβ) from the interstitial fluid (ISF) freely enter the semipermeable membrane of the microdialysis probe. (Ramanathan, Nelson et al. 2015).*

Microdialysis has been used as a collection tool for measurement of brain glucose; lactate, etc. with continuous microfluidics and electrochemical probes (Rogers and Boutelle 2013, Rogers, Feuerstein et al. 2013, Petit-Pierre, Bertsch et al. 2016). Compared to other sampling technologies microdialysis is particularly strong as a candidate for continuous monitoring due to its suitability for long term use in any tissue with no drainage of fluid from the sampling site (Chefer, Thompson et al. 2009). Microdialysis is now increasingly being used in human studies for monitoring tissue concentrations of metabolites, such as glucose and regulatory cytokines in response to homeostatic perturbation, as well as free and unbound drug concentrations in tissue (Westerink, Damsma et al. 1987, Stenken and Poschenrieder 2015). Generally, the semi-permeable membranes used do not allow cells, cellular debris, or lipophilic molecules to enter the probe reducing interference and enzymatic degradation. However, some probes for lipophilic analytes and with larger pore sizes have been tested (Plock and Kloft 2005), although recovery efficiency should decrease with increasing molecular weight of the analyte (Chefer, Thompson et al. 2009).

A major issue with microdialysis is the low temporal resolution due to the low flow rates used to accommodate diffusion and the time taken for collection of liquid volumes suitable for lab analysis. Recently the Kennedy group proposed the use of droplet microfluidics to digitise samples gathered by microdialysis (Wang, Roman et al. 2008). This method provides great improvement to the temporal resolution of measurements as described in Fig. 24 and may also reduce the sample volumes required for analysis.

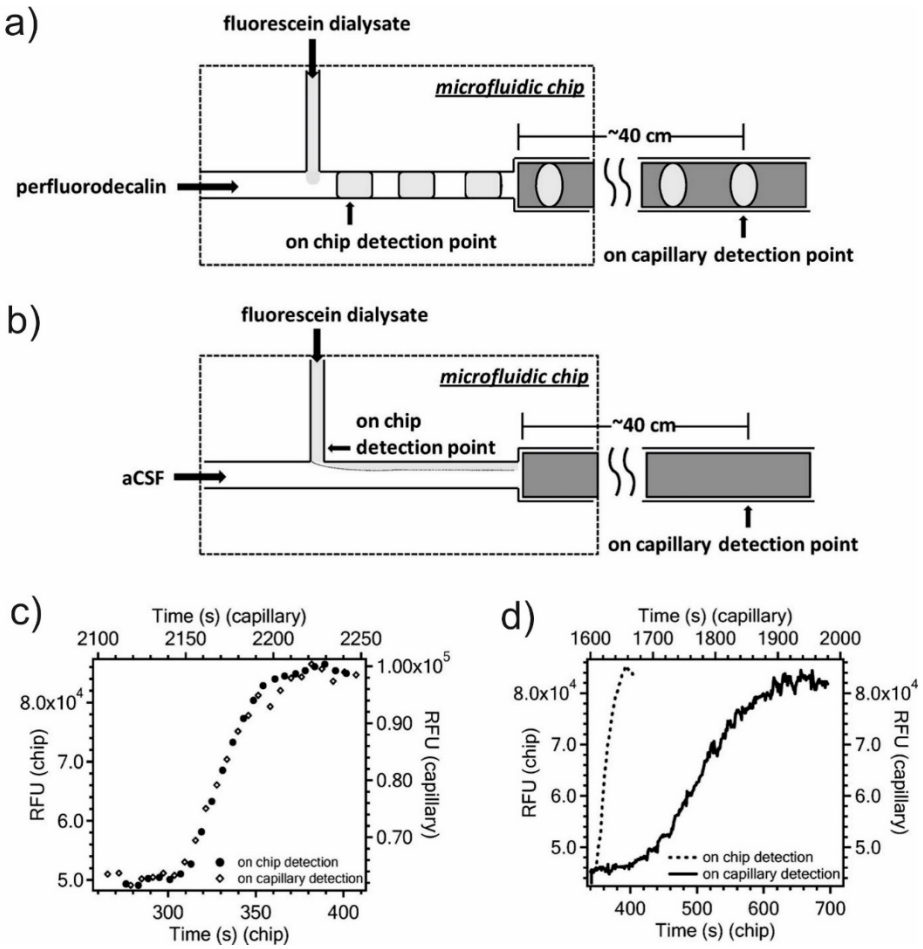

Figure 24 *Comparison of temporal resolutions achieved by segmented and continuous flow (Wang, Roman et al. 2008). Illustration of on chip and on-capillary detection points for comparing temporal resolution of segmented-flow (a) and continuous-flow (b) systems. Step change of fluorescein concentration from 50 to 100 nM was made at the probe surface, and response curves at the two detection points were recorded for segmented flow (c) and continuous flow (d). For (c), the data points represent the maximal fluorescence recorded from each sample plug as it passed through the detector. The top time axis is for the downstream (capillary) detection point and the bottom for the on-chip detection point in both graphs. Sampling flow rate was 200 nL/min, and cross-sectional flow rate (perfluorodecalin or aCSF) was 1 µL/min.*

This approach to sample collection combining microdialysis and droplet microfluidics has great potential to improve how we monitor tissue chemistry at the point-of-care. However, their fluidic system used a bulky syringe pump instrumentation, which was sensitive to disturbances in flow conditions and hence may not be suitable for widespread POC use.

Calibration of these microdialysis probes "recovery rate" is also important for calculating true sample concentration due to the long time required for molecules to diffuse across the membrane. *In-vitro* calibration by one of the established methods e.g. flow rate, no-net-flux or retrodialysis (Jacobson, Sandberg et al. 1985, Lonnroth, Jansson et al. 1987, Olson and Justice 1993, Wang, Wong et al. 1993) prior to implantation is often recommended. However, since *in-vitro* recovery will differ from recovery in tissue, *in-vivo* determination may also be required (Stahl, Bouw et al. 2002, Chaurasia, Müller et al. 2007). *In-vivo* calibration techniques tend to be derived from the *in-vitro* methods but are more difficult due to changes in tissue conditions, temperature and variance between probes. In-vivo

calibration often takes a prohibitively long time so new methods of *in-situ in-vivo* calibration may need to be developed for continuous monitoring purposes.

There are still challenges, which must be addressed for the development of continuous monitoring platforms based on droplet microfluidics such as the development of robust, portable and low power fluid handling solutions and of miniaturised sensing solutions with *in-situ* calibration. The work presented in the following chapters describes my research into tools and techniques, which will hopefully allow for droplet microfluidics to become a powerful analysis tool.

Chapter 2 – Pulsed droplet generation by programmable peristaltic micropump

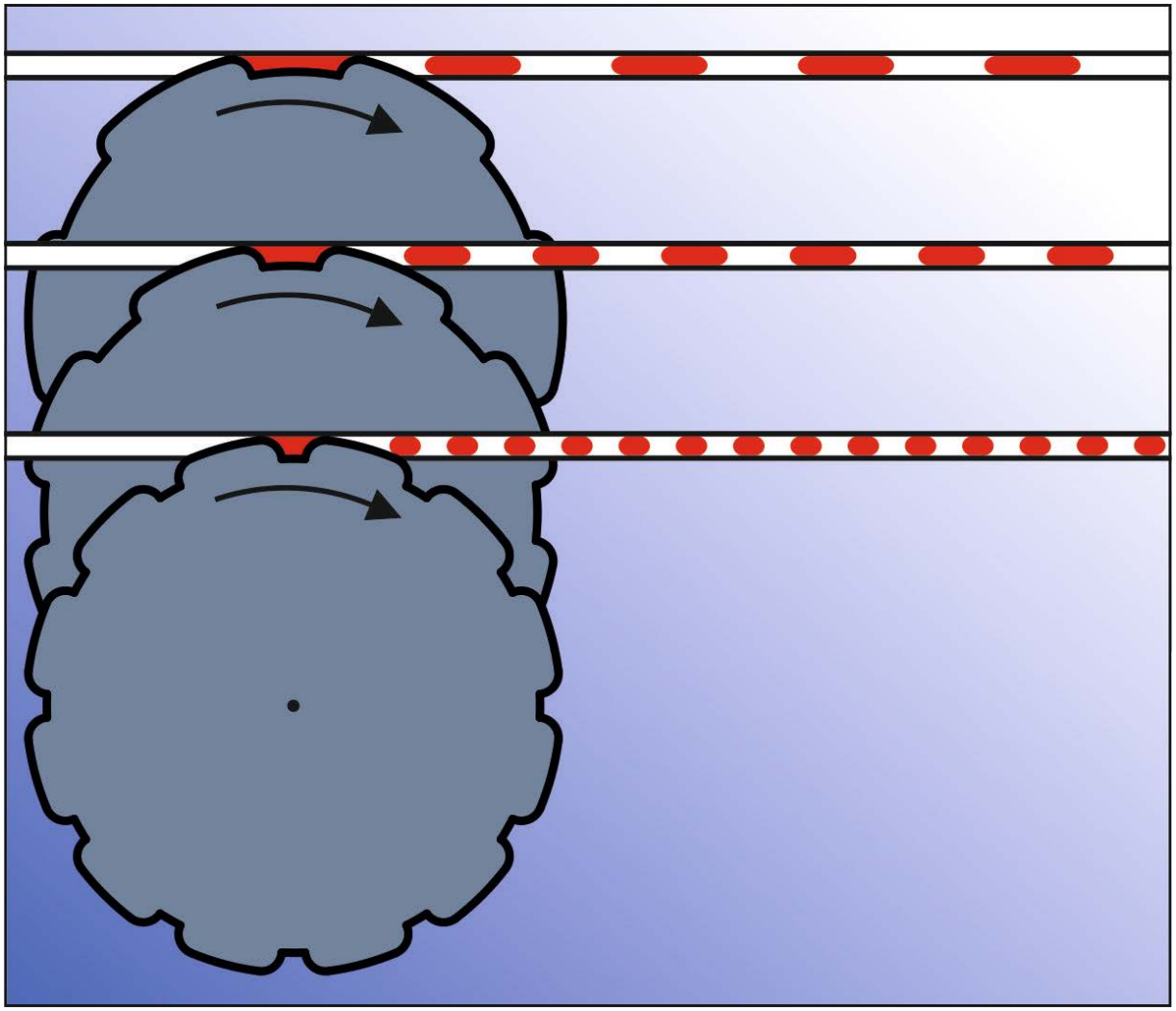

Presented in this chapter is the development of a robust, flow invariant and field deployable sampling and droplet generation method based around a peristaltic micro-pump delivering pulses of fluids.

As described in the previous chapter, passive droplet generation using pressure driven pumps is the most commonly used method of producing microdroplets. However, these methods are unsuitable for point-of-care (POC) application as the instrumentation is large and typically requires long 'ramping up' time (a few minutes). Additionally, the droplet size, generation, frequency and composition are likely to vary depending on ambient condition and operational variability. Presented in this chapter is a robust, flow invariant and field deployable sampling and droplet generation method based around temporally separate pulsed pumping of the aqueous and oil phases. This method is accomplished by implementing a 3D printed push-pull peristaltic micro-pump and PDMS droplet generation chip. The device is able to sample directly from fluid and tissue and perform assays *in-situ*. The method described here is able to produce droplets of a designed size regardless of changes in fluid properties or dynamics (flow rate, viscosity, surface tension, etc.) Moreover, different assay conditions can be directly 'hard coded' into the geometry of the pump, for example to change the concentration of sample or reagents.

The work presented in this chapter was carried out in collaboration with Dr Adrian Nightingale, Dr Sammer Ul Hassan and Byung Jae Kim and has led to two presentations at Microtas 2016 in Dublin (shown in appendices). This method of droplet generation and technological approach has also been further optimised with added functionality and taken forward to a variety of applications (as detailed in the following chapters).

2.1 Design rationale

In 2015 the Niu Group produced a simple peristaltic micropump used for generating droplets (Niu 2015) schematically shown in Fig. 25. This uses a screw-driven mechanism similar to (Wonsei and Toshiro 2010) as described in the literature review. This design exploits the pulsatile flow of the peristaltic micropump to produce droplets of uniform volume and sample-to-reagent ratio. The screw thread compresses pumplines forcing fluid along the tubing as the screw turns. Aqueous lines are positioned together on one side, with oil lines opposite, producing pulsatile flow profiles that are exactly out of phase. The screw thread disengages causing negative backpressure and breaking the neck of the droplet triggering droplet generation. This has been successful in generating droplets, robustly generating one droplet per turn of the screw thread. However, this approach is limited in its functionality by the number of tubing that can fit around the screw channel sizes. Channel position and sizes must be carefully controlled to ensure that this pump setup can robustly produce one droplet per turn (rather than per two or three turns). Additionally, the screw thread requires precise custom fabrication in metal, thus it cannot be as quickly prototyped as the later designs.

To overcome the issues of the previous screw driven pump a 3D printed peristaltic micropump was produced with monolithic microfluidic chip, including pumplines cast in PDMS by the method shown in section 2.2.2. An initial design (shown in Fig. 25b) based on a more conventional rotorhead peristaltic configuration was developed by Byung Jae Kim (undergraduate summer intern) extensively using 3D printing for rapid prototyping and simple fabrication.

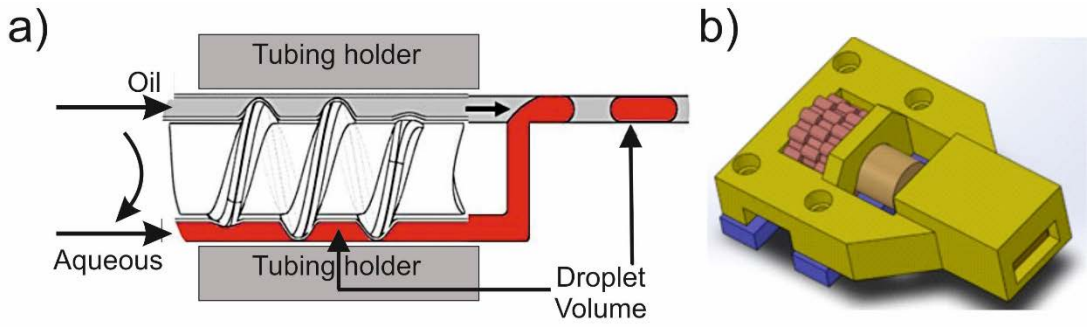

Figure 25 *Previous designs of peristaltic micropump from the Niu Group a) Peristaltic micropump utilising a screw thread b) 3D printed peristaltic micropump with circular features.*

Like all peristaltic pumps, this pump operates by positive displacement, as microchannels on the surface of the PDMS chip are compressed by the rotorhead. As the rotorhead turns, fluid in the pumplines (not shown in Fig. 25b) is trapped and pumped in the spacing between rotorheads raised circular features. The volume pumped during each pulsation should be determined by the topology of features around the circumference of the rotorhead. Unlike the screw driven pump, here the number of pumplines is not limited, new rotorhead designs can be rapidly prototyped, and crucially the size and timing of each pulsation can be arbitrarily specified.

However, this design produced droplets with a relatively high degree of polydispersity in droplet volume and irregular droplet composition (data not shown), due to a period of co-flow between pulsation peaks. To address this problem, I produced a new version of the 3D printed micropump with an altered rotorhead design. The features were wider and includes “shoulders” that overlap such that the two phases (oil/aqueous) never flow simultaneously. Figure 26a shows, the features of the rotorhead that pump the aqueous and oil phases, drawn solid and flat for easy understanding, with the hypothetical flow rate shown in Fig. 26b. This design should produce highly pulsatile flow and be able to deliver two immiscible fluids (e.g. oil and aqueous) to a droplet generation T-junction channel in anti-phase pulses (as shown in Fig. 26c). In this method, the fluid injected during the aqueous pulse defines droplet volume and composition, and the oil pulse defines oil spacing between the droplets. In contrast to co-flowing droplet generation regimes described in section 1.6.2, droplet size and generation frequency in this regime should be solely defined by the pump design and not affected by flow conditions such as total flow rate and ratio, interfacial tensions or viscosity thanks to a lack of shear flow during the aqueous incursion.

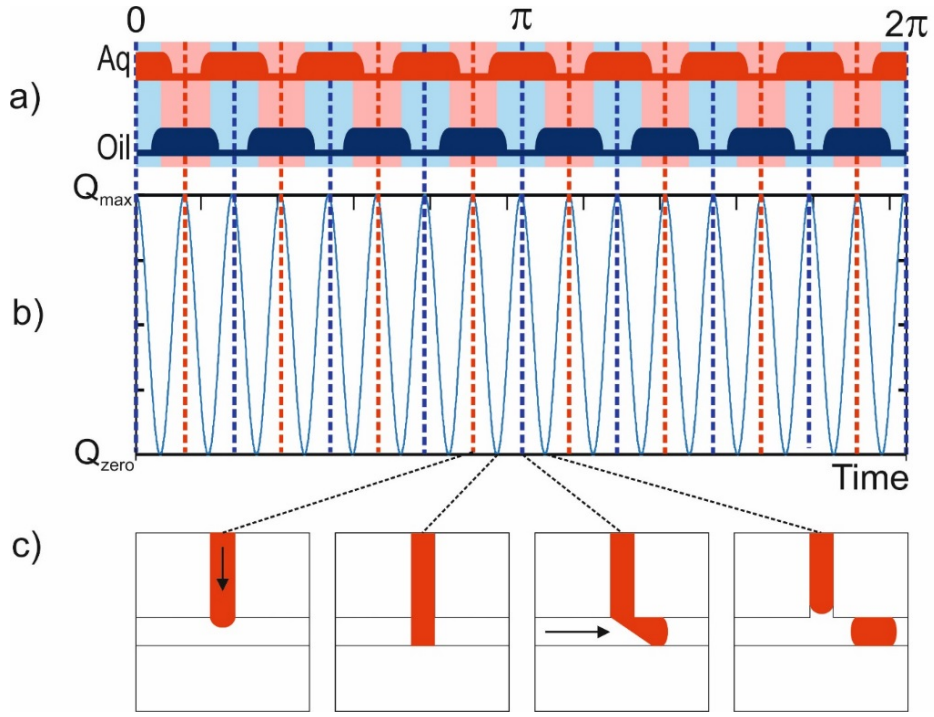

Figure 26 *Description of pulsed droplet generation regime. a) Schematic of rotorhead topography over one full turn (2π) b) Hypothetical average flow rate over time for the pulsed droplet generation regime. c) Relation of droplet generation to the theoretical flow rate b).*

The push-pull nature of the peristaltic pump design for droplet generation and pumping offers several advantages for point-of-care microfluidics such as its ability to self-prime, simplifying the required "chip to world" interface with no extra sample collection step required. The pump can be run continuously, intermittently or in reverse if required. Figure 27a shows a schematic of my redesigned push-pull micro-peristaltic pump (photograph Fig. 27b). For robust pumping, at least two features occlude the channel to move the fluid downstream as shown in Fig. 27c, a schematic side view of the pump. It is vitally important that the channel be completely occluded to ensure predictable repeatable pulsations for the intended pulsed droplet generation regime.

.

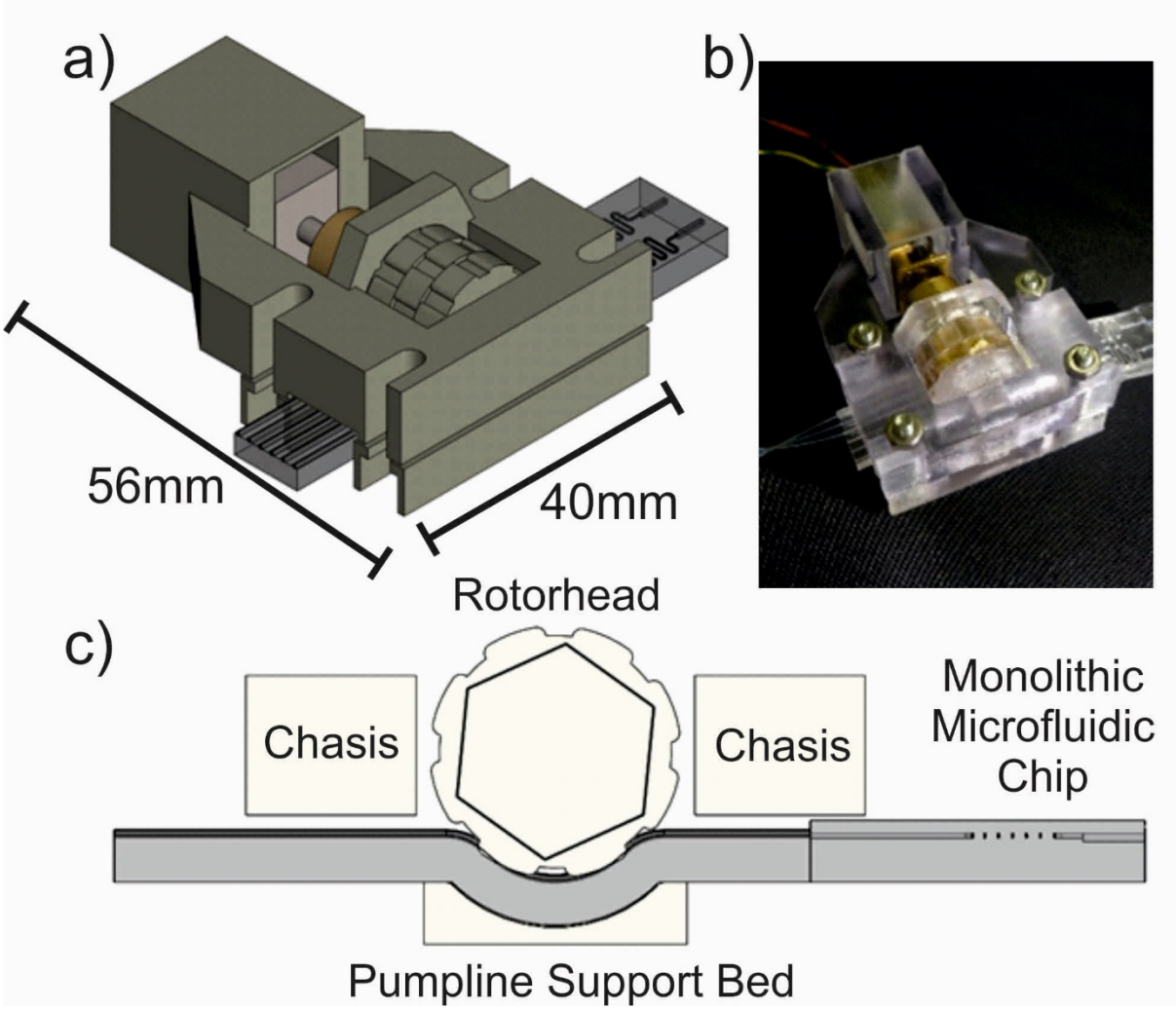

Figure 27 *3D-printed peristaltic micropump a) Schematic of peristaltic micropump b) Photo of peristaltic micropump c) Schematic side view of the pump.*

2.2 Methods and Materials

2.2.1 Design and fabrication of the first generation peristaltic micropump

As shown in the exploded schematic Fig. 28, the key components of the prototype peristaltic micropump/droplet generator are a monolithic microfluidic chip containing raised pumplines and a T-Junction (for droplet generation) geometry cast with polydimethylsiloxane (PDMS) (Dowsil Sylgard 184); and a rotorhead (16.25 mm in diameter), 3D printed with veroClear material (Objet500 Connex3 printer). A pumpline support 'bed' and a chassis were also 3D printed to fix the microfluidic chip onto the rotorhead. A DC motor (Pololu 210:1 Micro Metal Gearmotor) was used to drive the rotorhead. 3D printing was widely used in this pump fabrication allowing alternative feature topography and chassis to be easily fabricated as required by the application. A silicon lubricant (Rocol Silicone Grease SAPPHIRE Aqua-Sil) was used to lubricate the movement of the rotorhead with respect to the chassis and pumplines, decreasing the torque and ultimately increase pumpline lifetime.

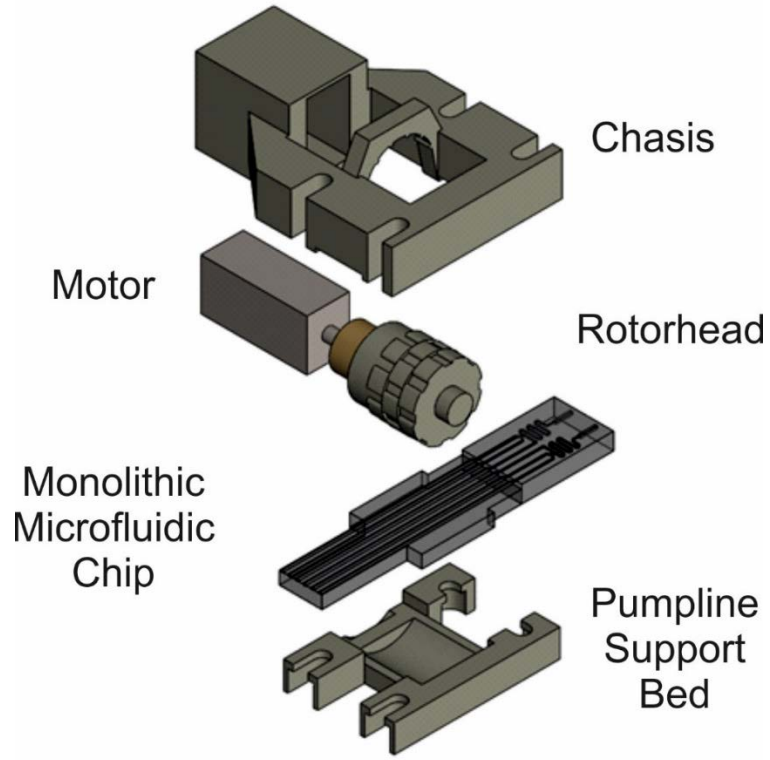

Figure 28 *Exploded view of the peristaltic micropump displaying all key components: 3D-printed chassis, DC motor (Pololu 210:1 Micro Metal Gearmotor) 3D-printed rotorhead monolithic PDMS chip featuring pumplines and two droplet generation T-junction and pumpline support bed.*

2.2.2 Fabrication of the monolithic microfluidic chip

The integrated microfluidic chip is a PDMS monolith containing both parallel 'pumplines' and channels forming a T-junction. Figure 29 shows the pumplines with uniform circular cross-section. These pumplines join immediately to a T-junction droplet generation chip. Direct connection of the pumplines to the droplet generation portion of the chip reduces the detrimental effect of Taylor dispersion as described in section 1.5 compared to long connections using channel or tubing. The short distance also avoids smoothing of the pulsatile flows from compliance (flexibility) of the PDMS channel material, as pulsed flow is key to the proposed approach to droplet generation. These pumplines are raised to help ensure complete occlusions, which is important for reliable pulsations.

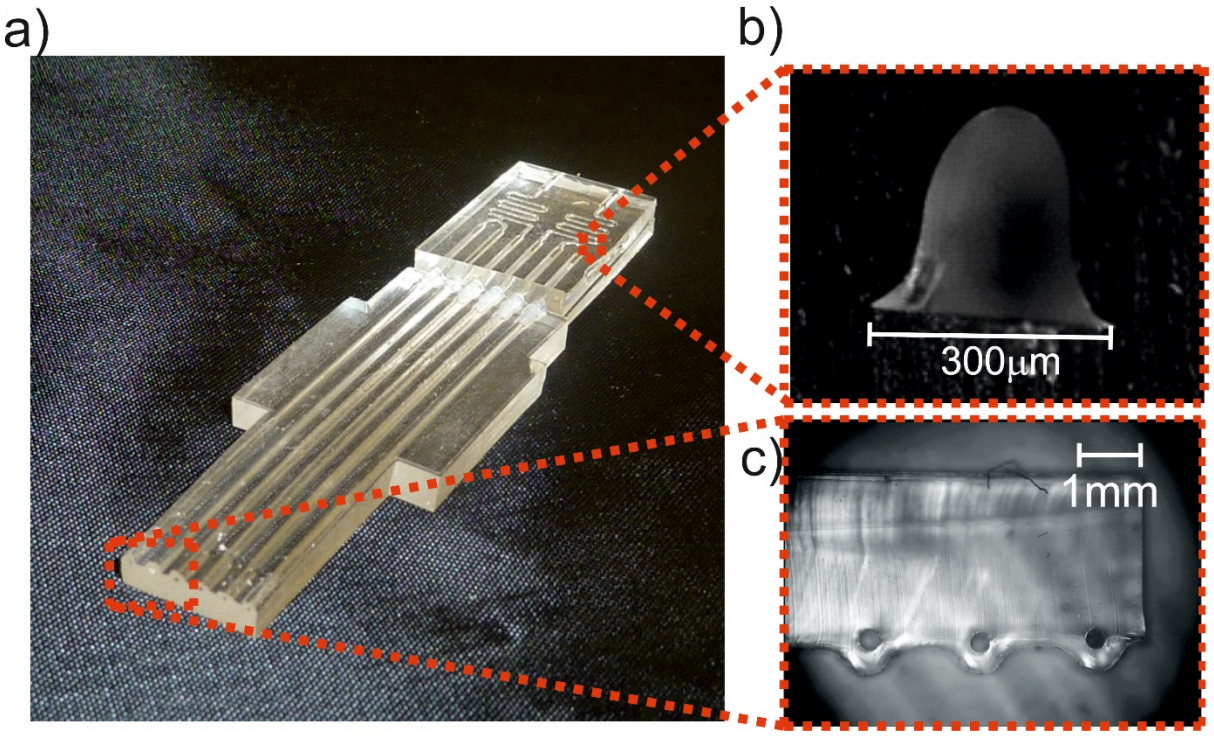

Figure 29 *Photographs of the monolithic microfluidic chip used in this peristaltic micropump a) Photograph of whole finished monolithic microfluidics chip b) Micrograph of channel c) Micrograph of raised pumplines.*

The monolithic chip was produced from two parts, the pumplines and droplet generation portion. The raised pumpline channels were cast with a monolithic procedure shown schematically in Fig. 30 with a method similar to that reported by Skafte-Pedersen and colleagues (Skafte-Pedersen, Sabourin et al. 2009). First, a mould was designed using CAD software (SolidWorks, Dassault Systemes) and printed in VeroClear material using an Objet500 Connex3 3D printer (Stanford Marsh Ltd). The printed mould was dried overnight at 70 ^{o}C to ensure no solvent was present in the material. The mould was further treated by wiping with a lint free wipe dipped in "Aquapel" (PPG Industries) to aid removal of the PDMS chip after casting. Optic fibres (Thorlabs) were used to mould the pumplines. The sizes of the fibres were chosen to provide the designed pumpline diameter typically, 245 µm diameter fibres were used for the two aqueous lines and 320 µm diameter fibre for the oil line. This establishes similar overall water and oil volumes with the same size of rotorhead features.

During chip fabrication, the fibres were mounted inside the semi-circular channels at the surface of the 3D-printed mould, so that the resultant PDMS channels would be raised in the finished chip (see Fig. 29). Short lengths of PVC tubing (Gradko International Ltd.) were used to hold the fibre optics in position in the mould. Liquid PDMS (10:1 ratio of elastomer to curing agent) was poured into the mould and oven cured at 70 ^{o}C overnight. The 10:1 ratio was chosen as it is the recommended and most often used in the literature (Friend and Yeo 2010), however the ratio could be altered to create a more optimal distensibility as required. The fibre optics were then removed, and the chip peeled off from the mould. The chip was then cut along guidelines included in the mould to a shape designed so that it can fit snugly into the bed later.

For initial testing a chip composed of two simple T-junctions each composed of two aqueous inlets and one oil inlet as in Fig. 29 (this was later further simplified to a single T-junction per chip). The droplet generation chip was fabricated by simple PDMS casting procedures, where the fluidic structures were moulded in PDMS from a 3D printed channel mould and then sealed with a layer of half-cured PDMS. After printing, the mould was baked overnight at 70 °C to remove any uncured precursor materials and treated with a non-stick coating by wiping with a lint free wipe dipped in "Aquapel" (PPG Industries). PDMS was added to the mould (Sylgard 184, 10:1 ratio of elastomer to curing agent) and baked at 70 °C until fully cured. After removal from the mould, the chips were cut to shape and then sealed to a flat piece of PDMS using the "half-cure" method (where pdms is allowed to cure until non-flowing but still adhering) (Go and Shoji 2004, Eddings, Johnson et al. 2008, Peng, Zhang et al. 2008). Due to the pulsed droplet generation regime, the volume and channel shape of the droplet generation chip should not affect the droplet volume so long as the aqueous incursion fills the width of the channel at the junction. The pumpline and droplet generation parts were linked by ~4 mm long PTFE tubing (0.4 mm ID, 0.15 mm wall), Adtech Polymer Engineering Ltd.) and then permanently bonded by sealing the connection with a small amount of liquid PDMS on a hotplate (Fisher Scientific) at 105 °C for 5 minutes. After fabrication, the inside of the chip was then treated with a hydrophobic coating (Aquapel, PPG Industries) to ensure that the fluorous oil phase preferentially wets the channel. This was done by filling the channels with Aquapel (PPG Industries) using a syringe and blunt dispensing needle, waiting for approximately 5 minutes, and then flushing the channels with air. The chips were then left overnight in an oven at 70 °C. PTFE tubing (I.D. 500 µm; outer diameter, OD, 700 µm; Adtech Polymer Engineering, UK) was inserted into the inlet/outlet sections and then fixed in place by placing the chip and tubing on a hotplate at 110 °C and applying uncured PDMS to the join.

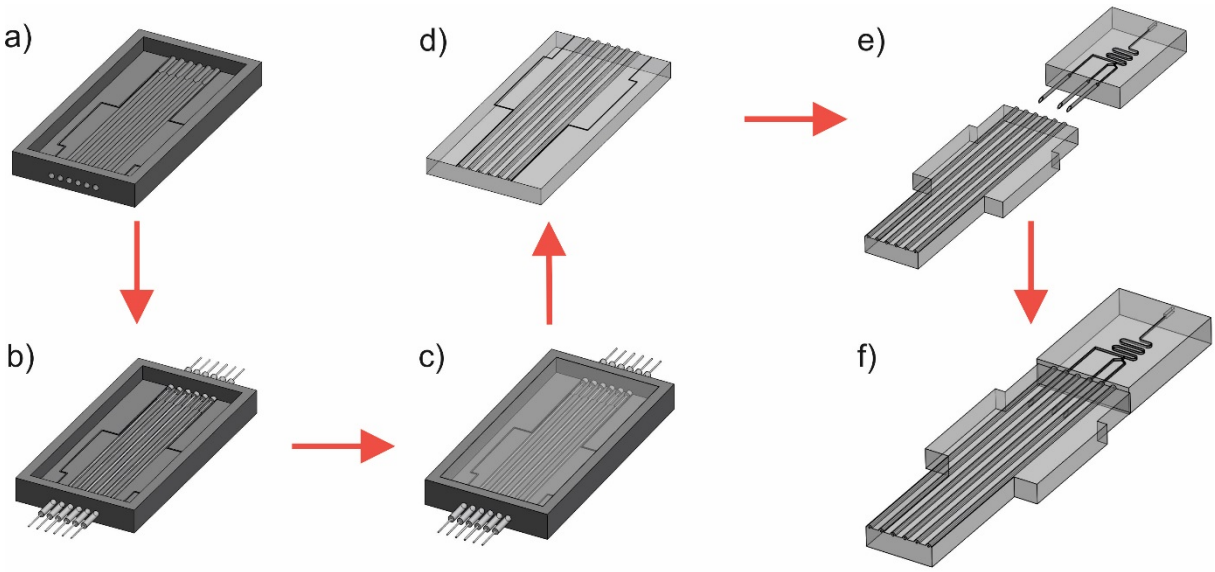

Figure 30 *Manufacture of the monolithic microfluidic chip. a) 3D printed mould. b) Insertion of the fibre optics that form the channel. c) PDMS is poured into the mould and fully cured at 70°C. d) Chip is removed from the mould and the fibre optics carefully removed. e) Chip is cut to fit the pumpline support bed. f) Pump chip is bonded to a droplet generation chip (produced by standard multilayer PDMS casting procedures) by a short connection of 0.4mm tubing encased in PDMS.*

Once fully assembled the pump is small enough to fit easily in the palm of a hand. The full pump and chip assembly are able to run for several hours while carrying our tests (provided correct fabrication with adequate lubrication) and when further tests are to be carried out the chip containing all fluidic components may be disposed of and replaced. The modular nature of the pump design allows for the replacement of each component when they are damaged or worn out, or substitution of different chips for a variety of different applications. Required fluids such as reagents and fluorous oil (FC-40) can be held in reservoirs such as small Eppendorf tubes or plastic bags (made in house using 250 gauge Polythene Tubing), while samples can be taken directly from tissue or other environments. A fluorinated oil was used in the experiments (FC-40) (3M, UK) containing a 1.8 %, w/w concentration of biocompatible and non-ionic tri-block copolymer surfactant (PEG-PFPE-PEG) synthesised in-house.

2.2.3 The hard coding of chemical operations

It is important to note that the features of the rotorhead can be designed with any size and this size does not have to be constant across pumplines or between droplets generated per turn. One exciting feature of this pump is ability to “hard code” chemical operations by changing the feature dimensions on a single rotorhead, allowing for the generation of a “train” of droplets every rotation, where each droplet in the train has different predefined size, composition or oil spacing. Figure 31 shows a rotorhead and microfluidic chip designed to produce a train of droplets with varied concentrations of sample. The chip features three aqueous inlets that meet at a single junction, which is then introduced into a stream of fluorous oil.

As shown in Fig. 31 pumphead topography and resulting droplet sequence, the composition of droplets is varied by sequentially reducing the pumping volume in one pipeline (line 1) containing sample by reducing the rotorhead feature spacing and increasing the pumping volume in another pumpline (line 3) containing buffer by increasing rotorhead feature spacing. Therefore, when the pumplines join into one channel at the T-junction, the droplets generated will have the same volume but different sample concentration.

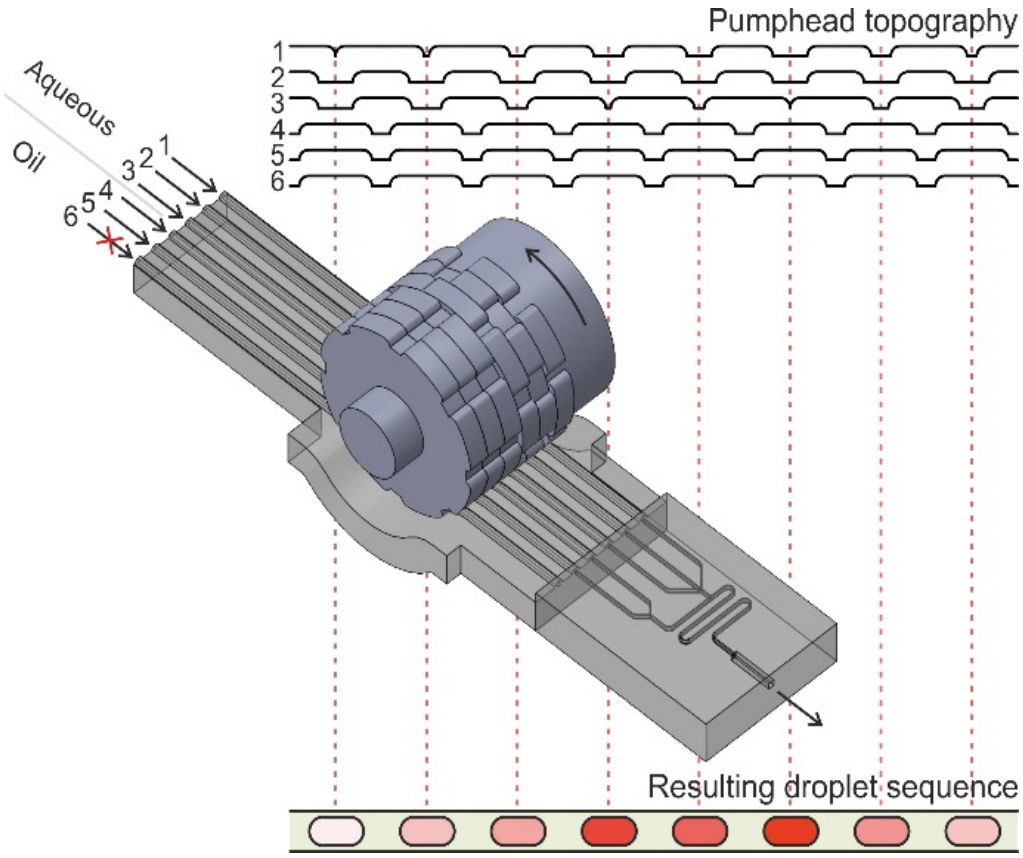

Figure 31 *Schematic of rotorhead and chip with dilution series 'hard coded' by pumphead topography (line 1 Sucrose solution, 2 Trinder assay reagent, 3 DI water 4-5 oil 6 unused) related to the resulting droplet sequence*

2.2.4 Recording and analysis of data

To characterise the pump and the generated droplets, a portable microscope camera (dnt Digimicro Mobile Mikroskope) was used to record either directly at the T-junction area of the chip or the droplet flow in a PTFE tubing (0.4 mm I.D., Adtech Polymer Engineering Ltd.) connected to the chip, as shown in Fig. 32a&b. The videos recorded were analysed using Droplet Morphology and Velocimetry (DMV) software (Basu 2013) an algorithm implemented in Matlab 2011. Unlike particle-image-velocimetry (PIV) which has been commonly used in microfluidics research DMV does not require the use of particles within the droplet for tracking instead relying on image processing alone with a single droplet granularity. Figure 32c shows a screenshot of the DMV GUI panel, which provides a wealth of data such as: the flow rate, droplet length, spacing between droplets etc.

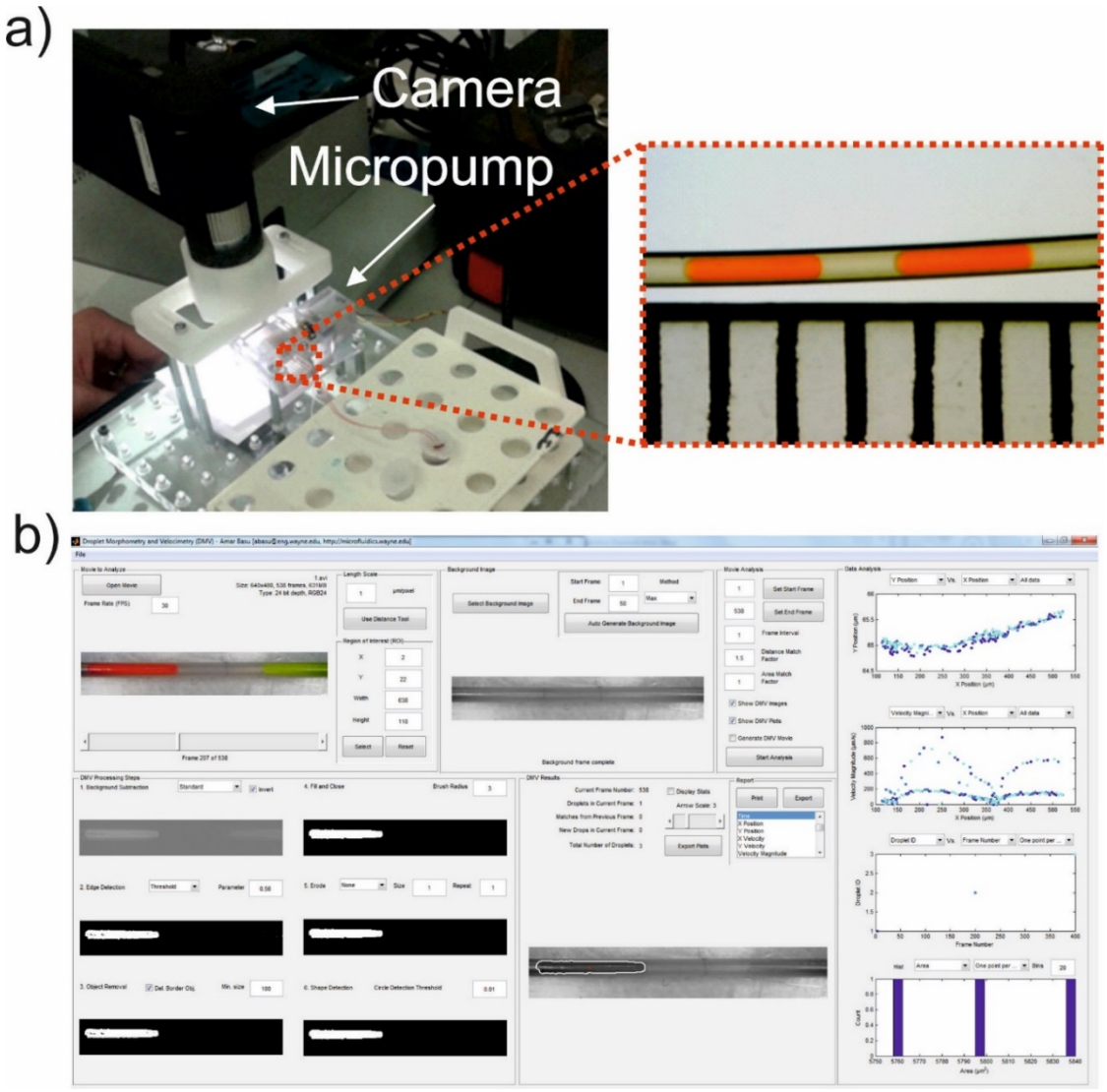

Figure 32 *Method of analysis used for characterisation of droplet dynamics thoughout this thesis. a) dnt Digimicro Mobile Mikroskope camera setup for video recording b) Example frame of recorded droplets in 0.4μm tubing c) Screenshot of DMV software during analysis*

To analyse these videos DMV requires droplets to be moving across a fixed background. A background was taken using an inbuilt feature to set the maximum, minimum or average light intensity of each pixel over a set period of frames. In this case, the maximum pixel intensity was taken as the background converted to greyscale and inverted. Intensity thresholding was then used for edge detection of the droplets (gradient-based algorithms may also be used), and other image processing techniques are also applied to each frame. A scale (μm/pixel) was set using the inbuilt feature for each video. The DMV programme was then run through all of the frames to pick up all of the droplets and exported as a .txt file ready for analysis. The data was then exported to a .txt file and processed using a Matlab programme developed in house to determine: a) Droplet generation rate (Hz); b) Mean droplet length (μm); c) Standard deviation of droplet length. Figure 33 shows an example of the figures generated by the Matlab programme after analysing videos recorded from an 8-featured rotorhead

with a droplet generation rate of 3.80 Hz. The mean droplet length is 3.03 mm in a 400 μm I.D. tubing, with a standard deviation of droplet length of 0.133 mm and a relative standard deviation of droplet length to be 4.39 %).

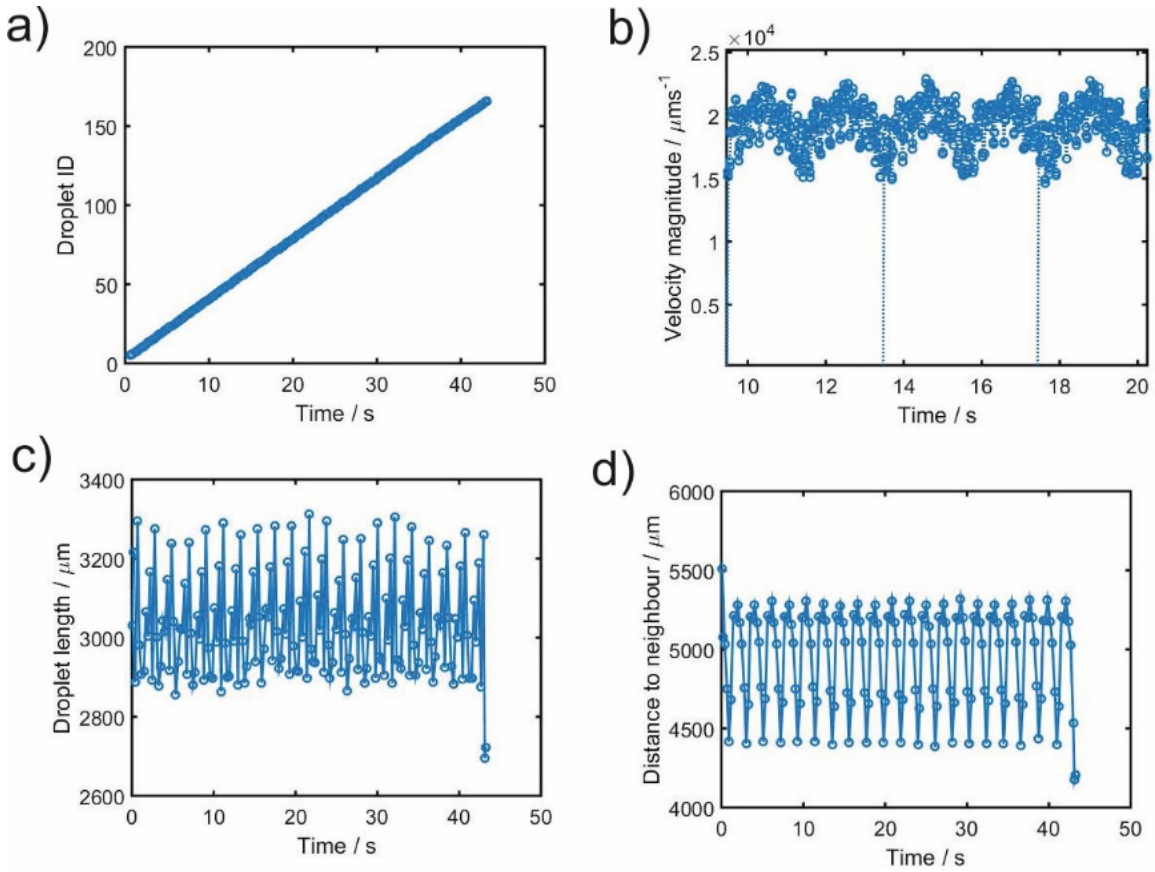

Figure 33 *Example output of Matlab script for analysis of droplet dynamics throughout this thesis. (droplets generated by peristaltic micropump and an eight featured rotorhead at 3V) a) Droplet ID vs time (s) where the gradient is the droplet generation rate b) Velocity magnitude of droplets in frame (μms^{-1}) vs time (s) c) Droplet length (μm) vs time (s) d) Distance to nearest neighbour (μm) vs time (s).*

2.3 Results and discussion

2.3.1 Characterisation of the pump

The first characterisation of the pump carried out was flow rate in single pumplines (without the droplet generation chip attached). Here the linear flow velocity (velocity magnitude) of a droplet was used to characterise the total flow rate with the DMV method mentioned in section 2.2.3. Droplets were manually formed by aspirating fluorous oil and dyed aqueous fluids alternately (by moving the pumpline inlets between fluorous oil and dyed aqueous fluids both contained in a small Eppendorf sample vial).

The flow produced was pulsed as expected with peristaltic pumping Fig. 34 shows the variation in flow for two motor speeds (0.33Hz and 0.59Hz) and rotor head design (1.7mm and 0.52mm spacing), where pumpline diameter ($\varnothing$) is $245\mu m$. In all cases, the flow rate was seen to periodically rise and fall with each period (peak and trough) corresponding to a single feature on the rotor head (red line average flow rate). Figure 34a & 34b show the resulting flow rates when using the same channel diameter (245 µm) and rotor head at two motor speeds. When the motor speed is increased from 0.33 Hz to 0.59 Hz, the pulse period reduces accordingly (from 375 to 175 ms) and both the peak flow rate and the mean flow rate double. Regardless of motor speed, the area under each peak remains relatively constant as the volume delivered in a single pulse remains constant, depending on the volume captured between features on the rotorhead.

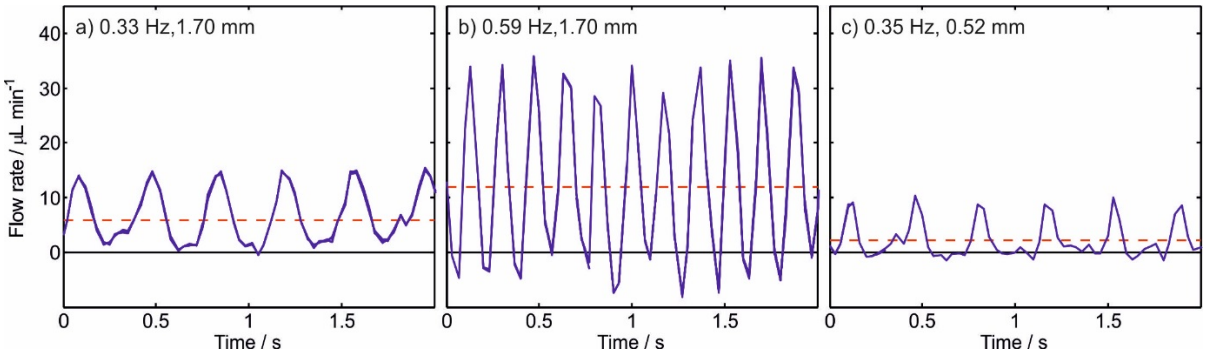

Figure 34 *Characterisation of the pulsed nature of flow in a single line of the peristaltic micropump a&b) Flow rate data for differing motor speeds (0.35 Hz-0.59Hz). c) Flow rate data for reduced feature spacing (1.70mm to 0.52 mm) motor speed (0.35Hz) (red line denotes average flow rate).*

As shown in Fig. 34a and Fig. 34c, flow rate can also be altered by altering the spacing between the rotorhead features (here from 1.70 to 0.52 mm) while motor speed, number of features (n=8) and channel diameter remains constant. With smaller feature spacing, the peak and mean flow rates are greatly reduced, and the resulting flow rate peaks are narrower, demonstrating the control offered by the design of rotorhead topology on the relative flow profile of each pumpline. The predictability of these pulsations demonstrates the robustness of this method and remained stable throughout the testing carried out which lasted several hours. The flow rates produced by this pump are low in comparison to those which may be desired for some applications, but for continuous monitoring in the medical and environmental fields, sampling rates generally do not require droplet generation rates and flow rates that high. Additionally low flow rates make for easier detection by miniaturised in-line

spectrophotometer flow cells like those described in (Hassan, Nightingale et al. 2016) and used throughout this thesis.

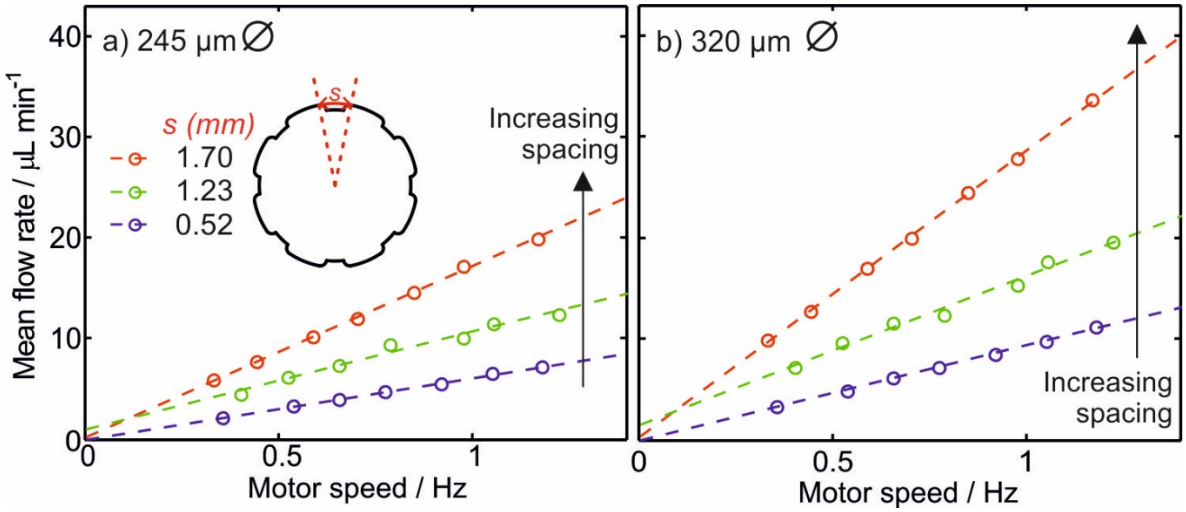

Figure 35 *Characterisation of the mean flow rate of a single line of the peristaltic micropump a) Mean flow rate vs motor speed showing how flow rate increases with motor speed and for increasing spacing⌀ (245µm) and b) for an increased channel diameters ⌀(320µm) (each data point represents approx.. 100 measurements).*

Figure 35a&b further demonstrate the level of precise control offered by the peristaltic micropump. Motor speed was varied, and the resulting flow rate measured for three sizes of rotorhead feature's spacing's and two channel sizes (245 µm and 320 µm). As would be theoretically expected, increasing the motor speed caused a linear increase in the mean flow rate given by equation 13.

Total flow rate $$Q = nVf \quad (13)$$

Where *Q* is the total flow rate, *n* is the number of features, *V* is the fluidic volume pinched between features and *f* is the motor speed (frequency). It is important to note that all these relationships assume complete occlusion of the channel. A linear fitting of the data produces a straight line passing through the origin with a gradient corresponding to the volume delivered with one turn of the rotorhead (*nV*). As shown in Fig.35a and Fig. 35b the gradient increases with the increase of feature spacing, due to increased volume delivered in each individual pulse with wider spacing. The volume (*V*) pumped per rotorhead feature can be given by equation 14.

Volume pumped per feature space $$V = ksA \quad (14)$$

Where *A* is the channel cross section, s is the spacing between features and *k* is a coefficient that allows for the channel's deviation from a perfect cylinder to complete compression, when pinched by the rotorhead features. Equation 15 shows a combined flow rate equation

Combined flow rate equation $$Q = nksAf \quad (15)$$

The same qualitative trends are seen in both Fig. 35a and Fig. 35b, with the increases in flow rates approximately equal to the ratio of the channel cross sectional area. These results show that the flow rate in the pump can be tuned as desired by carefully choosing the design parameters such as: the

diameter of the pumpline, the number of features, the width of feature spacing and the motor speed (frequency).

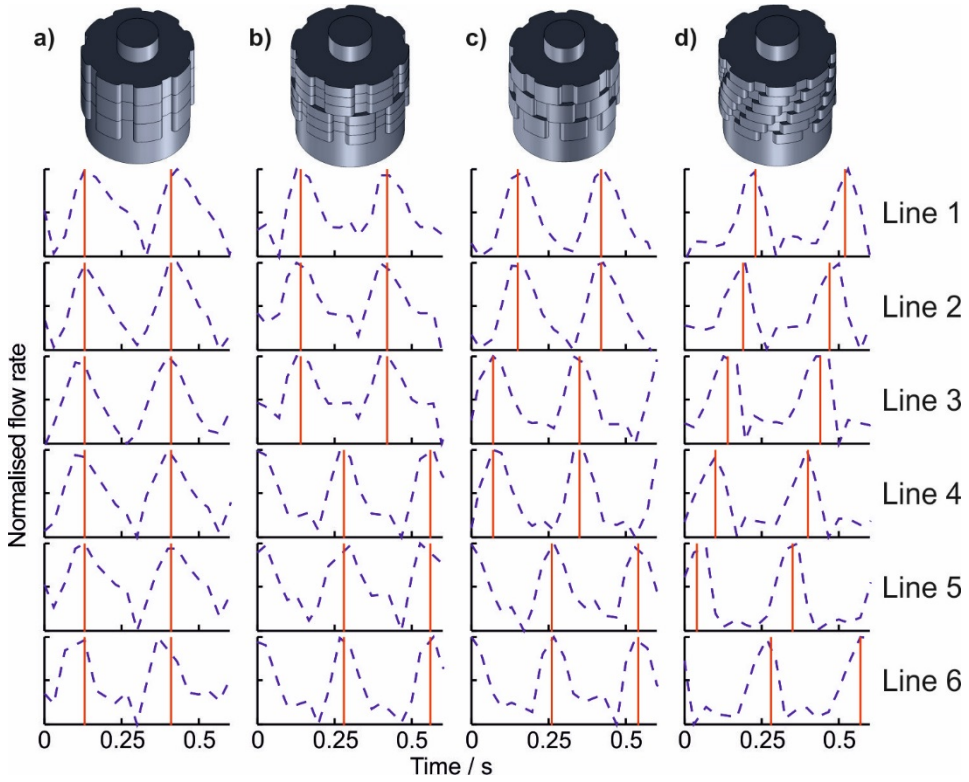

Figure 36 *Relative flow profiles of four different rotorhead geometries demonstrated by the normalised flow rate measured downstream a) lines 1-6 in phase b) line 1-3 in phase and lines 4-6 in phase with each other directly out of phase with lines 1-3 c) lines 1&2 in phase a third out of phase with lines 3&4 in phase a third out of phase with lines 5&6 d) Lines 1-6 sequentially a sixth out of phase.*

In addition, as shown in Fig. 36, the relative position of features for each pumpline and hence the timing of the pulse for each pumpline may be changed arbitrarily. Figure 36 shows the relative flow profiles obtained when using a series of rotor heads with the same number of features and spacing of these features, but with different offset around the rotorhead. These rotorheads were used to pump all six pumplines and the resulting downstream flow analysed simultaneously to measure the phase difference of the pulses. Column a) of Fig. 36 shows the case where all features are aligned and the resultant flow profiles of the fluid exiting all six pumplines were in phase. In column b), features on the top half of the rotorhead were anti-phase to those on the bottom half; hence flows in lines 1-3 were in phase, but exactly anti-phase to flows in lines 4-6. The phase offset can be arbitrarily designed for the application, with column c) showing an offset one third of the period and column d) one-sixth period offset. If desired it should be possible to combine antiphase flows into one channel to offset pulses in the overall flow, this could be particularly useful in continuous microfluidics when a smooth pumping and constant flow rate are required. However here I apply this antiphase approach to robust pulsed droplet generation as shown in the next section.

2.3.2 Characterisation of the droplet generation

Experiments were carried out to characterise pulsed droplet generation using the peristaltic micropump. Here two aqueous streams of coloured dye (East End Foods plc) representing a sample and a reagent are merged and introduced into a fluorous oil stream in a T-Junction chip (Channel height 800µm) as shown in Fig. 37. Rotorhead features were designed so that there is no overlap between the pulses from the oil and aqueous flows, as shown in Fig. 36c. This design ensures that the two phases are never pumped at the same time and are always delivered in anti-phase pulses. The aqueous pumplines used had a 245 µm ID, and a 320 µm ID pumpline was used for the fluorous oil. These pumplines were chosen to deliver roughly equal volumes for the combined aqueous phase and the oil phase. The motor was driven at 2 V DC to turn at 0.406 Hz. The setup used for this experiment was capable of simultaneously generating two droplet steams at two separate T-junctions. However, only one was used at a time in the experiments due to the limited view of camera for recording.

Figure 37 shows images of the T-junction correlated to the variation in droplet velocity downstream measured after the first turn of the serpentine channel (determined by the method described in section 2.2.3). As expected for the eight-featured rotorhead used, the frequency of the peaks (6.5 Hz) was exactly 16 times the frequency of the motor speed, with each peak in velocity generated by the injection of either the aqueous or the oil phase. As evidenced by the images shown in Fig. 37 the first peak clearly correlates to the injection of the aqueous stream (dyed red) into the main channel (t = 0 – 133 ms) with the second peak resulting from the aqueous phase being pushed downstream by the injection of the oil phase (t = 166 – 300 ms). The interface between the phases stretches (at 233 ms) and breaks a discrete amount of aqueous fluid from the main aqueous stream to form a droplet which is then carried further downstream (t = 266 – 300 ms).

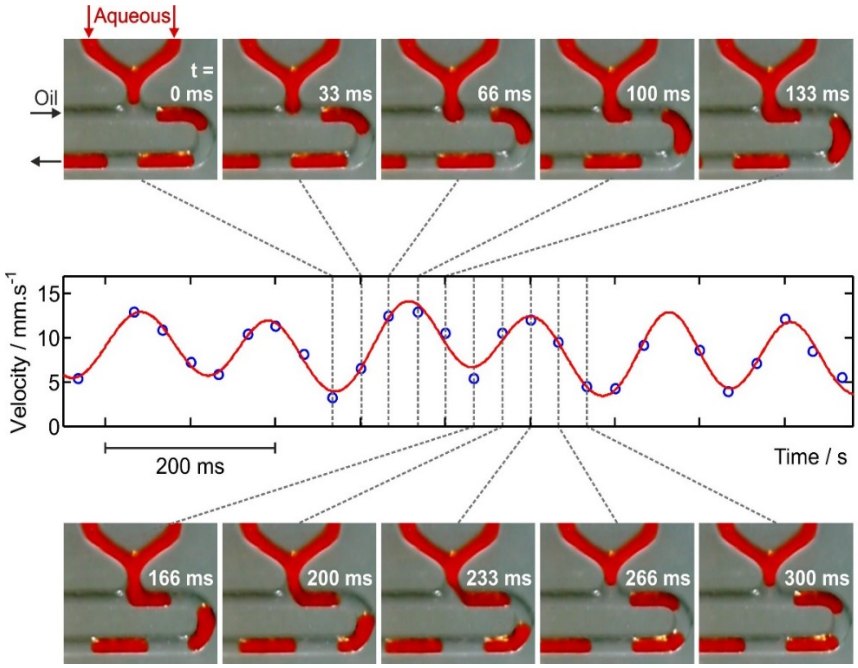

Figure 37 *Characterisation of the pulsed' regime of droplet generation: Images of T-Junction related to droplet velocity (mms^{-1}) measured downstream. t=0ms-t=133ms representing the aqueous pulse and t=166ms-300ms representing the oil pulse.*

The pulsed droplet generation regime should result in droplets with a volume defined solely by the volume injected into the main channel during each aqueous pulse, with one droplet generated for each complete pulse period (the time taken for both an aqueous and oil pulse). Hence when plotted the droplet generation rate should increase linearly with respect to motor speed (Hz) with a gradient matching the number of features on the rotorhead. To test these relationships, I designed a series of rotorheads with varied feature spacing from 0.88 mm to 2.40 mm, hence varying the volume delivered in each pulse. As with the previous experiment each of these rotors was designed with an overlap of the aqueous and oil rotorhead features to ensure no period of co-flow and the oil rotorhead feature spacing was varied exactly the same as the aqueous. Number of features *n* was also varied from 6-12 as rotorhead feature spacing (number of features and the relative overlap of oil/aqueous features cannot be varied independently). Figure 38 shows how the resultant droplet generation frequency (Figure 38a) and droplet length in 0.4 mm tubing (Figure 38b&c) varied for the range of rotorheads used when run at different motor speeds. Pumpline diameters again were 245 µm ID for the two aqueous pumplines and 320 µm ID for the fluorous oil chosen to deliver roughly equal volumes for each pulse of the aqueous and oil phases.

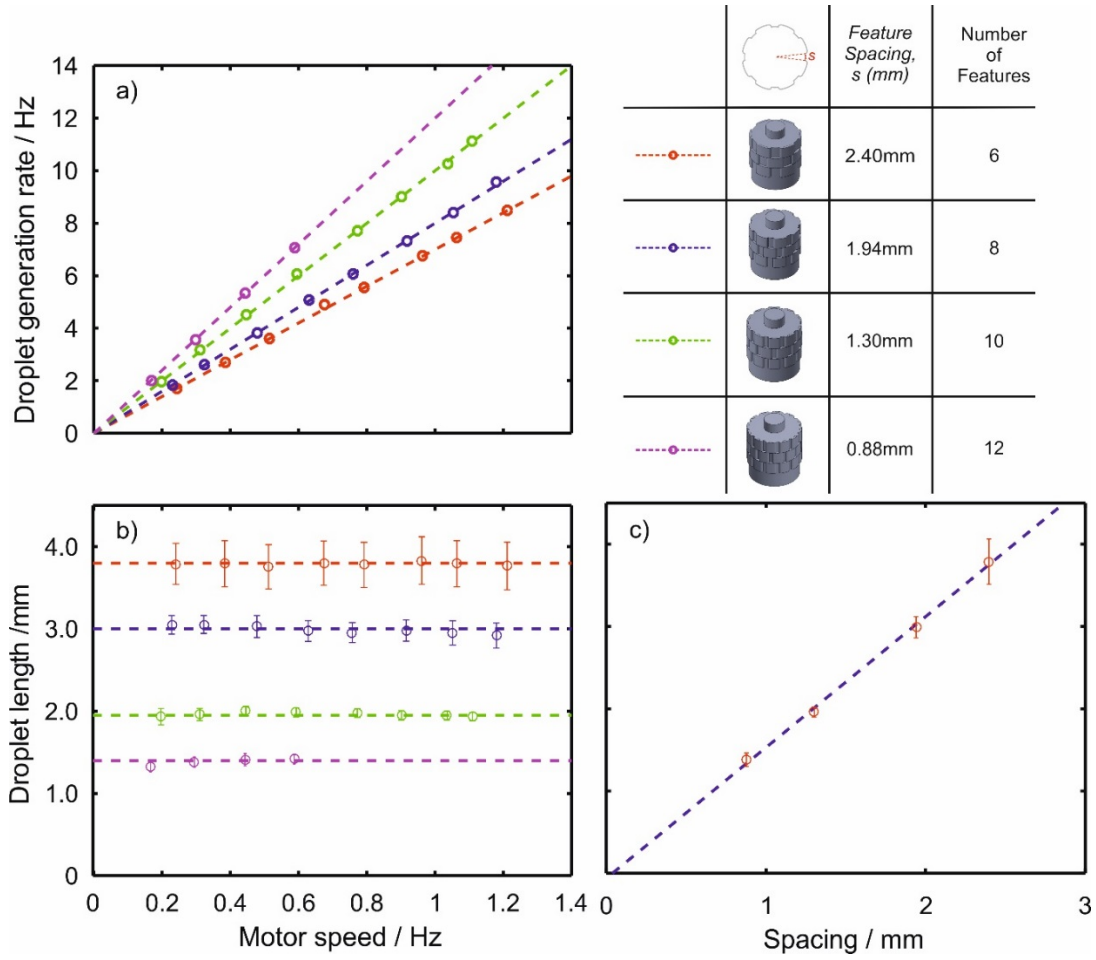

Figure 38 *Calibration data of pulsed droplet generation by micro peristaltic pump with a range of rotorhead dimensions. a) Droplet generation rate (Hz) vs Motor Speed (Hz). b) Droplet length (mm) vs Motor Speed (Hz). c) Droplet Length (mm) vs spacing (mm). Error bars in b) and c) represent the standard deviation of droplet length with each point representing over 100 droplets d) Rotorhead parameters used during characterisation.*

It is evident from Fig. 38a that for the wide range of droplet generation rates demonstrated, droplet generation rate increases linearly with motor speed, indicating the robust nature of pulsed droplet generation. (Note for higher motor speeds using the 12-featured rotorhead, the speed of the droplet flow could not be characterised due to the insufficient frame rate of the camera (30 fps)). Figure 38b demonstrates that for the pulsed method of droplet generation, droplet volume is defined solely by the liquid volume pumped into the channel during the aqueous pulse while the oil pulse defines droplet spacing. Figure 38b also demonstrates the flow rate invariance of the pulsed droplet generation regime, as when droplet generation rate is varied by altering motor speed, droplet size remains constant. The error bars in Fig. 38b and Fig. 38c show the standard deviations of droplet length with each point representing over 100 droplets. The relative standard deviation (RSDs) of droplet length were all between 4 and 6 %. The motor speed and hence flow rate invariance of droplet volume demonstrated here is in stark contrast to the traditional droplet generation strategies described in section 1.6, where constant and steadily co-flowing immiscible fluids are utilised, and the resulting droplet sizes are highly responsive to changes in the flow dynamics. Figure 38b also demonstrates that increasing the rotorhead feature spacing resulted in larger droplets generated as expected. Figure 38c shows the linear relationship between the mean droplet size and feature spacing, from experiments using a range of motor speeds. This is consistent with the relationship proposed earlier by equations 13-15 and shows that the size of droplets can be tuned by the rotorhead design as per the desired application.

2.3.3 Comparison to passive droplet generation

An experiment was designed to compare pulsed volumetric control-based droplet generation by the peristaltic micropump to “classic” passive methods using a syringe pump. Two syringe pumps (PHD 2000, Harvard Apparatus, with 1mL BD plastic syringes used) were used to drive fluorous oil and red food dye solution into the same PDMS chip that was used for the pulsed droplet generation (but without peristaltic pumping). The oil:aqueous flow ratio from the syringe pumps was set to be equal to the peristaltic pump ratio determined by the relative diameter of the pumplines (320:245).

Syringe pumps for these experiments were first run at a 40 µL/min total flow rate to prime the fluidic lines and to remove air from the lines. The flow was then stopped to allow the fluid to come to a complete standstill. Flow was re-started at 40 µL/min total flow rate and the resulting droplets were recorded in PTFE tubing out of the chip. The video was analysed by the same method described in section 2.2.3 and the results compared with an experiment using the peristaltic pump and the same chip, at the same linear velocity for the droplet flow as the syringe pump. The variations in droplet size and velocity are shown in Fig. 39a and Fig. 39c. Here the blue markers and line represent the droplets produced by the peristaltic pump and red markers and lines represent those from the syringe pump. Figure 39a show that as expected, due to the time taken for syringe pumps to come up to pressure and deliver a stable flow rate, the syringe pump took a much longer time to generate droplets of the same size than the peristaltic (this does not include the time taken for the plunger to come into contact with the syringe). The syringe pump’s flow rate instability can be seen in Fig. 39c; these show the linear velocity for the syringe pump, as it goes through multiple peaks and troughs before finally

becoming stable at approximately two minutes (not including time taken for the plunger to come into contact with the syringe). This is caused by the force required to compress the plunger of the syringe and for the system to come up to pressure. In contrast, the peristaltic pump was capable of delivering stable flow and droplet generation in a matter of seconds while the syringe pump system began generating very large droplets (approaching 10 mm in length) before stabilizing at 1.75 mm long droplets.

The experiment was also repeated at 80 µL/min total flow rate with the resulting droplet sizes and linear velocities shown in Fig. 39b and Fig. 39d respectively. For the increased flow rate, the syringe pump took approximately three minutes to build up the pressure and stabilize the droplet generation with very large initial droplet sizes. The same procedure was carried out with the peristaltic pump and the droplet generation stabilised within few seconds. It is important to note that droplets generated by the syringe pump at the higher flow rate were approximately 15% smaller than those generated by the slower flow rate. Reduction in droplet size can be attributed to the increase in shear forces with higher flow rate, which also increases the droplet generation rate. The peristaltic pump does not rely on these shear forces to generate droplets and so the droplet size remains the same.

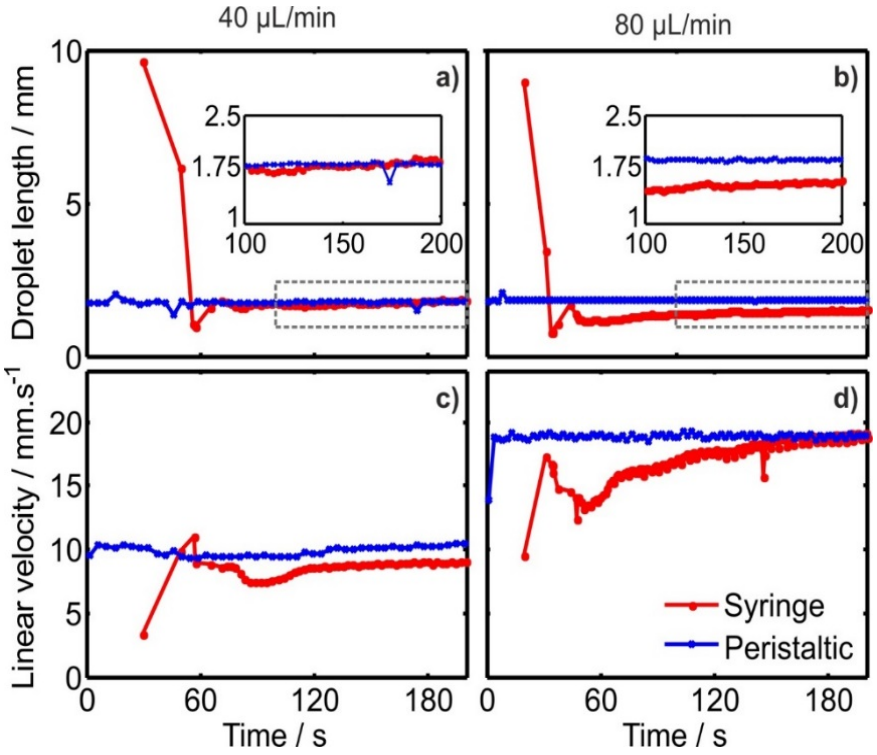

Figure 39 *Comparison of pulsed droplet generation to passive droplet generation at 40 µL/min (a) and c) and 80 µL/min (b) and d) total flow rate comparing droplet length (mm) (a) and b) and droplet linear velocity (c) and d) over time (s).*

2.4 The hard coding of chemical operations

In all previous experiments, the features on the rotorhead were designed with the same dimensions. However, this does not need to be so. As described in section 2.2.3 one exciting feature of this pump

is ability to “hard code” chemical operations by changing the feature dimensions on a single rotorhead, allowing for the generation of a “train” of droplets every rotation, where each droplet in the train has different predefined size, composition or oil spacing. This had been explored here to generate a dilution series

The system was first calibrated to quantify the range and reproducibility of concentrations of substrate that could be achieved. Red food dye solution was pumped through line 1, DI water through lines 2 and 3 and fluorous oil through lines 4 and 5 to generate sequences of droplets with different concentrations of dye. The droplets were filmed to ascertain the size distribution by the method described in section 2.2.3, the concentration of the dye in the droplets was measured using an inline spectrophotometer (Hassan, Nightingale et al. 2016) built in-house from a 516.5 nm light emitting diode (LED) and photodiode pair. The droplets were seen to be relatively uniform, with a relative size distribution of <5 % similar to my previous studies shown in section 2.3.2. Figure 40a shows the raw signal from the miniaturised in-line spectrophotometer flow cell, showing the intensity of light passing through the flow cell as a function of time. The signal is seen to fluctuate as oil and then droplets alternately pass through the light path. The food dye within the droplets absorbs some of the light and consequently, when a droplet is in the light path, the signal decreases. The responses corresponding to droplets vary in magnitude indicating the range of dye concentration in the droplets. The periodic nature of these responses clearly indicate that the system can generate droplets with a range of dye concentrations and with high reproducibility.

Absorbance colorimetry can be used to quantify the concentration of dye in the droplets with the light intensity transmitted through each droplet converted to an absorbance value, as shown in Fig. 40b. As absorbance is linearly related to concentration via the Beer-Lambert law, we can also express the concentration of each droplet in relation to the solution of dye supplied to line 1 as shown in Fig. 40c. It is interesting to note that considering the relative spacing of features on the rotorhead, we might expect a much larger range of concentrations. The reduced range recorded here is likely due to "carry-over" in the short channel in between the point at which the aqueous streams meet and the T-junction where the droplets form. Larger concentration ranges should be possible with optimisation of this structure; however, the measured 3.2 relative range was deemed sufficient to demonstrate the possibility.

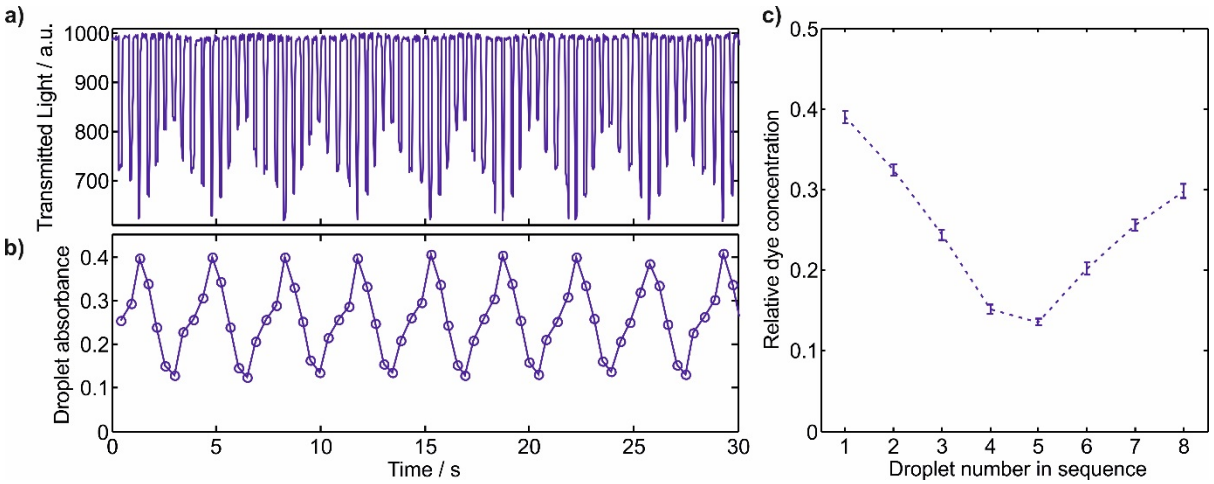

Figure 40 *Dilution series calibration with dye a) raw signal from the inline spectrophotometer, light intensity passing through the miniaturised in-line spectrophotometer flow cells against time b) Absorbance of droplets passing through the flow cell against time c) Relative dye concentration of droplets in the sequence.*

Following calibration with food dye, the system was applied to the quantification of the kinetics of the Trinder assay - a colorimetric glucose assay that uses a reagent based on glucose oxidase (Trinder 1969). The system is capable of performing rapid and continuous measurement of enzyme reaction kinetics by changing the concentration of substrate in each individual droplet of a droplet train and measuring absorbance in real time.

A 30 mM solution of glucose was supplied to line 1, premixed enzymatic reagent (Trinder 1969) was supplied to line 2 (with the same volume delivered to each droplet ensuring each droplet in the train contains the same amount of enzyme) and DI water was supplied to line 3. Fluorous oil was pumped through lines 4 and 5 (line 6 was not used). Repeated sequences of droplets were generated with glucose concentrations ranging from 4.1 mM to 11.7 mM (as calculated from the calibration data). The enzymatic glucose assay is described in equation 16.

Trinder assay

$$\text{glucose} + H_2O + O_2 \xrightarrow{\text{glucose oxidase}} \text{gluconic acid} + H_2O_2$$
$$2H_2O_2 + \text{4-AAP} + \text{TOPS} \xrightarrow{\text{peroxidase}} \text{quinoneimine} + 4H_2O \quad (16)$$

When the droplets exited the droplet generation chip the absorbance of the coloured product (quinoneimine) was measured by an optical method developed by Hassan et al. (Hassan, Nightingale et al. 2016) using multiple miniaturised in-line spectrophotometer flow cells for multiple detection points of the colorimetric reaction. The flow cells determine the initial reaction rate by measuring the colour development during the first 30 seconds after droplet generation (where the reaction starts).

The Michaelis-Menten equation 17 describes the relationship between the concentration of the substrate (in this case the target analyte of the assay) and the kinetics of the enzyme-based reaction.

Michaelis-Menten

$$V_0 = \frac{V_{max}[S]}{K_m + [S]} \quad (17)$$

Where V_0 is the initial reaction rate, [S] is the concentration of the substrate, V_{max} is the maximum possible rate (where [S] is in large excess) and K_m is the Michaelis constant representing the value of [S] at which $V_0 = ½V_{max}$ (Laurell, Drott et al. 1995). The standard practice of obtaining these values from the Michaelis-Menten equation is performed by running the reaction multiple times varying [S] and measuring V_0 in each case. The measured values of V_0 are then plotted against their respective [S] values and fitted to a Michaelis-Menten curve giving the values of K_m and V_{max}. In traditional spectrometry or well plate based assays, the repeated measurements can be very time-consuming and require very accurate execution and analysis of multiple experiments. This process may be made even longer if other parameters which affect the rate of reaction are to be tested such as temperature or the presence of molecular inhibitors.

Figure 41a and 41b show how the K_m and V_{max} values are obtained for a single sequence of droplets. Figure 41a shows the absorbance of each droplet in the sequence as it increases over time and passes through the detectors. The absorbing species in this assay is the product (quinoneimine) and consequently the rate of increase of the absorbance over time is a measurement of the rate of reaction. Thus, the gradient of the lines of best fit shown in Fig. 41a are direct measures of the initial rate of reaction. These rates should vary with glucose concentration as described by the Michaelis-Menten equation (Eqn. 17) thus; the droplets containing higher concentrations of glucose had the faster rates of reaction (steepest gradients). When the rates are plotted against glucose concentration and fitted with a Michaelis-Menten curve using non-linear regression (as shown in Fig. 41b) a good fit is obtained indicating that the reaction followed standard Michaelis-Menten enzyme kinetics, as expected. The values of V_{max} and K_m can be obtained from the fit, with Fig. 41b yielding values of K_m = 3.25 mM and V_{max} = 0.01 A.U.

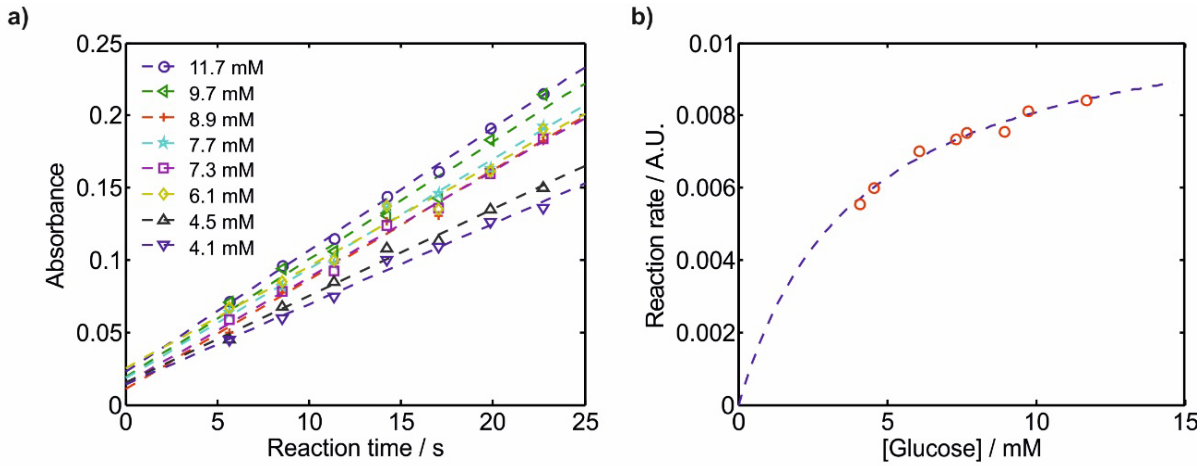

Figure 41 *Example of a single Michealis-Menten curve generated from a series of glucose concentrations measured over time generated from a single turn of the pump rotorhead measured using the multiple detector setup described in (Hassan, Nightingale et al. 2016) a) Absorbance of a number of different concentrations of glucose solutions over time. The gradient of which is the reaction rate b) Reaction rate of various concentrations of glucose in the trinder assay plotted against concentration denoting the Michealis-Menten equation.*

It should be noted that enzymatic kinematic measurements were achieved in the time taken to generate a sequence of droplets and flow them through the miniaturised in-line spectrophotometer

flow cells, less than 30 seconds in total. This process is automatic and the data for Fig.41b was obtained from a single sequence of droplets generated in a single turn of the pump motor. In contrast, if these values were to be obtained using standard benchtop procedures they would involve multiple manual experiments, take a long time and require much larger instrumentation.

With the pump continuously turning, it is possible to continuously monitor the K_m and V_{max} values. Figure 42a shows a sequence of Michaelis-Menten plots (like the individual plot shown in Fig. 41b) each of which were obtained from an individual sequence of droplets which were continuously generated and measured over 2 minutes. Values of K_m and V_{max} were obtained from each droplet sequence; thus, a continuous set of kinetic parameters can be obtained as shown in Fig. 42b and Fig. 42c. Continuous measurement such as this would be near impossible in bulk experimentation and allows the quantification of reaction kinetics in real-time. This could be used to explore the effect of perturbations such as variations in temperature or continuous monitoring of inhibiting species in real-time.

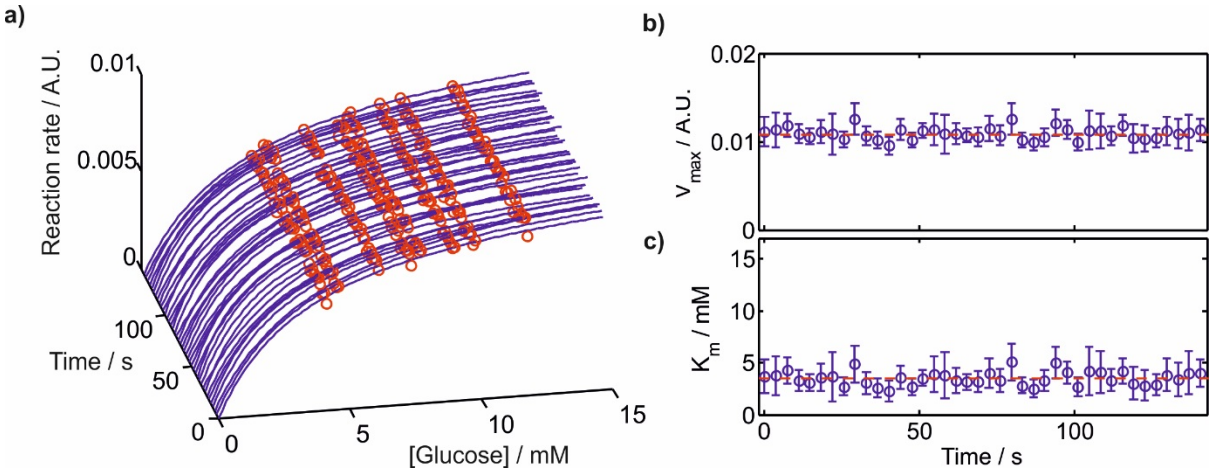

Figure 42 *Continuous analysis of glucose (trinder) assay kinematics a) Repeated dilution series reaction rates of various concentrations of glucose in the trinder assay plotted against concentration denoting the Michealis-Menten equation 20 repeats per minute over a 120 seconds period b&c) Calculated V_{max} and K_m values for repeated reaction rate experiments.*

With a single T-Junction, this device has potential in several research fields due to the relative ease of pre-programming a series of multiplexed assays, for example, the studying of reaction or crystallisation conditions, mass transfer or performing routine dilutions or titrations. It is also easy to imagine how this pump could be used to generate a droplet train where a number of assays are carried out in sequence to test for a variety of biomarkers or a system could be designed with standards and blanks to calibrate the measurements “on the fly”. This is further explored in chapter 4

2.5 Conclusions of Chapter 2:

In this chapter, I have:

a) Detailed the design and fabrication of the peristaltic micropump and novel monolithic microfluidic chip.

b) Characterised the pulsed nature of the micro peristaltic pump, which is the basis of the chosen droplet generation regime.
c) Characterised this pulsed droplet generation regime for a variety of droplet sizes, droplet generation rates etc., and described the invariance in droplet size with changes to flow rate.
d) Compared this invariance in droplet size demonstrated by the peristaltic micropump to 'classic' passive droplet generation with syringe pumps.
e) Furthermore, introduced this micropump design's ability to hard code chemical operations into the design, which will be further developed throughout this thesis.

The work presented in this chapter was presented as two poster presentations/conference papers in Microtas 2016 available in the appendices. In conclusion, this peristaltic micropump design shows promise for stable droplet generation both in the lab and in the field, with the invariance of droplet size for flow conditions and hard coding of chemical operations being key advantages over previously reported systems.

When compared to the traditional syringe pump/passive droplet generation, the flow rate invariance in droplet size, fast stabilisation and self-priming of the fluidic lines demonstrated by the peristaltic micropump, as well as its relatively small footprint and simple operation make it much better suited to a variety of field applications such as point-of-care monitoring. Additionally unlike passive droplet generation (Tice, Lyon et al. 2004) and many of the other active droplet generation regimes, the droplet size in this peristaltic pumping and pulsed droplet generation regime solely depends on the volume of liquid pumped in each period, unaffected by fluid properties such as viscosity and interfacial tension. This is explored in section 3.3.3 for a range of viscosities encompassing the viscosity of biological samples such as serum, plasma and whole blood (by dissolving various amount of sucrose in DI water) and in section 4.2, for the same range.

It is hypothesised that this invariance to all flow and fluid properties is due to the effect of this pulsed flow on the capillary number. As mentioned in chapter 1 this is a dimensionless number often used to determine the breakup regime of droplets in microfluidic channels. Equation 2 shows a form of the equation used to calculate the capillary number for this T-junction/Cross flow geometry (detailed in chapter 1)

Capillary number in Cross/co-flow geometry $$Ca = \frac{\mu_O U}{\gamma} \quad (2)$$

Delivering the fluids in pulsed flows results in a zero volumetric flow rate of the carrier fluid when the dispersed phase incursion occurs. In an ideal case, this should produce a zero capillary number no matter viscosity of the fluids, interfacial tension between them or the overall average volumetric flow rate. The instrumentation presented here is far from optimised. This peristaltic micropump and droplet generation method are further optimised in the following chapters and applied to prototype systems. Of particular importance is the optimisation presented in the further chapters.

Additionally in these experiments, I found a periodic variation in droplet length for many of the experiments. Figure 43 shows droplet length over time data using a particular poor performance pump with a relatively large RSD (15%) periodicity of the droplet length that clearly shows the periodicity.

Although many of the pumps provided a lower RSD, it was difficult to control the RSD to be lower than 5%, which is an indicator of 'good' droplet generator in comparison to a stabilised passive droplet generator.

Chapter 3 – Optimisation of the programmable peristaltic micropump for pulsed droplet generation

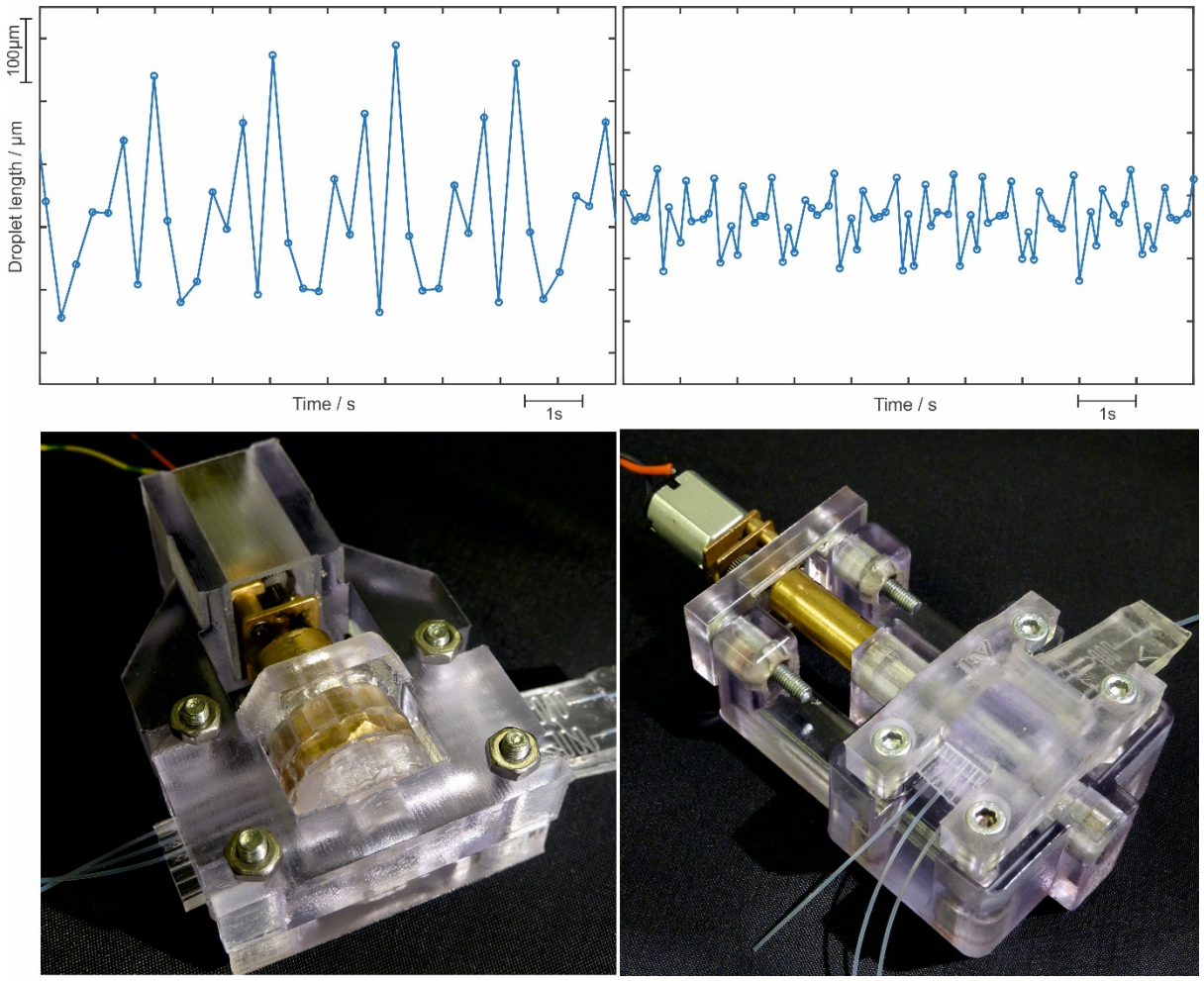

This chapter presents the optimisation of the push-pull peristaltic pump described in Chapter 3, with a focus on improving uniformity of the droplets produced. Here I also explore possible causes of variation and investigate new design elements to decrease this variation. Finally, I present data from the optimised version of this peristaltic micropump.

This chapter presents the further optimisation of the push-pull peristaltic pump described in Chapter 2, with a focus on improving uniformity of the droplets produced. Data presented within this chapter has informed a journal paper (Nightingale, Evans et al. 2017) in Lab on a chip in collaboration with Dr Adrian Nightingale and Dr Sammer Ul Hassan. In the previous experiments in Chapter 2, I found a periodic variation in droplet length for many of the experiments. Figure 43 shows droplet length over time data using a particular poor performance pump with a relatively large RSD (15%) periodicity of the droplet length that clearly shows the periodicity. Although many of the pumps provided a lower RSD, it was difficult to control the RSD to be lower than 5%, which is an indicator of 'good' droplet generator in comparison to a stabilised passive droplet generator. Possible reasons for this variation were explored and new design elements investigated. The new design provided greatly enhanced performance with RSD lower than 5%, with most copies of the pump providing uniform droplet generation with an RSD less than 2%.

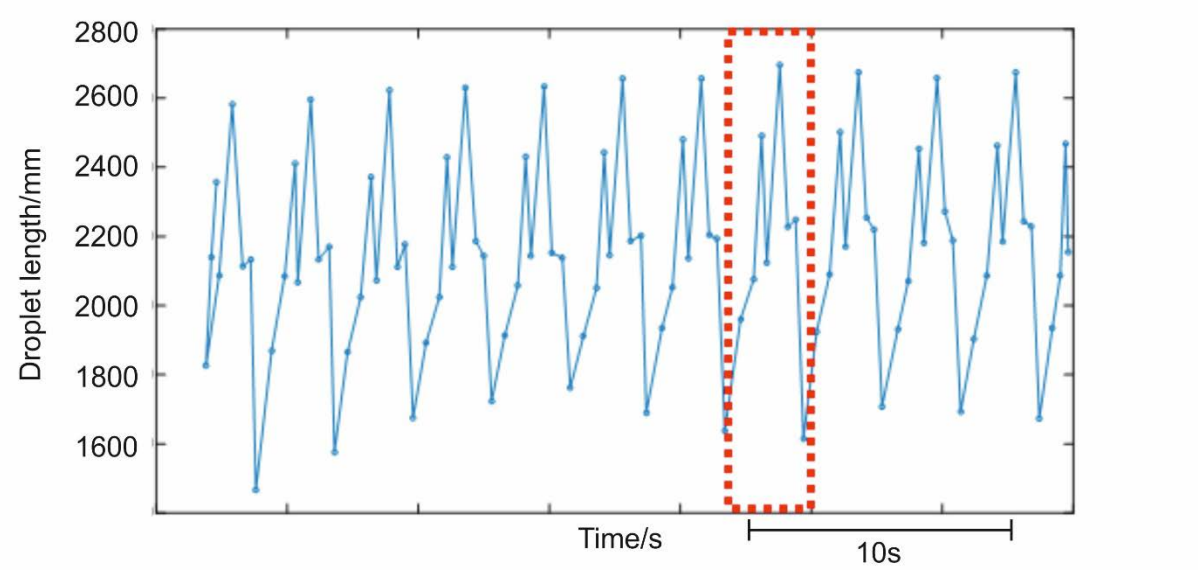

Figure 43 *Periodic nature of and particularly large variation of droplet length of the non-optimised peristaltic micropump 8 droplets generated per turn (Red box represents a single turn of the rotorhead).*

From Fig.43, the periodic variation of droplet size seems to be directly linked with the number of features on the rotorhead (here number of features in the rotorhead (*N*) is 8), with the period being equal to the time taken for one turn of the rotorhead. The pattern during the period is affected by the motor speed, but the maximum and minimum value of droplet length are unaffected. This periodicity in droplet sizes is undesirable for most applications, as they require stable droplet production with a low RSD in volume/size throughout the turn of the rotorhead. Manufacturing issues likely cause this periodic change in droplet size. After some investigation, it was found that the connecting bolt between the motor shaft and rotorhead was fabricated with an off centre hole and so the rotorhead

was off centre causing radial runout. Other possible reasons are axial run out caused by the motor wobble and the concentricity of the pumplines and rotorhead.

3.1 Iterative design

To carry out assays in droplets repeatedly for continuous monitoring it is vitally important to produce monodisperse droplets with reliable contents. The periodic variation and dispersity of droplet volume produced by the previous pump design (present in data shown in Fig. 43) is not sufficient moving forward. With the goal of reducing the dispersity so that the relative standard deviation of droplet volume produced to below 5% some of the device components were replaced and tested. To reduce run out and keep constant pressure on the pumplines as well as provide a smooth rotation of the rotorhead, the connecting bolt between the motor shaft and rotorhead (Fig. 44a) was replaced. The connecting bolt was first replaced by a 3D printed shaft extension (Fig. 44b) however during early testing this shaft was too susceptible to heat caused by friction and deformed during operation. The plastic shaft extension was replaced with an all-in one 3D printed approach shown in Fig. 44c and later replaced by a metal shaft extension (technical drawings in appendices) with ball bearings to decrease the friction in the optimised design (Fig. 45).

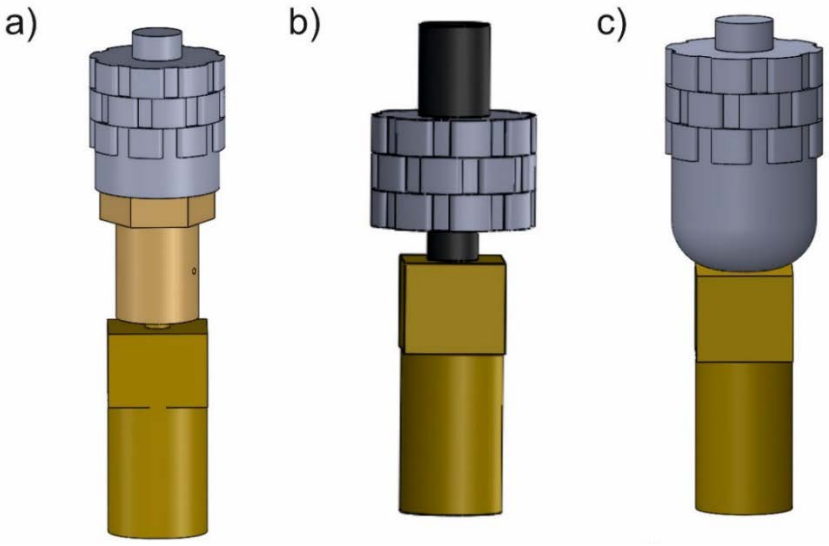

Figure 44 *Iterative pre-optimised designs a) Active components of the original design featuring brass bolt b) 3D-printed bolt replacement c) All-in-one (no-bolt) 3D printed rotorhead.*

During testing, some issues with concentricity of the bed were seen with a particularly inaccurately fabricated chip producing particularly erroneous results (not shown here). This highlighted the importance of concentricity and the fabrication of the chip as contributing factors to the run out seen in previous designs. Ensuring the pulsations are as robust and repeatable as possible is of paramount importance for droplet generation; the larger design was somewhat simplified a shaft extension and bearings used in the hope of further reducing axial run out from 'motor wobble'. The bed design was also modified to ensure that the chip is concentric with the rotorhead. In the improved design the chip is better held, with the diameter of the chip bed perfectly fitting the rotorhead outer diameter. The chip fabrication was more thoroughly regimented, with excess PDMS scraped from the mould and

great care taken throughout the whole process. After multiple rounds of modification, the new optimised design (shown in section 3.2) showed dramatic improvement, reliably producing droplet populations with relative standard deviations in length of less than 2%.

3.2 The optimised design

The optimised design is shown in Fig. 45. With further technical drawings included in the appendices. Data demonstrating the improvements to the droplet generation regime and droplet dynamics over time are shown in this chapter. As well as comparisons of this design to the standard continuous pressure driven flow method of droplet generation and a repeat of the example hard coding setup of droplet generation now using the optimised setup. Work presented in this chapter is the basis for a journal paper published in in Lab-on-a-Chip (Nightingale, Evans et al. 2017).

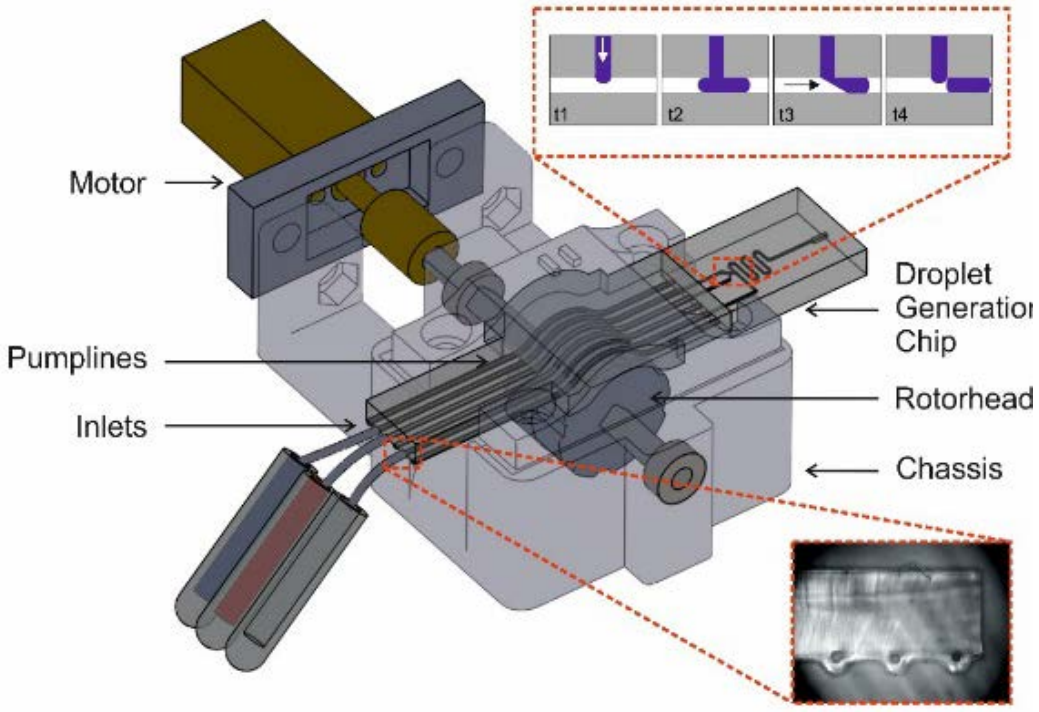

Figure 45 *Schematic showing pump operation. The 3D printed supporting chassis is shown semi-transparent to highlight the operational parts – motor, axle, rotorhead, PDMS pumpline chip and adjoining droplet generation chip. Inset top shows the method of droplet generation. Inset bottom shows the cross section of the monolithic pumpline chip.*

3.2.1 Fabrication of the optimised design

All components of the pump are shown in Fig. 46 detailed in the exploded diagram. The main pump chassis, rotorhead, pumpline support bed and motor attachment plate were all 3D-printed and shown in photograph inset. Each component was modelled in CAD software (SolidWorks, Dassault Systemes) and then printed in "VeroClear" material (VeroClear-RGD810) using an Objet500 Connex3 polyjet printer (Stanford Marsh Ltd) (3D models of the printed part files are available at http://pubs.rsc.org/en/content/articlelanding/2017/lc/c6lc01479h#!divAbstract). A DC motor (Pololu 210:1 Micro Metal Gearmotor) was attached to the chassis via the motor attachment plate. The motor was used to drive the rotorhead (16.25 mm in diameter including raised features), which was fixed on

a stainless-steel square shaft (~50 mm length, 3 x 3 mm cross section, Active Robots Ltd, UK), manually machined to give a 3 mm circular cross section at each end to fit the ball bearings (Technobots Ltd, UK). Additionally, a "D" cross section was machined into one end to enable attachment to the brass shaft coupler (Technobots Ltd, UK) which connected the main shaft to the motor. A silicon lubricant (Rocol Silicone Grease SAPPHIRE Aqua-Sil) was used to lubricate the movement of the rotorhead on the pumplines decreasing torque experienced in the pump and increasing pumpline lifetime.

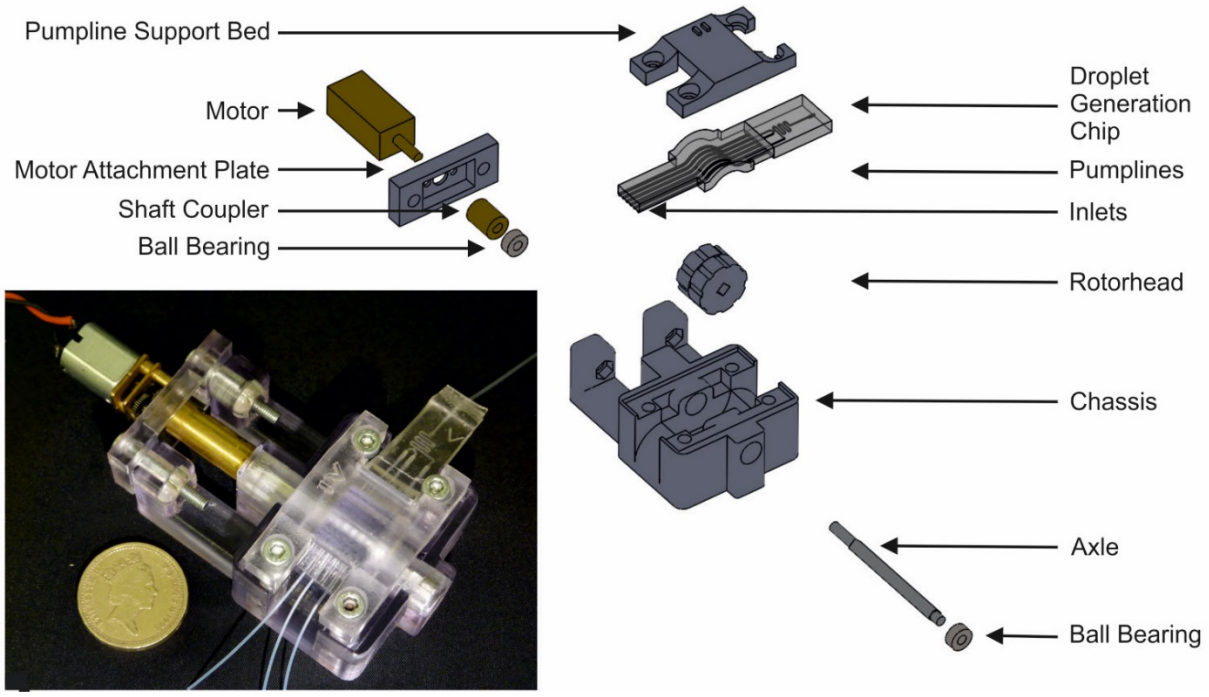

Figure 46 *Exploded view of the optimised peristaltic micro-pump (inset: Photograph of the micro-pump (pound coin for scale)).*

As in the previous design, the PDMS chip, which handles all fluidics, consists of two parts: the pumplines and a droplet generation chip which are fabricated separately and then joined as detailed in section 2.2.2. To assemble the pump M3 nuts and bolts are used to hold the pump support bed and the motor attachment plate to the chassis. Fluid was brought to the pumplines via PTFE tubing (ID 0.3 mm, 0.15 mm wall) inserted into the pumpline channels. The oil used for all testing was a low-viscosity fluorocarbon (FC-40, 3M, UK) containing a 1.8 % w/w concentration of non-ionic tri-block copolymer surfactant synthesised in-house. The aqueous phase varied depending on experiment. The fluid was pumped by supplying the motor with a constant power supply between 1.5 and 6 V and droplets were generated in the droplet generation chip (channel dimensions 300 µm wide, 450 µm deep). This channel size may not be completely reliable in the PDMS casting procedure due to the simple casting procedure and PDMS distensibility. However, the pulsed method is invariant to channel size so long as the volume delivered in the aqueous pulse (V) is larger than the volume of the T-junction (Vfill). Droplets are subsequently taken off-chip using PTFE tubing (0.4 mm ID, 0.15 mm wall) inserted into the chip outlet.

3.3 Characterisation of the pumping system

All the previous experiments to characterise the pumping system were repeated for this new design (Fig.s 47-54) and generally produced much more reliable and repeatable results with lower polydispersity. As with previous experiments to characterise the generated droplets, a portable microscope camera (dnt Digimicro Mobile Mikroskope) was used to record either directly at the T-junction of the chip or off-chip within the PTFE tubing. The videos recorded were analysed using Droplet Morphology and Velocimetry (DMV) software (Basu 2013) and the data subsequently processed in Matlab. Droplet volume etc. was calculated from DMV measurements of droplets recorded within tubing of known cross sectional area.

3.3.1 Characterisation of the pump in single lines

As with the previous design, the pump's ability to deliver accurate and tunable flow was first determined for individual lines pumping fluid in isolation; a summary of these tests is shown in Fig. 47. Fluid was pumped through pumplines of different diameter (245 μm and 320 μm), at different motor speeds and using different rotorhead designs (varying the spacing between pronounced features). The instantaneous flow rate was characterised by aspirating droplets (formed by moving the inlet between fluorous and dyed aqueous fluids), recording their movement downstream and then analysing the video. The improvements of this design are clear with a smaller variation in pulsation size.

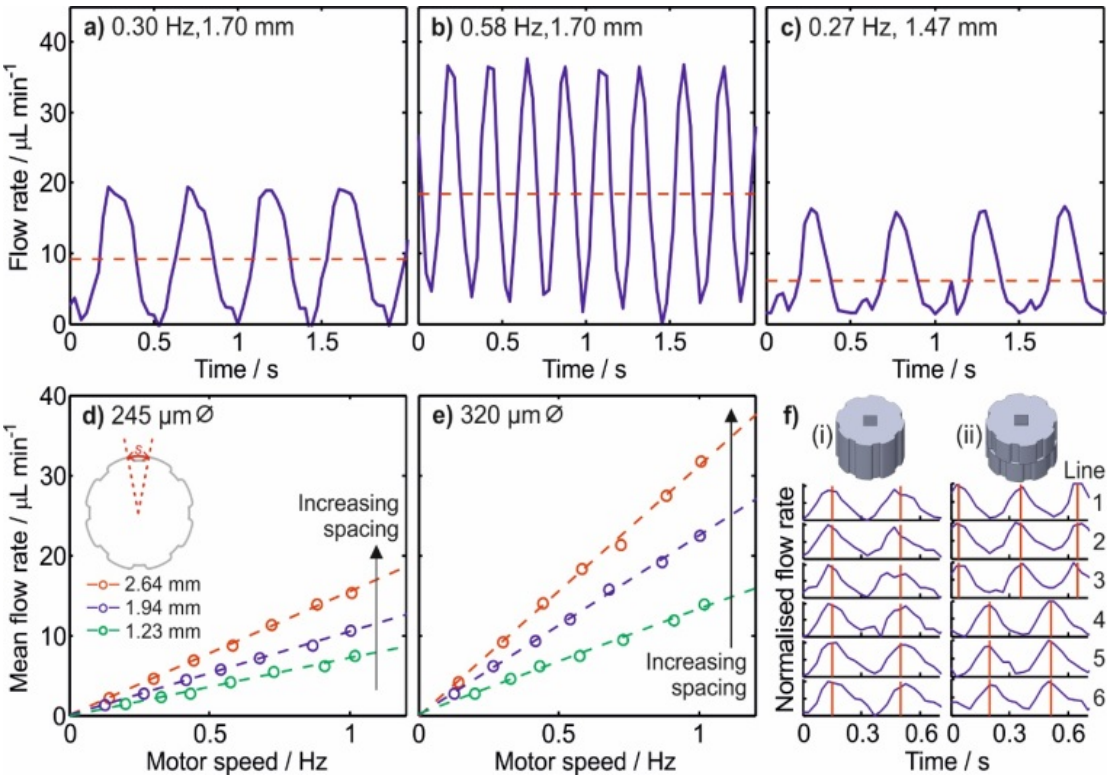

Figure 47 *Characterisation of flow in individual pump lines of the optimised peristaltic micropump. a-c) Volumetric flow rates for differing motor speeds and rotorhead feature spacings. Solid blue lines show transitory flow rate over time while dashed red lines show mean flow rates. d-e) Plots showing how mean flow rates can be tuned by controlling feature spacing, motor speed and cross-sectional area (each data point represents over 100 measurements). f) Plot showing the relative flow profiles for all six pumplines when using rotorheads with features aligned (i) and features anti-phase offset (ii).*

As expected for a peristaltic pump, the resulting flow was characteristically pulsatile. In all cases, the flow rate was seen to periodically rise and fall over time (Figure 47a-c), with each period (peak and trough) corresponding to a single feature on the rotorhead. Figure 47a and 47b show data for flow rate obtained using the same channel diameter (320 µm) and rotorhead spacing (1.7 mm, defined as shown in Fig. 47d inset) but with different motor speeds. As the motor rotation speed doubled from 0.30 Hz (Fig. 47a) to 0.58 Hz (Fig. 47b) the pulse period halved (375 to 175 ms) and both the peak flow rate and the mean flow rate (dashed red line) doubled. It should be noted that in both Fig. 47a and b, the area under each peak (which corresponds to the volume pumped in a single pulse) stayed constant regardless of motor speed, as each pulse corresponds to the volume in the pumpline occluded between adjacent features on the pump head. The average flow rate can also be changed by keeping the motor speed constant and changing the volume occluded between features as shown in Fig. 47c, where the space between the features was reduced from 1.70 mm in Fig. 47a to 1.47 mm.

To quantify how the pump could be rationally designed to tune net flow rate, flow rate was measured while systematically varying the motor speed for three different rotorhead feature spacings and constant cross-sectional area, as shown in Fig. 47d. In each case, the pumpline diameter was kept constant at 245 µm. For all rotorheads, increasing the motor speed had the effect of linearly increasing the mean flow rate. The gradient increased with feature spacing due to the increase in the volume

delivered in each individual pulse. Fig. 47e further shows that wider channels (diameter 325 µm) allow higher flow rates due to the increased volume delivered in each pulse, with the increase approximately equal to the ratio of the channel cross sectional areas. Thus, careful design of the pump can tune the flow rate as required, with multiple different design options available (channel cross-section, spacing of the feature, number of spacing and pumping frequency).

The relative position of the rotorhead features for each individual pumpline can determine the relative timing (phase) of pulsing in different pumplines. Fig. 47f shows the flow profiles obtained when using rotorheads with the same topology (i.e. the same number and size of features) but with the topology offset around the rotorhead. These rotorheads were used to pump all six pumplines and the resulting downstream flow analysed simultaneously so as to characterise the phase difference of the pulses. Where the features were aligned, as shown in Fig. 47f(i), the obtained flow profiles were in phase. By contrast where the features on the top half of the rotorhead (which contacts lines 1-3) were anti-phase to those on the bottom half (which contacts lines 4-6) the resulting flow profiles in lines 1-3 were in phase, but exactly anti-phase to those in lines 4-6, as shown in Fig. 47f(ii). The rotorhead can be easily redesigned to deliver any arbitrary phase offset that might be required for each individual line. Importantly, however, the ability to introduce oil and aqueous fluid in alternating pulses into a junction enables robust droplet generation. When compared to the previous characterisation data (2.3.1 Characterisation of the pump) it is clear that the new design delivers much more robust and repeatable pulsations as shown by the more uniform peak values and waveform shape. As the pulses define the droplet/oil segment volume, this is important for improving the droplet polydispersity.

3.3.2 Characterisation of droplet generation using anti-phased oil/aqueous pulses

To generate droplets, as shown in the images in Fig. 48, two aqueous streams were merged at a Y-shaped conjunction and then segmented into droplets by the oil at a T-junction. The relative cross sectional areas of the pumplines (245 µm ID aqueous pumplines and 320 µm ID oil pumpline) gave approximately equal volumetric flow of the different phases. The spacing between features on the rotorhead were deliberately offset, as shown in Fig. 47f(ii), so that the oil and aqueous flows were delivered in anti-phase pulses to the T-junction where the droplets were produced. The droplet velocity measured after the first bend of the channel shows clear periodicity against time. Each period is composed of two flow pulses as labelled with red and blue dashed lines respectively. A comparison of the video and flow velocity shows that the incursion of the red aqueous stream into the main channel (top images) gave rise to the pulse labelled with red dashed lines. While the following velocity peak (blue dashed lines) corresponds to the oil stream pushing the aqueous incursion downstream (bottom images), breaking it from the main aqueous stream to form a discrete droplet which is then carried downstream. In brief, each droplet was produced by firstly incursion of aqueous stream into the main channel and then ‘chopping’ of the aqueous incursion into a droplet by the pulse from oil stream. Compared to the characterisation of the previous design shown in Fig. 36 (Section 2.3.1) it is evident that the pulsations (hence volume delivered per pulsation and droplet volume) are much more reliable with this new design.

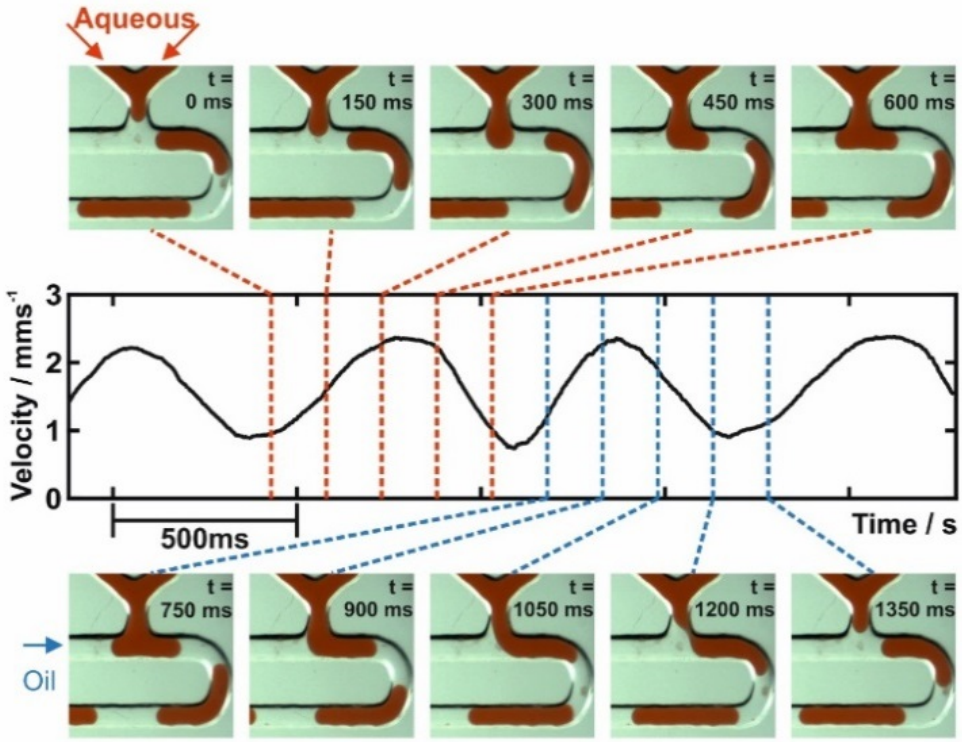

Figure 48 *Correlation of optical images of droplet generation at a T-junction with downstream flow velocity. Incursion of the aqueous phase into the main channel (images top) is associated with a single velocity pulse peak, while its subsequent break-up by oil flow (images bottom) is associated with the following velocity peak.*

This method for droplet generation implies that the volume of each droplet should be solely defined by the volume injected by the corresponding aqueous pulse. A series of rotorheads where the spacing between features (defined in Fig. 49 table) was systematically varied was designed to test this. Volume delivered in each pulse should vary linearly with feature spacing (see Fig. 49). For all rotorhead designs the droplet generation rate increased linearly with motor speed (Fig. 49a), indicating each pulse period universally generated a single droplet. A maximum generation rate of approximately 12 Hz was obtained here, however higher rates could be obtained by using rotorheads with more features, a more powerful motor or splitting the droplets downstream(Li and Ismagilov 2010).

The droplet size remained constant irrespective of motor speed (and hence total flow rate) and droplet generation rate, as shown in Fig. 49b, with larger rotorhead spacing producing larger droplets (Fig. 49c). With coefficients of variation in droplet volume as low 2% (as indicated by the error bars in Fig. 49b and c) which compares favourably with previously reported droplet generation methods (Tan, Murshed et al. 2008, Jung, Retterer et al. 2010, Abate, Kutsovsky et al. 2011). This low coefficient of variation in droplet volume was shown to be repeatable across many experiments a considerable improvement over the previous design.

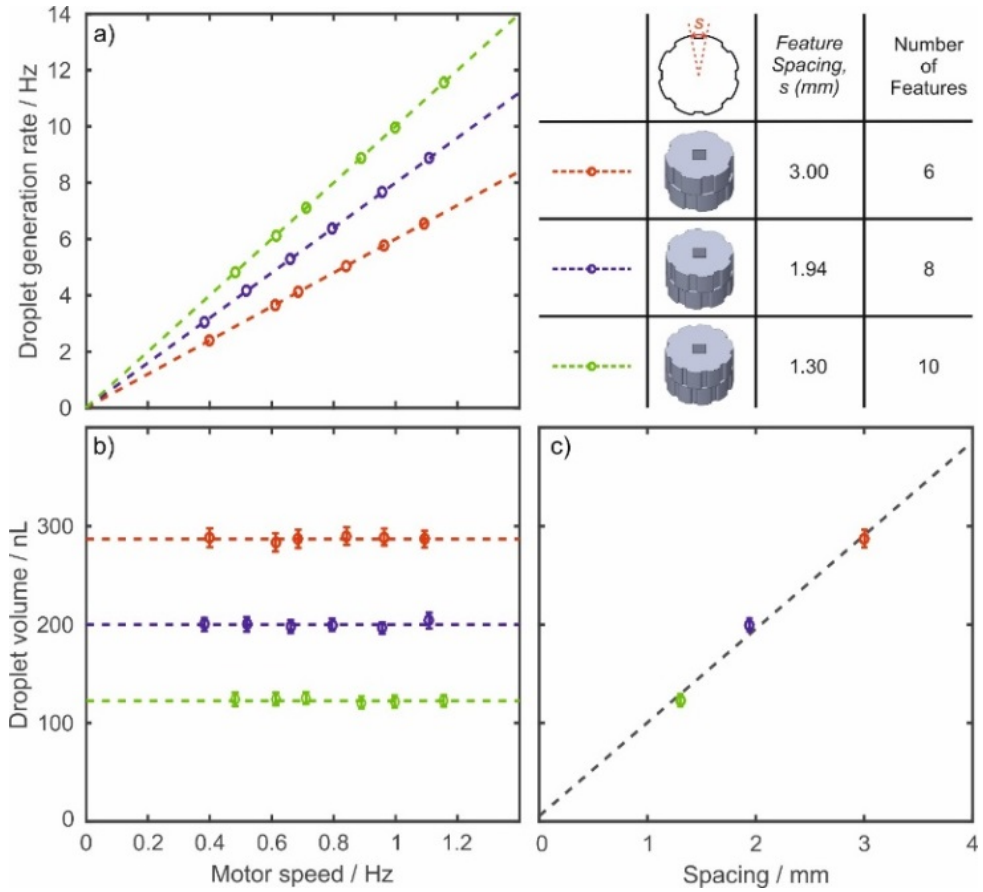

Figure 49 *Droplet generation dynamics for rotorheads with different feature spacing. a) Droplet generation rate increases linearly with motor speed, with the gradient corresponding to the number of features on the rotorhead. b) Droplet volume corresponding to each feature spacing remains constant irrespective of motor speed. Error bars show the standard deviation in droplet volume, typically between 2 and 5 % RSD c) Droplet volume increases linearly with feature spacing. Error bars represent the total standard deviation of droplet volume over different motor speeds.*

3.3.3 Invariance to viscosity

The effect of aqueous-phase viscosity on droplet generation was investigated as microfluidic systems are often applied to the manipulation and analysis of viscous biological media (Sackmann, Fulton et al. 2014). Solutions of varying viscosity were made by dissolving sucrose in water at concentrations between 0 and 60 % by mass. Droplets were generated using the same pump and droplet generation chip as previous tests, using a rotorhead with 8 features and a spacing of 1.94 mm and keeping the motor speed constant at 0.4 Hz. The droplets exited the chip into PTFE tubing (inner diameter 0.32 mm) where they were imaged using a USB microscope and the subsequent video analysed. Figure 50 shows the obtained droplet sizes as a function of the sucrose loading (top) and corresponding viscosity (bottom, obtained from reference values (Swindells, C.F. et al. 1958)). This range encompasses the viscosity of typical biological samples such as serum, plasma and whole blood.

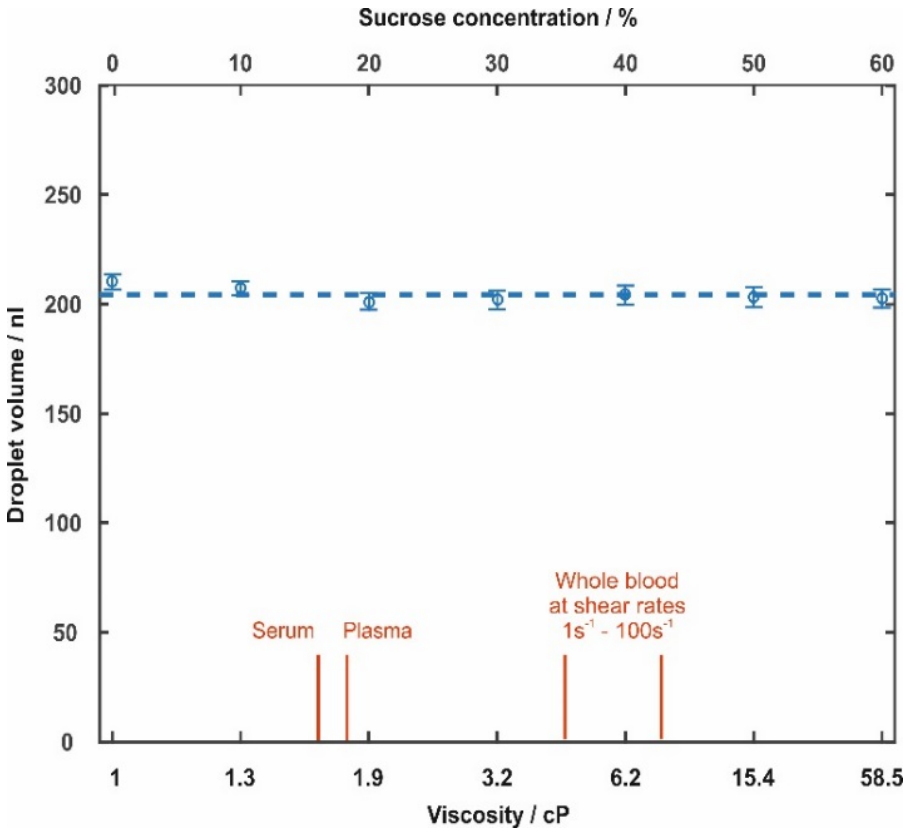

Figure 50 *Droplet volume (nl) vs viscosity (cP) for varying concentrations (by weight) of sucrose solution droplets produced by the improved peristaltic micropump design (with viscosities encompassing a range of biological sample viscosities). Error bars represent the standard deviation (%) of droplet volume.*

Mean droplet size was invariant with viscosity, consistent with the proposed method of droplet generation, showing how this droplet generation technique is suitable for applications where viscous biological fluids are sampled or processed or dealing with liquid samples with varied viscosities over time. Compared with traditional co-flowing droplet generation using syringe pumps, the anti-phase pulsed approach described here offers continuous operation (with no need to stop or refill) within a much smaller total package. More importantly, the short distance and small fluidic volume from rotorhead to droplet generation point (approximately 1 cm and 2 µL) means the system should achieve stabilised droplet generation much faster than syringe pumping. After disassembly and reassembly of the pump between experiments coefficient of variation in droplet volume remained low (below 2 %).

The ability of the pump to operate against an applied pressure was also tested by continuously pumping into a sealed container fitted with a pressure sensor (MPX4250A, RS, UK). The pump successfully operated above the pressure sensor's maximum of 1.6 bar.

3.4 Comparison to passive droplet generation

To compare the difference in droplet generation dynamics with traditional passive generation, droplets were first generated using two syringe pumps (PHD 2000, Harvard Apparatus, with 1mL BD plastic syringes used) pumping fluorous oil and red food dye solution into the same droplet generation chip. The velocity and size of droplets were measured downstream and then compared to droplets generated using the peristaltic pump under the same total flow rate and oil to aqueous ratio (0.85). At a total flow rate of 80 µL/min the syringe pumps took approximately 60 seconds to come up to pressure and deliver stable flow as shown in Fig. 51a and b.

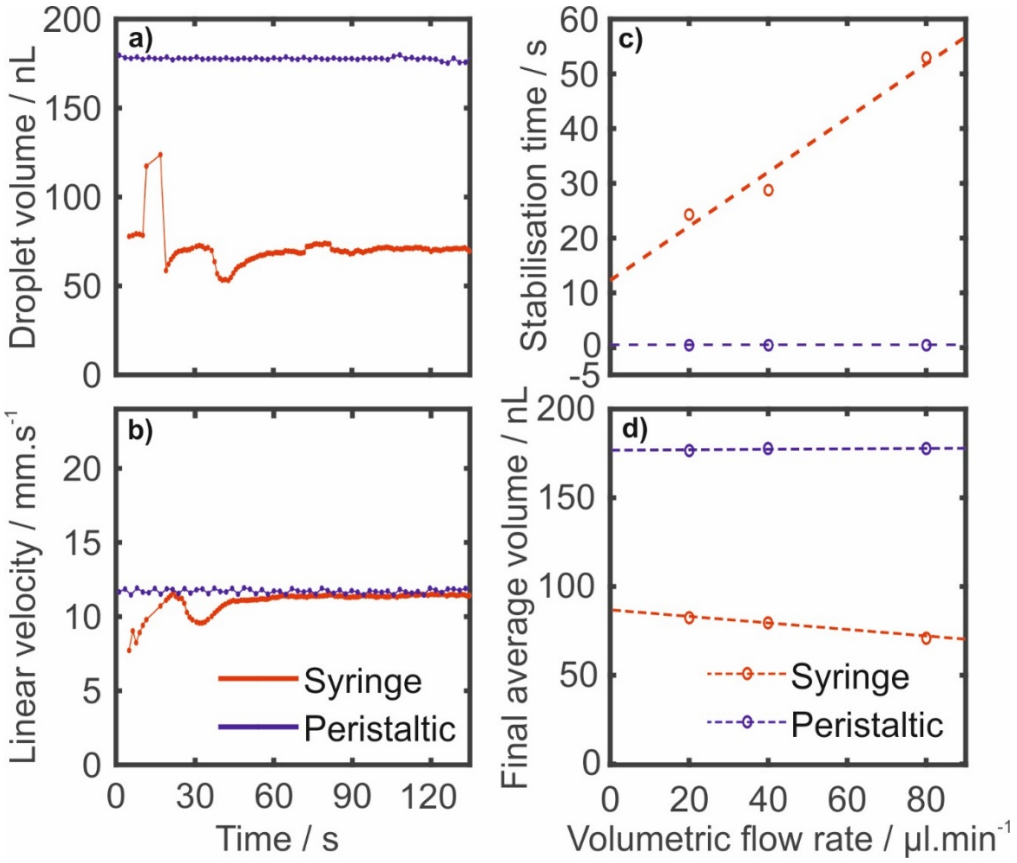

Figure 51 *Comparison of droplet generation via anti-phased peristalsis (blue) and syringe-pumped traditional passive co-flow (red). a) and b) show the variation of droplet volume (a) and droplet linear velocity (b) as a function of time following pump start-up. The time taken for the flow to stabilise and the stabilised droplet volume are recorded in c) and d) respectively as a function of the total volumetric flow rate.*

The size of the droplets varied from approximately 60 to 120 nL before stabilising at 71.0 nL. By contrast the peristaltic pump delivered stable droplet generation from the first droplet produced (in less than 0.5 second), also indicating that the pump could be operated in a stop/start fashion or for droplet generation-on-demand applications. For lower total flow rates at 40 and 20 µL/min, the stabilisation time required for the syringe pump improved (to a minimum of 25 s at 20 µL/min, see Fig. 51c) but were consistently much worse than the peristaltic device which generated droplets with negligible stabilisation time. Comparing the size of the droplets once stabilised, (Fig. 51d), it is notable that the syringe pumps produced droplets 14 % smaller at 80 compared to 20 µL/min (71.0 versus

82.5 nL). In contrast, the peristaltic pump gave droplets of equivalent size regardless of total flow rate with much lower variation than the previous design and showing that droplet size is determined by the physical design of the pump and is independent of the total flow rate as shown in Fig. 51.

3.5 "Hard-coding" chemical operations – rapid titrations

In all the experiments using the optimised pump design described thus far, rotorheads with multiple identical features around the rotorhead circumference were used. However, as with the previous design, each feature may be designed independently such that they each introduce a different volume of liquid. In this way, a single turn of the rotorhead can deliver a sequence of droplets with a range of arbitrarily predetermined sizes, spacing and/or compositions. This ability to generate an array of droplets with different pre-specified properties in a single turn of the rotorhead could be useful in changing reaction conditions for an array of applications e.g. screening reaction (Churski, Korczyk et al. 2010) or crystallisation conditions (Li and Ismagilov 2010), studying mass transfer (Bai, He et al. 2010) or performing routine dilutions (Niu, Gielen et al. 2011, Thakur, Amin et al. 2015) or titrations(Kawai, Fujii et al. 2009).

To demonstrate this a similar rotorhead to that described section 2.4 was designed to fit the new pump design. This rotorhead is capable of generating a dilution series once per turn allowing rapid and continuous measurement of enzyme reaction kinetics. The Michaelis-Menten equation (17) describes the relationship between the concentration of the substrate (in this case the target analyte of the assay) and the kinetics of the enzyme-based reaction.

Michaelis-Menten

$$V_0 = \frac{V_{max}[S]}{K_m + [S]} \tag{17}$$

Where V_0 is the initial reaction rate, [S] is the concentration of the substrate, V_{max} is the maximum possible rate (where [S] is in large excess) and K_m is the Michaelis constant representing the value of [S] at which $V_0 = ½V_{max}$. (Laurell, Drott et al. 1995, Berg JM 2002). The values of v_{max} and K_m are used to define the kinetics of the reaction and in benchtop testing are usually determined by running the reaction multiple times, varying [*S*] in each test and measuring v_0. The measured values of v_0 are then plotted against [*S*] and fitted with a Michaelis-Menten curve to obtain the values of v_{max} and K_m. As this involves accurate execution and analysis of multiple separate experiments, it can be a time-consuming process, even more so if additional reaction parameters such as temperature or the presence of molecular inhibitors need to be tested.

To continuously measure the Michaelis-Menten kinetics of an enzyme-based assay, a rotorhead and droplet generation chip shown in Fig. 52 were used to generate a sequence of droplets of constant size but varying composition. The chip features three aqueous inlets, which meet at a single junction and then introduced into the oil stream. The three aqueous lines supplied the substrate (line 1), the

reagent (line 2) and an additional stream of buffer (line 3). The size of the rotorhead features driving the substrate and buffer vary in opposition to each other, ensuring the volume of the droplets (and thus the final concentration of reagent) remained constant and producing a sequence of eight droplets with varied substrate concentrations. This droplet sequence were measured downstream by the miniaturised in-line spectrophotometer flow cells (Hassan, Nightingale et al. 2016) which could optically measure the progress of the reaction and hence the reaction rates shown in Fig. 53&54.

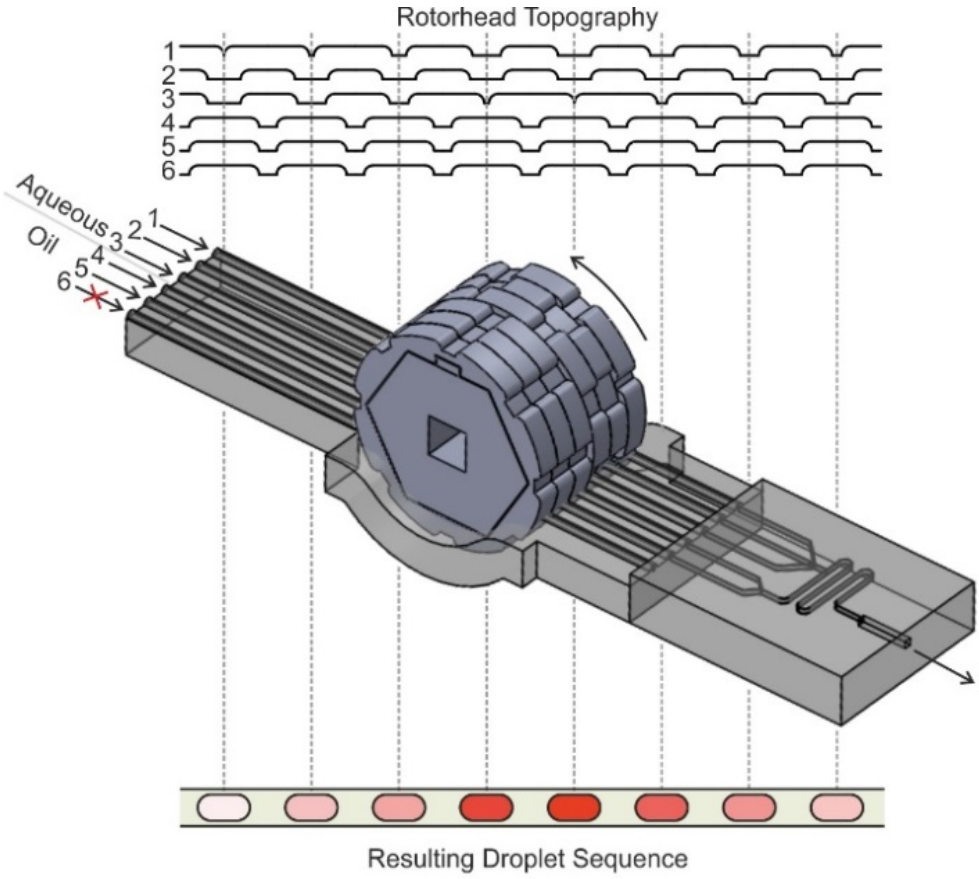

Figure 52 *Schematic of rotorhead and chip for creating a dilution series of droplets pre-specified by the pumphead design. The topography of the rotorhead circumference is shown top and demonstrates how the aqueous lines (1-3) and oil lines (4-6) are antiphase, and how lines 1 and 3 vary in opposition to each other to maintain a constant droplet volume. The droplet sequence corresponding to the rotorhead topography is shown bottom and qualitatively shows the colour range expected if red dye was supplied to line 1 and water to lines 2 and 3.*

As with the previous pump design, the system was first calibrated to quantify the range and reproducibility of droplet composition in each sequence by substituting the substrate for a food dye solution. As each droplet passed through the detection flow cell it produced a characteristic dip in the signal (Fig. 53a), with the consistent width of each dip indicating a uniform droplet size (confirmed via separate video analysis of the droplet flow, which gave a 4 % relative standard deviation consistent with the optimised pumping design). By comparison to a series of blank droplets (obtained by later replacing the dye with water) the light intensity transmitted through each droplet could be converted to an absorbance value, as shown in Fig. 53b. The periodic nature of those responses clearly indicates

that the system generated droplets with a highly reproducible range of dye concentrations. Fig. 53c shows that the dye content within the droplets varied by a factor of 4.6 (0.079 – 0.362 relative dye concentration) a significant improvement over the previous design (range 3.2). This indicates that the droplet volume variation was in fact affecting the dilution series with the new design producing a droplet sequence with relative dye concentrations ranging much closer to the ideal (5-fold dilution). "Carry over" in the continuous phase may account for the slight disparity between ideal and measured sequence.

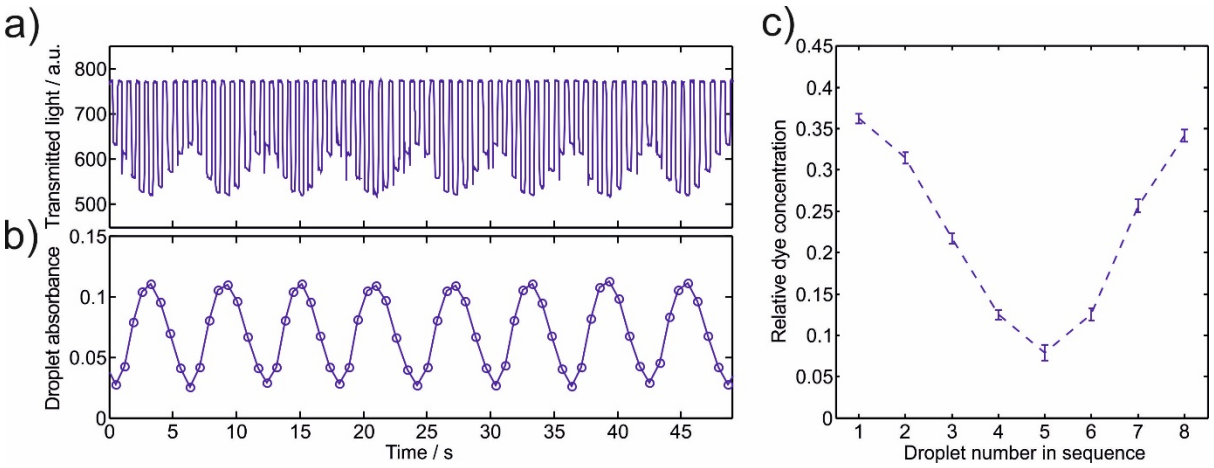

Figure 53 *Calibration of dilution series produced using the "hard-coded" rotorhead and dye. a) Raw signal from the miniaturised in-line spectrophotometer flow cell showing characteristic square-wave-like traces as droplets of different composition pass through the light path. b) Absorbance of the droplets passing through the flow cell against time, calculated from the raw data in (a). c) Mean droplet composition within the dilution sequence, shown relative to the undiluted dye. Error bars show the standard deviation of multiple sequences (n=12).*

Following calibration with food dye, the system was then used to quantify the kinetics of the Trinder assay - a colorimetric glucose assay that uses a reagent based on glucose oxidase (Trinder 1969). The premixed reagent was prepared using D-glucose, Glucose oxidase (GOx), horseradish peroxidase (HRP), 4-aminoantipyrine (4-AAP) and phenol purchased from Sigma-Aldrich (Dorset, UK) and used without further purification. Deionised water (18.2 MΩ cm, MilliQ) was used to prepare all the solutions and reagents. 0.1 M phosphate buffered saline (PBS, pH 7.0) was used throughout. The reagent consisted of 6.25 mM 4-AAP, 18.75 mM phenol, 22.5 U/mL HRP and 45 U/mL GOx in PBS. The enzymatic reagent was freshly made prior to the experiment and was covered from ambient light. The 15 mM glucose standards was also made up in 0.1 M PBS. A 15 mM solution of glucose in 0.1 M PBS was supplied to line 1, premixed reagent was supplied to line 2 and PBS to line 3, while fluorous oil was pumped through lines 4 and 5. Repeated sequences of droplets were generated with glucose concentrations ranging from 1.18 mM to 5.44 mM (as calculated from the calibration data). The absorbance is a direct measure of the assay product; hence, the rate of absorbance increase gives the reaction rate as shown in Fig. 54a.

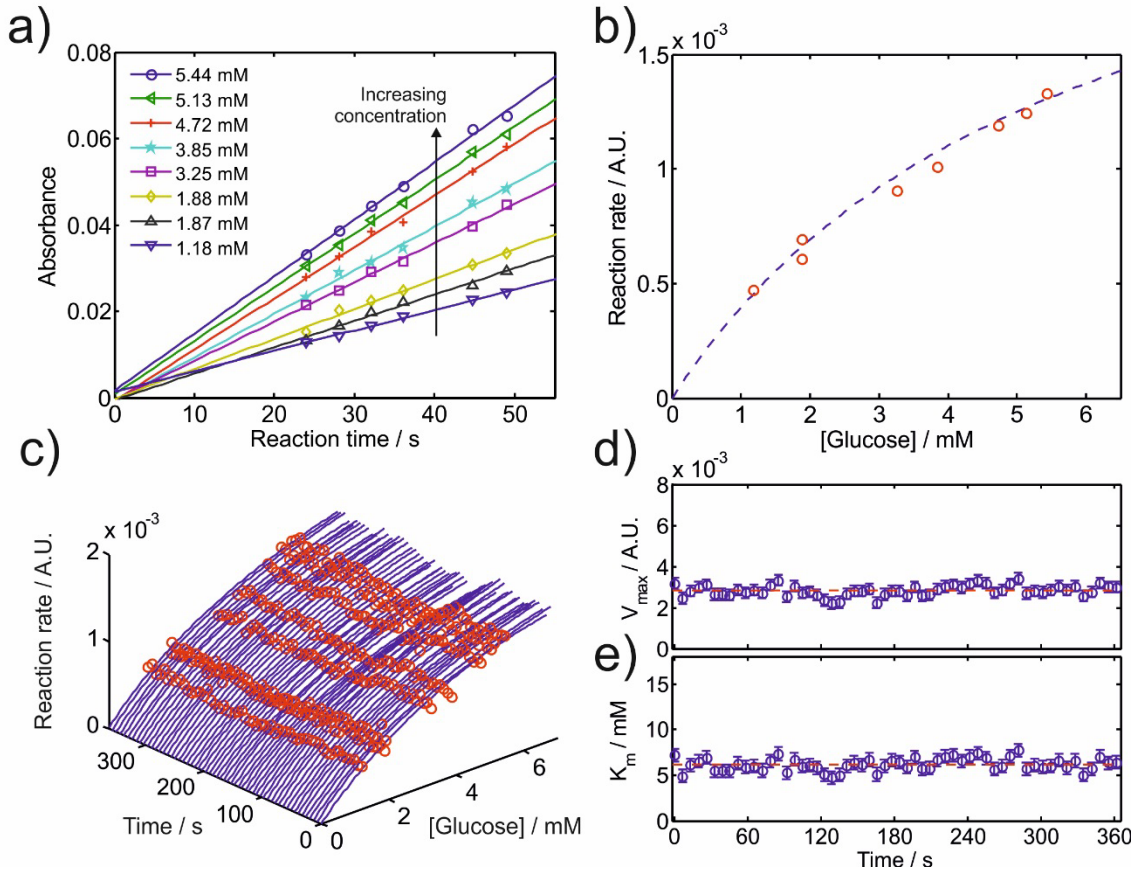

Figure 54 *Continuous analysis of glucose (Trinder) assay kinetics. a) Reaction rates for the different concentrations of glucose produced within a single dilution sequence. b) The data is fitted with a curve described by the Michaelis-Menten equation. c) Reaction rate measurement and corresponding Michaelis-Menten fits continuously obtained over a 6-minute period. c) & d) &e) Derived V_{max} and K_m values (respectively) obtained from the fits shown in (c).*

In Fig. 55b the reaction rates for a single sequence of droplets are plotted against glucose concentration and fitted with a Michaelis-Menten curve using non-linear regression (R2 = 0.98), indicating that the reaction followed standard Michaelis-Menten enzyme kinetics, as expected. The K_m value was obtained from the fit, yielding a value of 5.9 mM which was in good agreement with previously reported values (7.63 ± 2.22 mM, 6.47 ± 0.85 mM (Karmali, Karmali et al. 2004) for the same assay under the same reaction conditions (pH, temperature).

It should be noted that the Michaelis-Menten curve shown in Fig. 55b was obtained in the time taken to generate a single sequence of droplets (one turn of the motor) and flow them through the multi-detector flow cell, less than 60 seconds in total. By contrast, if these values were obtained using standard laboratory procedures they would involve multiple manual experiments and take much longer. Moreover, as the pump turns continuously, and no manual operation are required, it is possible to continuously monitor the kinetics. Fig. 55c shows a sequence of Michaelis-Menten plots (like that shown in Fig. 55b) obtained by continuously generating and measuring sequences of droplets over 6 minutes.

K_m and V_{max} values were obtained from each droplet sequence, allowing for continuous measurement of these kinetic parameters over the full 6 minutes as shown in Fig. 55d and e. Continuous measurement such as this would be impossible in bulk experimentation and allows the quantification of reaction kinetics in real-time. This could be used to explore the effect of perturbations such as variations in temperature (Peterson, Daniel et al. 2007) or continuous monitoring of inhibiting species (Nakamura and Ogura 1968) in real-time.

3.6 Comparison with previous design

The new design has shown dramatic improvement, reliably producing droplet populations with relative standard deviations in length of less than 2 %. Shown in Fig. 55 are example traces of droplet length over time of the original design and the optimised design. Rotorheads were designed with the same diameter and feature size with Fig.55a showing the non-optimised design with a droplet length RSD of ~10 % and Fig. 55b showing the optimised design with droplet length RSD ~2 % as measured using DMV in 0.5 mm PTFE tubing.

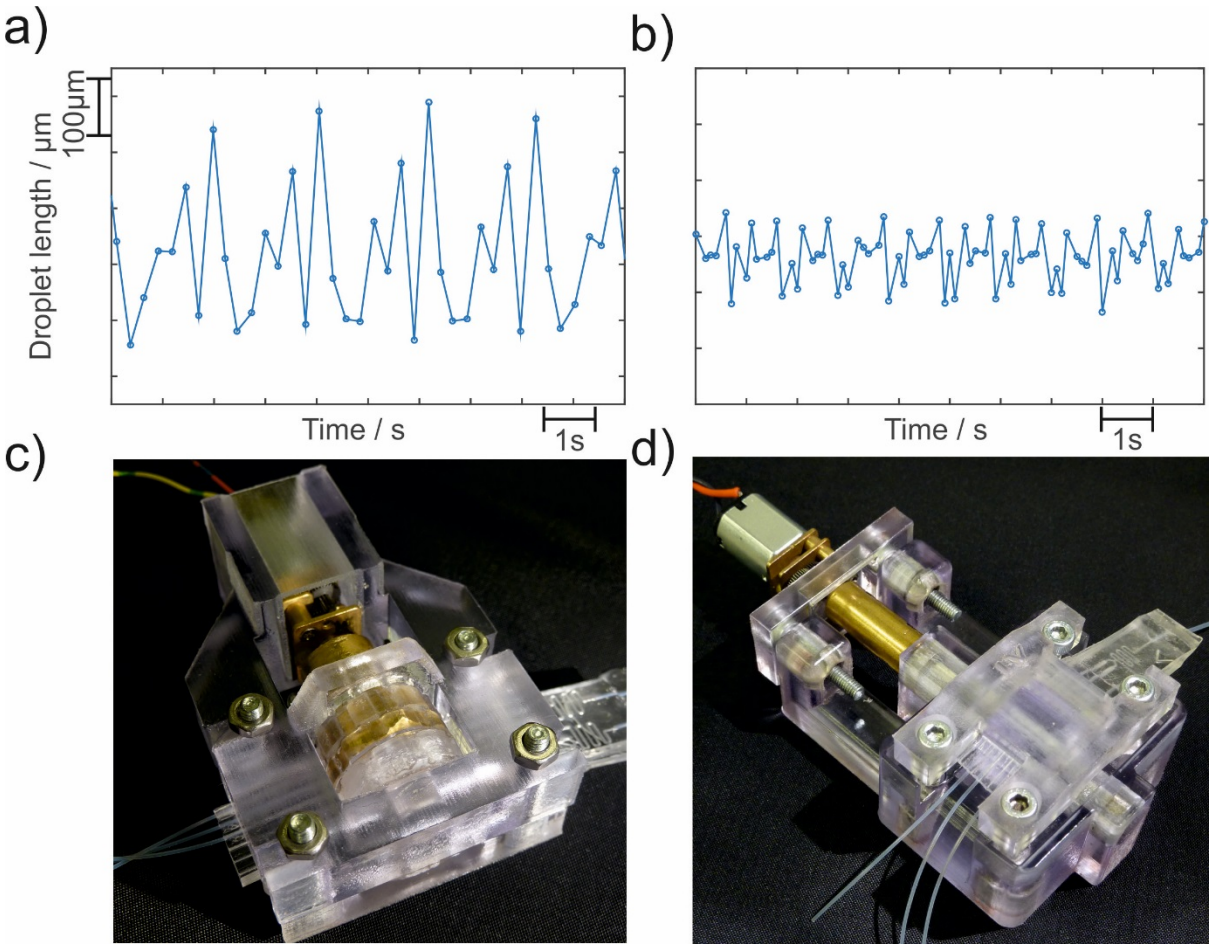

Figure 55 *Simple comparison of the variation (as shown by droplet length trace in a&b) in droplet size produced by the chapter 3 micropump device (photograph c) to the optimised micropump device (photograph d).*

3.7 Conclusions of Chapter 3

In this chapter, I have:

a) Shown the problems of periodicity of droplet size in generated droplet trains by the previous non-optimised micropump design.
b) Detailed the design and fabrication of an optimised peristaltic micropump design incorporating the monolithic microfluidic chip with greatly reduced periodicity of droplet size in the generated droplet trains.
c) Characterised the pulsed nature of the micro peristaltic pump, which is the basis of the chosen droplet generation regime.
d) Characterised this pulsed droplet generation regime for a variety of droplet sizes, droplet generation rates etc., and described the invariance in droplet size with changes to flow rate and viscosity on pulsed droplet generation.
e) Compared this invariance in droplet size demonstrated by the peristaltic micropump to 'classic' passive droplet generation with syringe pumps.
f) Demonstrated this micropump design's ability to hard code chemical operations into the design with a greater programmable range than the previous design (likely due to more reliable droplet generation), which will be further developed throughout this thesis.

Compared to my previous design droplet size periodicity has improved but is still present (although with less amplitude), further development to remove this periodicity may still be possible, such as a more solid frame of the chassis and more reliable fabrication of pumplines and other components. This peristaltic micropump and droplet generation regime could be further developed, applied as part of a continuous monitoring system and tested in a field and POC applications. The work presented in this chapter has led to publication in the journal Lab on a Chip (Nightingale, Evans et al. 2017) available in the appendices. In the following chapters, this method of droplet generation by pulsed flows generated by the peristaltic micropump design is further explored in a miniaturised platform generating sequences of droplets with varied contents to calibrate sensor devices and carry out more complex assays suitable for field applications. The full pump and chip assembly are able to run for several hours while carrying out tests (provided correct fabrication with adequate lubrication) and when further tests are to be carried out the chip containing all fluidic components may be disposed of and replaced.

Chapter 4 - Miniaturisation of the pumping system and fluid handling and multiplexing pulsed droplet generation

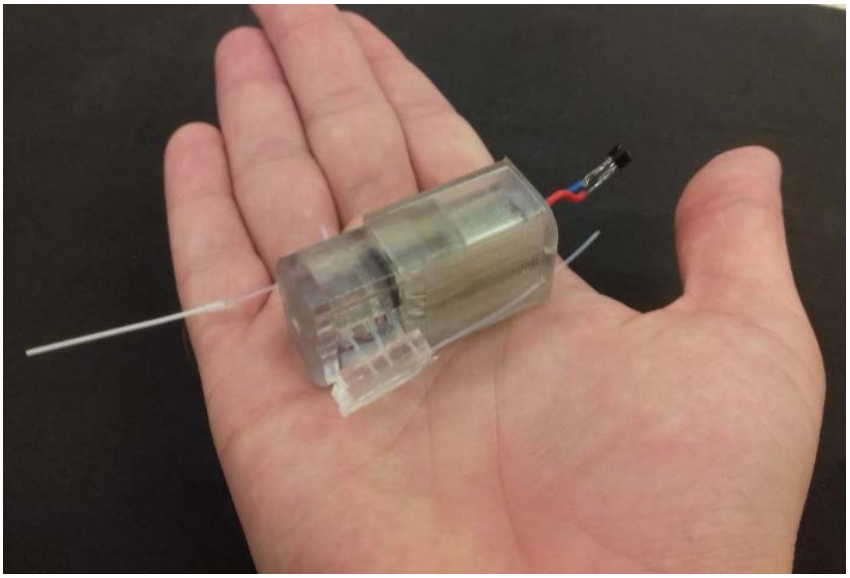

In this chapter is described a miniaturised and modular version of the peristaltic micropump/droplet generator. This pump is more robust and user-friendly than previous versions and better suited for field deployment. Also detailed is characterisation data displaying this platform's further utility over previous designs: generating trains of droplets, splitting and merging droplets.

This chapter details a miniaturised and modular version of the peristaltic micropump and droplet generation platform described in the previous chapter, which is more suited for field deployment. This platform utilizes the robust and flow invariant pulsed droplet generation regime detailed in the previous chapters but further expanded upon here for improved performance and utility. The pump has a smaller footprint than the previous platforms shown in chapters 2 & 3 and consumes little power (0.02W) whilst still generating monodisperse droplets by the pulsed regime. A tubing-based pumping head replaced the PDMS based monolithic chips, this pumping head was much simpler to fabricate and provided greater and more reliable life time capable of approximately two weeks of continuous operation. This is a considerable improvement over the PDMS based pump which was only capable of reliable continuous operation for a few hours.

Furthermore, detailed in this chapter is characterisation data displaying this platform's further utility over previous designs including the new platform's ability to generate droplet sequences for multiplexed and multiple step assays utilising the pulsed droplet generation regime (further applied in chapters 5 & 6) making it more suited to a variety of field and clinical applications.

4.1 Design of the further miniaturised peristaltic micropump

This iteration of the pump was designed with the aims of: decreasing the size and increasing the lifetime of the pump while providing easier assembly. A schematic including all components of the pumping head is shown in Fig. 56 with further technical drawing included in the appendices. Once fully assembled the pumping head has a total footprint of 44.5mm*31.6mm*18.2mm. This miniaturised micro-peristaltic pump has been shown to be capable of running for long periods of time with a very low power consumption (0.05W with 0.25Hz droplet generation rate). As with the previously described systems, patterned features on the rotorhead determine the timing and volume of the fluidic pulses introduced in the channel. Fluid samples were drawn into the system by peristalsis and delivered into a polydimethylsiloxane (PDMS) microfluidic chip. Here, sample and reagent mixes are then formed into droplets by the pulsed method described in the previous chapters.

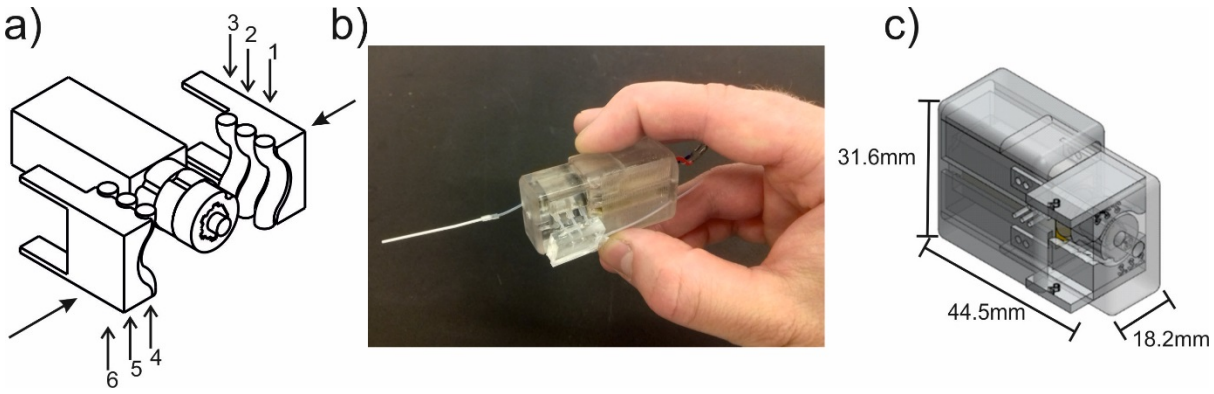

Figure 56 *Schematic of miniaturised peristaltic micropump. a) Schematic showing the active components of the micropump (DC motor, 3Dprinted rotorhead six silicone tubing pumplines 3D printed pumpline support bed). b) Image of the miniaturised peristaltic micropump/droplet generation device. c) Schematic showing the assembled micropump.*

Figure 57 shows an exploded view of the pump, as with the previous designs 3D printing was used extensively. The main pump chassis, cap, tubing support beds, rotorhead and spacer shims are all modelled in CAD software (SolidWorks, Dassault Systems, files available on request) and printed in "VeroClear" material using an Objet500 Connex3 polyjet printer (Stanford Marsh Ltd). Six silicone tubing pumplines (Gradko International Ltd., 0.5 mm wall, 0.5mm bore) were used for all the systems shown in this chapter, with pump outlets connected directly to the microfluidic chip, using PTFE tubing (ID 500 µm, OD 700 µm). The tubing pumplines are considerably easier to produce especially in large quantities than the PDMS pumpline chips used previously. However, this limits pumpline diameters to those commercially available unless custom tubing can be fabricated. The pumplines are glued into the 3D printed bed using a flexible cyanoacrylate adhesive (PERMABOND® 2050) after priming with Permabond Polyolefin Primer (POP). While six silicone tubing pumplines (three on each side of the rotorhead) are used for the studies presented here this can be extended for other studies. The use of the spacer shims and the design of the pump allows for the pressure on the pumplines to be adjusted to allow tubing to be replaced with tubing of different outer diameters or different materials such as PVC or Santoprene, which may increase lifetime. The same DC motor (Pololu 210:1 Micro Metal Gearmotor) as used in previous designs was used to drive the 3D-printed rotorhead, which compresses the pumplines. A silicon lubricant (Rocol Silicone Grease SAPPHIRE Aqua-Sil) was used to lubricate the movement of the rotorhead on the pumplines decreasing torque experienced in the pump and increasing pumpline lifetime.

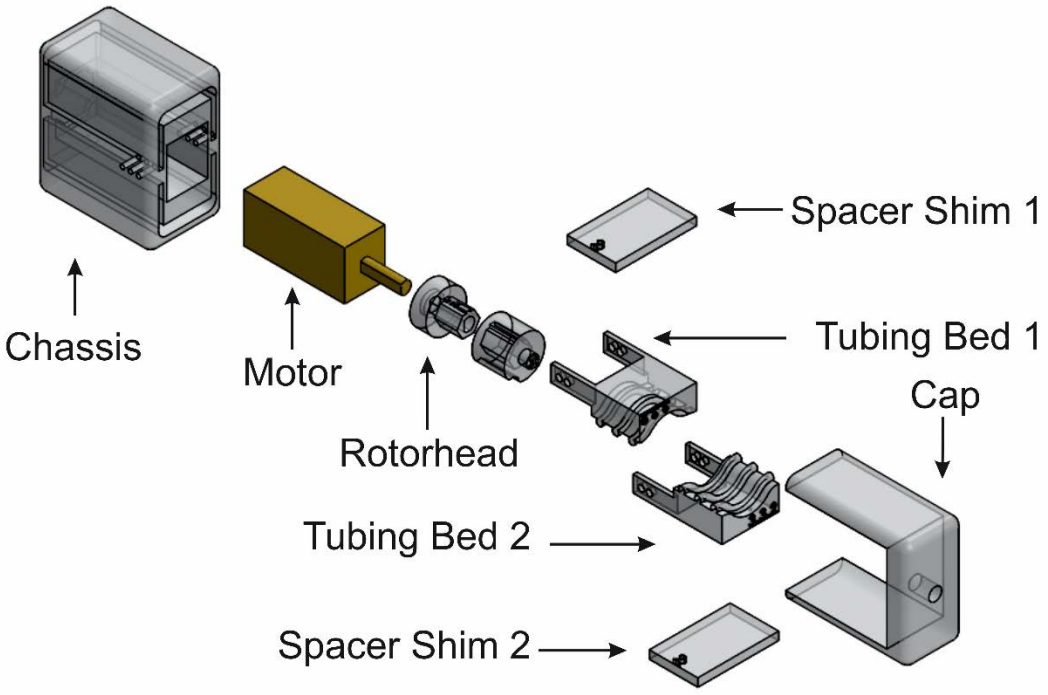

Figure 57 *Exploded schematic of the further miniaturised 3D printed micropump showing all components; 3Dprinted chassis, DC motor, 10mm 3D printed rotorhead, tubing beds featuring 0.5mmID silicone tubing, 3D printed spacer shims and cap.*

Three varieties of microfluidic chips have been utilised in this chapter. All chips were fabricated by standard PDMS casting procedures and mounted on the pump to keep fluidic connections as short as possible to minimise Taylor dispersion. Moulds were designed in CAD software (SolidWorks) and 3D

printed in “VeroClear” material (Objet500 Connex3 3D printer). Half-cured PDMS was used to seal the channel structure. Channels were surface functionalised with Aquapel rendering them hydrophobic and ensuring the oil phase preferentially wets the channel. PTFE tubing (Adtech Polymer Engineering Ltd.) was used to connect the pumplines to the chip and as the outlet from the chip. Simple T-junction chips were used in the early tests mounted onto the side of the pump and used to generate droplets with a relative standard deviation in droplet volume consistently <1%. In later tests, this same six-pumpline pump structure with an altered rotorhead and chip was used for multiplexing assays or for generating alternating droplets of sample and a standard. The two droplet populations are generated mirroring each other each meeting reagent at a Y-junction in a 1:1 ratio and then breaking off into droplets by the fluorous oil at a T-junction. Once generated droplets from both T-junctions head to a main Y-Junction and into the main reaction channel. Interspersing standard droplets between sample droplets allows continuous calibration of the sample measurement, an approach that has been successfully demonstrated in low-throughput continuous-phase microfluidic analysers (Beaton, Cardwell et al. 2012, Clinton-Bailey, Grand et al. 2017). These Y-Junction chips have also been used to merge droplets, which may be used for possibly adding reagents, diluting an assay to help extend dynamic range or multiplex assays by adding different reagent to a sample in a multiple branched structure. A chip featuring multiple inline T-junctions has also been developed to generate droplet trains. These may be used for multiplexed and multiple step reactions and has also been implemented for a “parked droplet splitting” approach.

4.2 Characterisation of the miniaturised pumping/droplet generation system

As previously described, the pulsed method of droplet generation generates droplets whose volume is solely defined by the volume injected by the corresponding aqueous pulse. A series of rotorheads was designed to test the capability of the new miniaturised pump design. Results of this testing are shown in Fig. 58, feature spacing was systematically varied (between 15^{o} and 30^{o} pitch for aqueous) in rotorheads with 10 mm diameter. As with the previous implementations of the pulsed method, the droplet generation rate increased linearly with motor speed (data not shown). This indicates one droplet is generated per pulse period of aqueous and oil. Droplet size remained constant with varying motor speed (and hence total flow rate) and droplet generation rate, with larger rotorhead spacing producing larger droplets (Fig. 58a). Coefficients of variation (relative standard deviation) in droplet volume were consistently <1% extremely favourable compared to other reported droplet generation methods (Tan, Murshed et al. 2008, Jung, Retterer et al. 2010, Abate, Kutsovsky et al. 2011). This low coefficient of variation in droplet volume was shown to be repeatable across many experiments, a considerable improvement over the previous design. The droplet size was also invariant with aqueous viscosity see Fig. 58b and interfacial tension (varied with surfactant concentration added to the oil (PFPE-PEG)) see Fig. 58c. This indicates the system may be used in the analysis of a huge variety of liquids including biological fluids (e.g. blood serum and whole blood), and deal with liquid samples with varied viscosities or interfacial tensions with the oil over time.

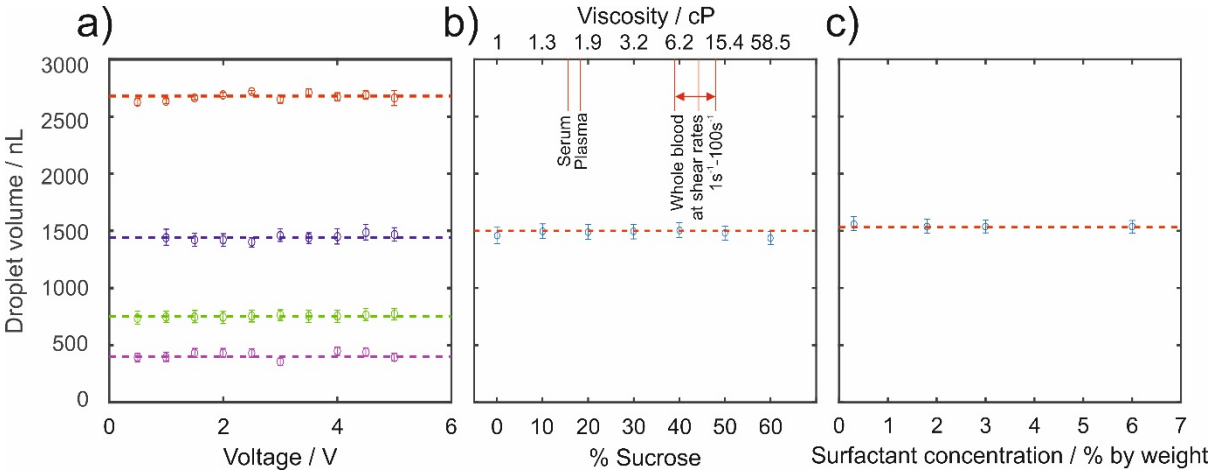

Figure 58 *Characterisation of miniaturised micro peristaltic pump. Droplet generation dynamics for rotorheads with different feature spacing. a) Droplet volume corresponding to each feature spacing remains constant irrespective of motor speed (controlled by voltage supplied to the motor). Error bars show the standard deviation in droplet volume (consistently <1%). Droplet volume increases with feature spacing. b) Droplet volume vs viscosity (controlled by sucrose concentration in the aqueous phase) c) Droplet volume vs interfacial tension (controlled by concentration of PFPE-PEG surfactant in the FC40 carrier fluid).*

4.3 Handheld μTAS tool

For years there has been research and industrial effort to create platforms which can be deployed in remote areas to be used for healthcare and scientific applications. These micro total analysis systems or μTAS tools have many possible applications particularly in the field of cell biology and biochemical assays (Kovarik, Gach et al. 2012). Technological approaches have varied from those using paper microfluidics and portable analysers (Knight 2002, Whitesides 2006, Dungchai, Chailapakul et al. 2009, Li, Ballerini et al. 2012) and those using electrochemistry (Bandodkar and Wang 2014).

To showcase the functionality of the miniturised peristaltic micropump/droplet generation platform I have developed, I have integrated it into a handheld μTAS tool (Total footprint 6cm*4cm*4cm) shown as a schematic explosion in Fig. 59a and photograph of the protoype handheld in Fig. 59b. Also included in the handheld tool is a miniaturised in-line spectrophotometer flow cell and accompanying electronics required for continuous monitoring of sample chemistry using a colourimeteric assay. A fluidics resevior is also included containing deformable liquid bags (made in house using 250 gauge Polythene Tubing) holding FC40 oil and all required reagents. All these components are enclosed within a 3D printed housing. An example of the intensity data trace reading droplets of sample and reagent (nitrite and Griess reagent as described in section 5.1.3) passing through the included detector is shown in Fig. 59b inset. Peaks in the data represent oil spacing and troughs represent droplets.

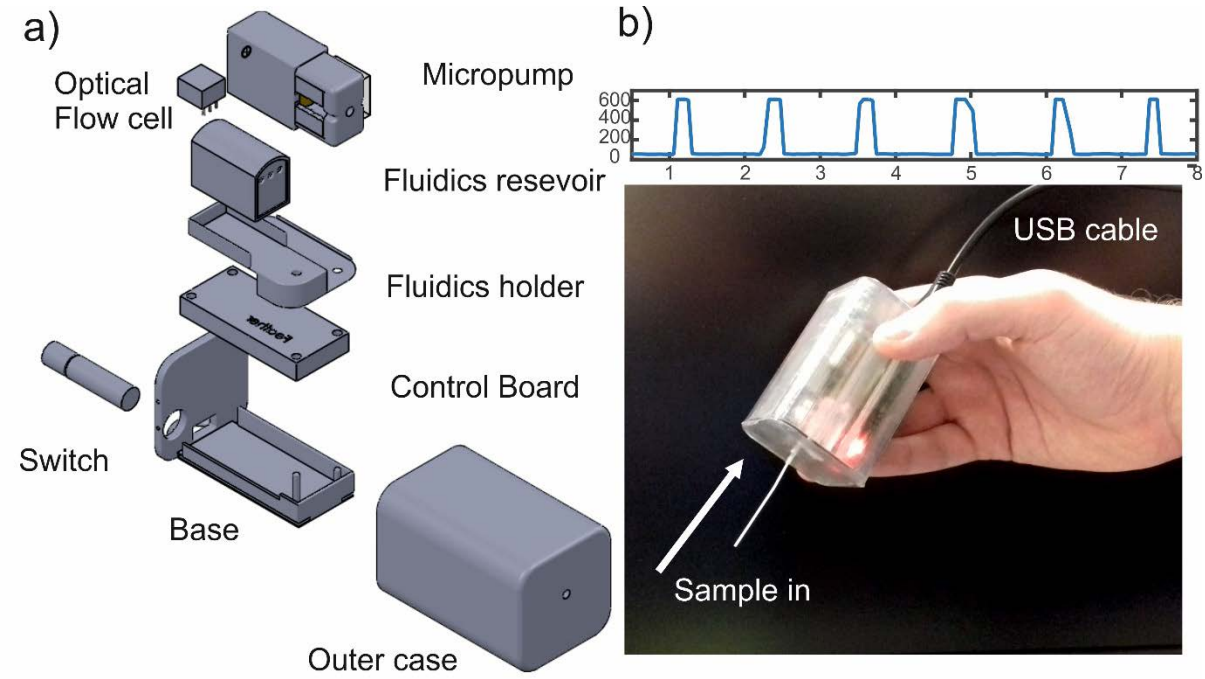

Figure 59 *Handheld lab device a) schematic explosion featuring all components of the handheld lab device b) photograph of the handheld lab device (inset above: raw light intensity data trace from the included miniaturised spectrophotometer flow cell (Hassan, Nightingale et al. 2016) while measuring nitrate with a modified Griess reagent assay).*

4.4 Generation of droplets 'trains'

Generation of droplet sequences with different pre-specified composition or 'trains' is an important task for droplet microfluidics research to create true μTAS devices capable of replacing lab systems. Droplet trains open up the possibility of performing multiplexed and multistep assays in a single channel as described in section 1.9.7. This has proven difficult to perform for continuous fluidic systems, with surface contamination from Taylor dispersion making it necessary to wash the channels between tests. Therefore, a switching of valves and pumps and large amount of washing buffer and liquid priming are unavoidable.

Droplet microfluidics holds potential to provide multiplexed or multistep assays in a higher throughput offering reduced surface contamination and 'digitalisation' of reactions within the droplet reactors. However, current droplet systems are still very limited in achieving this potential; (Ferraro, Champ et al. 2016) have designed a system to generate droplet trains utilising a single droplet generating orifice, robotic arms, valves, pressure driven pumps and control systems as shown in Fig. 60. (Gu, Zhang et al. 2011),(Zeng, Li et al. 2009) and (Ferraro, Lin et al. 2015) have also demonstrated other approaches to generate droplet trains using using a variety of valves.

These systems have demonstrated excellent functionality as lab instruments, increasing automation, decreasing contamination and sample sizes required, and making heterogeneous assays possible for droplet microfluidics. However, these systems are particularly large benchtop instruments with complicated controls of syringe pumps and valves unsuitable for POC use.

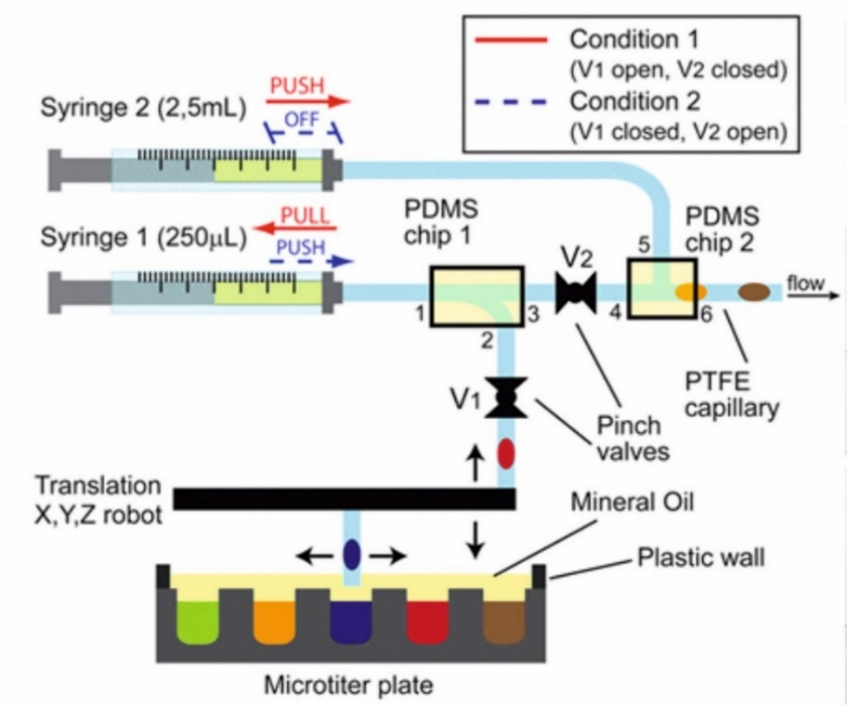

Figure 60 *Example lab based system for generation of droplet trains (Ferraro, Champ et al. 2016). Scheme of the droplet microfluidic generator module, which combines a microtiter plate placed under a motorized pipettor arm (Cetoni), two syringes, two pinch valves.*

In chapters 2&3 I have demonstrated that the pulsed method can generate droplet trains by hardcoded features to perform chemical operations such as dilution series and titrations within droplets. Here I will also describe its ability to generate trains of droplets with different contents suitable for multiplexed and multiple step assays.

4.5 Generation of a two-droplet train by branched chip and 4 phase rotorhead

Presented here is a method for the production of a two-droplet train and preliminary characterisation data. This may be implemented to introduce standards for assays calibrating sensors during continuous monitoring or multiplexing two assays continuously. This is accomplished by a chip geometry featuring two parallel T-Junctions which then join in a Y-junction shown schematically in Fig 61a (photograph Fig. 61b). Fluid is driven by a rotorhead and pumpline structure featuring four separate phases. Figure 61 shows a schematic of the rotorhead. Here a single feature is used to drive the upper and lower pumplines at different times therefore in each rotation the pumping head provides four out-of-phase pulsations.

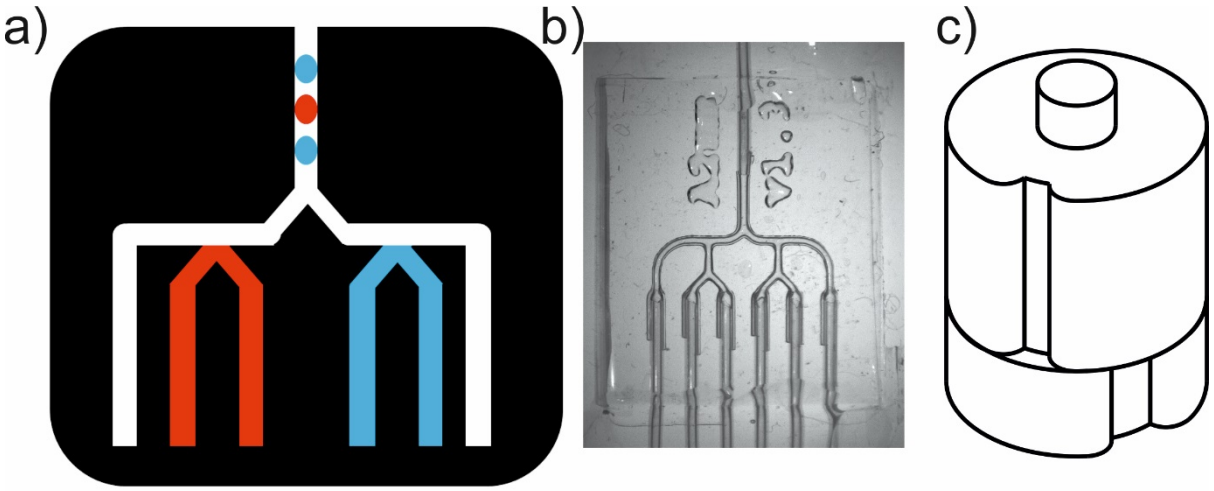

Figure 61 *Schematic of system for generating two-droplet train a) Schematic of double T-junction branched microfluidic chip b) photo of double T-junction branched microfluidic chip (channel cross section 100μm*600μmc) Schematic of four phase rotorhead (10mm diameter).*

As shown in the Fig. 61a schematic, two aqueous streams are merged at a Y-shaped junction and then segmented into droplets by the oil at a T-junction. This then joins a mirrored set of streams at a Y-shaped junction. Volume here is controlled by the feature spacing on the rotorhead and features are offset to deliver the oil and aqueous phases in anti-phase pulses to the T-junctions where the droplets are produced. Each mirrored T-Junction is also entirely out of phase with the other. Chips must be carefully designed to avoid undesired droplet breakup or merging in the main branched channel.

The pump and microfluidic chips were made with similar methods as previous experiments. A portable microscope camera (dnt Digimicro Mobile Mikroskope) was used to record either directly at the droplet generation chip or off-chip within the PTFE tubing. The videos recorded were analysed using Droplet Morphology and Velocimetry (DMV) software (Basu 2013) and the data subsequently processed in Matlab. Droplet volume was calculated from DMV measurements of droplets recorded within tubing of known cross sectional area.

Figure 62 displays images of the microfluidic chip over a full droplet generation period for one full turn of the rotorhead generating two droplets using four pulsations. The droplet velocity is measured downstream. Each droplet was produced from an incursion of an aqueous stream into the main channel and then 'chopping' of the aqueous incursion into a droplet by the pulse from oil stream which is then carried into the main junction downstream. Figure 62 demonstrates how the four phases of pulsations (as measured downstream) relate to the generation of the two separate droplet populations.

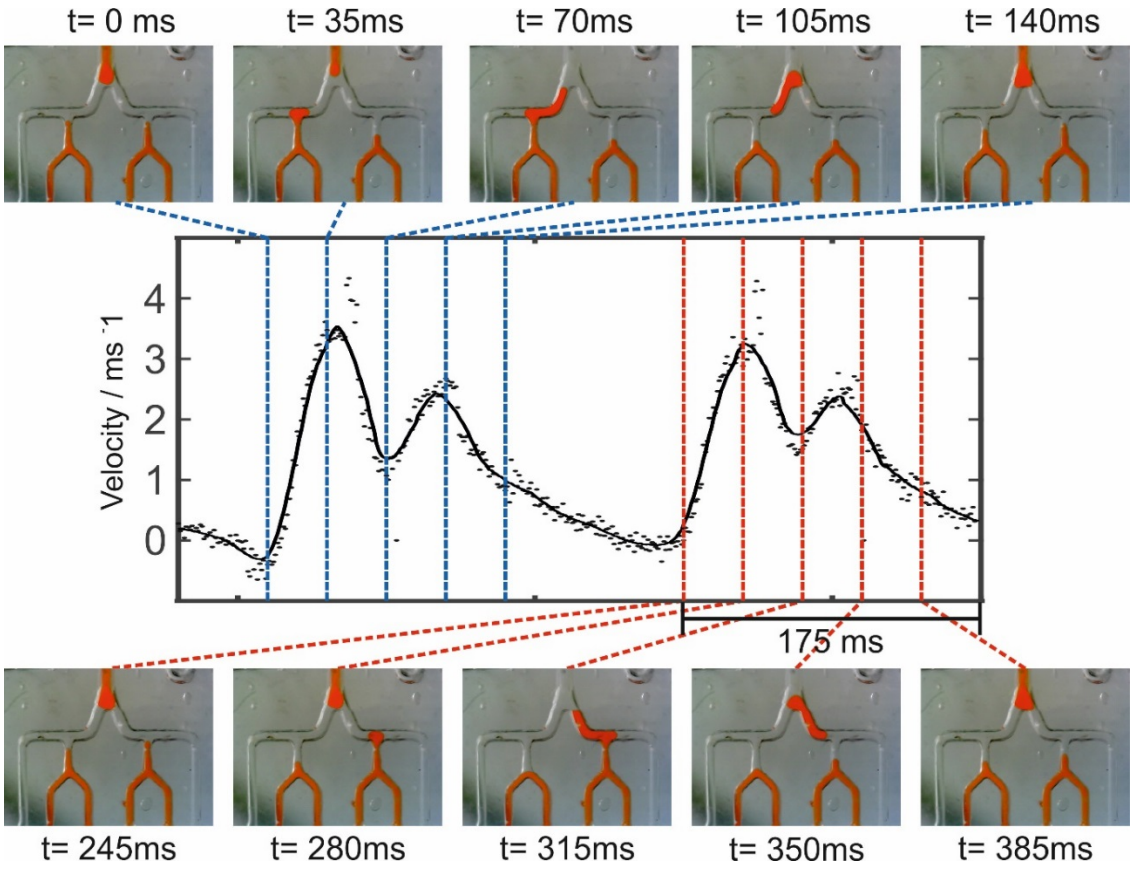

Figure 62 *Correlation of optical images of droplet generation chip for a four-phase generation of a two-droplet train by pulsed flows with downstream flow velocity. Incursion of the first aqueous phase into the main channel (images top) is associated with a single velocity pulse peak, while its subsequent break-up by oil flow (0.3% PEG-PFPE surfactant FC40 oil) (images top) is associated with the following velocity peak. The mirroring T-Junction pulsations follow the same pattern (images bottom).*

Two example tests were carried out (results shown in Fig. 63) utilising two different rotorheads with 30° pitch aqueous with 60° pitch oil, and 15° pitch aqueous with 30° pitch oil. Both rotorheads had a 10 mm diameter and were run at two speeds (droplet controlled by the motor voltage (3 V and 1.5 V). The different feature sizes translated into different droplet sizes as expected. The larger featured rotorhead producing droplets of 2650nl average volume and the smaller featured rotorhead producing droplets of 1540nl average volume. Both setups having a relative standard deviation under 1 % with regards to volume over the entire droplet population (both T-Junctions). As is expected varying motor speed has no effect on droplet volume. While, these are relatively large volumes for droplet microfluidics this method is extremely customisable and smaller droplets could be generated using smaller rotorhead features and smaller bore pumplines. As with previous studies on this pulsed method these droplet trains generated in branched structures should be invariant to flow rate (as shown in Fig. 63), interfacial tension and viscosity etc. although I have not tested this here.

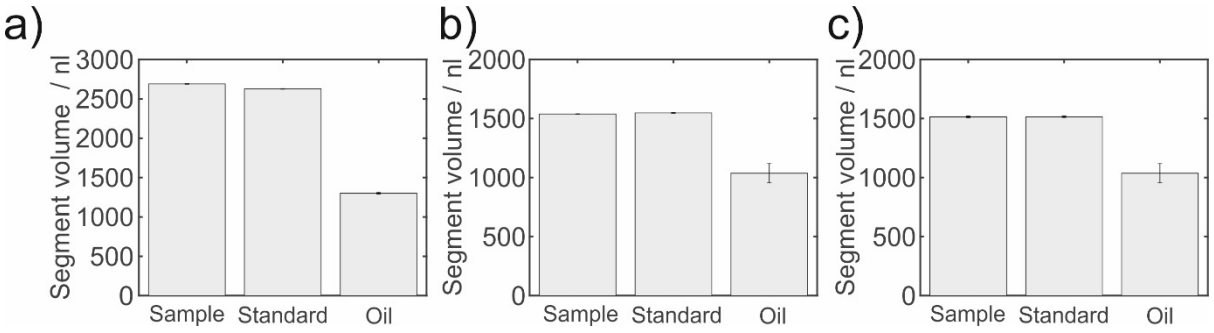

Figure 63 *Segment volumes of double droplet generation platform (error bars showing standard deviation) for two sizes of rotorhead pitch a) 30º pitch aq 60º pitch oil 3 V b) 15º pitch aq 30º pitch oil rotorhead diameter (10mm) motor voltage 3 V and c) 15º pitch aq 30º pitch oil rotorhead diameter (10mm) 1.5 V motor voltage.*

Each set of droplets is independent from the other and as such has potential uses in generating inline standards and multiplexing assays for multiple analytes. This method has been applied in Chapter 5 as part of an environmental monitoring platform for nitrite and nitrate in rivers. In that system, each sample droplet is accompanied by a standard droplet. As the reagent injected into the sample droplet and the standard droplet are the same any measurement drift due to degradation of reagents over time can be easily quantified and accounted for.

4.6 Droplet merging in a branched microfluidic chip

As previously stated, merging of droplets is particularly useful for assays where reagents must be combined at specific time points. For coalescence to occur the continuous phase between the droplets must be drained to bring them into close contact and this contact must be held for a critical minimum amount of time. As described in section 1.8.2 merging occurs when the surface tension at the interface between the water and oil phases fluctuates and destabilises.

A number of approaches both passive and active have been taken to cause merging of droplets with high throughput and efficiency; the simplest passive method is a widening of the channel (Tan, Fisher et al. 2004, Hung, Choi et al. 2006, Liu, Ding et al. 2007).

To demonstrate how the same chip design used to generate two interdigitated populations of droplets (Fig. 61a) could also be used to merge droplets, I redesigned the rotorhead as shown in Fig. 64a. also used in the pump shown in Fig. 57. As the rotorhead has an even number of features, aq and oil pulses are generated simultaneously in both the left and right sides of the microfluidic chip this means that the droplets should meet at the main Y-junction. Fig. 64b shows this approach in action. As you can see, the green and red droplets are generated simultaneously and immediately meet at the main junction merging. This approach could be tailored to combine droplets of reagents for complex assays at specific time points.

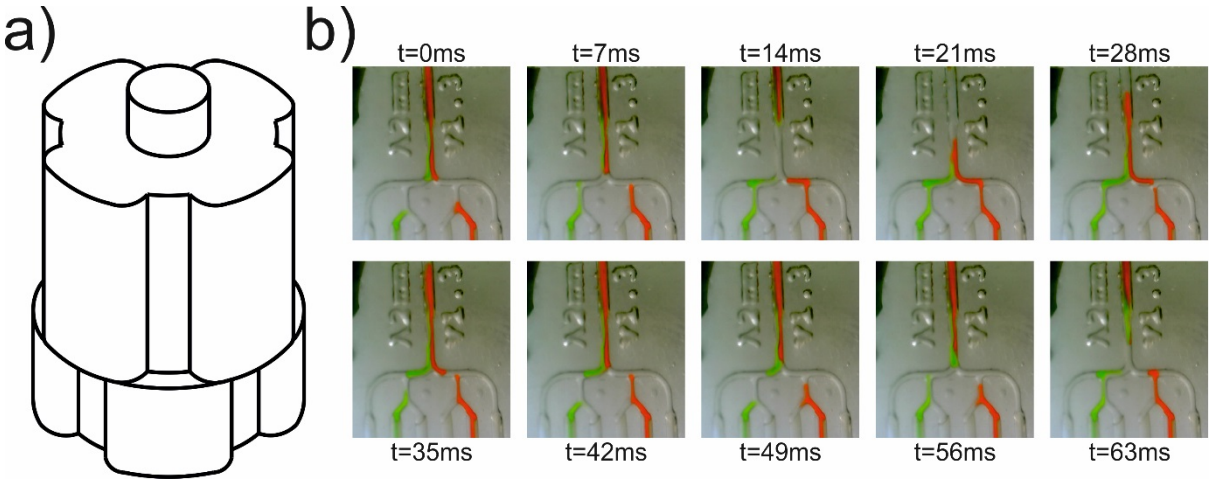

Figure 64 *Example droplet merging using the Y- junction geometry and two phase pulsations: Using the rotorhead a) 10mm diameter all aqueous incursions to this branched T-junction chip occur in phase and broken off by their corresponding oil to join at the Y-junction b) Photographic image sequence showing the droplet merging.*

4.7 Generation of droplet trains by multiple in line T-junctions and 6 phase rotorhead

Droplet trains can also be generated with multiple in line T-junctions. Presented here is a new method for the production of a four-droplet train and preliminary results. The system was designed to generate droplet trains with larger numbers of constituent droplets (>2). The chip geometry features four parallel T-Junctions sharing a main channel as shown in Fig 65a. Fluid is driven by a rotorhead and pumpline structure with six separate antiphase pulsations as shown in Fig. 65b.

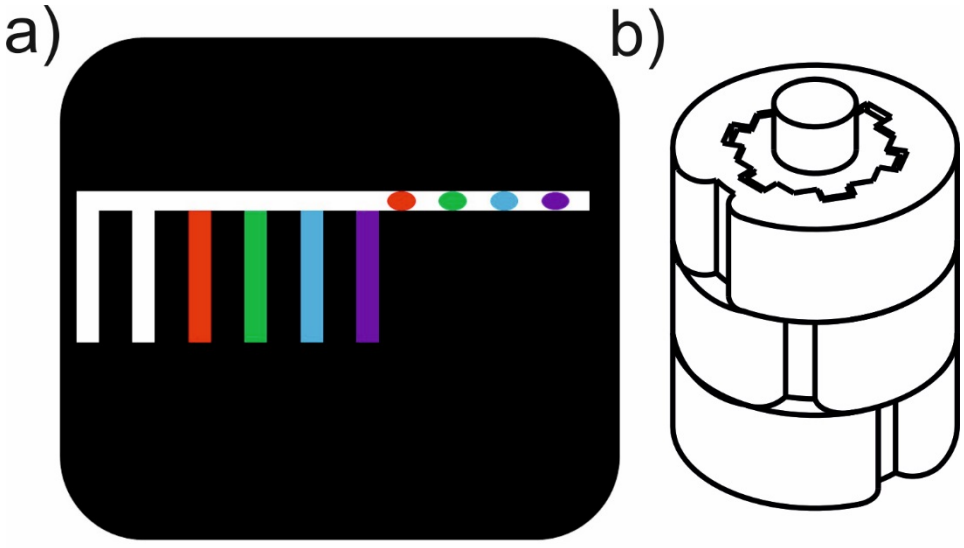

Figure 65 *Schematic of system for generating four-droplet train a) Schematic of multiple T-Junction and b) Schematic of six-phase rotorhead 10mm diameter.*

Figure 66 displays images of the microfluidic chip over a full droplet generation period for one full turn of the rotorhead generating four droplets using six pulsations. Each image is correlated to the droplet

velocity that is measured downstream (shown centre). As the rotorhead turned, each droplet was produced by firstly incursion of aqueous stream into the main channel and then broken off by the oil pushed forward by the aqueous incursion of next subsequent stream. The fifth and sixth pulsation deliver oil to move the whole train of droplets downstream out of the chip. Figure 66 demonstrates how the six phases of pulsations (as measured downstream) relate to the generation of the four separate droplet populations.

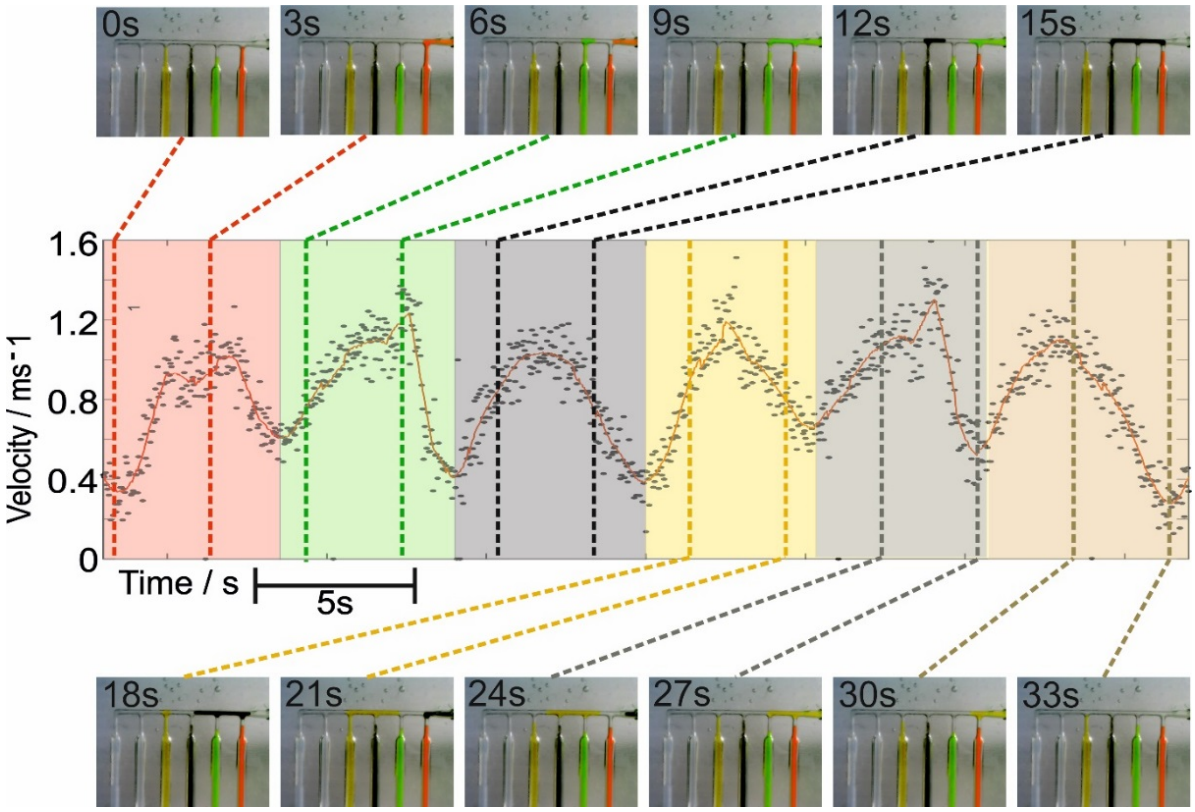

Figure 66 *Generation of a single 4-droplet train in a single turn of the six-phase rotorhead. The total flow velocity measured downstream of the droplet generation chip, during a single turn of the rotorhead. Six distinct peaks are seen in one period due to the incursion of the four aqueous and two oil pulses. Images of the chip during this generation of droplet trains with zero cross talk (2% Relative standard deviation of droplet volume across the entire droplet population (mean volume 834nL). (Carried out at 0.5V ad using 1.8% PEG-PFPE surfactant FC40 oil)) t=0-3s incursion into the main channel of red dye from right most inlet, t=6-9s incursion into the main channel of green dye, t=12-15s incursion into the main channel of black dye, t=18-21s incursion into the main channel of yellow dye, t=24-27s incursion into the main channel of oil from second channel from the left, t=30-33s incursion into the main channel of oil from the leftmost channel.*

Figure 67a shows an image of tubing filled with many droplet trains each composed of four coloured droplets populations generated during each rotation. This example test was carried out utilising a feature rotorhead pitch of 30^{o} and pumpline diameter of 0.5 mm producing an average droplet volume of 1314nL with a relative standard deviation under 4% over the entire droplet population (all T-Junctions). These were generated with 0.5 V supplied to the pump for a 0.12 Hz droplet generation rate.

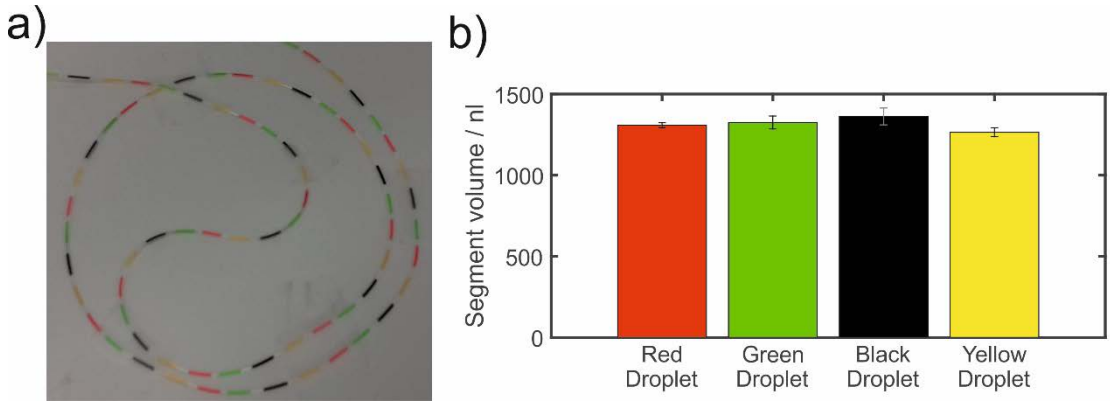

Figure 67 *Characterisation of the droplet train generation by multiple T-junctions a) photograph of a long sequence of droplets in 500um tubing (<4% Relative standard deviation of droplet volume across the entire droplet population (mean volume 1314nL). (Carried out at 0.5V ad using 1.8% PEG-PFPE surfactant FC40 oil)) b) Segment volume of the four-droplet train as generated by the multiple T-junction; error bars represent standard deviation for over 100 droplet trains.*

In this instance the stability and uniformity of droplet generation is comparable to the results shown in previous chapters. Strikingly, at the flow rate tested there is no noticeable cross talk (with regards to contents) and seemingly no-interference (with regards to size etc.) between the droplets. This method and system could be further refined and explored for use in multi-step immunoassays involving reactions and washing steps. However, generally it was found that issues with droplet contamination (dosing and merging) occurred when outside of optimal flow rates, pulsation volumes and timing. The contamination typically occurred due to droplets meeting the aqueous streams as they pass T-Junctions. Hence, I have focused on using branched chip structures for generating droplet trains.

4.8 Droplet splitting by multiple in line T-junctions

As mentioned in section 1.8.1 droplet fission is one of the many vital tools/operations in the development of droplet microfluidics as a tool for assays. Droplet splitting increases the system's ability to multiplex and replicate measurements or increase analytical throughput. Many methods of splitting droplets have been described. Earlier papers described how splitting may be accomplished by a simple bifurcation geometry. Similar to droplet splitting regimes described in section 1.8.1. Here I present the possibility to integrate programmable droplet splitting tuned by dimensions of the microfluidic chip and rotorhead dimensions droplet systems for further functionality. The same experimental setup demonstrated in section 4.7 can be adapted to controllably split droplets. Figure 68 shows an early attempt at droplet splitting by timed pulsations. Here droplets are parked in front of a T-Junction and then split by a pulsation of oil.

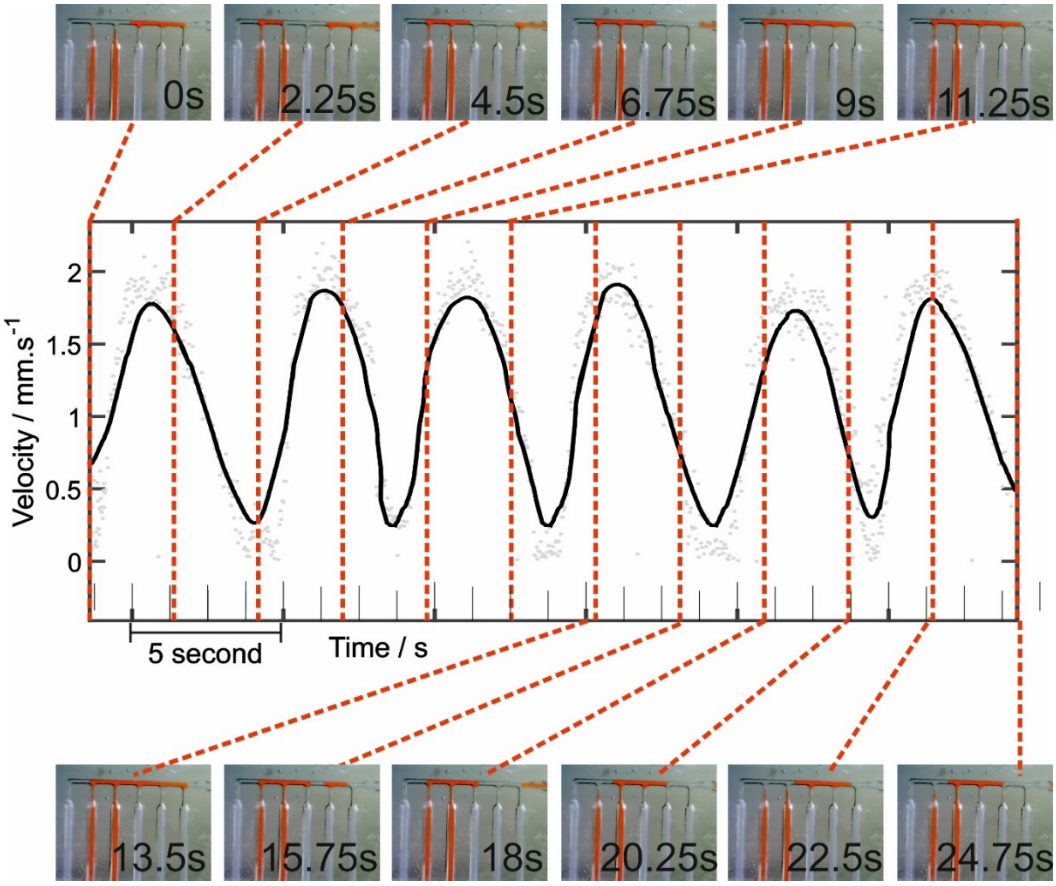

Figure 68 *Example of droplet splitting by timed pulsations and multiple T-Junctions: six separate pulsations two of aqueous and four of oil in the order 2,3,6,5,4,1 (numbering left to right) to generate a single large mother droplet from the two aqueous inlets which is then split into four aqueous droplets by oil pulsations and sent downstream. T = 0-2.25s aqueous incursion from inlet 2, T = 4.5-6.75s aqueous incursion from inlet 3, T = 9-11.25s FC40 incursion from inlet 6, T = 13.5-15.75s FC40 incursion from inlet 5, T = 189-20.25s FC40 incursion from inlet 4, T = 22.5-24.75s FC40 incursion from inlet 1.*

This could be further developed adding greater functionality to the droplet microfluidics platform. This method could be used to isolate single cells in droplets or remove unwanted substances from droplets. For continuous monitoring droplet splitting could allow a single sample droplet to be split multiple times, with different assays performed on each daughter droplet when combined with the droplet merging previously described. This allows monitoring of a screen of analytes.

4.9 Conclusions of chapter 4

In this chapter, I have:

a) Detailed the design and fabrication of the miniaturised peristaltic micropump.
b) Characterised the pulsed droplet generation regime's ability to generate two droplet trains of varying constituents with considerably small polydispersity by two parallel T-junctions joined at a Y-junction.
c) Characterised the pulsed droplet generation regime's ability to generate four droplet trains of varying constituents, with small polydispersity by parallel T-junctions sharing a main channel.

In conclusion, this peristaltic micropump design shows promise for stable generation of droplet trains both in the lab and in the field. Invariance of droplet size for flow conditions and generation of hard coded droplet trains are key advantages exhibited by this method over previously reported systems. The small overall system size and extremely low power consumption has provided additional advantages.

Lifetime of the fluid handling system has also been further improved in the following chapters by replacing the silicone tubing with more durable Santoprene tubing now able to last up to one month constant run time. However, the increased compression required for pumping with these tubing means that torque and therefore power consumption increases. Additionally, long-term usage will require chips that will remain hydrophobic for long periods to avoid contamination and smearing. Methods such as "whole Teflon microfluidic chips" developed by (Ren, Dai et al. 2011) for the production of perfluoroalkoxy (PFA) and fluorinated ethylenepropylene (FEP) could be integrated and used to fabricate chips for long term use in remote locations where replacing components would be too difficult.

This peristaltic micropump and droplet generation regime has been further developed, applied as part of a continuous monitoring system and tested in field. Described in Chapter 5 is the design, characterisation and preliminary data for the early field deployments of this method as part of a holistic device for the continuous monitoring of chemistry in waterways. Longer droplet trains are applied in Chapter 6 towards developing platforms to monitor low quantity biomarkers using more complex assays in droplets.

Chapter 5-Monitoring nitrite and nitrate levels in rivers and estuaries

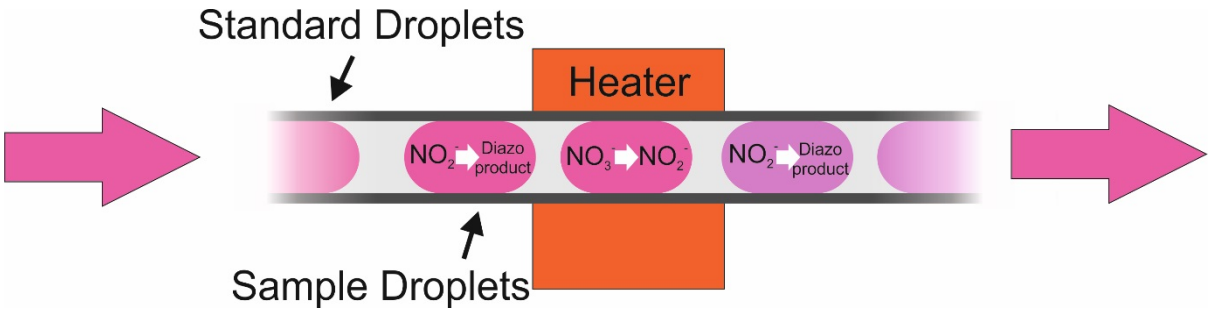

This chapter demonstrates the first ever field-deployable droplet-based system for analysis of water chemistry with *in-situ* calibration.

Traditionally, water chemistry has been measured by taking spot samples, either manually or using autosamplers (Nightingale, Beaton et al. 2015), transporting to a laboratory where the samples are then analysed. As described in section 1.3 measurement of aqueous nutrients such as nitrite and nitrate are extremely important for determining the health of aquatic ecosystems and studying biogeochemical cycles. Nitrate and nitrite are key nutrients in natural waters (rivers, lakes, oceans etc.) particularly for monitoring rivers susceptible to anthropogenic pollution as part of early warning systems for algal blooms and eutrophication (Burt, Howden et al. 2010).

In-situ measurement with small and low power analytical devices at the sampling site offers an exciting option for monitoring water chemistry. Removing the logistical problems of transporting samples reduces the risk of sample contamination and degradation, while measuring in even in remote locations. These sensors also raise the possibility of large scale networks of sensors deployed on moorings and autonomous vehicles such as profiling floats and gliders (Nightingale, Beaton et al. 2015). With many sensors larger data sets can be obtained, building up a detailed picture of water chemistry (Burt, Howden et al. 2010). When compared to competitor technologies such as voltammetry, microfluidic sensors offer high limits of detection and non-drifting measurements. However, they suffer from the need to replace fluids and are limited by temporal resolution (limits how easily they can be deployed on moving vehicles).

There have been numerous reports of field-deployable continuous-microfluidics based analysers, (Bende-Michl and Hairsine 2010, Nightingale, Beaton et al. 2015). However, droplet-based systems could offer several advantages, over the current state-of-the-art continuous microfluidics sensors. Moving to a droplet regime and removing Taylor dispersion offers the possibility of increased temporal resolution and remove the need to flush the system between samples. This could also potentially reduce the amount of fluid used in each measurement from millilitres to microliters, thus improving the long-term viability and economy of monitoring.

The work presented in this chapter demonstrates the first ever field-deployable droplet-based system for *in-situ* analysis of water chemistry. The system was tested both in the lab and in a local tidal river (Itchen). Additionally, I briefly describe a mathematical method of correction for a specific and interesting form of gas-mediated crosstalk developed by our group used in deployments to ensure accurate monitoring. The device development, calibration and studies presented here have produced presentations at international conference Microtas 2017 and 2018 (available in the appendices) and also contributed to a journal paper presented in Lab on a Chip (Nightingale, Hassan et al. 2018) available in the appendices.

This work was carried out as part of a larger project in collaboration with other members of my academic group. With the long-term goal of producing a field-deployable droplet-based system for *in-situ* analysis of nitrate and other important nutrients, metal ions etc. in waterways. Dr Adrian Nightingale collaborated on deployments and spearheaded the crosstalk correction method. Dr Sammer Ul-Hassan provided optical flow cells and collaborated on deployments of the field device. MSc student Ke Du carried out bulk assay measurements that informed the assay timings used in the droplet platform. The PID control of the heating unit was produced by MSc student Yang Li. Dr Sharon Coleman carried out bulk assays analysis of spot river samples to compare with the droplet platform.

My main contributions are on the hydraulics (pumping and droplet generation), integration of the various components, lab calibrations of the sensor and field deployments. Applying the peristaltic micropump and droplet pair generation I have developed and integrating it with the other sensor components.

5.1 Methods and Materials

5.1.1 Design of the droplet-based fluid handling system

The prototype system detailed in this chapter makes use of the pulsed droplet generation regime described in this thesis and the two-droplet train method detailed in Chapter 4. A schematic showing the fluidic pathway of the droplet-based nitrite/nitrate sensor is shown in Fig. 69.

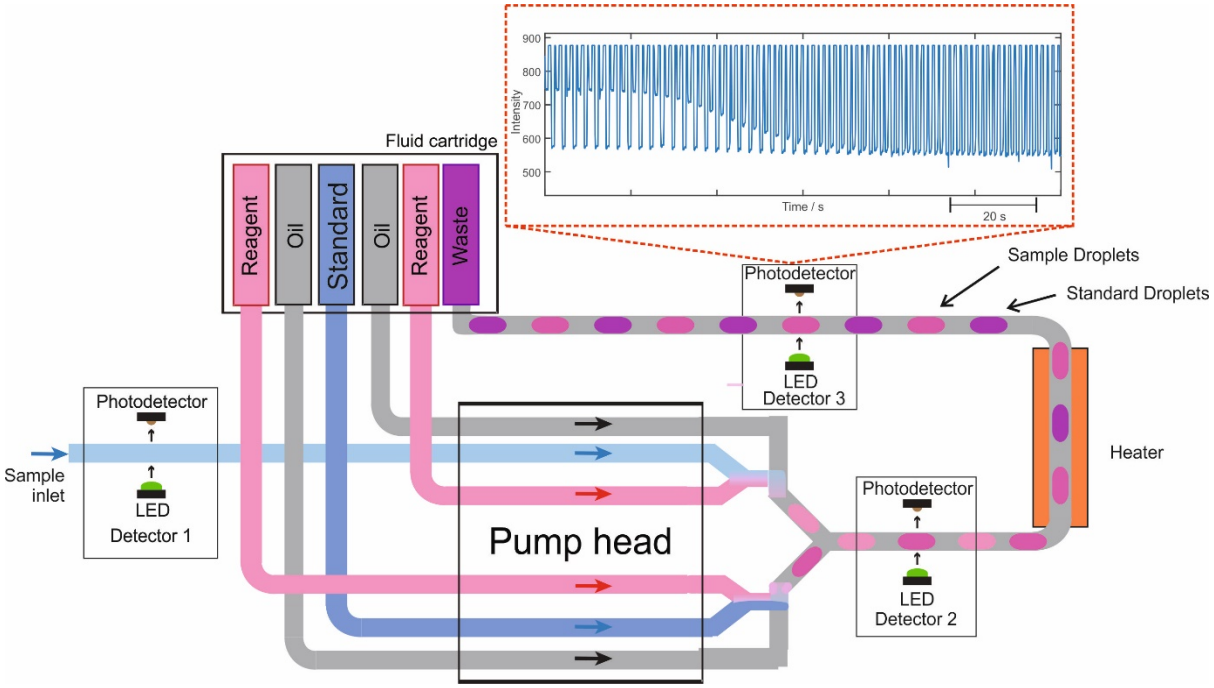

Figure 69 *Schematic 'map' of droplet microfluidics platform for continuous monitoring of environmental nitrite and nitrate with in-situ standard. Inset: Example droplet data featuring nitrate sample droplets changing concentration while standard droplet concentration is kept constant.*

Deformable liquid containers hold FC40 oil (containing 0.3% PEG-PFPE surfactant), Griess reagent and Vanadium (III) chloride solution, standard (containing 100µm nitrite and 300µm nitrate) for calibration and waste. A miniaturised peristaltic micropump drives all fluids to the PDMS chip for droplet generation. A heated reaction vessel and three miniaturised spectrophotometer flow cells are used in the sensor platform. One for measurement of incoming changes in refractive index by changes in salinity. Another for nitrite measurement by colorimetry placed between the droplet generation chip and heater. A third for measuring total oxidised nitrogen (combination of nitrite and nitrate) placed downstream from the heater to allow for the complete reduction of all nitrate in the sample to nitrite and reaction with Griess reagent to form the coloured complex. Electronic control/data

collection components are also integrated including: Arduino nano microcontroller board, SD card attachment for Arduino board thermal sensor, Mosfet, eight AA batteries and two 9V batteries for power over 48 hours.

5.1.2 Peristaltic micropump

At the heart of the prototype device is the peristaltic micropump. All pumping and droplet generation in the following calibrations and field deployments was carried out by a single built in-house peristaltic micropump (size: 44.5mm*31.6mm*18.2mm) described in Chapter 4. The pump is operated using a DC motor (Pololu 1000:1 Micro Metal Gearmotor) which turns a 3D-printed rotor mounted to the motor shaft (10mm diameter) . The patterning of features on the rotorhead contact the pumplines determining the timing and magnitude of the fluidic pulses. Fluid samples are drawn into the system by peristalsis passing through the first optical flow cell, for detection of any optical changes in the sample such as turbidity or refractive index which will be affected by the salinity and unfiltered particulates.

The sample is delivered into a polydimethylsiloxane (PDMS) microfluidic chip where it meets a stream of reagent (1:1 volumetric ratio) at a Y-shaped junction. The sample reagent mix is then formed into droplets by the previously described “anti-phased peristaltic pumping” method. A key feature of this system is the generation of alternating droplets containing sample and standard, as described in section 4.5. Standard droplets are generated mirroring the sample droplets meeting reagent at a Y junction in a 1:1 ratio and then broken off into droplets. These pairs of alternating droplets flow to a main Y-Junction and into the main reaction channel exiting the PDMS microfluidic chip into PTFE tubing (0.5 mm ID). Interspersing standard droplets between sample droplets allows continuous calibration of the sample measurement. This approach has also been successfully demonstrated in (low-throughput) continuous-phase microfluidic analysers (Beaton, Cardwell et al. 2012, Clinton-Bailey, Grand et al. 2017).

As with previous studies, the main pump chassis and the rotor were 3D printed in “VeroClear” material using an Objet500 Connex3 polyjet printer (Stanford Marsh Ltd). Six fluidic pumplines were used for the double droplet generation, with pump outlets connected to the microfluidic chip using PTFE tubing (ID 500 µm, OD 700 µm). For reliable droplet generation, channels were treated with Aquapel (PPG Industries) to ensure preferential wetting by the fluorous oil. PDMS microfluidic chips were replica moulded from a 3D-printed master as described in Chapter 2. The 3D-printed master was designed with nominal channel dimensions of 600 µm height for all channels, a main channel 200 µm wide and inlets 100 µm wide. Limitations in printing resolution and feature shrinkage with post-treatment resulted in final channels with a Gaussian profile and dimensions of 590/350 µm height/full-width-half-maximum for the 200 µm nominal-width channels and 480/320 µm for the 100 µm nominal-width channels. The entry/exit points featured enlarged channels (660 µm nominal width and 550 µm nominal height) so that tubing could be later inserted. After printing, the mould was baked overnight at 65 °C to remove any uncured precursor materials. PDMS was added to the mould (Sylgard 184, 10:1 ratio of elastomer to curing agent) and baked at 65 °C for a minimum of one hour. After removal from the mould, the chips were cut to shape and then sealed to a flat piece of PDMS using the “half-cure”

method(Go and Shoji 2004, Eddings, Johnson et al. 2008, Peng, Zhang et al. 2008). To generate the alternating sample/standard droplets, the rotorhead was designed to pump fluids in the order: 1. Sample and reagent; 2. Oil; 3. Standard and reagent; 4. Oil. A silicon lubricant (Rocol Silicone Grease SAPPHIRE Aqua-Sil) was used to lubricate the movement of the rotorhead with respect to the chassis and pumplines, decreasing the torque and ultimately increase pumpline lifetime.

5.1.3 Assay choice and reaction control

The device made use of a modified version of the well-documented Griess reagent, a mixture of sulfanilamide and N-naphthyl-ethylenediamine (NEDD) (Grasshoff, Kremling et al. 1999) (Miranda, Espey et al. 2001, Garcia-Robledo, Corzo et al. 2014, Schnetger and Lehners 2014). Griess reagent produces a pink diazonium product when mixed with nitrite suitable for detection using the 516nm green LEDs for illumination. For detection of nitrate, it must be reduced to nitrite and the total oxidised nitrogen measured. Previously reduction of nitrate to nitrite was achieved in field-deployable systems by flowing the sample over a copperised-cadmium surface. However, this is not appropriate for droplet microfluidics, where the droplet contents must be contained away from surfaces. A homogenous method, based on the method previously reported by (Miranda, Espey et al. 2001), in which vanadium (III) chloride is added to the Griess reagent and heat applied to accelerate the reaction, is used in the prototype. When heated, the vanadium reduces nitrate (NO_3^-) to nitrite (NO_2^-) which then reacts with the standard Griess reagent to produce a coloured diazonium product. As described in Fig. 70 this nitrate reduction takes place during the approximately eight minutes taken to move droplets through the heater, which is kept at a constant 50°C. After the sample and reagent met, they co-flowed into a T-junction to meet a fluorous oil (Fluorinert FC-40, with 1.8% non-ionic triblock co-polymer surfactant) which broke the co-flow into droplets (which we will refer to as “sample” droplets). While fluorous capillary tubing and T-connectors could have been feasibly used for droplet generation, a microfluidic chip was used here for space economy and ease in tailoring fluid paths as required. It should be noted that the rate-determining step in this reaction is the reduction of the nitrate by the vanadium (III) chloride. In the equivalent nitrite-based reaction the reaction kinetics are much faster with all reactions complete within one minute. This is highly advantageous for the droplet sensor as it means the nitrite reaction will go to completion and colour development measured before the droplets enter the heater in which the nitrate reduction takes place, so the combined nitrate and nitrite content can be measured.

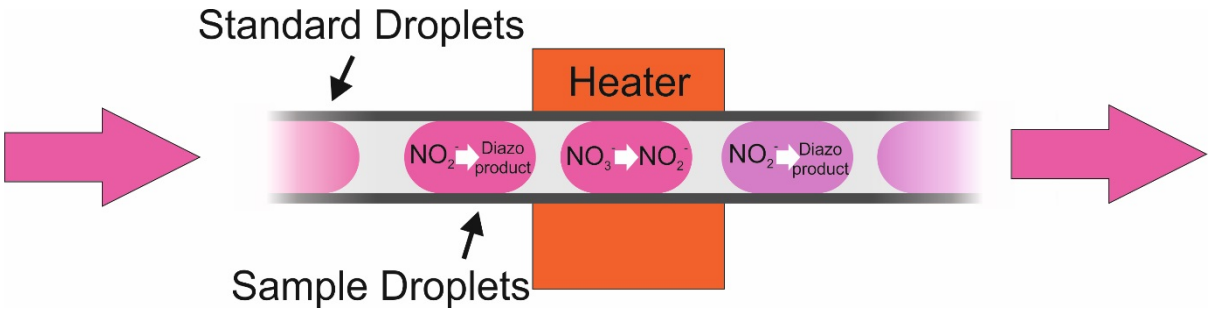

Figure 70 *Schematic of the important assay steps carried out in droplets with nitrate reduced to nitrite in the heated section of the device by vanadium (III) chloride and then converting the Griess reagent to the coloured diazo product.*

The modified Griess reagent was formulated by first weighing out 2.5 g of vanadium (III) chloride and adding to a 250 ml volumetric flask along with 50ml of ultrapure water to form a dark brown solution. 15 ml of concentrated (37 %) hydrochloric acid was added which caused the solution to turn a dark turquoise colour. 1.25 g of sulfanilamide and 0.125 g of NEDD was added, dissolved and the solution finally made up to the volumetric mark using ultrapure water. Hydrochloric acid (37 %), potassium nitrate (≥99 %), vanadium (III) chloride (97.0 %), sulphanilamide (≥99.0 %), N-(1-napthyl) ethylenediamine dihydrochloride (NEDD, >98 %), sodium nitrite (99.0 %), were obtained from Sigma Aldrich, UK. Unless otherwise stated, water was ultrapure grade (18.2 MΩ, Barnstead EASYpure RODI). Fluorinert FC40 oil was obtained from Acota Ltd, UK. The tri-block co-polymer surfactant (perfluorinated polyether / polyethylene glycol / perfluorinated polyether) was synthesised in-house using the previously reported protocol (Chokkalingam, Tel et al. 2013).

The heater was fabricated in-house by winding PTFE tubing (500 µm ID, 700 µm OD) around a 1 cm length of copper tubing. 3D-printed end-pieces (polylactic acid, Ultimaker 2) were attached to each end of the tube to help keep the PTFE tubing in place. A resistive polyimide thin film heater (Watlow Kapton K05711980AL-L 1/2" x 1.1/8") was placed on the inside surface of the tubing and a digital thermometer (Maxim DS18b20) was placed in the centre of the tubing. The whole assembly was wrapped in an approximately 3 cm-thick blanket of cotton wool. The heater was powered by a 9 V battery *via* a metal oxide semiconductor field emission transistor (MOSFET, Vishay TO-220AB) controlled by the same microcontroller used to handle the flow cell data. The microcontroller was programmed with custom pulse width modulation (PWM) code to control the power supplied to the heater and maintain its temperature (as determined by the digital thermometer) at 50 °C.

5.1.4 Detection of droplet contents

Three inline spectrophotometers were used to monitor contents of droplets as described in previous chapters. The detection flow cells (shown schematically in Fig. 71a) are fabricated in black polymethylmethacrylate (PMMA) micromilled with two channels. One channel holds a short length of PTFE tubing (ID 500 µm, OD 700 µm, Adtech Polymer Engineering, UK) and another defines a light path directly transecting the tubing. A 516nm LED (Cree CLM4B-GKW-CWBYA693, Farnell Onecall) and light-to-voltage converter (TSL257, Texas Advance Optical Solutions, UK) were positioned at either end of the light path using a 3D-printed support (polylactic acid, printed on an Ultimaker 2 fused deposition modelling printer). The LED was powered by a constant current while the light-to-voltage converter was connected to a microcontroller (Arduino Nano) and continuously measured the signal voltage. Data was saved to on-board SD card or passed back to a PC running Labview 2012 (National Instruments). The three detectors were placed one at the inlet to measure incoming turbidimetry (detector 1), one before heating to measure nitrite concentration (detector 2), and one after the heater to measure nitrite and nitrate concentration (detector 3). Figure 71b shows example raw data output representing light intensity measured in the pre-heater flow cell (flow cell2) with peaks in intensity representing oil and dips representing droplets of 50 µM nitrite and reagent. Figure 71c shows the same for the post-heater flow cell (flow cell3) with peaks in intensity representing oil and

dips representing droplets 100μM nitrate solution. Absorbance data traces for both of these flow cells calculated by the Beer-Lambert method is shown in Fig. 71 d&e respectively.

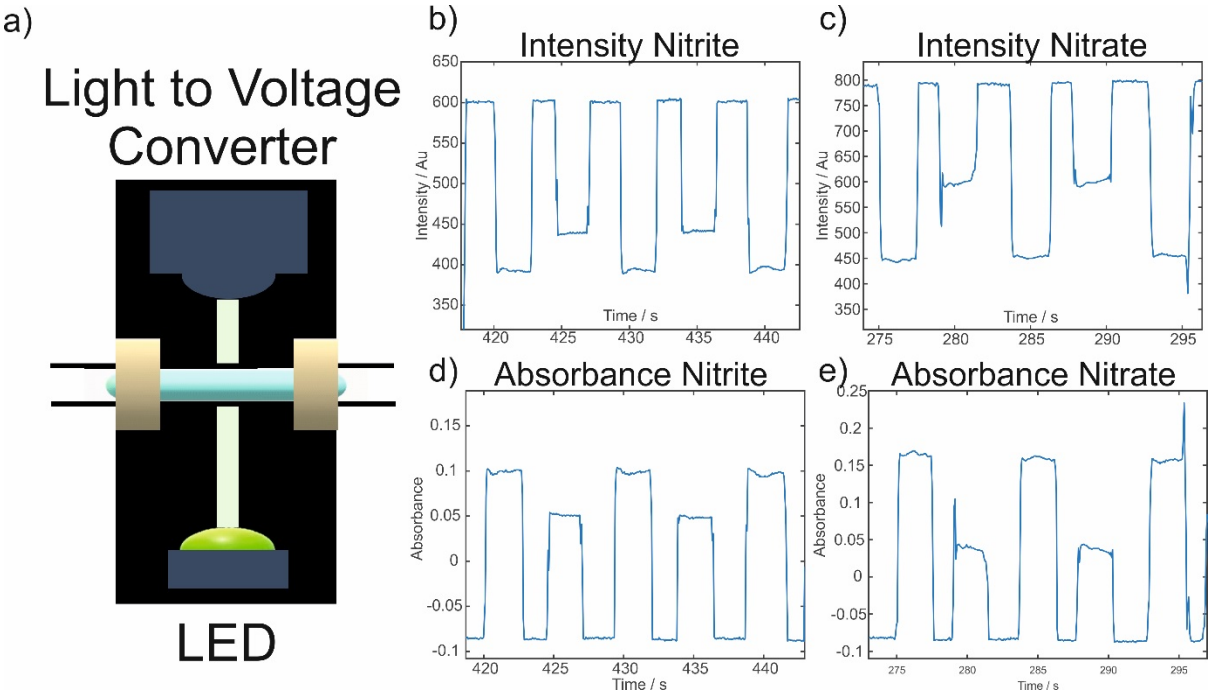

Figure 71 *Miniaturised in-line spectrophotometer flow cells used for detection of droplet contents a) Schematic of a built in house optical flow cell b) Raw intensity data trace output from the pre-heater flow cell with peaks in intensity representing oil and dips representing droplets of 50μM nitrite solution c) Raw intensity data trace output from the post-heater flow cell with peaks in intensity representing oil and dips representing droplets 100μM nitrate solution d) Absorbance data trace of the pre-heater flow cell from raw data in b) e) Absorbance data trace of the post-heater flow cell from raw data in c).*

5.1.5 Calibration of the three optical flow cells

Calibration of the optical flow cells is required to accurately calculate the quantity of analyte in the sample. I first quantified the flow cells response to refractive index change. This is important as the changing water salinity (e.g. in estuaries) can affect absorbance measurements. The refractive index and hence measured intensity in flow cell 1 will change with the quantity of dissolved salts in water. Figure 73a correlates changes in refractive index with salinity from 0-100% (100 % equal to 1 g of NaCl per 1 g pure water). The linear response means the effect of refractive index change can be measured in flow cell 1 and used to correct the other flow cells. The analytical performance of the device was then tested by flowing different concentrations of nitrate and nitrite standards through the device. A selection of standards were used to relate measured absorbance to the quantity of nitrite and nitrate in the sample. Figure 73b shows how quantity of nitrite in the sample relates to the measured absorbance of flow cell 2 (pre-heater) while Fig. 73c shows how nitrate relates to the measured absorbance of flow cell 3 (post-heater).

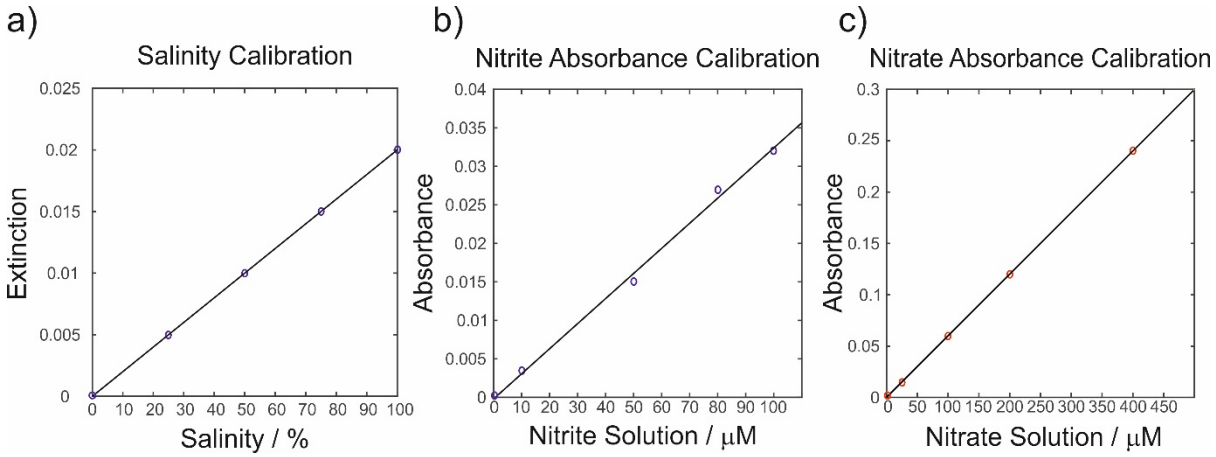

Figure 72 *Calibration of the three miniaturised in-line spectrophotometer flow cells used in the prototype river monitoring device (see Fig. 69 for schematic) a) Calibration of incoming sample salinity (100% equal to 1g of salt per 1g pure water) as this relates to changes in extinction of the sample droplets b) Calibration of measured absorbance values against sample amount of nitrite for flow cell 2 (pre-heater) c) Calibration of measured absorbance values against sample amount of nitrate for flow cell 3 (post-heater).*

Detector 2 gave a strong response to nitrite concentrations, with a linear relation that passed through the origin. Detector 3 positioned after the heater gave a strong response for both nitrite and nitrate, consistent with the heater having successfully accelerated the nitrate reduction. The limit of detection was determined using the 3-sigma method to be 10 μM with the flow cells 0.4 mm optical path length. Compared with other existing microfluidic systems, limit of detection is quite high, due to the relatively short (0.4 mm) optical path length and crude flow cell fabrication. While more than adequate for monitoring riverine and other hydrological waters, the sensor in its current form would be unsuitable for use in low-nitrate environments such as the oligotrophic ocean. This may be overcome by extending the optical path length in flow cells by axially illuminating droplets that have been elongated by constricted channels as is planned for the future (limit of detection has been improved to ~0.7 μM recently by other group members after my PhD studies).

5.2 Results and discussion

5.2.1 Calibration of fluidic lengths for optimal assay conditions and flow rate

The second optical flow cell is located downstream at a location corresponding to one minute's reaction time after the droplet generation. This ensures any nitrite will have reacted, but negligible nitrate will have been reduced to nitrite hence this signal reflects the quantity of nitrite in the sample. The droplets then carry on through the PTFE tubing, which is routed through a heater unit at 50 °C controlled via a made in house PID controller (proportional–integral–derivative) controller with an optimal residence time 8 min. From there, the droplets exit the heater, pass through the third optical flow cell measuring total oxidised nitrogen (combination of nitrite and nitrate) and are then collected in a waste bag.

There are many conditions to consider for optimal function of the device including: changeover time which should be kept to a minimum by short inlet tubing (reducing Taylor dispersion) and is also affected by inlet flow rate of the inlet, fluid consumption which for field deployments should also be kept to a minimum (further improved with oil recycling), but most critical are the residence times for the assay which must be kept constant, also the oil spacing and droplet volumes appropriate for robust generation even at relatively high back pressures caused by long tubing length downstream for assay residence. Tubing lengths flow rates etc. from the inlet through the entire system to the waste bag must be calculated to match to the optimal assay conditions.

Ten different configurations of the "Evans" pump (detailed in chapter 4) were tested at different flow rates and also compared to a previously designed system utilising a screw-driven peristaltic pump (shown in Fig. 25). Table 1 displays the optimisation of motor type, voltage supplied, rotorhead feature pitch and tubing length from the droplet generation chip to detector 2 optimised for the measurement of nitrite for a range of pump configurations. The optimal residence time of 1 minute for this reaction was determined using uv/vis spectrometry (Lambda-35 spectrometer) by MSc student Ke Du.

After passing through detector 2, droplets enter the heated reaction vessel where the reduction of nitrate to nitrite takes place. Table 2 displays the optimisation of motor type, voltage supplied, rotorhead features and tubing length for the heated section. The optimal residence time in the heater unit of 8 minutes was determined using uv/vis spectrometry (Lambda-35 spectrometer) by MSc student Ke Du. The same ten pump configurations were tested at different flow rates again compared to a previously designed system utilising a screw-driven peristaltic pump. As long as the residence times and reaction conditions for the assay are kept constant, the results of the assay carried out in each droplet will be unaffected. Therefore, the tubing lengths and flow rate are correlated in the design of the fluidics, to guarantee a fixed residence time.

Three rotorhead variations (15^{o}aq 30^{o} oil, 30^{o} aq 60^{o} oil and 15^{o}aq 60^{o} oil pitch) were used each with equal quantities of reagent and sample or standard delivered to each droplet (volumes detailed in Fig. 63). These rotorhead dimensions were chosen to produce droplet volumes, droplet generation rates, flow rates etc. in the approximate desired range at the rotation rates which the pump is capable of (particular at low voltages). Following this calibration, it was decided to use the "Evans pump" (Pololu 1000:1 Micro Metal Gearmotor, RS components) with rotorhead featuring a 15^{o} pitch features for the aqueous pumplines and 60^{o} for the fluorous oil pumplines running the pump at 1.5 V (highlighted thoughout). Due to this configuration satisfying all needs for the device including: short changeover time, low fluid consumption (further improved with oil recycling), correct assay residence times, oil spacing and droplet volumes appropriate for robust generation even at relatively high back pressures caused by long tubing length downstream for assay residence.

Table 1 *Calibration of a variety of micropump parameters and fluidics (length of tubing from droplet generation to detector 2 (see Fig. 69)) required for optimal assay conditions (Tubing ID 0.5mm).*

Pump details	Measured velocity (mm/s)	Total flow rate (ul/min)	Distance to Det 2 (cm)	Residence time (s)
Screw pump, 5mm pitch, (Pololu 210:1 Micro Metal Gearmotor, RS components) 1.5V	0.36	4.25	2	55
Evans pump, Aq pitch 30°, oil pitch 60°, (Pololu 210:1 Micro Metal Gearmotor, RS components), 1.5V	7.14	84.1	42.9	60
Evans pump, Aq pitch 15°, oil pitch 60°, (Pololu 210:1 Micro Metal Gearmotor, RS components), 1.5V	5.50	64.8	33	60
Evans, Aq pitch 15°, oil pitch 60°, (Pololu 1000:1 Micro Metal Gearmotor, Chinese OEM), 1.5V	0.53	6.20	3.16	60
Evans, Aq pitch 15°, oil pitch 60°, (Pololu 1000:1 Micro Metal Gearmotor, Chinese OEM), 4.5V	3.47	40.9	20.8	60
Evans, Aq pitch 30°, oil pitch 60°, (Pololu 1000:1 Micro Metal Gearmotor, Chinese OEM), 1.5V	1.09	12.8	6.52	60
Evans, Aq pitch 30°, oil pitch 60°, (Pololu 1000:1 Micro Metal Gearmotor, Chinese OEM), 3.0V	3.03	35.7	18.2	60
Evans, Aq pitch 30°, oil pitch 60°, (Pololu 1000:1 Micro Metal Gearmotor, Chinese OEM), 4.5V	4.76	56.1	28.6	60
Evans, Aq pitch 30°, oil pitch 60°, (Pololu 1000:1 Micro Metal Gearmotor, RS components), 1.5V	3.75	44.2	22.5	60
Evans, Aq pitch 15°, oil pitch 60°, (Pololu 1000:1 Micro Metal Gearmotor, RS components), 1.5V	2.50	29.5	15.0	60
Evans, Aq pitch 15°, oil pitch 30°, (Pololu 1000:1 Micro Metal Gearmotor, RS components) 1.5V	1.67	19.6	10.0	60

Table 2 *Calibration of a variety of micropump parameters and fluidics (Length of tubing in heater required for optimal assay condition) for a variety of micropump parameters (Tubing ID 0.5mm).*

Pump details	Measured velocity (mm/s)	Total flow rate (ul/min)	Heated Section (cm)	Residence time (s)
Screw pump, 5mm pitch, (Pololu 210:1 Micro Metal Gearmotor, RS components) 1.5V	0.36	4.25	18.5	513
Evans pump, Aq pitch 30°, oil pitch 60°, (Pololu 210:1 Micro Metal Gearmotor, RS components), 1.5V	7.14	84.1	343	480
Evans pump, Aq pitch 15°, oil pitch 60°, (Pololu 210:1 Micro Metal Gearmotor, RS components), 1.5V	5.50	64.8	264	480
Evans, Aq pitch 15°, oil pitch 60°, (Pololu 1000:1 Micro Metal Gearmotor, Chinese OEM), 1.5V	0.53	6.20	25	480
Evans, Aq pitch 15°, oil pitch 60°, (Pololu 1000:1 Micro Metal Gearmotor, Chinese OEM), 4.5V	3.47	40.9	167	480
Evans, Aq pitch 30°, oil pitch 60°, (Pololu 1000:1 Micro Metal Gearmotor, Chinese OEM), 1.5V	1.09	12.8	52	480
Evans, Aq pitch 30°, oil pitch 60°, (Pololu 1000:1 Micro Metal Gearmotor, Chinese OEM), 3.0V	3.03	35.7	145	480
Evans, Aq pitch 30°, oil pitch 60°, (Pololu 1000:1 Micro Metal Gearmotor, Chinese OEM), 4.5V	4.76	56.1	229	480
Evans, Aq pitch 30°, oil pitch 60°, (Pololu 1000:1 Micro Metal Gearmotor, RS components), 1.5V	3.75	44.2	180	480
Evans, Aq pitch 15°, oil pitch 60°, (Pololu 1000:1 Micro Metal Gearmotor, RS components), 1.5V	2.50	29.5	120	480
Evans, Aq pitch 15°, oil pitch 30°, (Pololu 1000:1 Micro Metal Gearmotor, RS components) 1.5V	1.67	19.6	80	480

5.2.2 Temporal resolution of the droplet-based system

Increased temporal resolution (especially at lower flow rates) when compared to continuous flow microfluidics is one of the key advantages of droplet microfluidic platform, when compared to other bulk and microfluidic systems. Figure 72 shows the temporal response of a prototype device with a particularly long inlet (15 cm) due to difficulties in assembly at different pump speeds (1.5 V - 5 V, Aq pitch 15°, oil pitch 60°). This was accomplished by stopping the pump and moving the sample inlet of the device to a standard containing 100 µm nitrite. As would be expected temporal resolution decreases with decrease of pumping speed, controlled by the voltage delivered to the pump. A linear trend line is included as a guide to the eye in the linear portion of the calibration. As would be expected the changeover time decreased linearly with increased rotation rate, up until a point where the fluid in the inlet has not full come to rest between pulsations.

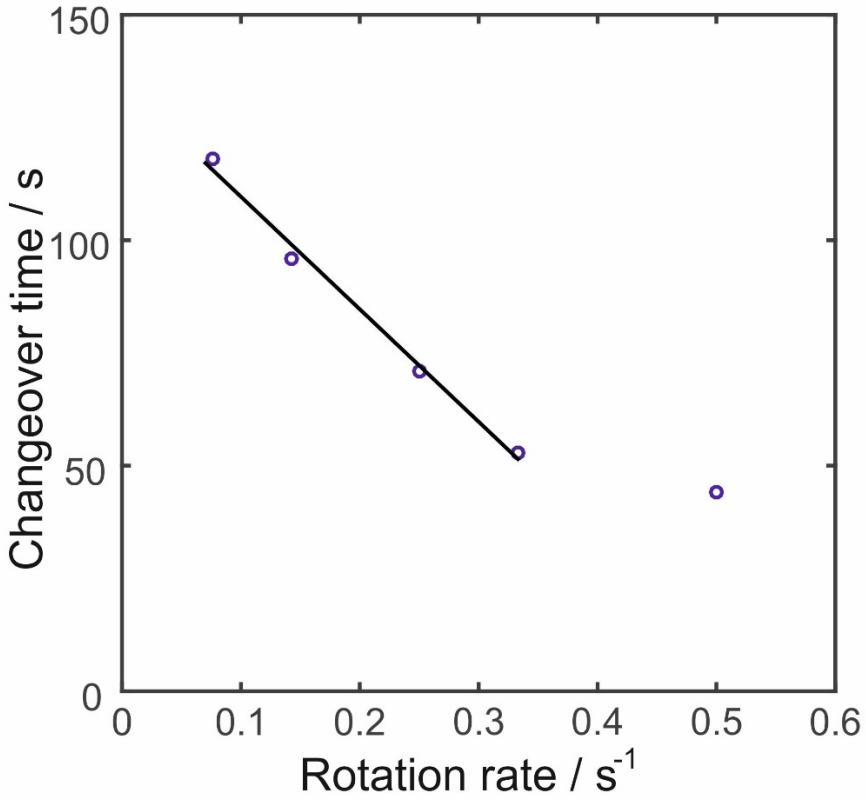

Figure 73 *Temporal Resolution of the nitrite & nitrate monitoring device - changeover time plotted against changing pump speed/flow rate by voltage (linear portion trend line R^2 = 0.992) (Inlet length = ~15cm, rotorhead pitch Aq pitch 15°, oil pitch 60°)e.*

The volume and distance that the sample must travel in the continuous phase (before splitting into droplets) will also affect the temporal resolution due to Taylor dispersion in the continuous flow stage. Therefore, the volume of continuous fluidics must be minimised. Table 3 details additional tests varying motor type, voltage supplied, rotorhead features and tubing length for the heated section all with a smaller inlet length of 6.5cm in order to display the improved changeover time and determine the predict changeover time of the fluidic structure used in field deployments.

Table 3 Changeover times between two concentrations of nitrites for a variety of micropump parameters.

Pump details	Measured velocity (mm/s)	Total flow rate (ul/min)	Changeover time (s)
Screw pump, 5mm pitch, (Pololu 210:1 Micro Metal Gearmotor, RS components) 1.5V	0.36	4.25	150
Evans pump, Aq pitch 30°, oil pitch 60°, (Pololu 210:1 Micro Metal Gearmotor, RS components), 1.5V	7.14	84.1	7.57
Evans pump, Aq pitch 15°, oil pitch 60°, (Pololu 210:1 Micro Metal Gearmotor, RS components), 1.5V	5.50	64.8	9.83
Evans, Aq pitch 15°, oil pitch 60°, (Pololu 1000:1 Micro Metal Gearmotor, Chinese OEM), 1.5V	0.53	6.20	103
Evans, Aq pitch 15°, oil pitch 60°, (Pololu 1000:1 Micro Metal Gearmotor, Chinese OEM), 4.5V	3.47	41.0	15.6
Evans, Aq pitch 30°, oil pitch 60°, (Pololu 1000:1 Micro Metal Gearmotor, Chinese OEM), 1.5V	1.09	12.8	49.7
Evans, Aq pitch 30°, oil pitch 60°, (Pololu 1000:1 Micro Metal Gearmotor, Chinese OEM), 3.0V	3.03	35.7	17.8
Evans, Aq pitch 30°, oil pitch 60°, (Pololu 1000:1 Micro Metal Gearmotor, Chinese OEM), 4.5V	4.76	56.1	11.4
Evans, Aq pitch 30°, oil pitch 60°, (Pololu 1000:1 Micro Metal Gearmotor, RS components), 1.5V	3.75	44.2	14.4
Evans, Aq pitch 15°, oil pitch 60°, (Pololu 1000:1 Micro Metal Gearmotor, RS components), 1.5V	2.50	29.5	21.6
Evans, Aq pitch 15°, oil pitch 30°, (Pololu 1000:1 Micro Metal Gearmotor, RS components) 1.5V	1.67	19.6	32.4

A faster flow rate would be desirable as this will reduce changeover times and increase temporal resolution. However, with increased flow rates comes an increased power consumption and fluid consumption (as detailed in table 4) which are especially important to consider for long term field-testing. Increased flow rate will also result in an increased backpressure due to the longer tubing lengths required for the reaction.

Table 4 *Estimated fluid usage per day for prototype river monitoring device with varying micropump parameters.*

Pump details	Measured v (mm/s)	Total flow rate (ul/min)	Fluid storage per day (ml)			
			Oil	***Rgt***	***Std***	***Waste***
Screw pump, 5mm pitch, 1.5V, (Pololu 210:1 Micro Metal Gearmotor)	0.36	4.25	3.06	1.53	0.76	6.11
Evans pump, Aq pitch 30°, oil pitch 60°, (Pololu 210:1 Micro Metal Gearmotor), 1.5V	7.14	84.1	60.6	30.3	15.1	121
Evans pump, Aq pitch 15°, oil pitch 60°, (Pololu 210:1 Micro Metal Gearmotor), 1.5V	5.50	64.8	56.0	18.7	9.33	93.3
Evans, Aq pitch 15°, oil pitch 60°, (Pololu 1000:1 Micro Metal Gearmotor, Chinese OEM), 1.5V	0.53	6.20	5.36	1.79	0.89	8.93
Evans, Aq pitch 15°, oil pitch 60°, (Pololu 1000:1 Micro Metal Gearmotor, Chinese OEM), 4.5V	3.47	40.9	35.3	11.8	5.89	58.9
Evans, Aq pitch 30°, oil pitch 60°, (Pololu 1000:1 Micro Metal Gearmotor, Chinese OEM), 1.5V	1.09	12.8	9.22	4.61	2.30	18.4
Evans, Aq pitch 30°, oil pitch 60°, (Pololu 1000:1 Micro Metal Gearmotor, Chinese OEM), 3.0V	3.03	35.7	25.7	12.9	6.43	51.4
Evans, Aq pitch 30°, oil pitch 60°, (Pololu 1000:1 Micro Metal Gearmotor, Chinese OEM), 4.5V	4.76	56.1	40.4	20.2	10.1	80.8
Evans, Aq pitch 30°, oil pitch 60°, (Pololu 1000:1 Micro Metal Gearmotor, RS components), 1.5V	3.75	44.2	31.8	15.9	7.95	63.6
Evans, Aq pitch 15°, oil pitch 60°, (Pololu 1000:1 Micro Metal Gearmotor, RS components), 1.5V	2.50	29.5	21.2	10.6	5.30	42.4
Evans, Aq pitch 15°, oil pitch 30°, (Pololu 1000:1 Micro Metal Gearmotor, RS components) 1.5V	1.67	19.6	14.1	7.07	3.53	28.3

5.3 *In-situ* estuarine deployment

Following laboratory calibration, the system was validated by measuring nitrite and nitrate levels over a 24-hour period in an estuarine deployment. The River Itchen, a chalk stream-fed river on the south coast of the UK (which feeds into the Solent estuary and ultimately into the English Channel), was chosen for the deployments due to its unique double tide variation which perturbs the nutrient levels within rivers. The deployment location (50°56'02.1"N 1°22'48.0"W) is approximately 200 m downstream of the Woodmill tidal barrier, 3-4 miles upstream of Southampton docks, and is subject to a tidal height variation of several meters. The prototype device was ballasted with approx. 3 kg weights and suspended from a pontoon, such that the intake was a constant ~15 cm under the surface throughout the deployment.

The prototype device was deployed for a minimum period of 24 hours sampling once every 10 seconds (over 8000 measurements in 24 hours) each deployment capturing two tidal cycles. Figure 74 shows data from an early field deployment of this system with standard ensuring flow cell data is self-calibrated.

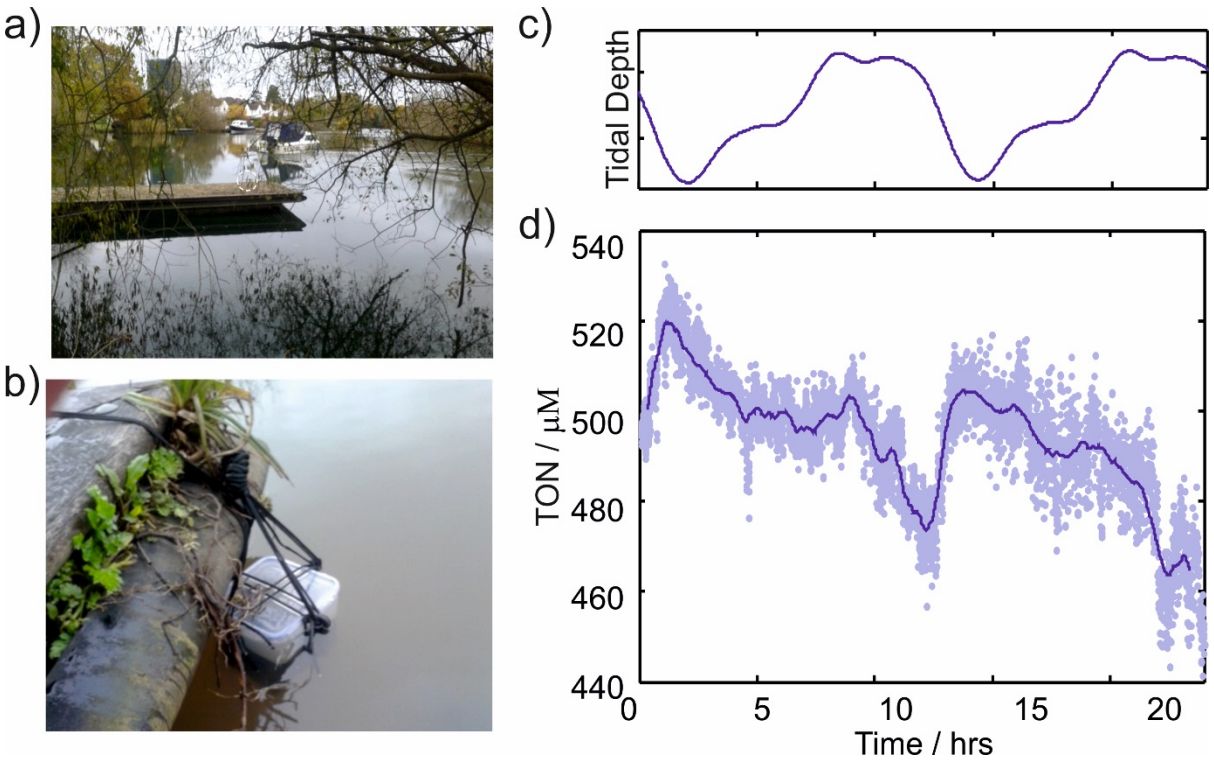

Figure 74 *Example of preliminary estuarine field measurements of total oxidised nitrogen (TON) (measured in detector3) a) photograph of deployment sight (end of pontoon) taken during the deployment b) Photograph of device during deployment c) Data showing the tidal depth of the river (http://sotonmet.co.uk) d) Total oxidised nitrogen levels measured by the prototype device (combination nitrate and nitrite levels) measured over a 24 hour deployment .*

All sensor fluidics and electronics (including batteries and fluid reservoirs for oil, reagent, standard and waste) were held within a watertight plastic housing 19 x 15.4 x 8.6 cm in size. The on-board standard was composed of 100 µM nitrite and 200 µM nitrate. The housing featured an unfiltered

inlet to intake river water and a USB cable that allowed data to be streamed to an external laptop during installation. All data was also stored on an on-board SD card and later processed using Matlab.

As would be expected the nutrient levels drop as the tide comes in, as seawater is considerably less nutrient dense than fresh river water. Spot samples were also taken at the chosen deployment site for testing in the lab by UV-vis spectrophotometry (PE Lambda 35 spectrometer). Data provided by Dr S. Coleman shows that at high tide nitrite levels are negligible while nitrate levels were shown to be 542uM while at low tide nitrite levels were 3.57uM and nitrate was 605uM.

During this deployment, there was an observed reduction in the absorbance of both the sample and standard droplets and a reduced frequency of droplets over time. This was due to reduced power fed to the motor during the testing, as batteries were depleted by the increased power consumption of the heater due to cold temperatures in the river.

While for a large portion of this deployment the quantitative value of the data was suspicious, this serves as a qualitative proof of principle before moving forward to further deployments after some improvements are made to the platform to address these issues. Future deployments feature increased power storage, a filter at the inlet and a form of crosstalk correction detailed in the next section.

5.4 Crosstalk Gas mediated crosstalk and correction

While trialling the droplet-based system for quantifying nitrate in water, we seemingly encountered crosstalk between the sample and standard droplet during some of the deployments. Fig. 75a shows some data from a test performed in the lab where this crosstalk was particularly apparent. As is explained in (Nightingale, Hassan et al. 2018), this crosstalk was driven by an uncommon mechanism wherein the analyte (nitrite) was converted into a gaseous intermediate (nitric oxide) at low pH which then diffused between droplets as described in Fig. 75b. Importantly it was found that the crosstalk occurred predictably, could be experimentally quantified, and measurements rationally post-corrected.

The inherent acidity of the Griess reagent (Giustarini, Rossi et al. 2008) (typical pH < 3) causes nitric oxide to be generated within each droplet as soon as the nitrate has been reduced to nitrite. Nitric oxide will then be able to diffuse through the droplet/oil barrier aided by the enhanced solubility of nitric oxide in fluorocarbon oils over water (Ortiz, Cabrales et al. 2013). However, this is a competitive process as shown in Fig. 75b which illustrates the various reaction, diffusion, and convection processes occurring within the system. Following nitric oxide generation there will be an ensuing competition between the chemical reactions that remove nitric oxide (regenerating nitrite and then converting to the diazonium dye) and transport of nitric oxide from the droplet. This competition determines how much nitric oxide leaves the droplet and thus the extent of the crosstalk. With the constant consumption of the nitrite in the generation of the diazo product there should be no remaining nitric oxide in the oil.

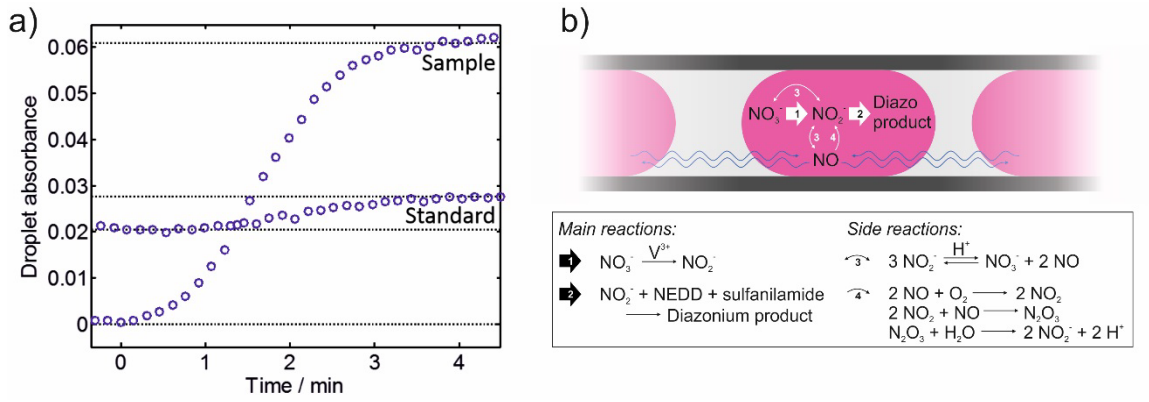

Figure 75 *Gas mediated crosstalk a) Absorbance of the two droplets sample and standard converted from raw light intensity as measured by the miniaturised in-line spectrophotometer flow cell where the standard is held constant at 100 µM $NO3^-$ and the incoming sample changes from 0 to 200 µM $NO3^-$. b) Schematic illustrating the processes occurring within each droplet in the original experimental setup, adapted from (Nightingale, Hassan et al. 2018).*

The presence of this crosstalk may seem strange as previously stated, within the field of droplet microfluidics droplets are often thought of as self-contained reaction chambers. However in recent years some research groups have shown that solutes can leave droplets under routine conditions, travelling into the oil phase and on into neighbouring droplets (Sandoz, Chung et al. 2014, Janiesch, Weiss et al. 2015) (Woronoff, El Harrak et al. 2011, Gruner, Riechers et al. 2016). With elevated pH not an option for carrying out the Griess assay not an option and no suitable alternative assay available

other than those which use highly caustic (Cogan, Cleary et al. 2013) or unstable reagents.(Patton, Fischer et al. 2002, Campbell, Song et al. 2006) a mathematical correction method was developed and applied to future deployments.

5.4.1 Mathematical correction of gas mediated crosstalk

After determining that the magnitude of the crosstalk is a fixed proportion of the source droplet, and that it is independent of the destination droplet concentration, a mathematical method of correcting for this gas mediated inter-droplet crosstalk was developed by Dr Adrian Nightingale (Nightingale, Hassan et al. 2018). Previous mathematical descriptions of surfactant driven crosstalk have used diffusion-based models, (Chen, Wijaya Gani et al. 2012, Gruner, Riechers et al. 2016). However, this empirical model requires minimal prior knowledge of the mechanistic process of the crosstalk and its associated kinetics. Using a crosstalk ratio it is possible to derive the absorbance we would expect if there were no crosstalk (corrected absorbance), based on measured absorbance of the two sets of droplets as shown by equation 18. It is important to note, given the gas-mediated crosstalk mechanism, the crosstalk ratio will change with reaction temperature. However, for fixed reaction conditions it should remain constant as in our tests.

Gas mediated cross talk correction equation $$A_{a,corrected} = \left(\frac{1+\alpha}{1-\alpha^2}\right)(A_a - \alpha A_b) \qquad (18)$$

Where A_a is the measured absorbance of droplet "a" (sample or standard), A_b is the measured absorbance of the neighbouring droplets, "b" (standard or sample) and α the crosstalk ratio defined as ratio of the amount of analyte that transfers to neighbouring droplets relative to that which remains in the source droplet (henceforth referred to as the crosstalk ratio, α). This ratio is defined by the quantities found in the droplets *after* crosstalk has occurred, and so can be experimentally determined. The crosstalk ratio α can be determined by including a blank droplet (contains no analyte) and measuring the ratio of concentration in the two droplet populations (This method is dependent on one droplet having zero analyte concentration before crosstalk). When both droplets initially contain analyte, another method must be used but only if one population (the standard) is kept constant while the analyte concentration in the other varies. This second method in effect performs a single-point calibration for each individual sample and can compensate for calibration drift but does require multiple measurements (Beaton, Cardwell et al. 2012, Yucel, Beaton et al. 2015, Clinton-Bailey, Grand et al. 2017). As the NO in the droplets is continuously removed forming the coloured diazo product, with the greiss reagent in excess there should be no NO remaining in the FC40 oil. While not necessary for laboratory-based testing, inline calibration is critical for field-deployable microfluidic chemical analysers where aging reagents and/or changing ambient conditions can shift the calibration. This method was used to correct for the data shown in Fig. 76 and 77. Full derivation of equation 18 is detailed in the ESI of (Nightingale, Hassan et al. 2018).

5.5 Further field deployments

Following the success of the mathematical crosstalk correction the same method as described in (Nightingale, Hassan et al. 2018) was applied to further deployments of the prototype device carried out alongside colleagues Dr Adrian Nightingale, Dr Sammer ul-Hassan. A 48-hour deployment shown in figure 76 and 24-hour period shown in figure 77. Additionally, the device was tested alongside a WTW pocket conductivity meter (TetraCon 325 conductivity cell) so that TON levels could be correlated to conductivity measurements.

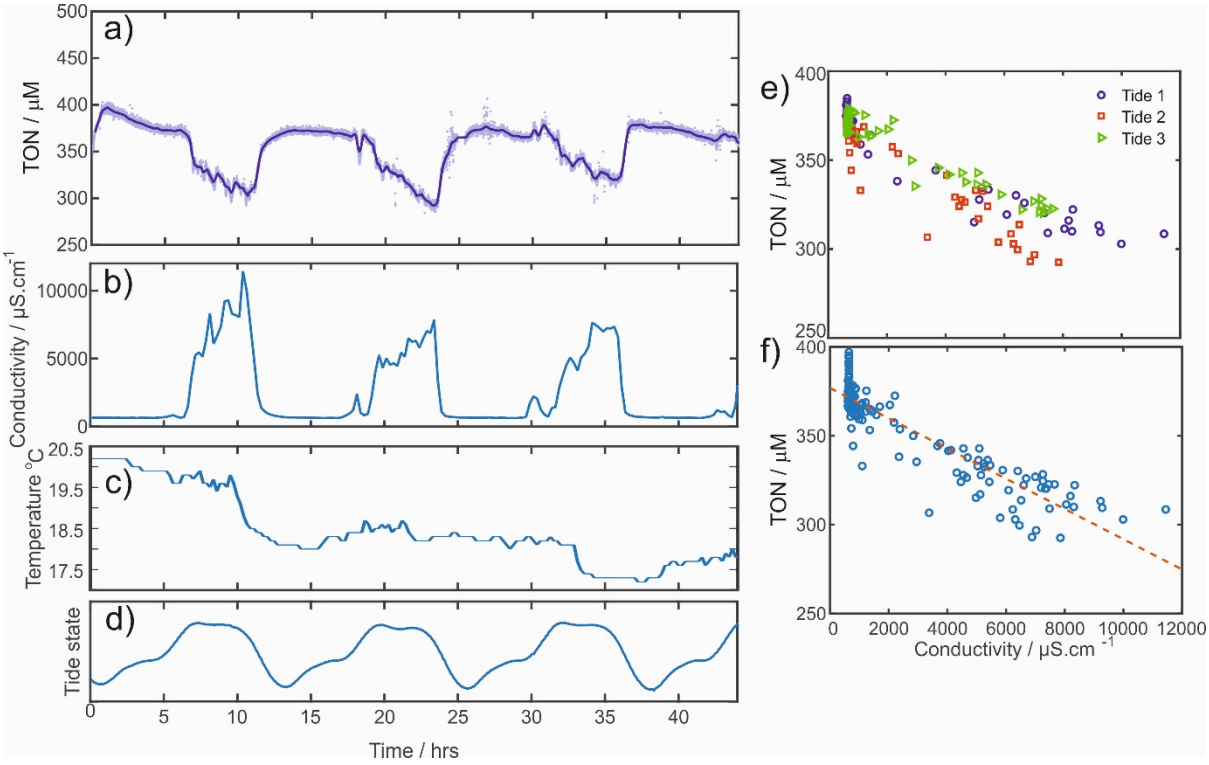

Figure 76 *Second field deployment of the prototype river monitoring device over a 48hour period including filter and comparison with conductivity measurements (WTW pocket conductivity meter) a) TON measured by the prototype device b) Conductivity of the sample water over the 48hour deployment c) Water temperature during the deployment d) Tidal state throughout the deployment (http://sotonmet.co.uk) e) TON vs conductivity over each tidal cycle f) TON vs conductivity over the whole field deployment* $R^2 = 0.8369$.

As was seen with the previous deployments nutrient levels dropped as the tide rises, confirmed by conductivity increase as measured by WTW pocket conductivity meter. This is to be expected as seawater is considerably less nutrient dense that fresh river water and has a higher concentration of ions. However, compared to the previous deployment there was a much greater dip in TON measurement at high salinity levels. It is hypothesised that this was due to the addition of a copper filter, which may have released copper ions over the course of the deployment interfering with the Griess assay. This was later corroborated by empirical testing carried out in the lab by Dr Sharon Coleman. For further deployments, this copper filter was removed. Fig. 77 displays a 24 hour deployment without the copper filter and utilising the mathematical method for crosstalk correction(Nightingale, Hassan et al. 2018).

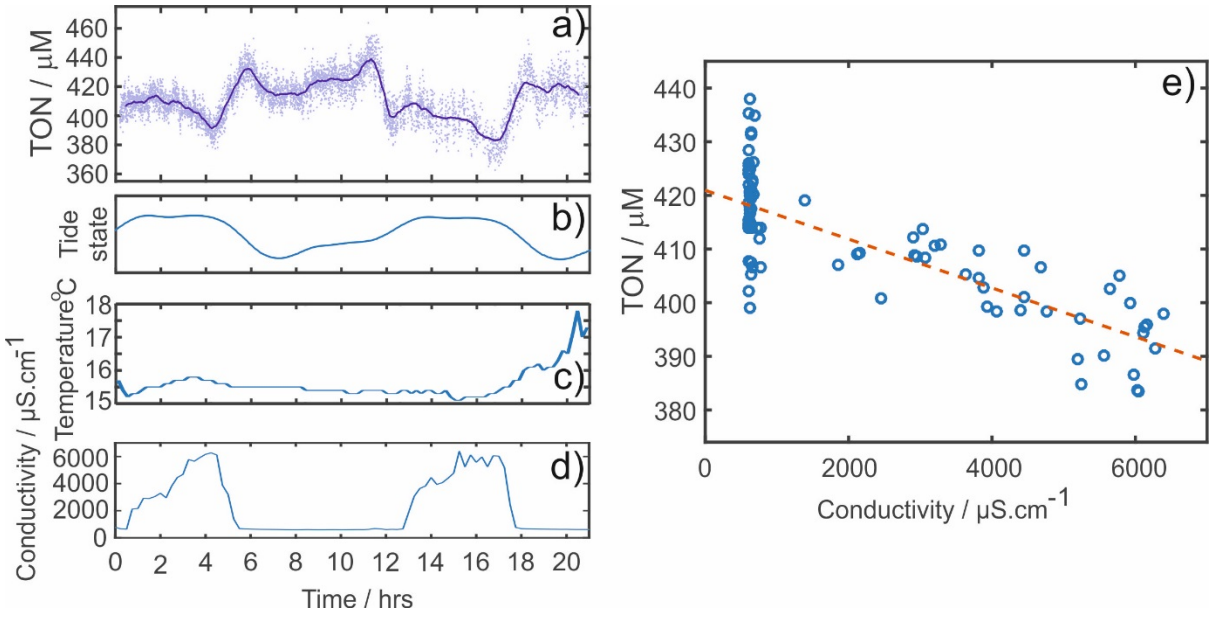

Figure 77 *Third field deployment of the prototype river monitoring device over a 24hour period (no filter) and comparison with conductivity measurements (WTW pocket conductivity meters) a) TON measured by the prototype device b) Conductivity of the sample water over the 48hour deployment c) Water temperature during the deployment d) Tidal state throughout the deployment (http://sotonmet.co.uk) e) TON vs conductivity over the whole tidal cycle* $R^2 = 0.6335$.

Figure 77 shows much smaller dips in TON measurement. While the conductivity measurements varied consistently with the tidal cycle, the tidal influence on TON concentrations was not consistent. The tidal effect is most obvious at the start of the deployment however later nitrite reduction seems to be out of phase with the conductivity and tidal changes which may be due to the lagging of internal timing from the simple Arduino chip. An independent crystal was added in the circuit in the further versions of the sensor after my PhD, and the problem was eventually solved.

Nevertheless, these early deployments show a compelling proof of principle for this method of using droplet microfluidics to monitor chemistry in the field. The system demonstrated here was capable of generating a wealth of data due to its relatively fast sampling rate (every ten seconds). Despite the high measurement frequency, the fluid consumption of the sensor was extremely low compared to the bulk procedure. Reagent was consumed at a rate of 2.8 ml/day, the total fluid consumption for the sample and standard was 2.8 ml/day, while the oil was recycled and hence not consumed. The droplet approach offers higher temporal resolution and the easy introduction of standards and blanks etc. compared with a continuous flow approach. Unlike electrochemical sensors that are capable of similar temporal resolutions, the microfluidic approach allows for the target analyte to be easily changed by swapping the reagents. Critically the wet chemistry method is robust for both freshwater and sea water monitoring and does not drift in the way standard electrochemical sensors do.

5.6 Conclusions of Chapter 5

In this chapter, I have:

a) Described a droplet microfluidics and colorimetric sensing platform for the continuous monitoring of biomolecules in waterways.
b) Shown this platform's favourable changeover times and low power consumption.
c) Described early calibrations of this platform for nitrite and nitrate sensing and salinity.
d) Shown some early preliminary field data for an estuarine deployment of this system.
e) Described an uncommon droplet crosstalk mechanism which was prevalent in these measurements
f) Utilised a mathematical crosstalk correction method developed by our group to correct for 2 further deployments showing nutrient levels in an estuarine river

In conclusion, this continuous monitoring platform shows promise for the monitoring of molecules related to biogeochemistry in waterways. Incorporating both droplet microfluidics generated by pulsed flows (Nightingale, Evans et al. 2017) and inline spectrophotometers (Hassan, Nightingale et al. 2016) allows for high temporal resolution and accurate measurement of both nitrite and nitrate. The further development and testing of this platform is being taking forward by the spinout company founded by my academic supervisor Dr Xize Niu South West Sensors and the new prototype device utilising the techniques etc. developed in this thesis are shown in Fig. 78.

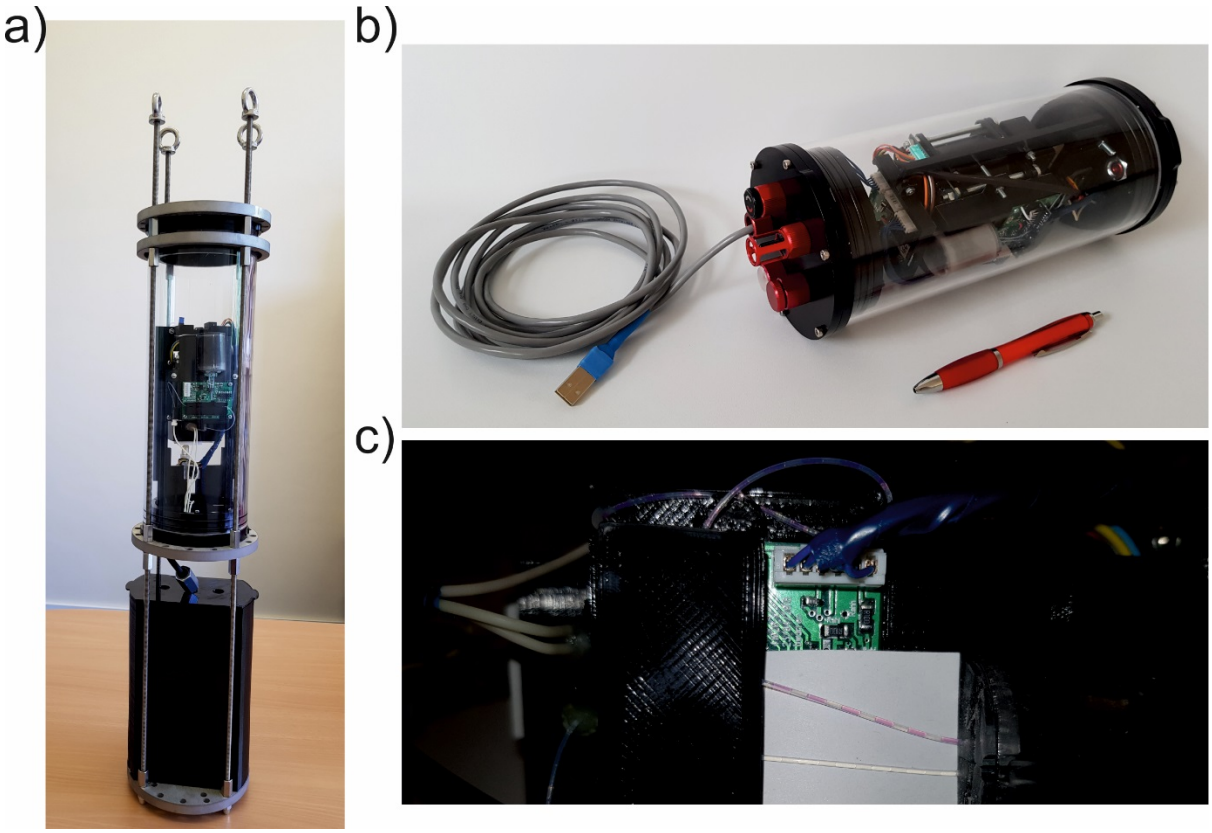

Figure 78 *South West Sensors new prototype device which uses this same technological approach of chemical assays droplet microfluidics for monitoring of water*

Chapter 6 – Continuous heterogeneous assays in droplets for monitoring cortisol

In this chapter, I describe an application of the pulsed droplet generation technique applied in conjunction with a magnetic bead trap and an inline spectrophotometer. This is a new method for performing heterogeneous assays continuously with a high temporal resolution utilizing droplet microfluidics in a miniaturised platform suitable for point-of-care monitoring. While this platform could be tailored for a wide variety of target analytes, here I have chosen to demonstrate a competitive assay for cortisol, a stress related steroid hormone relevant to several disease states.

6.0 Continuous heterogeneous assays in droplets for monitoring cortisol

In the previous chapters I have reported novel droplet microfluidic systems for continuous *in-situ* sampling and analysis using homogenous 'mix and read' assays. While these assays can be used to accurately measure a wide range of analytes, they lack the specificity and sensitivity required for some important biomarkers such as interleukins, cytokines, and hormones such as cortisol. As described in section 1.9 heterogeneous immunoassays utilise the specificity of immune interactions and are capable of detecting low quantities of analytes making them particularly suitable for measuring dilute biomarkers.

Microfluidic systems have been designed for carrying out heterogeneous immunoassays (Pamme 2006, Peyman, Iles et al. 2008, Peyman, Iles et al. 2009, Phurimsak, Tarn et al. 2014, Ferraro, Champ et al. 2016). However these systems use large expensive lab-based instrumentation and require specialist operation, and critically they are not designed for continuous operation. The droplet platform described in the previous chapters has shown great potential for performing biochemical assays and could be adapted and developed to automate the sampling, mixing, washing and extraction steps required in a heterogeneous assay.

Towards this end, I have designed a droplet-based platform that can carry out a heterogeneous assay in a repeated continuous fashion with a high degree of accuracy and temporal resolution. Cortisol was selected as an example analyte and a competitive colourimeteric assay developed by industrial collaborator LGC group was used to quantify it. Hence, there is a negative relationship between the intensity of colour development in the marker Tetramethylbenzidine (TMB) and the amount of test sample bound to the solid substrate.

Cortisol is a steroid hormone produced by the HPA axis as part of the bodys main response to stress (discussed in section 1.2.3). A variety of assay and sensing technologies have been implemented for monitoring cortisol However, many of these lab based assays are not suitable for point-of-care use requiring, pre-treatment steps, large expensive analysis equipment, and long assay times (several hours). If these assays are to be applied to continuous monitoring at the point-of-care, sampling rate and throughput will need to be greatly increased. This will provide an accurate picture of short-term events and long-term trends present in the circadian rhythms of analytes such as cortisol.

To this end I have chosen to apply a fully automated droplet microfluidics approach to perform a competitive heterogeneous colourimeteric assay initially developed (for a lab-based test) by my collaborator Dr. Susan Pang (LGC group). Sample collection is automated by the push-pull peristaltic micropump removing the possibility of manual error and throughput is greatly increased in the droplet microfluidics platform. This system was developed alongside PhD student Wahida Bhuiyan, Dr. Sharon Coleman, Dr. Susan Pang (LGC group) and Brett Warren (SWS). Work carried out in this chapter has informed presentation at MicroTAS 2018 and BioMedEng 2018 and a journal paper currently under preparation.

6.1 Bulk assay testing

The assay was carried out in a bulk lab procedure before transferring to the automated droplet platform. It is common procedure for these heterogeneous assays to be carried out with one of the capture antibodies anchored on the walls of a microwell plate, where samples and reagents can be washed over them. However, here we use a magnetic microbead-based approach as this is most translatable to the droplet platform with a similar approach presented by (Ferraro, Champ et al. 2016).

In our assay, cortisol competes with cortisol-HRP for binding sites on the magnetic microbeads, the beads are then purified and washed, and a marker added for quantification of the amount of bound cortisol-HRP. Hence, the measured signal is inversely proportional to the quantity of cortisol in the sample. A variety of marker molecules may be used for quantification including colourimeteric, radiological, or fluorometric markers. In this assay, we use 1-Step Ultra tetramethylbenzidine (TMB) for colourimeteric detection at 456nm. TMB is a sensitive chromogenic substrate that requires no preparation and unlike other commercially available substrates, contains no dimethylformamide (DMF) or dimethyl sulfoxide (DMSO). This makes it particularly suitable for integration into the POC droplet microfluidics platform.

6.1.1 Protocol for grafting of antibodies onto magnetic beads

Magnetic micro-particles (tosyl-activated Dynabeads by Invitrogen) were coated with anti-cortisol-3-BSA antibody (Calbioreagents) according to a protocol optimised by Dr S. Pang from the London Government Chemist Group (LGC). 250 µL of 100 mg/mL tosyl-activated beads were rinsed twice in 1 mL of coating buffer (0.1M sodium borate buffer, pH 9.5). They were re-suspended in 100 µL coating buffer and mixed thoroughly using a vortex mixer. For a quantity of 500 µg of coating antibody 12.1 µL of the antibody (suspended in phosphate buffered saline, PBS) was added to 722.9 µL of coating buffer and the full 735 µL added to the bead suspension with 415 µL of 3 M ammonium sulphate. The beads were incubated with the antibody at room temperature under slow tilt rotation for 24 hours. The beads were removed from the coating buffer, placed in 1250 µl of blocking buffer (PBS with 2 % w/v bovine serum albumin and 0.05 % Tween20) and incubated again for 24 hours with a slow tilt rotation. On the third day the beads were washed twice and resuspended in storage buffer (PBS, 0.1 % bovine serum albumin and 0.05 % Tween), giving a final concentration of 1 mg/mL assuming a 100 % recovery, and stored at 4°C. All reagents unless otherwise stated were from Sigma Aldrich. A set of neodynium magnets were used to retain the beads when washing and resuspending the beads.

6.1.2 Assay carried out in 96-well plate

In the bulk procedure 96-well microtitre plates (StarLab Ltd) and low protein binding tubes (Eppendorf) were used throughout. Anti-cortisol capture antibodies were coupled on the surface of the magnetic beads using the protocol as described in section 6.1.1. For the cortisol immunoassay, 0.1 mg of the antibody-conjugated beads were dispensed into individual wells within a 96-well skirted

PCR plate and placed onto a magnetic plate stand for 2 minutes. The resultant supernatant from each reaction well used was removed by manual pipetting. Serial dilutions of cortisol (CalBioreagents) were made from 100 ng/mL to 1.56 ng/mL in a background of PBS wash buffer. A tracer solution was prepared from cortisol-3-carboxymethyloxime horseradish peroxidase conjugate (CalBioreagents) with a 1:2500 dilution in PBS wash buffer (2μL tracer and 5mL buffer). Equal volumes of working tracer solution was added to each cortisol calibrant standard and from this 100 μL used to resuspend the pellet of magnetic beads in each well was subsequently resuspended by repeated gentle manual pipetting with each calibrant (NIST 921) for the standard curve. The plate was then transferred to a plate shaker for 15 minutes at 37 °C shaking at 1200 rpm. Following this incubation step, the beads were recovered using the magnetic plate stand and the recovered bead pellets were washed with a phosphate buffer. The beads were washed three times using fast rotation for two minutes and resuspending in wash buffer. For detection, the beads were incubated for 10 minutes at room temperature with 100 μL of 1-step Ultra tetramethylbenzidine (TMB) ELISA from Thermo Scientific. The reaction vessel was then placed on the magnetic plate stand and the resultant supernatant from each well was transferred to individual wells of a fresh clear flat-bottomed plate. The absorption was measured in a BMG Labtech OMEGA fluorostar plate reader at 450 nm. Resulting in the calibration shown in Fig. 79 (a linear trend line is included as a guide to the eye in the linear portion of the calibration).

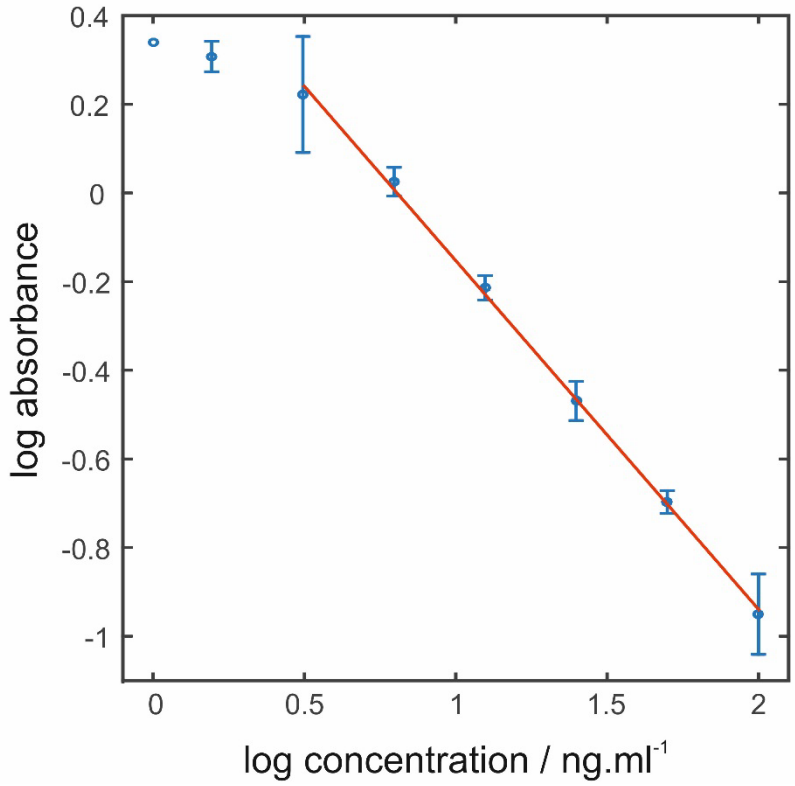

Figure 79 *Calibration carrying out the competitive cortisol assay by the bulk laboratory procedure (NIST serum 0-100ng/ml) Tecan Infinite M200 plate reader - The calibration was constructed from the magnetic bead based immunoassay for cortisol in a background of 6-fold diluted charcoal stripped serum encompassing a working range of 1.5625 ng/mL – 100 ng/mL of cortisol. (Tetramethylbenzidine (TMB) was used as the colorimetric substrate for the signal output, which entailed the measurement of OD at 450 nm) Errorbars represent standard deviation across 3 repeats (max 0.09).*

As shown in Fig. 79 the competitive assay carried out in the bulk lab procedure displayed very good linearity between 3.175 ng/ml and 50 ng/ml. However, the variation seen in this procedure was particularly large for some of the calibrant points on the curve (as high as 80 % RSD). This may be due to a variety of factors, but human error is a prime suspect as some of the other calibrants have much lower variation (as low as 1.7 % RSD). This procedure also took a considerable amount of time to complete (~4 hours) due to various washing and mixing steps as well as lengthy incubation times. This is vastly improved upon by moving to a droplet platform, which is capable of carrying out an assay every 10 seconds with 10 minutes from sampling to data.

6.2 Design of the droplet platform

After the bulk testing had shown its ability to quantify cortisol, a droplet system was developed integrating it. The prototype device shown schematically in Fig. 80 integrates: the pulsed droplet generation regime detailed in previous chapters and a branched microfluidic chip for continuously generating trains of droplets (repeated sequences). A set of miniaturised electromagnetic tweezers facilitate the extraction of the magnetic bead pellet from the droplet supernatant and re-disperse the pellet into the droplet containing the next assay step. Finally, once the full assay procedure is carried out a miniaturized spectrophotometer flow cell measures the colorimetric response. To perform the cortisol assay the device continuously generates droplet sequences composed of four droplets. The first droplet in this train contains the magnetic microbeads, cortisol-HRP competitor and the sample. The second and third droplets in the train are comprised solely of a phosphate buffered saline (PBS) washing buffer. The final droplet contains only the tetramethylbenzidine (TMB) colourimetric marker.

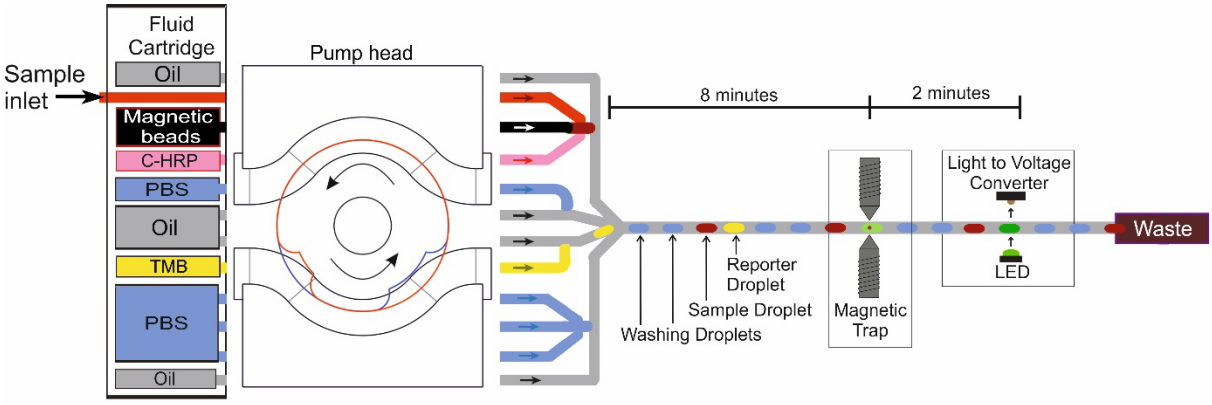

Figure 80 *Schematic 'map' of prototype droplet microfluidic platform for carrying out the competitive heterogeneous assay in droplets featuring peristaltic micropump and branched microfluidic chip for generating the train of four droplets, magnetic trap and in-line spectrometer.*

The assay procedure is shown schematically in Fig. 81. A lagrangian view of the assay procedure following a single antibody functionalised bead is shown in Fig. 81a. Sample cortisol first competes with cortisol-HRP to bind with the antibodies on the bead surface. The beads are then purified and washed in PBS wash buffer to remove interferrents and leftover cortisol-HRP. The cortisol-HRP

complex bound to the magnetic beads then acts as a catalyst for colour development in the tetramethylbenzidine (TMB) marker.

A Eulurian view fixed at the magnetic trap is shown in Fig. 81b. The sample/magnetic bead/cortisol-HRP droplet enters the trap; beads are captured and removed from the droplet. Beads are dragged through wash droplets to remove supernatant and then redispersed in final marker droplet. HRP catalyses colour change in the tetramethylbenzidine (TMB) marker. Once the assay procedure was completed (10 minutes in integrated system).colourimeteric detection was carried out by an inline spectrophotometer detailed in section 6.5.

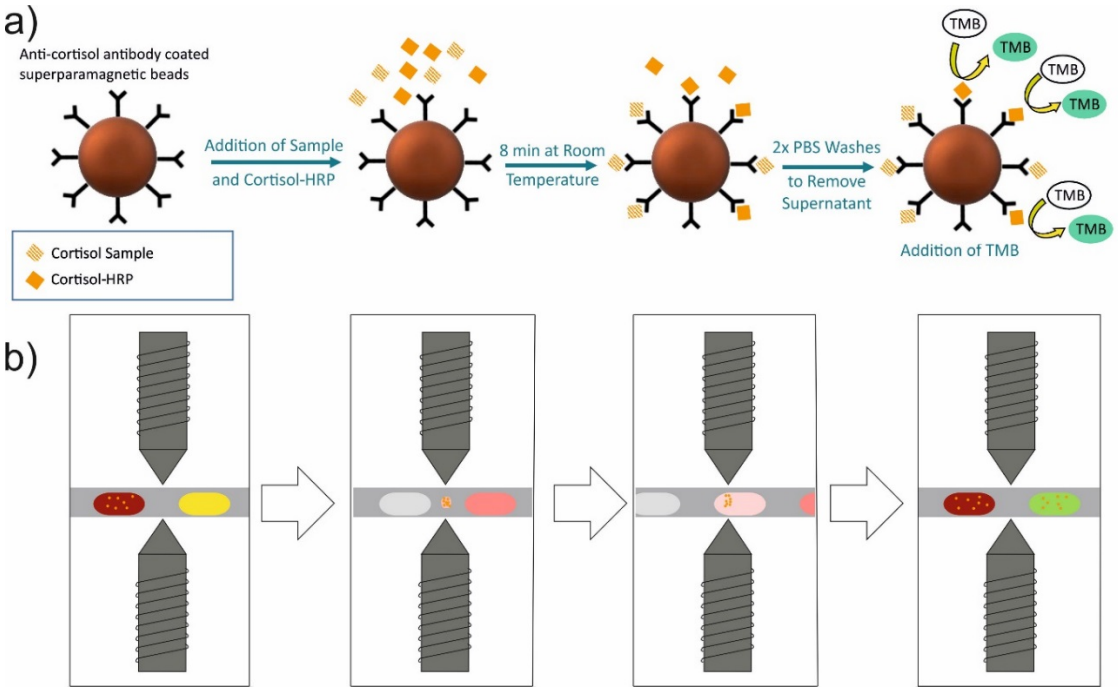

Figure 81 *Schematic of competitive heterogeneous cortisol assay in droplets procedure – a) Lagrangian view following a single antibody functionalised bead. Sample cortisol out competes Cortisol-HRP to form the final assay complex after washing in PBS to remove extra supernatant sample interferrents and leftover Cortisol-HRP, the Cortisol-HRP complex bound to the superparamagnetic beads acts as a catalyst for colour development in the Tetramethylbenzidine (TMB) marker. B) Eulurian steps of the assay procedure in the droplet procedure sample/magnetic bead/Cortisol-HRP droplet enters the trap beads are captured and removed from the droplet dragging through wash droplets to remove supernatant and then redispersed in final marker droplet where HRP catalysis colour change in the Tetramethylbenzidine (TMB) marker.*

6.2.1 Design and characterisation of the fluidic system

The device makes use of the pulsed droplet generation technique used throughout this thesis to produce a four-droplet train once per turn of the rotorhead. Fluid is driven by the rotorhead and pumpline structures (top and bottom) shown in Fig. 82 delivering fluid in eight separate phases. 1. Sample+beads+cortisol-HRP 2.FC40 oil 3.PBS 4. FC40 oil 5. PBS 6. FC40 oil 7. TMB 8. FC40 oil.

All components of the 12-line peristaltic micropump are shown in Fig. 82a and detailed in the exploded diagram Fig. 82c. The main pump chassis, rotorhead, pumpline support bed, and cap were all 3D-printed. Each was first modelled using CAD software (SolidWorks, Dassault Systemes) and then printed in “VeroClear” material using an Objet500 Connex3 polyjet printer (Stanford Marsh Ltd). A DC

motor (499:1 Metal Gearmotor 25Dx58L mm LP 6V) was used to drive the 3D printed rotorhead (12 mm in diameter including raised features) in contact with the twelve Santoprene (purchased from Megaflex Ltd., UK) pumplines. The droplet generation chip was fabricated by the PDMS casting procedure used throughout this thesis. A mould designed in CAD software (SolidWorks) was 3D printed in "VeroClear" material (Objet500 Connex3) and dried overnight at 70°C. Liquid PDMS (Sylgard 184, Farnell Onecall) was poured into the mould and oven cured at 70 °C overnight. The chip was then peeled from the mould, cut to shape and the channel structure sealed with a layer of half-cured PDMS. PTFE tubing (Adtech Polymer Engineering Ltd.) was used as inlets and outlets, sealed with PDMS. After fabrication, the microfluidic channels were surface functionalised with Aquapel rendering channels hydrophobic. Compared to the peristaltic micropump presented in the previous two chapters, the rotorhead diameter was expanded from 10 mm to 12 mm to allow for space for the 8 phases of pulsations of fluorous oil and aqueous solutions required to ensure robust generation of well-spaced droplets. Additionally, following some testing the small DC motor (Pololu 1000:1 Micro Metal Gearmotor) was replaced with a higher torque DC motor (499:1 Metal Gearmotor 25Dx58L mm LP 6V) as the original motor was operating far over its recommended running torque (25% stall torque) resulting in labouring and eventual stall/breakage during tests. A silicon lubricant (Rocol Silicone Grease SAPPHIRE Aqua-Sil) was used to decrease the torque experienced in the pump and to increase pumpline lifetime.

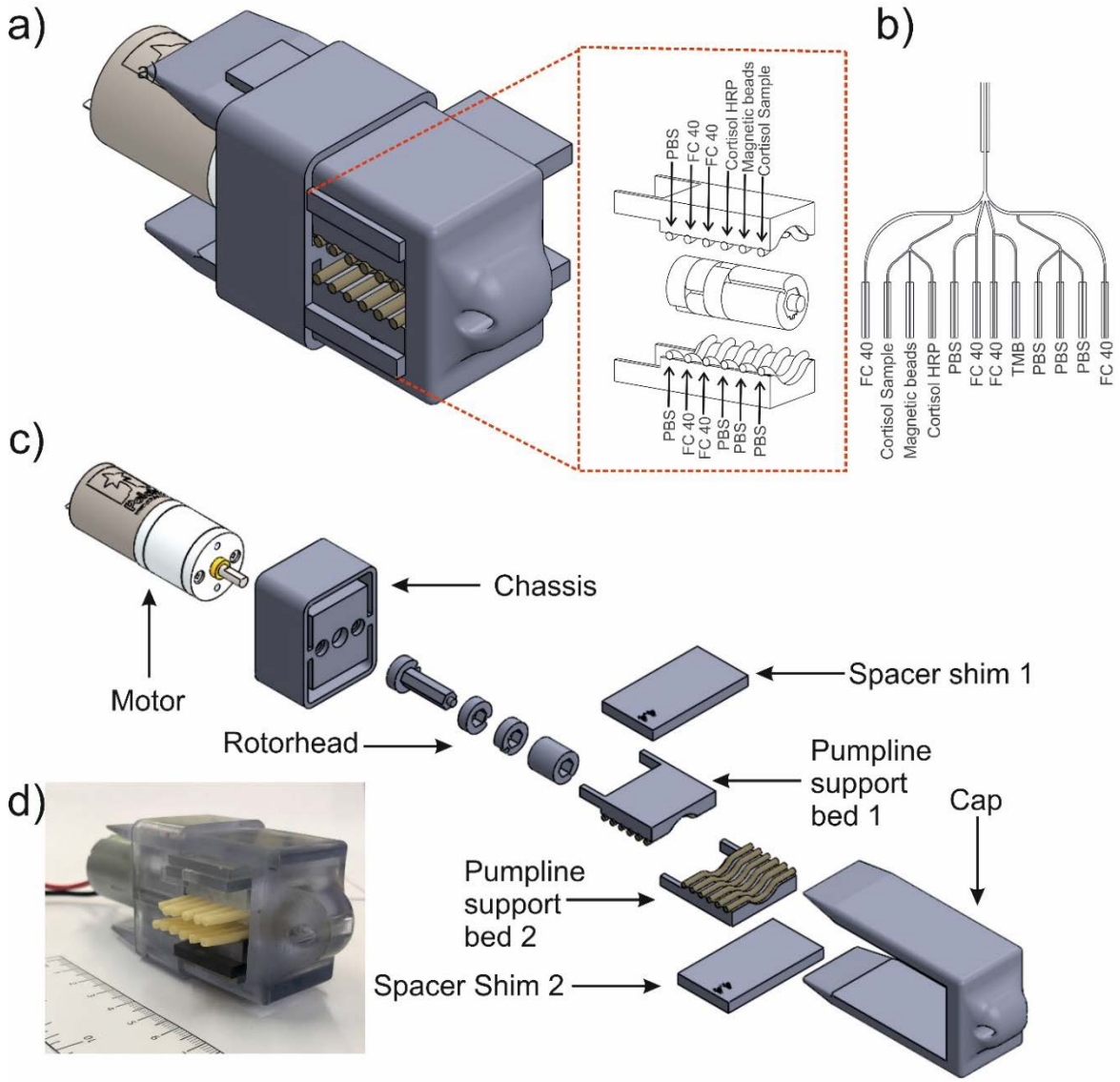

Figure 82 *Schematic of the 12 line peristaltic micropump tailored for generation of a four droplet train to carry out a competitive heterogeneous assay for cortisol: a) schematic of micropump with exploded rotorhead and pumplines b) microfluidic chip schematic with inlets related to pumplines shown in a) c) explosion of the micropump design showing all key components: DC motor (499:1 Metal Gearmotor 25Dx58L mm LP 6V) 3D printed chassis, rotorhead, pump-line support bed and cap d) photograph of the assembled 3D-printed micropump.*

One of the challenges in using magnetic particles or other heterogeneous suspensions in a microfluidic system is sedimentation which is particularly prevalent due to high surface to volume ratios (Pamme 2006). While the dynabeads are sold as having a slower sedimentation rate than other magnetic beads on the market, it became apparent from some early experimental setups that sedimentation would continue to be a problem that must be overcome. The beads were initially suspended in PBS and experiments were carried out to characterise this sedimentation and determine how to mitigate it. Two surfactants (BSA and Tween 20) were tested. As well as a chemically inert thickening agent (glycerol) to increase the viscosity as a mechanical method of reducing sedimentation of the microbeads. At higher concentrations, the surfactants did seem to slow the sedimentation of the

beads. However, neither of the surfactants tested (BSA and Tween 20) were added as these were found to reduce binding in later testing. The glycerol thickening agent had the greatest effect on the beads and bead stock was suspended in 50:50 glycerol:PBS in all testing to decrease the rate of sedimentation without interfering with the bead chemistry.

The whole droplet train generation process is shown in Fig. 83. The three aqueous inputs of sample, magnetic particles and cortisol HRP (represented by red food dye) meet and begin mixing at a Y-shaped conjunction. These are then segmented into droplets by the oil at a T-junction and finally move into another Y-shaped conjunction and into the main output channel out of the chip. After this droplet has reached the main junction, the aqueous pulse of the first of two PBS wash droplets (represented by green food dye) enters its T-Junction. This is then broken off into a droplet by an oil pulse, which also moves it into the main channel with the previous droplet being pushed further forward. The second PBS wash droplet (represented by black food dye) is generated from three PBS aqueous inputs merged in another Y-shaped conjunction and broken off by the oil mirroring the generation of droplet one. Droplet four is generated from a single pulse of aqueous Tetramethylbenzidine (TMB) (represented by yellow food dye), and broken off mirroring the generation of droplet two pushing droplet three forward in the main channel. This whole process can be repeated ad infinitum with droplet one pushing droplet four into the main channel.

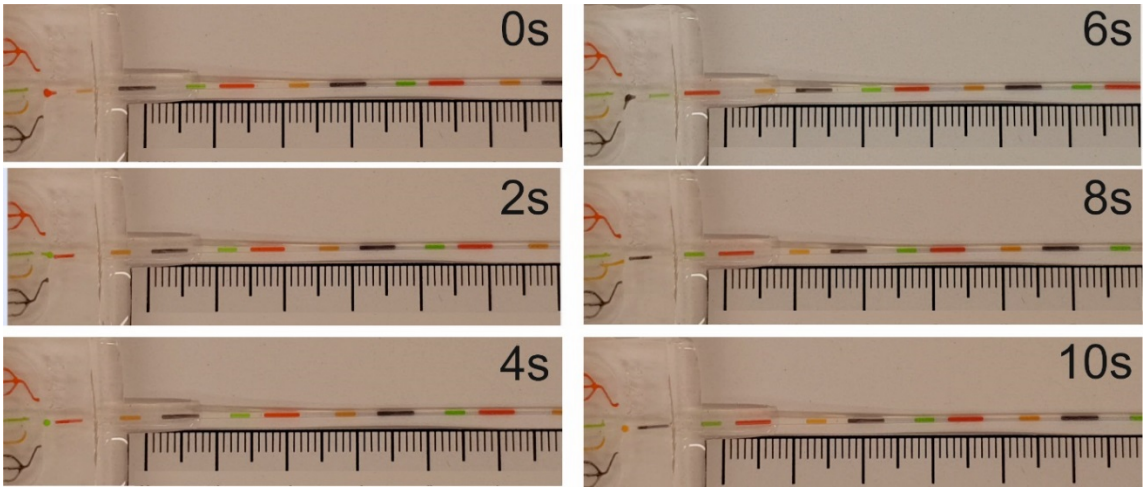

Figure 83 *Photographic image sequence showing the pulsed droplet train generation in the branched chip to generate a four droplet sequence suitable for carrying out heterogeneous cortisol assay and these droplets carried downstream by the exit tubing.*

Droplet generation dynamics were characterised similarly to previous experiment. A portable microscope camera (dnt Digimicro Mobile Mikroskope) was used to record either directly at the droplet generation chip or off-chip within the PTFE tubing. The videos recorded were analysed using Droplet Morphology and Velocimetry (DMV) software (Basu 2013) and the data subsequently processed in Matlab. Droplet volume was calculated from DMV measurements of droplets recorded within tubing of known cross sectional area.

The rotorhead was designed to deliver the four droplets with approximate volumes: droplet 1=1000nl delivering the sample, beads and competitor in a 1.1.1 ratio, droplet 2=500nl, droplet 3=1000nl,

droplet 4=500nl. With oil pulsations of 1000nl to push droplets into the main junction. As shown in Fig. 84 testing confirmed the volumes as 1060nl for droplets 1&3 and 550nl for droplet 2&4.

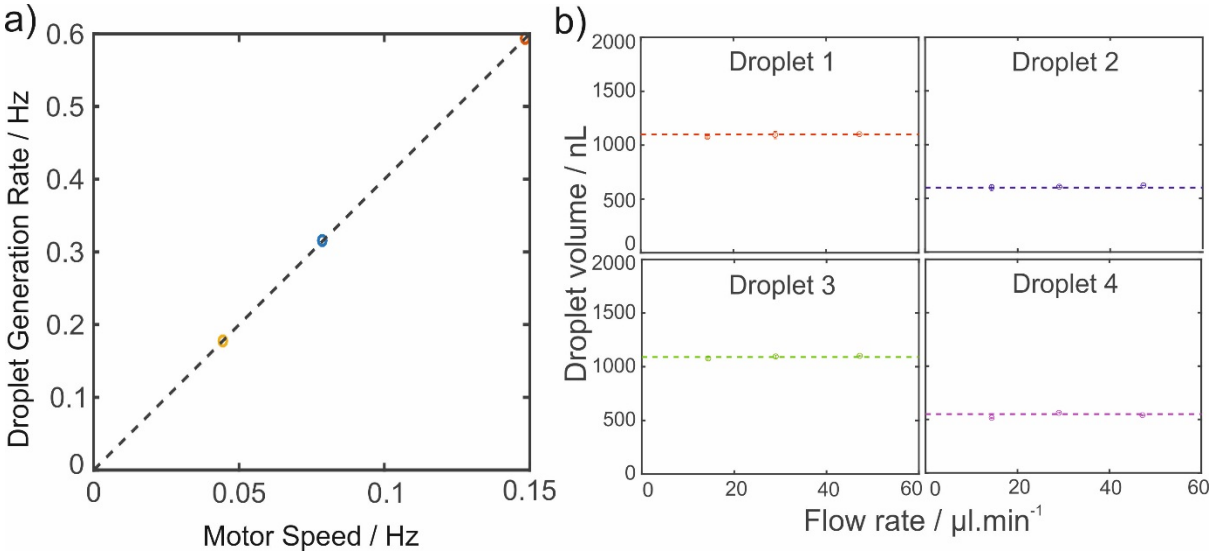

Figure 84 *Droplet train generation dynamics for the cortisol assay a) Droplet generation rate increases linearly with motor speed b) Droplet volume of each droplet in the train remains constant irrespective of flow rate Error bars show the standard deviation in droplet volume, <2%.RSD.*

Fig 84a shows how the droplet generation rate in the setup changed with motor speed (Hz). The gradient (4.0) and zero intercept display that there was no unwanted droplet breakup and exactly four droplets were produced in each rotation of the motor as expected. Figure 84b shows how the volume of each droplet in the sequence and how it remained invariant to total flow rate. Coefficients of variation in droplet volume for each droplet are consistently <2% (as indicated by the error bars in Fig. 84d) which compares favourably with previously reported droplet generation methods (Tan, Murshed et al. 2008, Jung, Retterer et al. 2010, Abate, Kutsovsky et al. 2011). This low coefficient of variation in droplet volume was shown to be repeatable across many experiments indicating the robustness of the pulsed droplet generation method. It is important to note that the fluids were of various viscosities, surface tension etc. with the magnetic particles having been suspended in a 50/50 mix of buffer and glycerol to slow sedimentation of the beads in the liquid storage during testing.

6.3 Magnetic trap and microbeads in microfluidics

One of the main components of the miniaturized heterogeneous assay platform technology is a magnetic trap comprising of a small pair of electromagnetic tweezers. This is used to extract the magnetic beads from a droplet dragging it through the fluorous carrier oil and then either dispensing it into the next droplet or dragging it *through* the droplet to wash the beads and then redistributing in the following droplet for the next assay step. As explained by Pamme et al. the force applied to a magnetic particle within a magnetic field can be described as a function of the volume of the particle (V), the variation between the magnetic susceptibilities (Δx) between the particle (x_p) and the medium (x_m) together with the gradient and strength of the magnetic field (B) (Pamme 2006):

Force required to extract magnetic particles

$$F = \frac{V.\Delta x}{\mu_0}(B.\nabla)B \quad (18)$$

For all the following experiments superparamagnetic 1 µm diameter Dynabeads MYone (Thermofisher) were used either in carboxyl or tosyl activated surfaces from Thermofisher. These beads are superparamagnetic, exhibiting magnetic properties while placed in a magnetic field with no residual magnetism once removed from the field. The polymer shell on each bead protects antibodies interaction with iron. The hydrophilic surface functionalisation of each bead reduces aggregation and means the beads will exhibit similar behaviour to the antibody-functionalised beads used in the assay. The initial magnetic tweezers design (shown in Fig. 85) is relatively simple but allows precise manual control (under microscope) of the magnetic beads

6.3.1 Design and fabrication of magnetic trap

The simplest magnetic trap used for these assays is shown in Fig. 85. This manually controlled version comprises of two ferrite cores (3 mm diameter, 25mm length) (RS Components) and windings of copper wire. A 3D printed PLA holder (Ultimaker 2$^+$) holds the ferrite cores and tubing in place so that the core tips are aligned and fit tightly around the PTFE tubing (0.3 mm ID and 0.5 mm OD) (Adtech Ltd.). Aligning the tweezer tip is of utmost importance as slight misalignment leads to unfocused magnetic field and unsuccessful trapping of beads. Each electromagnetic tweezer set was constructed by wrapping 200 windings of enamelled copper wire of 0.35 mm thickness around each ferrite rod. The length of the coil varied between 15-16 mm depending on the manual winding. The tips of the ferrite core were tapered to increase the magnetic field density and provide sufficient force for extraction of the magnetic beads. Current was supplied and manually controlled by a benchtop power supply (EL302RT - Bench Power Supply, Linear Regulated, Adjustable, 3 Output, AIM-TTI instruments). When energised the trap is capable of creating and extracting the magnetic bead pellet for carrying out the various steps of the assays as displayed in the inset image sequence.

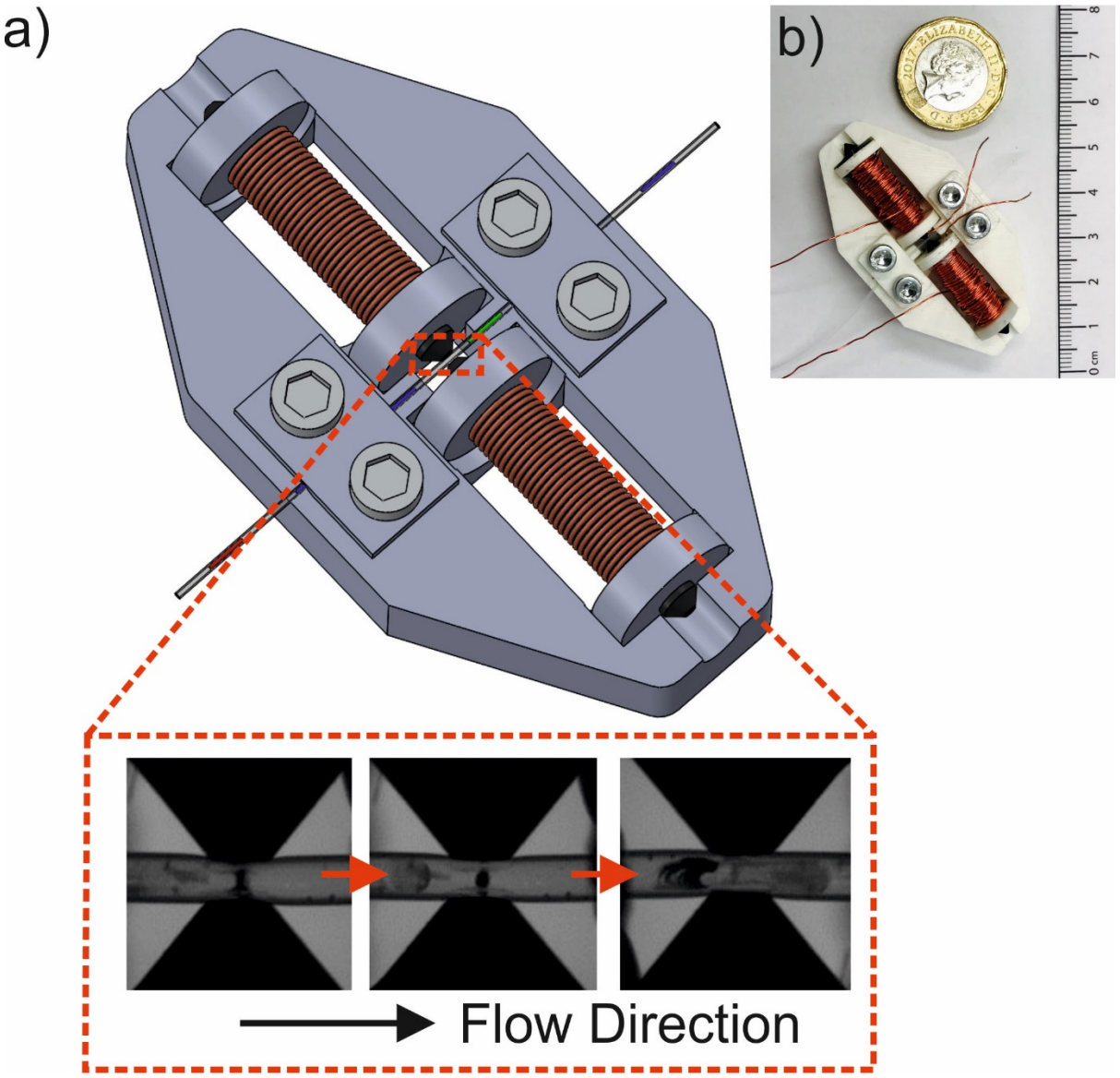

Figure 85 *Basic magnetic bead trap (manually operated) consisting of: two RFID cores tapered to a point and wrapped in 200turns of copper wire and a 3D-printed housing to hold the 'tweezers' and tubing a) schematic and image sequence of the trap in operation b) photograph of the trap (pound coin for scale).*

6.3.2 Field strength of electromagnets

To test and characterise the effect of distance from the tip, number of windings, and current on magnetic field density. A low power 3.3V Adafruit Feather 32u4 board and a bipolar Hall effect sensor (DRV5053VAQLPG) with a sensitivity of -90mV/mT was used in order to measure the field density. Number of coil windings was varied from 50, 100 to 200 (coil wire thickness 0.35 mm) and the tweezers were excited with currents ranging from 0 to 1 A. The distance between the tweezer tip and sensor was also varied from 0.5 mm to about 5 mm. Figure 86 shows the variation in magnetic field density with current for tweezers with increasing number of windings.

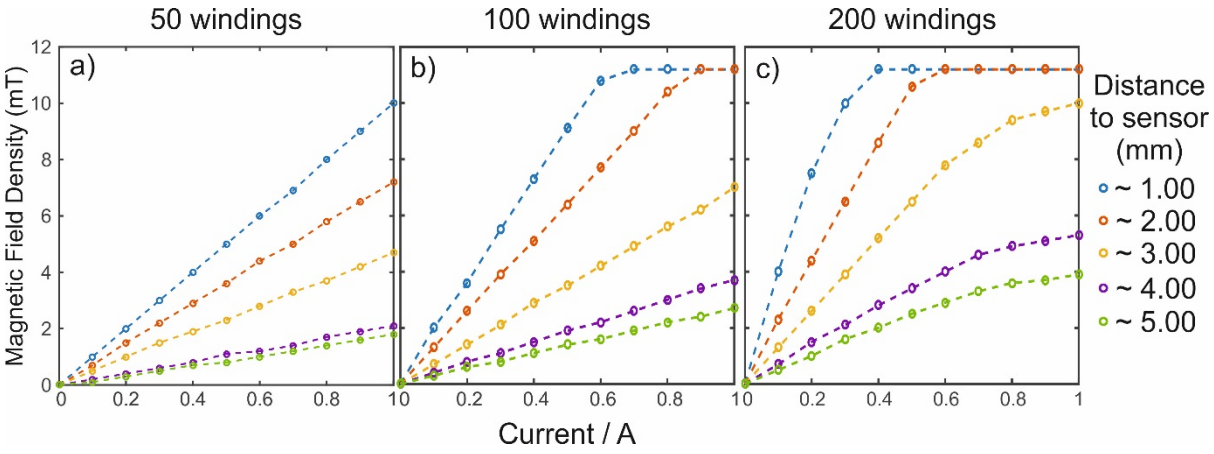

Figure 86 *Characterisation of field strength of a single electromagnet' tweezer' a) Magnetic field density (mT) vs. Current (A) for tweezer with 50 windings b) Magnetic field density (mT) vs. Current (A) for tweezer with 100 windings c) Magnetic field density (mT) vs. Current (A) for tweezer with 200 windings at varying distance to hall effect sensor.*

As expected, the magnetic field density increased with current, increasing proportionally for the three different windings. Also increasing the distance from the tip deceased field density as expected. The hall effect sensor had a saturation limit of 11.2 mT which the 100 and 200 winding tests reached (the 50 windings test highest field density was ~ 10 mT) for future tests 200 windings were used (the largest number of windings practically allowed by the core) to allow lower currents to hopefully be used for bead capture.

6.3.3 Exploring magnetic tweezer tip shape and capture

It is important to produce a strong and focused field to ensure that the bead pellet breaks the droplet oil interface with as little loss as possible. The shape of the tips can have a profound effect on the focussing of the field. Three designs of the ferrite core (RS Components) were tested with varied tip size each using the same 200 windings of 0.35 mm enamelled copper wire (RS Components) shown in Fig. 87. A 3d printed holder (Ultimaker 2^+) holds the ferrite cores and tubing in place so that the core tips are aligned and fit tightly around the PTFE tubing (0.3mm ID and 0.5mm OD) (Adtech Ltd.). The unaltered (flat) ferrite rod 3mm in diameter shown in Fig. 87a, rods sharpened to a point using hand tools shown in Fig. 87b and those sharpened to have a diameter ~1mm shown in Fig. 87c.

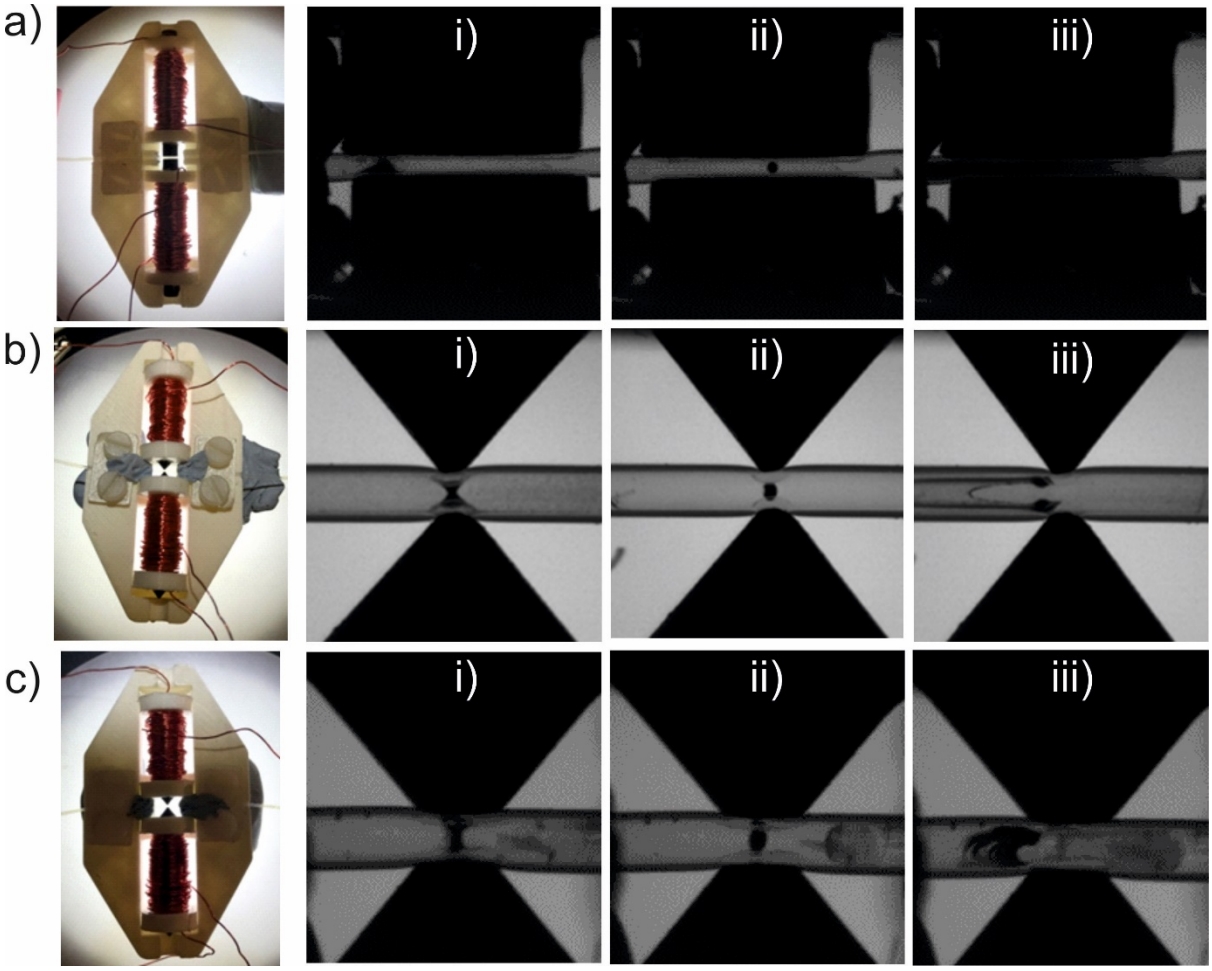

Figure 87 *Photographs of capture of magnetic beads in the basic trap (flow right to left) - (i) Capture, (ii) retention and (iii) re-dispersion of beads using a) flat tips (3mm) b) sharp tips (<1mm)and c) blunt tips (1mm).*

All three of the tip types have demonstrated their ability to capture the magnetic particles. During capture Fig. 87ai the flat tips struggled to hold the beads in place with the majority moving to the downstream side of the tips, it is unknown whether or not there will be loss due to this. Post capture, the flat tips bead droplet had a tendency to move the centre of the flat tips indicating that the magnetic field strength is strongest in the centre of the flat tips. Both capture and redistribution of beads took place over a larger area and the magnetic beads seemed to align with respect to different field lines. This behaviour indicated that the flat tips are not best suited for capture and retention of beads but possibly could be used to increase mixing by advection when pulsed. Both the sharp and blunted tips Fig. 87b&c respectively exhibit good ability to collect and capture the magnetic beads displayed by the characteristic hourglass shape i). Both demonstrated an ability to redisperse beads. However, the blunted tips seemingly offer better redispersion.

Rather than spend extensive time modelling the field etc. to find the best arrangement of electromagnet a series of experiments were carried out to test the effectiveness of the sharp and blunt tweezer tips. The bead stock used in the experiment was prepared using 50 µl of bead in 500 µl of Phosphate Buffered Saline (PBS) with 1 % Bovine Serum Albumin (BSA) and 1 % Tween20. FC40

carrier was used without any surfactant. Droplets were generated by manual aspiration using a syringe pump (Harvard Apparatus PHD 2000), using the withdrawal mode set at 10 µl/min. Figure 88 displays the effect of current (A) versus concentration of magnetic beads (µg/ml) for different total flow rate of the droplets for the two different tweezer tips.

As shown in Fig. 88 increasing current delivered to the coil or bead quantity increases the probability of bead capture (bead capture represented by red points) as there is an increased magnetomotive force which allows the magnetic beads to break the droplet interface and increased total flow rate decreases probability of capture for both setups due to stronger hydrodynamic forces and reduced time for beads to sediment in the droplet and form a pellet. We would expect better performance from the sharp tips due to a more focused field. However, it can be seen that the blunt tips provide more reliable capture (especially at higher bead quantities). The lower capture probability and inconsistencies for the sharp tips could be due to two hypothesised reasons: oversaturation of the tips resulting in field density leakage, and misalignment of the tips. This is also likely the cause of some anomalous data present in Fig. 88c with 0.2A current delivered to the tweezers not being sufficient for capture, most likely due to misalignment. The blunt tip tweezers easily fit tightly around the PTFE tubing and the larger surface area of the tips makes them easier to align for high field density in the centre of the channel. The larger surface area of the tips may also in fact produce a greater field density due to reduced leakage. High field density is vital for good extraction of the magnetic beads. Therefore, the blunt tips were chosen as the most suitable configuration for the assay based on the experimental results.

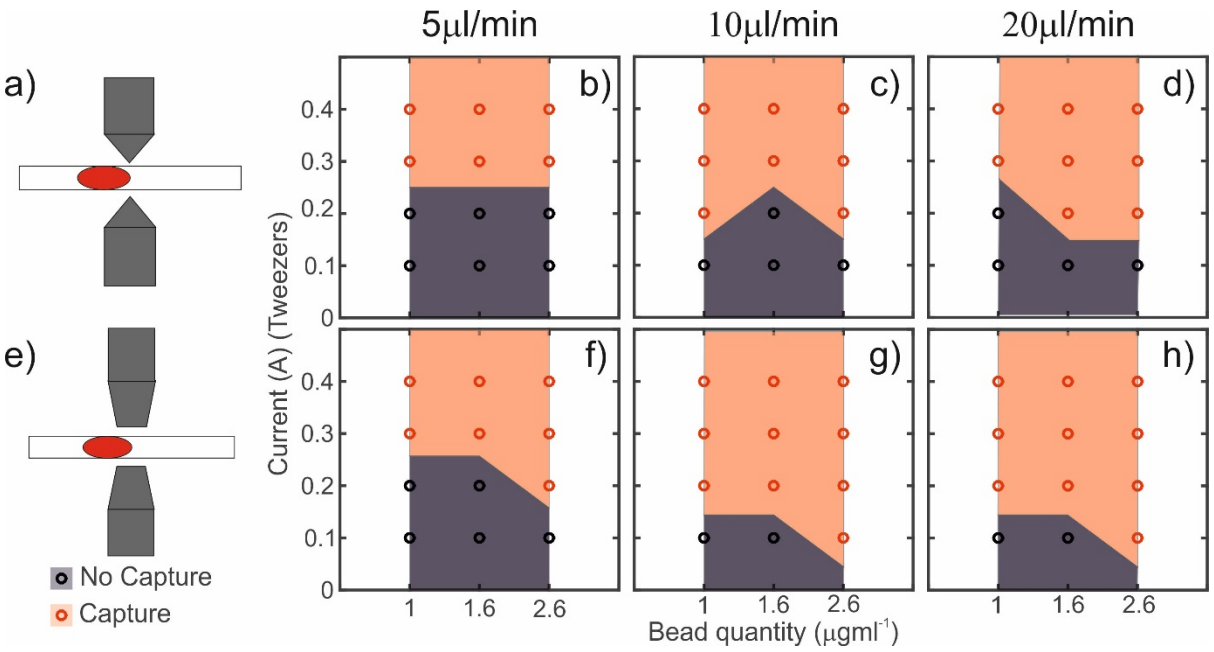

Figure 88 *Capture of magnetic beads in the basic trap for a range of current (0.1-0.5 A) flow rates (5, 10 and 20µl/min) and bead quantities 1-2.6ugml^{-1} using (a-d) sharp tip and (e-h) blunt tip cores.*

6.4 Automation and integration

In the testing described thus far, operation of the trap required a user to watch droplets under a microscope and manually energise the tweezers to trap and then redisperse the beads. In order for this technique to be viable as part of a point-of-care monitoring device it must be automated (Chin, Linder et al. 2012).

Figure 89 describes the system used to automate the process of bead extraction, washing and redistribution. A pair of 'light gates'(spectrophotometers) as shown in Fig. 89a were added before and after the trap as close to the magnetic tip as possible along with a control circuit. The control circuit determines when to energise the trap or re-disperse the beads into a new droplet based on the light transmittance measured by the light gates. These light gates are based on the previously described miniaturised in-line spectrophotometer flow cells (section 1.9.2). Channels and sockets for the two 527 nm Green LEDs (Cree PLCC4 1-in-1 SMD LED CLM4B-BKW/GKW) and two detectors (TSL 257 photodiode with amplifier) were micromilled by Dr. Sammer-Ul Hassan.

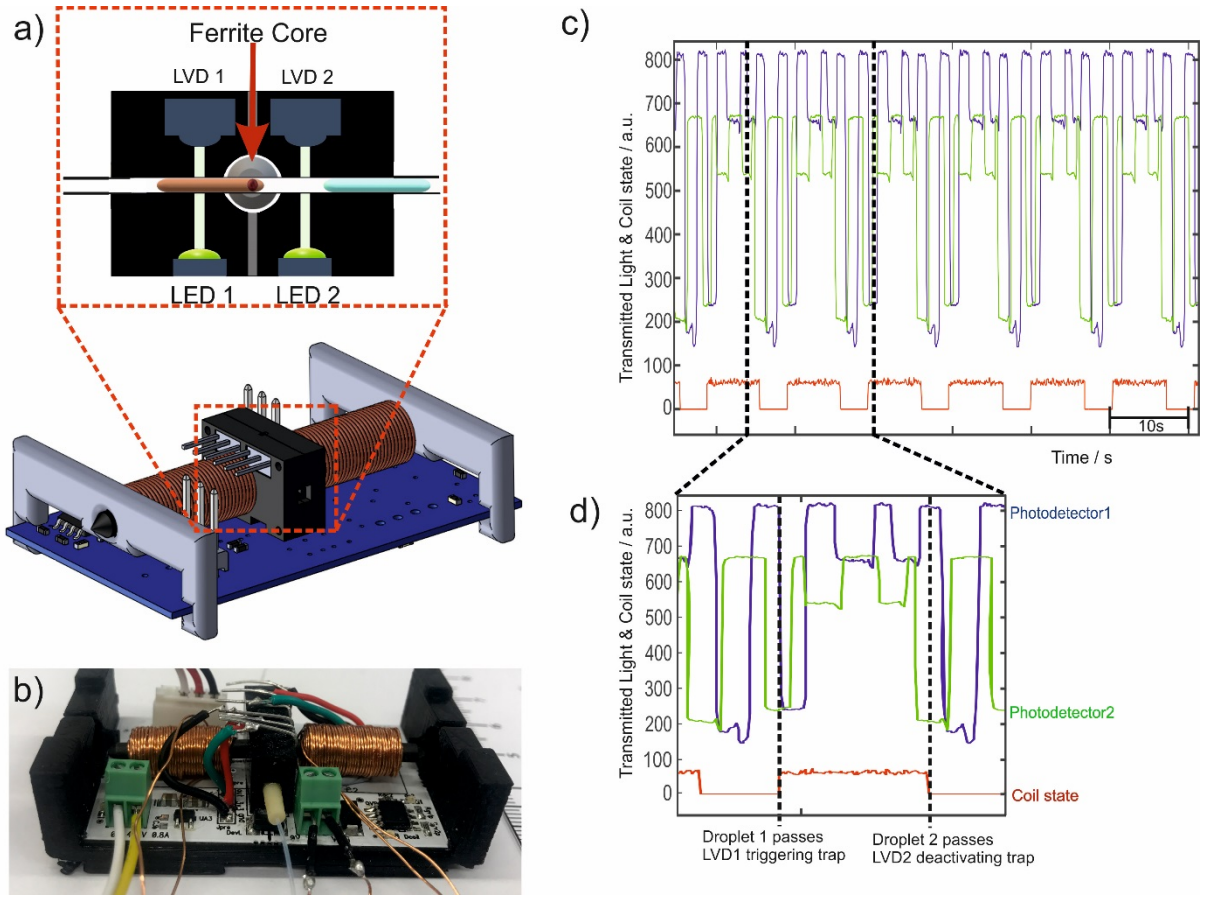

Figure 89 *Automated magnetic bead trap and readout from the built in house GUI used during these tests – a) schematic of the automated magnetic bead trap featuring two 'light gates' (spectrophotometers) which are used to determine when to activate the trap and when to re-disperse the beads into a new droplet. b) Photograph of automated magnetic bead trap c) Isolated traces of the most important data lines from the in house built GUI used during these tests Photodetector 1 determines when to activate the trap and Photodetector 2 determines when to deactivate the trap re-dispersing the bead pellet in a droplet d) A single trains worth of trace shown in the GUI as the coil energises to capture beads.*

The automated magnetic trap is mounted directly on its control board as shown in Fig. 89b. An Adafruit Featherboard 32u4 integrated circuit board allows the activity of the unit to be recorded and presented on a nearby PC. The control circuit of the automated magnetic trap circuit was designed by Brett Warren (SouthWestSensor ltd.) using DipTrace and exported in Gerber format for the PCB to be manufactured. AVRStudio was used to develop the software and to control an Atmel ISP chip programmer. Arduino IDE was used to develop and program the connection software running on the control board. A graphical user interface (GUI) was also developed using Embarcadero C++ Builder. The GUI allows the user to either manually energise the tweezers or set the unit in to automatic mode. In automatic mode, the GUI is used to view, define and upload different control parameters of the tweezers such as the coil current and light intensity thresholds required to trigger the switching of the tweezers.

To illustrate the automated systems operation, Fig. 89c shows raw data from a one minute period of automated function (shorter period shown in Fig. 89d). The blue and green plots shows the transmitted light reaching the inlet and outlet photodetectors respectively. While the red plot represents the state of the current flowing through the coil of the electromagnetic tweezers. When droplets pass between the LED and detector there is a drop in transmitted light. The intensity value from the inlet detector indicates when a droplet is going to pass through the tweezers and whether the droplet contains magnetic beads (determined by user defined threshold values). As can be seen in the data shown in Fig. 89c, to assist in bead capture the tweezers are activated before the droplet arrives in the trap. The beads are then dragged through the two wash droplets. Finally, the change in intensity value in the outlet detector indicated when a droplet is fully situated between the tweezer tips. When droplet four reaches the trap, the beads can be released for redispersion. As the beads must overcome the tension of the droplet interface to redisperse safely release is triggered by the outlet detector while droplet four is in the centre of the trap.

6.5 In-line spectrophotometer

After leaving the magnetic trap the droplets travel downstream. Within droplet four a colour change in the TMB marker is catalysed by the cortisol-HRP. After two minutes the droplets arrive at a spectrometer to quantify the colour development. As with previous studies an inline miniaturised spectrophotometer was used similar to that detailed in (Hassan, Nightingale et al. 2016) a 456 nm blue LED (Cree PLCC4 1-in-1 SMD LED CLM4B-BKW/GKW) and detector (TSL257 photodiode with amplifier) pair are used in a PMMA micromilled (LPKF Protomat S100-LPKF Laser & Electronics Ltd, Berkshire, UK) holder to quantify a droplets extinction for a particular wavelength of light. A schematic of the miniaturised in-line spectrophotometer flow cell is shown in Fig. 90a and the output for two concentrations of cortisol 3.175 ng/ml in Fig. 90b and 100 ng/ml in Fig. 90c) after carrying out the full competitive heterogeneous assay procedure.

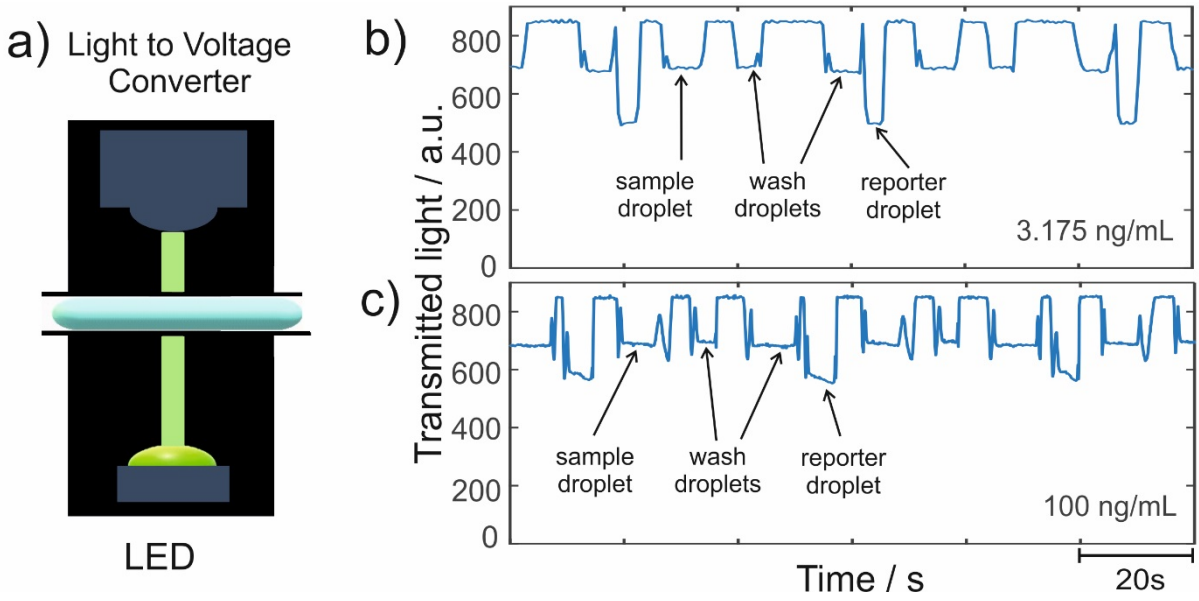

Figure 90 *Miniaturised in-line spectrophotometer used for detection of droplet contents a) Schematic of the built in house miniaturised in-line spectrophotometer flow cell b&c) Raw intensity data trace outputs from detector after the whole assay process has taken place (3.175 ng/ml and 100 ng/ml cortisol standards).*

6.6 Purification efficiency of droplet washing

It is important to determine the efficacy of the washing steps in the droplet assay procedure. This informs the volume and quantity of washes required to remove any uncomplexed cortisol-HRP and ensure there is no remaining interferrents. Hence, after deciding upon a suitable tweezer design (tip diameter ~1mm) a test was carried out to determine the efficacy of the washing buffer droplets for purifying the magnetic beads. Beads were moved from a highly concentrated droplet of Rose bengal dye through PBS wash droplets and redispersed in another PBS droplet.

Droplets were generated using the rotorhead and pump design shown in Fig. 82 mimicking the steps of a droplet heterogeneous assay. The first droplet in the four-droplet train consisted of (1 $mgml^{-1}$) magnetic beads with Rose bengal dye in 50% PBS and 50% glycerol with the other three droplets consisting of PBS buffer. For these tests, FC40 oil with 0.1% PFPE-PEG surfactant was used as the carrier phase (surfactant aiding in redispersion).

The magnetic trap was energised as the first droplet approached and magnetic beads were captured. The tweezers remained energised and the bead 'pellet' was held in place while washing droplets passed through the trap. As the beads pass through each wash droplet, the bead pellet was observed to deform indicating partial redispersion reforming the pellet as they passed into the oil. The beads were then released into the third PBS buffer droplet.

After the full washing procedure, the final droplet now containing the magnetic beads displayed no Rose bengal dye by naked eye (as seen in photograph Fig. 91b). To quantify the dye concentration remaining the droplets were passed through an inline spectrophotometer. Figure 91a shows the

intensity of the transmitted light versus time as the droplet train travels through the flow cell. The first droplet to reach the flow cell contained the Rose Bengal dye from which the beads have been extracted. The next two droplets were PBS buffers and the last droplet was the PBS droplet containing re-suspended beads. There is a change in intensity due to the release of beads in the fourth droplet. To determine the absorbance of the dynabeads alone a 1mg/ml droplet of bead stock was also passed through the inline spectrophotometer flow cell (blue line in Fig. 91c).

Four purification regimes were tested shown in Fig. 91c. Regime 1 in which droplets were simply captured removed from the dye droplet and redispersed (0 nl wash volume). Regime 2&3 where beads were washed in a single droplet of 550 nl and 1060 nl respectively. Regime 4 in which two wash droplets totalling 1610 nl volume were used. After this testing it was chosen to use purification regime four to ensuring there is no remaining supernatant. However, this does cause loss of some beads, which will reduce the strength of the signal.

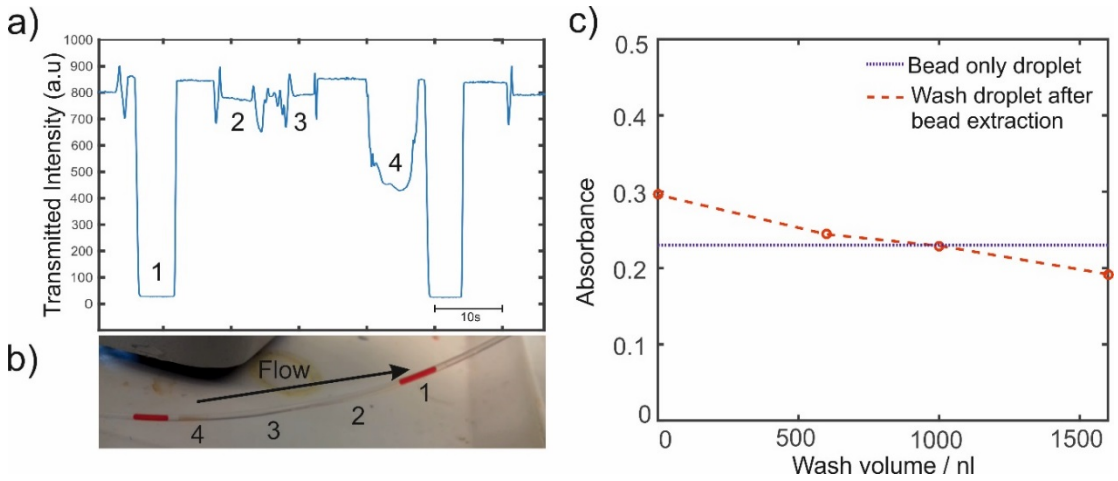

Figure 91 *Calibration of purification efficiency of the droplet in flow method as measured by a built in house miniaturised spectrophotometer a) Raw data trace (light intensity) from mini spectrophotometer after beads have been removed from droplet 1 containing the rose Bengal dye and washed through two PBS wash droplets (2&3) and redispersed in another PBS droplet b) Photograph of the droplet train after purification procedure) c) Characterisation of total wash volume vs absorbance for the droplet train with blue line indicating the absorbance of a droplet containing magnetic beads (no dye) which have not undergone the procedure.*

6.7 Heterogeneous immunoassay carried out in droplets

The system was then tested with the cortisol assay as described earlier utilising all of the techniques described in this chapter. All tests were carried out at room temperature. During the test the motor was supplied 1.33 V and 0.13 A and the magnetic trap when energised drew 2.68 V and 0.7 A.

All fluids were stored in 2 ml Eppendorph tubes during the test. Serial dilutions of cortisol (CalBioreagents) were generated from 100 ng/mL to 1.56 ng/mL in a background of wash buffer. Cortisol sample concentrations from 3.175-100 ng/mL concentration were used to test and generate a calibration. The tracer solution was kept constant at 100 ng/mL prepared from cortisol-3-carboxymethyloxime horseradish peroxidase conjugate (CalBioreagents) with a 1:2500 dilution in wash buffer (2 μL tracer and 5 mL buffer). Antibody functionalized magnetic beads (MyOne

Dynabeads) were suspended in PBS and 50 % glycerol. Washing buffer was prepared from Phosphate Buffered Saline (PBS) with 0.1 % Bovine Serum Albumin (BSA) and 0.05 % Tween20. 1 step Ultra TMB (3,3',5,5'-tetramethylbenzidine) ELISA was used as supplied Thermo Scientific. FC-40 oil with 0.1% of PFPE-PEG surfactant was used as the carrier phase throughout.

All fluids were delivered to the microfluidic chip and the aqueous assay components broken up into drops by the carrier oil by the pulsed method, incubated in-line (in tubing) for 8 minutes during the binding step of the assay. The magnetic beads were then trapped passing through the two washing droplets. The beads then redispersed in the final TMB droplet with the Cortisol-HRP catalysing the colour change (mixing for 2 minutes). This colour change was then measured by the inline spectrophotometer. The light intensity values of each droplet and the carrier oil were measured and the absorbance calculated by the modified Beer-Lambert law described in section 1.9.2. After each of the samples were tested 10 times these measurements were used to generate a calibration with error bars representing standard deviations all less than 0.01 shown in Fig. 92 (a linear trend line is included as a guide to the eye in the linear portion of the calibration).

As shown in Fig. 92 the total measured absorbance of the assay carried out in the droplet platform was considerably less than observed in the bulk lab procedure (Figure 79) it is hypothesised that this and the shorter period of linearity is due to the considerably shorter incubation time used in droplets as assay may not be at its most optimal. Additionally, the droplet platform displayed very good linearity between 12.5ng/ml and 100ng/ml while the bulk assay had a linear period of 3.125ng/ml to 100ng/ml. This may also be due to the shorter non-optimal incubation period. In the future, the assay will be carried out in a heated reaction vessel similar to that used in chapter 5.

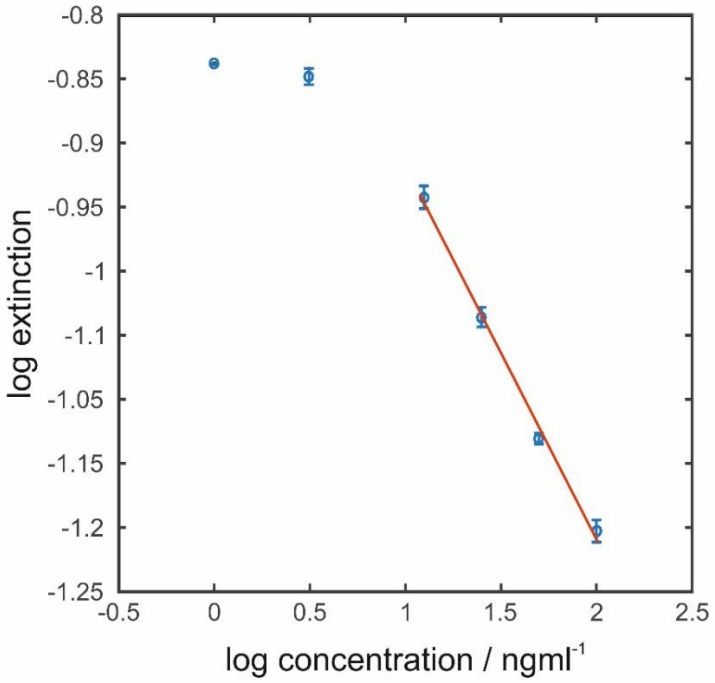

Figure 92 *Competitive heterogeneous assay for cortisol carried out in our droplet microfluidic platform - featuring ten repeats of cortisol assay carried out in droplets (all standard deviation <0.01) displaying similar trend as the bulk plate reader tests (with lower amplitude due to shorter gestation period).*

The advantages of the droplet platform compared to the lab procedure are derived from the benefits of droplet microfluidics for performing assays, and the high degree of automation. The assay takes considerably less time to perform in the droplet platform and all washing steps etc. can be automated. The droplet platform is capable of carrying out an assay approximately every ten seconds taking advantage of the high temporal resolution offered by droplet microfluidics. Results are delivered with a ten minute delay when carried out at room temperature due to the time required for the competitive binding process. The high degree of automation also removes the possibility of human error contributing to the consistently low total error and anyone with basic training should be able to use this platform.

This system has been developed for application in POC monitoring offering sensitivity and robustness on par with lab based assays with high temporal resolution in a small and low power platform. All of the components required for the assay have been integrated in a generic portable platform shown in Fig. 93. The device can collect samples directly from the sampling site (e.g. bodily fluids such as interstitial fluids), making it possible to perform complex assays continuously at the point-of-care. The programmable and modular nature of this platform makes tailoring the platform to other assays such as those for cytokines, RNA markers etc. providing exciting research and development opportunities in a variety of fields.

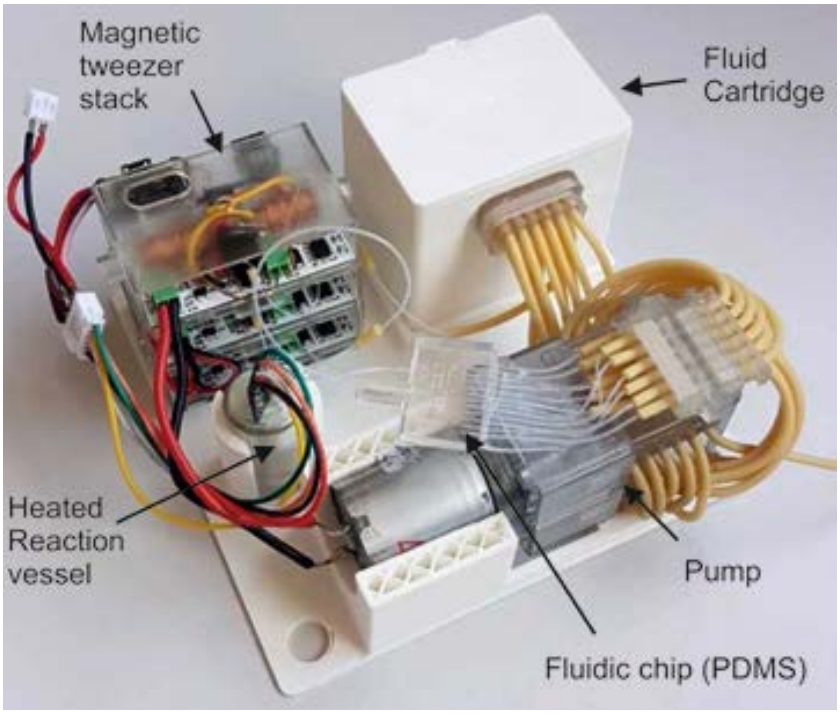

Figure 93 *Photograph of the fully integrated prototype platform device for carrying out the competitive heterogeneous cortisol assay in droplets continuously (also suitable for tailoring to a wide variety of assays).*

6.8 Conclusions to Chapter 6

In this chapter, I have:

a) Described the development of a novel implementation of a competitive heterogeneous immunoassay for the steroid hormone cortisol (an important biomarker of physiological stress).
b) Described and characterised a novel method of generating droplet trains by pulsed droplet generation and a branched microfluidic chip structure.
c) Described a miniaturised automated magnetic bead trap for integration into a microfluidic platform and characterised its efficacy in bead capture and purification.
d) Described a fully integrated droplet microfluidics and competitive heterogeneous colorimetric assay based and sensing platform for the continuous sensing of low quantity biomolecules in clinical monitoring.
e) Presented early calibration data of an assay for cortisol carried out in the droplet microfluidic platform.

In conclusion, this continuous monitoring platform shows promise for the monitoring of low quantity biomarkers in a clinical setting. Incorporating trains of droplets generated by pulsed flows (Nightingale, Evans et al. 2017), an automated in-flow magnetic bead trap for carrying out heterogeneous assays in droplets and inline spectrophotometers (Hassan, Nightingale et al. 2016) allows for high temporal resolution and accurate measurement of the steroid hormone cortisol.

In the future, this platform will be tested in a clinical setting as part of the EPSRC doctoral prize award grant, which I have been awarded. I will continue to develop this platform alongside industrial and academic collaborators South West Sensors ltd and LGC. Further testing will be carried out to validate this method and extensively test this device's analytical performance over long periods.

Chapter 7 – Conclusions and Future work

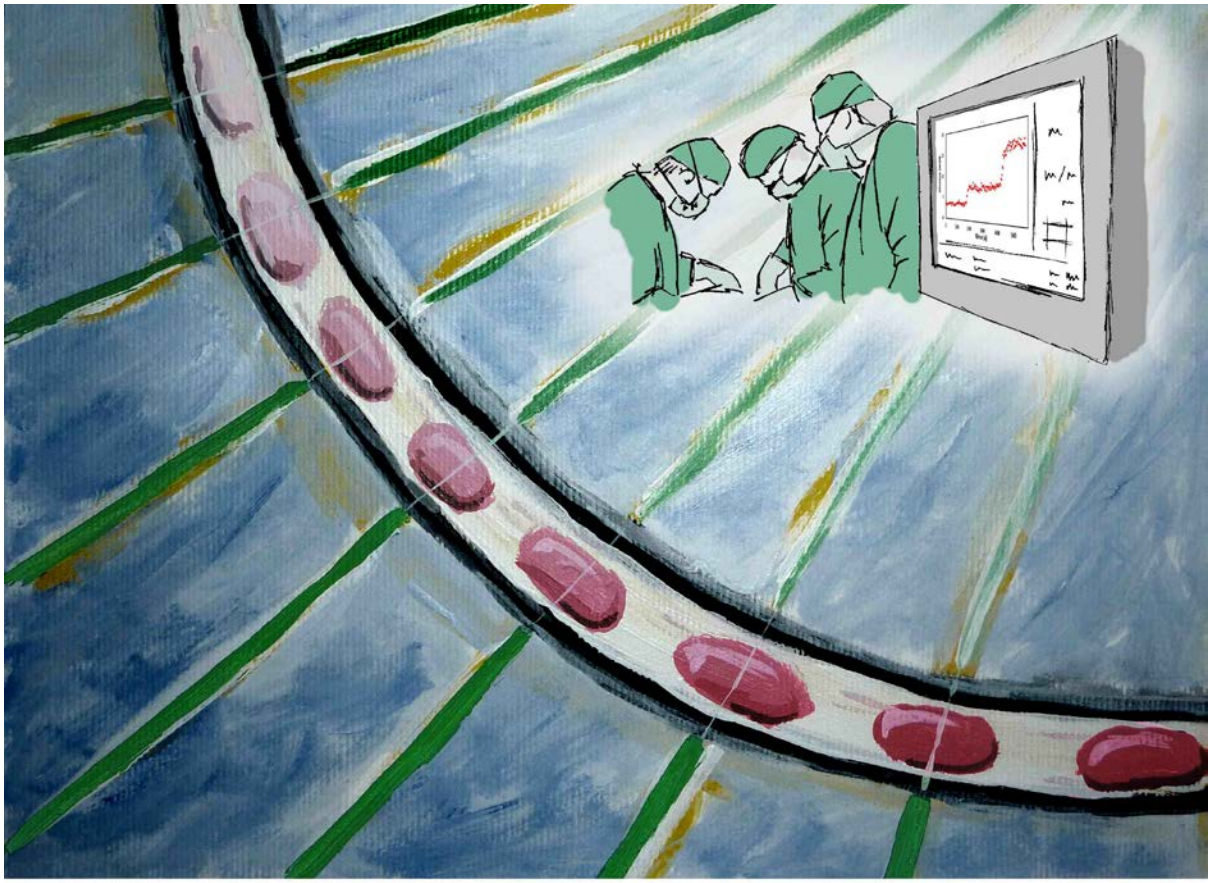

This thesis describes the development of a droplet platform technology that can be tailored to different chemical monitoring applications such as clinical monitoring and environmental science.

After developing a novel approach for robust and field-deployable droplet microfluidics two example sensor systems were developed. The first is a field deployable sensor for simultaneously measuring nitrate and nitrite in water featuring: a small overall footprint and power consumption providing high temporal resolution and *in-situ* calibration, a true step change over previously reported systems. The second is a system for monitoring cortisol using a novel competitive immunoassay. The system features a high temporal resolution and a high degree of automation in a portable platform suitable for use at the point-of-care.

The key contributions of my thesis include:

1. The development and characterisation of a novel pulsed droplet generation regime, which is programmable and requires no 'ramp-up' period. Importantly, the droplet generation is invariant to both fluid and flow properties (viscosity, interfacial tension and flow rate).
2. The development of a 3D-printable peristaltic micropump for robust sample collection and droplet generation by the pulsed regime.
3. The evolution of this micropump and specialised droplet generation strategy to generate trains of droplets.
4. The integration of this micropump and specialised droplet generation strategy with chemical assays and optical detection into a first of its kind platform for environmental science applications. The platform was also successfully tested in field deployments monitoring nitrite and nitrate in natural water.
5. The development of a droplet microfluidic platform including an automated magnetic trap and the peristaltic micropump, for continuous heterogeneous immunoassays in droplets. The platform has been tailored and characterized for the monitoring of cortisol, in droplets.

7.1 Pulsed droplet generation by peristaltic micropump

Over the course of this thesis, I have developed and thoroughly characterised a novel method for droplet generation utilising the pulsed flows generated by a 3D-printed peristaltic micropump. This pulsed droplet generation regime produces uniform droplets close to the sampling site with no 'ramp-up' period. The droplet generation is also completely invariant to fluid and flow properties such as: viscosity, interfacial tension and flow rate. This is in stark contrast to passive droplet generation methods. Here droplet size and sample/reagent concentrations can be pre-specified by careful design of the peristaltic micropump. The robustness of this method, combined with the ability to pre-specify droplet properties make this droplet generation method particularly well suited for integration into continuous monitoring devices.

I have carried out extensive characterisation and optimisation of the pulsed droplet generation regime and peristaltic micropump design. The droplet volume and contents variation has relative standard deviations under <2%, which is suitable for most of the analytical applications. I have incorporated the

pumping system into an exemplar miniature droplet generation system measuring only 2 cm x 2 cm x 4 cm, which still produced droplets with a volume RSD of 2%. I have further developed the method to allow generation of droplet trains (pre-specified sequences of droplets with different composition). Demonstrating this using a variety of structures including parallel T-junctions and multiple T-junctions in a branched channel structure. These droplet trains are well suited for multiplexed testing or multiple step testing, or the addition of standards *in-situ* for calibration of sensors.

7.2 Application to environmental monitoring

I have combined the droplet generation technology with a wet chemical assay to create a first of its kind platform using droplet microfluidics to continuously monitor environmental water chemistry. The platform has been tailored for the monitoring of both nitrite and nitrate utilising a modified Griess assay but could be tailored for a wide variety of chemical species. I have detailed the calibrations carried out in preparation for field deployments of the prototype device. I have also shown some of the early field deployment data in an estuarine river, which demonstrate the high temporal resolution, and accuracy of this platform. High temporal resolution and the inclusion of an internal standard are key advantages of this system over previously reported systems. Other advantages include small overall system size, low power consumption and reagent usage.

This platform has shown great promise and further development and testing of this platform will be taken forward by our industrial collaborator SouthWestSensors ltd. This could include further improvements to the device's longevity for deployments in remote locations where replacing components is unfeasible by including more durable pumplines and "whole Teflon" microfluidic chips similar to those described by Ren and others (Ren, Dai et al. 2011).

7.3 Continuous Heterogeneous assays in droplets

I have also demonstrated the application of the continuous droplet train generation by the pulsed droplet generation method, to perform a heterogeneous microbead based assay. This platform integrated a newly developed automated magnetic bead trap and a miniaturised spectrophotometer flow cell. This new method is similar in principle to previously described lab based droplet microfluidics heterogeneous assay platforms as described by Ferraro (Ferraro, Champ et al. 2016), however, is executed in a smaller platform with a high degree of automation. This method has been applied to perform a novel competitive heterogeneous assay for cortisol continuously in droplets, with the long-term goal of developing a point-of-care monitoring device. This platform could be tailored for a variety of heterogeneous assays such as ELISA assays to monitor rare protein biomarkers and ultralow concentration metabolites, cytokines etc..

Future work

The droplet microfluidics method developed in this thesis has shown the potential to improve the current practices of sampling and chemical sensing for both clinical and environmental monitoring. Real-time sampling and monitoring allows for the study of biochemical, physiological or pathological processes faster and more efficiently than ever before. For medical applications, we can record biochemical response caused by both chemical stimuli and physical stimuli in real time.

This could also form the basis of sensor systems for the study of drug metabolism and allow the development of new 'smart' therapies that use biochemical marker levels to guide treatment in real time and at the point-of-care (POC). Huge impact in environmental science can also be expected; particularly in the study of biogeochemistry and anthropogenic pollution with the potential to support data based policymaking.

The new approach of droplet train generation that I have developed during the course of my PhD will hopefully also allow for many exciting research opportunities such as for single cell studies, the generation of nanoparticles with differing quantities of starter materials etc.

7.4 Clinical validation of the continuous heterogeneous assays in droplet microfluidics

In the next year, I intend to carry out the research laid out in my plan for my EPSRC doctoral prize award by further developing the C.H.A.D. method and testing it in a clinical setting. I expect that this project will generate meaningful data that will inform both my own continued research and others within the field. A high degree of collaboration is expected between academic group, industrial partners such as LGC Group on biochemistry and SouthWestSensor Ltd. on clinical prototype development.

Several improvements will be made to the prototype before clinical testing. Currently a single pump is used to generate the sequence of droplets as defined by the rotorhead design. In the future, the pump will be decentralised from a single pump and many tubing to multiple smaller pumps synchronised by a microcontroller. This will allow arbitrary sequences of droplets to be generated as required, for an enhanced ability to perform multiplexed assays etc. with standard sample droplet interspersed. The modular design should also allow for reduced complication in the design of each of the pump modules, reducing the possibility for fabrication error. The magnetic trap design will be improved to ensure the tweezer tips can be easily aligned with high precision. The optical detection flow cell may be improved upon in a variety of ways including extending the optical path length by axial illumination of the droplets by elongating the droplet in constricted channels (Yang, Stavrakis et al. 2017). Furthermore, I intend to integrate other sensing technologies e.g. electrochemical (Rogers, Leong et al. 2011), fluorescent and chemiluminescence (Shi, Xu et al. 2009) assays into these devices to sense a greater variety of analytes with high sensitivity. Sample collection and preparation are also crucial for any continuous monitoring system and so some development may be required to integrate sample collection tools such as microdialysis with the current system including the development of in-situ calibration.

7.5 Microdialysis calibration

As previously mentioned *in-situ,* calibration is extremely important for creating complete continuous monitoring platform. As mentioned in section 1.10.2, *in-vivo* calibration of microdialysis probes can be difficult (Chefer, Thompson et al. 2009), as is the determination of the absolute concentration of an analyte in tissue.

Building on the fixed droplet size produced by the pulsed droplet generation regime and the ability to hard code chemical operations within the peristaltic micropump. It should be possible to design a rotorhead geometry for the *in-situ* calibration of microdialysis probes, and determination of the absolute concentration of an analyte in tissue (with a method similar to the flow rate method (Jacobson, Sandberg et al. 1985)). This could potentially be accomplished with a rotorhead design where feature spacing (and hence droplet size) is kept constant but feature size is varied around the rotorhead circumference. This will result in a train of droplets with defined constant volume but with different amounts of retention time in the probe, equivalent to varying flow rate through the probe in continuous flow systems. After completing one full turn of the rotorhead the effective flow rate of each droplet can be plotted against the measured concentration by an inline spectrophotometer flow cell (Hassan, Nightingale et al. 2016). It should then be possible to extrapolate the trend to a 100% recovery state and to determine the absolute concentration of the analyte in tissue.

7.6 Additional assays and applications

While liquid handling for the continuous monitoring device detailed in this thesis is well developed, some new developments may improve performance in clinical or field deployment. Similar to the regimes described in Chapter 4, it should be possible to integrate merging and dosing for multiple step assays into the continuous monitoring device. Also based on a similar multiple T-Junction geometry and timed pulsations it should also be possible to split samples into multiple droplets to carry out a variety of assays as described in the literature (Lee, Abbaspourrad et al. 2014).

Another interesting endeavour, which may be explored in the future, is the miniaturisation of a simple form of the peristaltic micropump/droplet generation device into a pill sized ingestible sampler device. This could be applied for time-displaced measurements of analytes present through the gastrointestinal tract or for temporary implantation. Transferring this to the lab, these droplets could be used to analyse markers of inflammation or to study bacteria inside the gut.

In the future, a wide variety of assays may be integrated into this platform technology, making it possible to monitor a wider variety of molecules at the point-of-care such as those for troponin (an important cardiac marker) and interleukins such as IL6 (another stress marker). The droplet microfluidics approach detailed in this thesis will also allow for the monitoring of a wide variety of chemistry in waterways for the study of biogeochemistry and anthropogenic pollution. Integrating new assays such as those for phosphate and silicate with the potential to support data based policymaking and could be applied to the search for disease markers in waterways to ensure that contaminated water is not being used.

In this thesis I have presented that droplet microfluidics has many favourable characteristics for the application of continuous monitoring. It is my hope that the work presented in this thesis may be built upon to create a wide variety of research and devices, which will be applied for the public good.

Bibliography

Abate, A. R., T. Hung, P. Mary, J. J. Agresti and D. A. Weitz (2010). "High-throughput injection with microfluidics using picoinjectors." Proceedings of the National Academy of Sciences of the United States of America **107**(45): 19163-19166.
Abate, A. R., M. Kutsovsky, S. Seiffert, M. Windbergs, L. F. V. Pinto, A. Rotem, A. S. Utada and D. A. Weitz (2011). "Synthesis of Monodisperse Microparticles from Non-Newtonian Polymer Solutions with Microfluidic Devices." Advanced Materials **23**(15): 1757-1760.
Abate, A. R., P. Mary, V. van Steijn and D. A. Weitz (2012). "Experimental validation of plugging during drop formation in a T-junction." Lab on a Chip **12**(8): 1516-1521.
Abdelgawad, M. and A. R. Wheeler (2009). "The Digital Revolution: A New Paradigm for Microfluidics." Advanced Materials **21**(8): 920-925.
Adamson, D. N., D. Mustafi, J. X. J. Zhang, B. Zheng and R. F. Ismagilov (2006). "Production of arrays of chemically distinct nanolitre plugs via repeated splitting in microfluidic devices." Lab on a chip **6**(9): 1178-1186.
Ahn, C. H., C. Jin-Woo, G. Beaucage, J. H. Nevin, L. Jeong-Bong, A. Puntambekar and J. Y. Lee (2004). "Disposable smart lab on a chip for point-of-care clinical diagnostics." Proceedings of the IEEE **92**.
Ahn, K., C. Kerbage, T. P. Hunt, R. M. Westervelt, D. R. Link and D. A. Weitz (2006). "Dielectrophoretic manipulation of drops for high-speed microfluidic sorting devices." Applied Physics Letters **88**(2): 024104.
Ambrosi, B., S. Peverelli, E. Passini, T. Re, R. Ferrario, P. Colombo, A. Sartorio and G. Faglia (1995). "Abnormalities of endocrine function in patients with clinically "silent" adrenal masses." European Journal of Endocrinology **132**(4): 422-428.
Anna, S. L. (2016). "Droplets and Bubbles in Microfluidic Devices." Annual Review of Fluid Mechanics **48**(1): 285-309.
Anna, S. L., N. Bontoux and H. A. Stone (2003). "Formation of dispersions using “flow focusing” in microchannels." Applied Physics Letters **82**(3): 364-366.
Baca, J. T., D. N. Finegold and S. A. Asher (2007). "Tear Glucose Analysis for the Noninvasive Detection and Monitoring of Diabetes Mellitus." The Ocular Surface **5**(4): 280-293.
Bai, Y., X. He, D. Liu, S. N. Patil, D. Bratton, A. Huebner, F. Hollfelder, C. Abell and W. T. S. Huck (2010). "A double droplet trap system for studying mass transport across a droplet-droplet interface." Lab on a Chip **10**(10): 1281-1285.
Baker, M. (2010). "Clever PCR: more genotyping, smaller volumes." Nature Methods **7**(5): 351-356.
Balaban, N. Q., J. Merrin, R. Chait, L. Kowalik and S. Leibler (2004). "Bacterial Persistence as a Phenotypic Switch." Science **305**(5690): 1622-1625.
Bandodkar, A. J. and J. Wang (2014). "Non-invasive wearable electrochemical sensors: a review." Trends in Biotechnology **32**(7): 363-371.
Banfi, G., M. Marinelli, G. S. Roi and V. Agape (1993). "Usefulness of Free Testosterone/Cortisol Ratio during a Season of Elite Speed Skating Athletes." Int J Sports Med **14**(07): 373-379.
Baret, J.-C. (2012). "Surfactants in droplet-based microfluidics." Lab on a Chip **12**(3): 422-433.
Baret, J.-C., O. J. Miller, V. Taly, M. Ryckelynck, A. El-Harrak, L. Frenz, C. Rick, M. L. Samuels, J. B. Hutchison, J. J. Agresti, D. R. Link, D. A. Weitz and A. D. Griffiths (2009). "Fluorescence-activated droplet sorting (FADS): efficient microfluidic cell sorting based on enzymatic activity." Lab on a Chip **9**(13): 1850-1858.
Baroud, C. N., J.-P. Delville, F. Gallaire and R. Wunenburger (2007). "Thermocapillary valve for droplet production and sorting." Physical Review E **75**(4): 046302.

Baroud, C. N., M. Robert de Saint Vincent and J.-P. Delville (2007). "An optical toolbox for total control of droplet microfluidics." Lab on a Chip **7**(8): 1029-1033.
Barron, J. L., T. D. Noakes, W. Levy, C. Smith and R. P. Millar (1985). "Hypothalamic Dysfunction in Overtrained Athletes*." The Journal of Clinical Endocrinology & Metabolism **60**(4): 803-806.
Basu, A. S. (2013). "Droplet morphometry and velocimetry (DMV): a video processing software for time-resolved, label-free tracking of droplet parameters." Lab Chip **13**(10): 1892-1901.
Beaton, A. D., C. L. Cardwell, R. S. Thomas, V. J. Sieben, F. E. Legiret, E. M. Waugh, P. J. Statham, M. C. Mowlem and H. Morgan (2012). "Lab-on-Chip Measurement of Nitrate and Nitrite for In Situ Analysis of Natural Waters." Environmental Science & Technology **46**(17): 9548-9556.
Beaton, A. D., V. J. Sieben, C. F. A. Floquet, E. M. Waugh, S. Abi Kaed Bey, I. R. G. Ogilvie, M. C. Mowlem and H. Morgan (2011). "An automated microfluidic colourimetric sensor applied in situ to determine nitrite concentration." Sensors and Actuators B: Chemical **156**(2): 1009-1014.
Bende-Michl, U. and P. B. Hairsine (2010). "A systematic approach to choosing an automated nutrient analyser for river monitoring." Journal of Environmental Monitoring **12**(1): 127-134.
Berg JM, T. J., Stryer L (2002). Biochemistry. Biochemistry. New York, W.H.Freeman & Co Ltd.
Bertocci, U., F. Huet, R. P. Nogueira and P. Rousseau (2002). "Drift Removal Procedures in the Analysis of Electrochemical Noise." CORROSION **58**(4): 337-347.
Bhat, V., M. Tiwari, P. Chavan and R. Kelkar (2012). "Analysis of laboratory sample rejections in the pre-analytical stage at an oncology center." Clinica Chimica Acta **413**(15): 1203-1206.
Bibette, J., F. L. Calderon and P. Poulin (1999). "Emulsions: basic principles." Reports on Progress in Physics **62**(6): 969.
Bock, J. L. (2000). "The New Era of Automated Immunoassay." American Journal of Clinical Pathology **113**(5): 628-646.
Bouchoucha, M., F. Callais, P. Renard, O. G. Ekindjian, P. H. Cugnenc and J. P. Barbier (1997). "Relationship between Acid Neutralization Capacity of Saliva and Gastro-Oesophageal Reflux." Archives of Physiology and Biochemistry **105**(1): 19-26.
Boybay, M. S., A. Jiao, T. Glawdel and C. L. Ren (2013). "Microwave sensing and heating of individual droplets in microfluidic devices." Lab on a Chip **13**(19): 3840-3846.
Brehm-Stecher, B. F. and E. A. Johnson (2004). "Single-Cell Microbiology: Tools, Technologies, and Applications." Microbiology and Molecular Biology Reviews **68**(3): 538-559.
Brezina, P. R., E. Haberl and E. Wallach (2011). "At home testing: optimizing management for the infertility physician." Fertility and Sterility **95**(6): 1867-1878.
Brossaud, J., D. Ducint, B. Gatta, M. Molimard, A. Tabarin and J. Corcuff (2012). "Urinary cortisol metabolites in corticotroph and adrenal tumours." Endocr. Abstr. **29**.
Brosseau, Q., J. Vrignon and J.-C. Baret (2014). Microfluidic Dynamic Interfacial Tensiometry (??DIT).
Brügmann, L. and K. Kremling (2007). Sampling. Methods of Seawater Analysis, Wiley-VCH Verlag GmbH**:** 1-25.
Burt, T. P., N. J. K. Howden, F. Worrall and M. J. Whelan (2010). "Long-term monitoring of river water nitrate: how much data do we need?" Journal of Environmental Monitoring **12**(1): 71-79.
Campbell, W. H., P. F. Song and G. G. Barbier (2006). "Nitrate reductase for nitrate analysis in water." Environmental Chemistry Letters **4**(2): 69-73.
Carpenter, L. L., T. T. Shattuck, A. R. Tyrka, T. D. Geracioti and L. H. Price (2011). "Effect of childhood physical abuse on cortisol stress response." Psychopharmacology **214**(1): 367-375.
Carter, P. J. (2006). "Potent antibody therapeutics by design." Nat Rev Immunol **6**(5): 343-357.
Chabert, M. and J.-L. Viovy (2008). "Microfluidic high-throughput encapsulation and hydrodynamic self-sorting of single cells." Proceedings of the National Academy of Sciences **105**(9): 3191-3196.

Chapin, T. P., J. M. Caffrey, H. W. Jannasch, L. J. Coletti, J. C. Haskins and K. S. Johnson (2004). "Nitrate sources and sinks in Elkhorn Slough, California: Results from long-term continuous in situ nitrate analyzers." Estuaries **27**(5): 882-894.
Chapin, T. P., H. W. Jannasch and K. S. Johnson (2002). "In situ osmotic analyzer for the year-long continuous determination of Fe in hydrothermal systems." Analytica Chimica Acta **463**(2): 265-274.
Chaurasia, C. S., M. Müller, E. D. Bashaw, E. Benfeldt, J. Bolinder, R. Bullock, P. M. Bungay, E. C. M. DeLange, H. Derendorf, W. F. Elmquist, M. Hammarlund-Udenaes, C. Joukhadar, D. L. Kellogg, C. E. Lunte, C. H. Nordstrom, H. Rollema, R. J. Sawchuk, B. W. Y. Cheung, V. P. Shah, L. Stahle, U. Ungerstedt, D. F. Welty and H. Yeo (2007). "AAPS-FDA Workshop White Paper: Microdialysis Principles, Application and Regulatory Perspectives." Pharmaceutical Research **24**(5): 1014-1025.
Chefer, V. I., A. C. Thompson, A. Zapata and T. S. Shippenberg (2009). "Overview of Brain Microdialysis." Current protocols in neuroscience / editorial board, Jacqueline N. Crawley ... [et al.] **CHAPTER**: Unit7.1-Unit7.1.
Chen, C. T. and G. B. Lee (2006). "Formation of Microdroplets in Liquids Utilizing Active Pneumatic Choppers on a Microfluidic Chip." Journal of Microelectromechanical Systems **15**(6): 1492-1498.
Chen, D., W. Du, Y. Liu, W. Liu, A. Kuznetsov, F. E. Mendez, L. H. Philipson and R. F. Ismagilov (2008). "The chemistrode: A droplet-based microfluidic device for stimulation and recording with high temporal, spatial, and chemical resolution." Proceedings of the National Academy of Sciences **105**(44): 16843-16848.
Chen, D. L., L. Li, S. Reyes, D. N. Adamson and R. F. Ismagilov (2007). "Using Three-Phase Flow of Immiscible Liquids To Prevent Coalescence of Droplets in Microfluidic Channels: Criteria To Identify the Third Liquid and Validation with Protein Crystallization." Langmuir **23**(4): 2255-2260.
Chen, Y., A. Wijaya Gani and S. K. Y. Tang (2012). "Characterization of sensitivity and specificity in leaky droplet-based assays." Lab on a Chip **12**(23): 5093-5103.
Chin, C. D., V. Linder and S. K. Sia (2012). "Commercialization of microfluidic point-of-care diagnostic devices." Lab on a Chip **12**(12): 2118-2134.
Chin, C. S., K. H. Coale, V. A. Elrod, K. S. Johnson, G. J. Massoth and E. T. Baker (1994). "In situ observations of dissolved iron and manganese in hydrothermal vent plumes, Juan de Fuca Ridge." Journal of Geophysical Research: Solid Earth **99**(B3): 4969-4984.
Chin, C. S., K. S. Johnson and K. H. Coale (1992). "Spectrophotometric determination of dissolved manganese in natural waters with 1-(2-pyridylazo)-2-naphthol: application to analysis in situ in hydrothermal plumes." Marine Chemistry **37**(1): 65-82.
Cho, S. K., H. Moon and C. J. Kim (2003). "Creating, Transporting, Cutting, and Merging Liquid Droplets by Electrowetting-Based Actuation for Digital Microfluidic Circuits." JOURNAL OF MICROELECTROMECHANICAL SYSTEMS **12**(1): 70-80.
Choi, K., A. H. C. Ng, R. Fobel and A. R. Wheeler (2012). "Digital Microfluidics." Annual Review of Analytical Chemistry **5**(1): 413-440.
Chokkalingam, V., J. Tel, F. Wimmers, X. Liu, S. Semenov, J. Thiele, C. G. Figdor and W. T. Huck (2013). "Probing cellular heterogeneity in cytokine-secreting immune cells using droplet-based microfluidics." Lab Chip **13**(24): 4740-4744.
Chokkalingam, V., J. Tel, F. Wimmers, X. Liu, S. Semenov, J. Thiele, C. G. Figdor and W. T. S. Huck (2013). "Probing cellular heterogeneity in cytokine-secreting immune cells using droplet-based microfluidics." Lab on a Chip **13**(24): 4740-4744.
Christensen, H., H. H. Johannesen, A. F. Christensen, K. Bendtzen and G. Boysen (2004). "Serum Cardiac Troponin I in Acute Stroke Is Related to Serum Cortisol and TNF-α." Cerebrovascular Diseases **18**(3): 194-199.

Christopher, G. F., N. N. Noharuddin, J. A. Taylor and S. L. Anna (2008). "Experimental observations of the squeezing-to-dripping transition in T-shaped microfluidic junctions." Physical Review E **78**(3): 036317.
Churski, K., P. Korczyk and P. Garstecki (2010). "High-throughput automated droplet microfluidic system for screening of reaction conditions." Lab on a Chip **10**(7): 816-818.
Clausell-Tormos, J., D. Lieber, J.-C. Baret, A. El-Harrak, O. J. Miller, L. Frenz, J. Blouwolff, K. J. Humphry, S. Köster, H. Duan, C. Holtze, D. A. Weitz, A. D. Griffiths and C. A. Merten (2008). "Droplet-Based Microfluidic Platforms for the Encapsulation and Screening of Mammalian Cells and Multicellular Organisms." Chemistry & Biology **15**(5): 427-437.
Clinton-Bailey, G. S., M. M. Grand, A. D. Beaton, A. M. Nightingale, D. R. Owsianka, G. J. Slavikt, D. P. Connelly, C. L. Cardwell and M. C. Mowlem (2017). "A Lab-on-Chip Analyzer for in Situ Measurement of Soluble Reactive Phosphate: Improved Phosphate Blue Assay and Application to Fluvial Monitoring." Environmental Science & Technology **51**(17): 9989-9995.
Cogan, D., J. Cleary, T. Phelan, E. McNamara, M. Bowkett and D. Diamond (2013). "Integrated flow analysis platform for the direct detection of nitrate in water using a simplified chromotropic acid method." Analytical Methods **5**(18): 4798-4804.
Collins, D. J., T. Alan, K. Helmerson and A. Neild (2013). "Surface acoustic waves for on-demand production of picoliter droplets and particle encapsulation." Lab on a Chip **13**(16): 3225-3231.
Collins, D. J., A. Neild, A. deMello, A.-Q. Liu and Y. Ai (2015). "The Poisson distribution and beyond: methods for microfluidic droplet production and single cell encapsulation." Lab on a Chip **15**(17): 3439-3459.
Corbalán-Tutau, D., J. A. Madrid, F. Nicolás and M. Garaulet (2014). "Daily profile in two circadian markers “melatonin and cortisol” and associations with metabolic syndrome components." Physiology & Behavior **123**: 231-235.
Craighead, H. (2006). "Future lab-on-a-chip technologies for interrogating individual molecules." Nature **442**(7101): 387-393.
Cubaud, T. and T. G. Mason (2008). "Capillary threads and viscous droplets in square microchannels." Physics of Fluids **20**(5): 053302.
Cui, F., M. Rhee, A. Singh and A. Tripathi (2015). "Microfluidic Sample Preparation for Medical Diagnostics." Annual Review of Biomedical Engineering **17**(1): 267-286.
Czeisler, C. A., M. C. Moore Ede, Q. R. Regestein, E. S. Kisch, V. S. Fang and E. N. Ehrlich (1976). "Episodic 24-Hour Cortisol Secretory Patterns in Patients Awaiting Elective Cardiac Surgery." The Journal of Clinical Endocrinology & Metabolism **42**(2): 273-283.
Darhuber, A. A., J. P. Valentino and S. M. Troian (2010). "Planar digital nanoliter dispensing system based on thermocapillary actuation." Lab on a Chip **10**(8): 1061-1071.
De Kloet, E. R. M. J. (2005). "Holsboer Florian Stress and the brain: from adaptation to disease." Nature Rev. Neurosci. **6**(6): 13.
De Menech, M. (2006). "Modeling of droplet breakup in a microfluidic T-shaped junction with a phase-field model." Physical Review E **73**(3): 031505.
Delahanty, D. L., A. J. Raimonde and E. Spoonster (2000). "Initial posttraumatic urinary cortisol levels predict subsequent PTSD symptoms in motor vehicle accident victims." Biological Psychiatry **48**(9): 940-947.
deMello, A. J. (2006). "Control and detection of chemical reactions in microfluidic systems." Nature **442**(7101): 394-402.
Dettling, A. C., M. R. Gunnar and B. Donzella (1999). "Cortisol levels of young children in full-day childcare centers: relations with age and temperament." Psychoneuroendocrinology **24**(5): 519-536.

Dimov, I. K., L. Basabe-Desmonts, J. L. Garcia-Cordero, B. M. Ross, A. J. Ricco and L. P. Lee (2011). "Stand-alone self-powered integrated microfluidic blood analysis system (SIMBAS)." Lab on a Chip **11**(5): 845-850.
Dittrich, P. S., K. Tachikawa and A. Manz (2006). "Micro Total Analysis Systems. Latest Advancements and Trends." Analytical Chemistry **78**(12): 3887-3908.
Dobell, C. and A. v. Leeuwenhoek (1932). Antony van Leeuwenhoek and his "Little animals"; being some account of the father of protozoology and bacteriology and his multifarious discoveries in these disciplines; collected, translated, and edited from his printed works, unpublished manuscripts, and contemporary records, by Clifford Dobell ... Published on the 300th anniversary of his birth. New York, Harcourt, Brace and company.
Dobson, H. and R. F. Smith (2000). "What is stress, and how does it affect reproduction?" Animal Reproduction Science **60-61**: 743-752.
Dollet, B., W. van Hoeve, J.-P. Raven, P. Marmottant and M. Versluis (2008). "Role of the Channel Geometry on the Bubble Pinch-Off in Flow-Focusing Devices." Physical Review Letters **100**(3): 034504.
Dressman, D., H. Yan, G. Traverso, K. W. Kinzler and B. Vogelstein (2003). "Transforming single DNA molecules into fluorescent magnetic particles for detection and enumeration of genetic variations." Proceedings of the National Academy of Sciences of the United States of America **100**(15): 8817-8822.
Dreyfus, R., P. Tabeling and H. Willaime (2003). "Ordered and Disordered Patterns in Two-Phase Flows in Microchannels." Physical Review Letters **90**(14): 144505.
Du, W., L. Li, K. P. Nichols and R. Ismagilov (2009). "SlipChip." Lab on a Chip **9**(16): 2286-2292.
Dungchai, W., O. Chailapakul and C. S. Henry (2009). "Electrochemical Detection for Paper-Based Microfluidics." Analytical Chemistry **81**(14): 5821-5826.
Dutkiewicz, S., M. J. Follows and P. Parekh (2005). "Interactions of the iron and phosphorus cycles: A three-dimensional model study." Global Biogeochemical Cycles **19**(1): n/a-n/a.
Eddings, M. A., M. A. Johnson and G. B.K. (2008). "Determining the optimal PDMS–PDMS bonding technique for microfluidic devices." Journal of Micromechanics and Microengineering **18**(6): 067001.
Eddings, M. A., M. A. Johnson and B. K. Gale (2008). "Determining the optimal PDMS-PDMS bonding technique for microfluidic devices." Journal of Micromechanics and Microengineering **18**(6).
Edwards, O., J. M. Galley, R. J. Courtenay-Evans, J. Hunter and A. Tait (1974). "CHANGES IN CORTISOL METABOLISM FOLLOWING RIFAMPICIN THERAPY." The Lancet **304**(7880): 549-551.
Eggers, J. and E. Villermaux (2008). "Physics of liquid jets." Reports on Progress in Physics **71**(3): 036601.
El-Ali, J., P. K. Sorger and K. F. Jensen (2006). "Cells on chips." Nature **442**(7101): 403-411.
El-Laboudi, A., N. S. Oliver, A. Cass and D. Johnston (2013). "Use of Microneedle Array Devices for Continuous Glucose Monitoring: A Review." Diabetes Technology & Therapeutics **15**(1): 101-115.
Ellerbee, A. K., S. T. Phillips, A. C. Siegel, K. A. Mirica, A. W. Martinez, P. Striehl, N. Jain, M. Prentiss and G. M. Whitesides (2009). "Quantifying Colorimetric Assays in Paper-Based Microfluidic Devices by Measuring the Transmission of Light through Paper." Analytical Chemistry **81**(20): 8447-8452.
Engvall, E. and P. Perlmann (1971). "Enzyme-linked immunosorbent assay (ELISA) quantitative assay of immunoglobulin G." Immunochemistry **8**(9): 871-874.
Fan, H. C., J. Wang, A. Potanina and S. R. Quake (2011). "Whole-genome molecular haplotyping of single cells." Nat Biotech **29**(1): 51-57.
Fan, S.-K., T.-H. Hsieh and D.-Y. Lin (2009). "General digital microfluidic platform manipulating dielectric and conductive droplets by dielectrophoresis and electrowetting." Lab on a Chip **9**(9): 1236-1242.

Ferraro, D., J. Champ, B. Teste, M. Serra, L. Malaquin, J.-L. Viovy, P. de Cremoux and S. Descroix (2016). "Microfluidic platform combining droplets and magnetic tweezers: application to HER2 expression in cancer diagnosis." Scientific Reports **6**: 25540.
Ferraro, D., Y. Lin, B. Teste, D. Talbot, L. Malaquin, S. Descroix and A. Abou-Hassan (2015). "Continuous chemical operations and modifications on magnetic [gamma]-Fe2O3 nanoparticles confined in nanoliter droplets for the assembly of fluorescent and magnetic SiO2@[gamma]-Fe2O3." Chemical Communications **51**(95): 16904-16907.
Fidalgo, L. M., C. Abell and W. T. S. Huck (2007). "Surface-induced droplet fusion in microfluidic devices." Lab on a Chip **7**(8): 984-986.
Fidalgo, L. M., G. Whyte, D. Bratton, C. F. Kaminski, C. Abell and W. T. S. Huck (2008). "From Microdroplets to Microfluidics: Selective Emulsion Separation in Microfluidic Devices." Angewandte Chemie International Edition **47**(11): 2042-2045.
Finch, M. S., D. J. Hydes, C. H. Clayson, W. Bernhard, J. Dakin and P. Gwilliam (1998). "A low power ultra violet spectrophotometer for measurement of nitrate in seawater: introduction, calibration and initial sea trials." Analytica Chimica Acta **377**(2): 167-177.
Flynn, K. J. (2001). "A mechanistic model for describing dynamic multi-nutrient, light, temperature interactions in phytoplankton." Journal of Plankton Research **23**(9): 977-997.
Fradet, E., C. Bayer, F. Hollfelder and C. N. Baroud (2015). "Measuring Fast and Slow Enzyme Kinetics in Stationary Droplets." Analytical Chemistry **87**(23): 11915-11922.
Friend, J. and L. Yeo (2010). "Fabrication of microfluidic devices using polydimethylsiloxane." Biomicrofluidics **4**(2): 026502.
Funfschilling, D., H. Debas, H. Z. Li and T. G. Mason (2009). "Flow-field dynamics during droplet formation by dripping in hydrodynamic-focusing microfluidics." Physical Review E **80**(1): 015301.
Furuberg, L., M. Mielnik, A. Gulliksen, L. Solli, I.-R. Johansen, J. Voitel, T. Baier, L. Riegger and F. Karlsen (2008). "RNA amplification chip with parallel microchannels and droplet positioning using capillary valves." Microsystem Technologies **14**(4-5): 673-681.
Gao, W., Q. Xie, J. Jin, T. Qiao, H. Wang, L. Chen, H. Deng and Z. Lu (2010). "HPLC-FLU detection of cortisol distribution in human hair." Clinical Biochemistry **43**(7): 677-682.
Garcia-Robledo, E., A. Corzo and S. Papaspyrou (2014). "A fast and direct spectrophotometric method for the sequential determination of nitrate and nitrite at low concentrations in small volumes." Marine Chemistry **162**: 30-36.
Garstecki, P., M. J. Fuerstman, H. A. Stone and G. M. Whitesides (2006). "Formation of droplets and bubbles in a microfluidic T-junction-scaling and mechanism of break-up." Lab on a Chip **6**(3): 437-446.
Garstecki, P., I. Gitlin, W. DiLuzio, G. M. Whitesides, E. Kumacheva and H. A. Stone (2004). "Formation of monodisperse bubbles in a microfluidic flow-focusing device." Applied Physics Letters **85**(13): 2649-2651.
Garstecki, P., H. A. Stone and G. M. Whitesides (2005). "Mechanism for Flow-Rate Controlled Breakup in Confined Geometries: A Route to Monodisperse Emulsions." Physical Review Letters **94**(16): 164501.
Gatti, R., G. Antonelli, M. Prearo, P. Spinella, E. Cappellin and E. F. De Palo (2009). "Cortisol assays and diagnostic laboratory procedures in human biological fluids." Clinical Biochemistry **42**(12): 1205-1217.
Ghimenti, S., T. Lomonaco, M. Onor, L. Murgia, A. Paolicchi, R. Fuoco, L. Ruocco, G. Pellegrini, M. G. Trivella and F. Di Francesco (2011). "Measurement of Warfarin in the Oral Fluid of Patients Undergoing Anticoagulant Oral Therapy." PLoS ONE **6**(12): e28182.
Giavarina, D. and G. Lippi (2017). "Blood venous sample collection: Recommendations overview and a checklist to improve quality." Clinical Biochemistry **50**(10): 568-573.

Gielen, F., L. van Vliet, B. T. Koprowski, S. R. A. Devenish, M. Fischlechner, J. B. Edel, X. Niu, A. J. deMello and F. Hollfelder (2013). "A Fully Unsupervised Compartment-on-Demand Platform for Precise Nanoliter Assays of Time-Dependent Steady-State Enzyme Kinetics and Inhibition." Analytical Chemistry **85**(9): 4761-4769.
Gijs, M. A. M. (2004). "Magnetic bead handling on-chip: new opportunities for analytical applications." Microfluidics and Nanofluidics **1**(1): 22-40.
Gill, S. R., M. Pop, R. T. DeBoy, P. B. Eckburg, P. J. Turnbaugh, B. S. Samuel, J. I. Gordon, D. A. Relman, C. M. Fraser-Liggett and K. E. Nelson (2006). "Metagenomic Analysis of the Human Distal Gut Microbiome." Science (New York, N.Y.) **312**(5778): 1355-1359.
Giustarini, D., R. Rossi, A. Milzani and I. Dalle-Donne (2008). Nitrite and Nitrate Measurement by Griess Reagent in Human Plasma: Evaluation of Interferences and Standardization. Methods in Enzymology, Academic Press. **440:** 361-380.
Glawdel, T. and C. L. Ren (2012). "Droplet formation in microfluidic T-junction generators operating in the transitional regime. III. Dynamic surfactant effects." Physical Review E **86**(2): 026308.
Go, J. S. and S. Shoji (2004). "A disposable, dead volume-free and leak-free in-plane PDMS microvalve." Sensors and Actuators a-Physical **114**(2-3): 438-444.
Gordillo, J. M., A. Sevilla and F. Campo-Cortés (2013). "Global stability of stretched jets: conditions for the generation of monodisperse micro-emulsions using coflows." Journal of Fluid Mechanics **738**: 335-357.
Gowers, S. A., V. F. Curto, C. A. Seneci, C. Wang, S. Anastasova, P. Vadgama, G. Z. Yang and M. G. Boutelle (2015). "3D Printed Microfluidic Device with Integrated Biosensors for Online Analysis of Subcutaneous Human Microdialysate." Anal Chem **87**(15): 7763-7770.
Grasshoff, K. and H. Johannsen (1974). "Notes on techniques and methods for sea water analysisA critical review of the method by Benesch and Mangelsdorf for the colorimetric determination of ammonia in sea water." ICES Journal of Marine Science **36**(1): 90-92.
Grasshoff, K., K. Kremling and M. Ehrhardt (1999). Methods of Seawater Analysis, Wiley-VCH.
Gruner, P., B. Riechers, L. A. Chacòn Orellana, Q. Brosseau, F. Maes, T. Beneyton, D. Pekin and J.-C. Baret (2015). "Stabilisers for water-in-fluorinated-oil dispersions: Key properties for microfluidic applications." Current Opinion in Colloid & Interface Science **20**(3): 183-191.
Gruner, P., B. Riechers, B. Semin, J. Lim, A. Johnston, K. Short and J. C. Baret (2016). "Controlling molecular transport in minimal emulsions." Nature Communications **7**.
Gu, H., M. H. G. Duits and F. Mugele (2011). "Droplets Formation and Merging in Two-Phase Flow Microfluidics." International Journal of Molecular Sciences **12**(4): 2572-2597.
Gu, S.-Q., Y.-X. Zhang, Y. Zhu, W.-B. Du, B. Yao and Q. Fang (2011). "Multifunctional Picoliter Droplet Manipulation Platform and Its Application in Single Cell Analysis." Analytical Chemistry **83**(19): 7570-7576.
Guo, M. T., A. Rotem, J. A. Heyman and D. A. Weitz (2012). "Droplet microfluidics for high-throughput biological assays." Lab Chip **12**(12): 2146-2155.
Han, K. N., C. A. Li and G. H. Seong (2013). "Microfluidic Chips for Immunoassays." Annual Review of Analytical Chemistry **6**(1): 119-141.
Han, M., X. Gao, J. Z. Su and S. Nie (2001). "Quantum-dot-tagged microbeads for multiplexed optical coding of biomolecules." Nat Biotech **19**(7): 631-635.
Hart, J. K. and K. Martinez (2006). "Environmental Sensor Networks: A revolution in the earth system science?" Earth-Science Reviews **78**(3): 177-191.
HARTE, J. L. and G. H. EIFERT (1995). "The effects of running, environment, and attentional focus on athletes' catecholamine and cortisol levels and mood." Psychophysiology **32**(1): 49-54.
Hartings, J. A., M. R. Bullock, D. O. Okonkwo, L. S. Murray, G. D. Murray, M. Fabricius, A. I. R. Maas, J. Woitzik, O. Sakowitz, B. Mathern, B. Roozenbeek, H. Lingsma, J. P. Dreier, A. M. Puccio, L. A. Shutter,

C. Pahl and A. J. Strong (2011). "Spreading depolarisations and outcome after traumatic brain injury: A prospective observational study." The Lancet Neurology **10**(12): 1058-1064.
Hassan, S., A. M. Nightingale and X. Niu (2016). "Continuous measurement of enzymatic kinetics in droplet flow for point-of-care monitoring." Analyst **141**(11): 3266-3273.
Hayes, C. J. and T. M. Dalton (2015). "Microfluidic droplet-based PCR instrumentation for high-throughput gene expression profiling and biomarker discovery." Biomolecular Detection and Quantification **4**: 22-32.
Hersini, K. J., L. Melgaard, P. Gazerani and L. J. Petersen (2014). "Microdialysis of inflammatory mediators in the skin: a review." Acta Derm Venereol **94**(5): 501-511.
Hibbard, T. and A. J. Killard (2011). "Breath Ammonia Analysis: Clinical Application and Measurement." Critical Reviews in Analytical Chemistry **41**(1): 21-35.
Holsboer, F. and M. Ising (2010). "Stress Hormone Regulation: Biological Role and Translation into Therapy." Annual Review of Psychology **61**(1): 81-109.
Holt, D. J., R. J. Payne, W. Y. Chow and C. Abell (2010). "Fluorosurfactants for microdroplets: Interfacial tension analysis." Journal of Colloid and Interface Science **350**(1): 205-211.
Hosokawa, K., K. Sato, N. Ichikawa and M. Maeda (2004). "Power-free poly(dimethylsiloxane) microfluidic devices for gold nanoparticle-based DNA analysis." Lab on a Chip **4**(3): 181-185.
Huang, X., C. Leduc, Y. Ravussin, S. Li, E. Davis, B. Song, Q. Wang, D. Accili, R. Leibel and Q. Lin (2012). "Continuous Monitoring of Glucose in Subcutaneous Tissue Using Microfabricated Differential Affinity Sensors." Journal of Diabetes Science and Technology **6**(6): 1436-1444.
Huh, D., J. H. Bahng, Y. Ling, H.-H. Wei, O. D. Kripfgans, J. B. Fowlkes, J. B. Grotberg and S. Takayama (2007). "A Gravity-Driven Microfluidic Particle Sorting Device with Hydrodynamic Separation Amplification." Analytical chemistry **79**(4): 1369-1376.
Humphry, K. J., A. Ajdari, A. Fernández-Nieves, H. A. Stone and D. A. Weitz (2009). "Suppression of instabilities in multiphase flow by geometric confinement." Physical Review E **79**(5): 056310.
Hung, L.-H., K. M. Choi, W.-Y. Tseng, Y.-C. Tan, K. J. Shea and A. P. Lee (2006). "Alternating droplet generation and controlled dynamic droplet fusion in microfluidic device for CdS nanoparticle synthesis." Lab on a Chip **6**(2): 174-178.
Hunter, G. W., J. C. Xu, A. M. Biaggi-Labiosa, D. Laskowski, P. K. Dutta, S. P. Mondal, B. J. Ward, D. B. Makel, C. C. Liu, C. W. Chang and R. A. Dweik (2011). "Smart sensor systems for human health breath monitoring applications." Journal of Breath Research **5**(3): 037111.
Jacobson, I., M. Sandberg and A. Hamberger (1985). "Mass transfer in brain dialysis devices—a new method for the estimation of extracellular amino acids concentration." Journal of Neuroscience Methods **15**(3): 263-268.
Janiesch, J. W., M. Weiss, G. Kannenberg, J. Hannabuss, T. Surrey, I. Platzman and J. P. Spatz (2015). "Key Factors for Stable Retention of Fluorophores and Labeled Biomolecules in Droplet-Based Microfluidics." Analytical Chemistry **87**(4): 2063-2067.
Jannasch, H. W., K. S. Johnson and C. M. Sakamoto (1994). "Submersible, Osmotically Pumped Analyzer for Continuous Determination of Nitrate in situ." Analytical Chemistry **66**(20): 3352-3361.
Jannasch, H. W., C. G. Wheat, J. N. Plant, M. Kastner and D. S. Stakes (2004). "Continuous chemical monitoring with osmotically pumped water samplers: OsmoSampler design and applications." Limnology and Oceanography: Methods **2**(4): 102-113.
Janssen, P. J. A., H. E. H. Meijer and P. D. Anderson (2012). "Stability and breakup of confined threads." Physics of Fluids **24**(1): 012102.
Jin, B. J., Y. W. Kim, Y. Lee and J. Y. Yoo (2010). "Droplet merging in a straight microchannel using droplet size or viscosity difference." Journal of Micromechanics and Microengineering **20**(3): 035003.

Johnson, K. S. and L. J. Coletti (2002). "In situ ultraviolet spectrophotometry for high resolution and long-term monitoring of nitrate, bromide and bisulfide in the ocean." Deep Sea Research Part I: Oceanographic Research Papers **49**(7): 1291-1305.
Johnson, K. S., L. J. Coletti and F. P. Chavez (2006). "Diel nitrate cycles observed with in situ sensors predict monthly and annual new production." Deep Sea Research Part I: Oceanographic Research Papers **53**(3): 561-573.
Johnson, K. S., S. C. Riser and D. M. Karl (2010). "Nitrate supply from deep to near-surface waters of the North Pacific subtropical gyre." Nature **465**: 1062.
Jones, T. B. (2002). "On the Relationship of Dielectrophoresis and Electrowetting." Langmuir **18**(11): 4437-4443.
Jung, S.-Y., S. T. Retterer and C. P. Collier (2010). "On-demand generation of monodisperse femtolitre droplets by shape-induced shear." Lab on a Chip **10**(20): 2688-2694.
Junker, R., H. Schlebusch and P. B. Luppa (2010). "Point-of-Care Testing in Hospitals and Primary Care." Deutsches Ärzteblatt International **107**(33): 561-567.
Karmali, K., A. Karmali, A. Teixeira and M. J. M. Curto (2004). "Assay for glucose oxidase from Aspergillus niger and Penicillium amagasakiense by Fourier transform infrared spectroscopy." Analytical Biochemistry **333**(2): 320-327.
Kaur, J. and R. Sharma (2006). "Directed Evolution: An Approach to Engineer Enzymes." Critical Reviews in Biotechnology **26**(3): 165-199.
Kaushik, A., A. Vasudev, S. K. Arya, S. K. Pasha and S. Bhansali (2014). "Recent advances in cortisol sensing technologies for point-of-care application." Biosensors and Bioelectronics **53**: 499-512.
Kawai, K., M. Fujii and S. Shoji (2009). Pricise Titration Microfluidic System using Sub-Picoliter Droplet Injection. Micro Electro Mechanical Systems, 2009. MEMS 2009. IEEE 22nd International Conference on.
Keenan, D. B., J. J. Mastrototaro, G. Voskanyan and G. M. Steil (2009). "Delays in Minimally Invasive Continuous Glucose Monitoring Devices: A Review of Current Technology." Journal of Diabetes Science and Technology **3**(5): 1207-1214.
Kibria, G., M. M. Hossain, D. Mallick, T. C. Lau and R. Wu (2016). "Monitoring of metal pollution in waterways across Bangladesh and ecological and public health implications of pollution." Chemosphere **165**: 1-9.
Kirschbaum, C. and D. H. Hellhammer (1994). "Salivary cortisol in psychoneuroendocrine research: Recent developments and applications." Psychoneuroendocrinology **19**(4): 313-333.
Kirschbaum, C., K.-m. Pirke and D. H. Hellhammer (1995). "Preliminary evidence for reduced cortisol responsivity to psychological stress in women using oral contraceptive medication." Psychoneuroendocrinology **20**(5): 509-514.
Klespitz, J. and L. Kovács (2014). Peristaltic pumps — A review on working and control possibilities. 2014 IEEE 12th International Symposium on Applied Machine Intelligence and Informatics (SAMI).
Klimant, I., V. Meyer and M. Kühl (1995). "Fiber-optic oxygen microsensors, a new tool in aquatic biology." Limnology and Oceanography **40**(6): 1159-1165.
Knight, J. (2002). "Honey, I shrunk the lab." Nature **418**: 474.
Kobayashi, Y., K. Amitani, F. Watanabe and K. Miyai (1979). "Fluorescence polarization immunoassay for cortisol." Clinica Chimica Acta **92**(2): 241-247.
Koster, S., F. E. Angile, H. Duan, J. J. Agresti, A. Wintner, C. Schmitz, A. C. Rowat, C. A. Merten, D. Pisignano, A. D. Griffiths and D. A. Weitz (2008). "Drop-based microfluidic devices for encapsulation of single cells." Lab on a Chip **8**(7): 1110-1115.
Kovarik, M. L., P. C. Gach, D. M. Ornoff, Y. Wang, J. Balowski, L. Farrag and N. L. Allbritton (2012). "Micro Total Analysis Systems for Cell Biology and Biochemical Assays." Analytical Chemistry **84**(2): 516-540.

Latré, B., B. Braem, I. Moerman, C. Blondia and P. Demeester (2011). "A survey on wireless body area networks." Wireless Networks **17**(1): 1-18.
Laurell, T., J. Drott and L. Rosengren (1995). "Silicon wafer integrated enzyme reactors." Biosensors and Bioelectronics **10**(3): 289-299.
Le Bris, N., P. M. Sarradin, D. Birot and A. M. Alayse-Danet (2000). "A new chemical analyzer for in situ measurement of nitrate and total sulfide over hydrothermal vent biological communities." Marine Chemistry **72**(1): 1-15.
le Roux, C. W., G. A. Chapman, W. M. Kong, W. S. Dhillo, J. Jones and J. Alaghband-Zadeh (2003). "Free Cortisol Index Is Better Than Serum Total Cortisol in Determining Hypothalamic-Pituitary-Adrenal Status in Patients Undergoing Surgery." The Journal of Clinical Endocrinology & Metabolism **88**(5): 2045-2048.
Lecault, V., M. VanInsberghe, S. Sekulovic, D. J. H. F. Knapp, S. Wohrer, W. Bowden, F. Viel, T. McLaughlin, A. Jarandehei, M. Miller, D. Falconnet, A. K. White, D. G. Kent, M. R. Copley, F. Taghipour, C. J. Eaves, R. K. Humphries, J. M. Piret and C. L. Hansen (2011). "High-throughput analysis of single hematopoietic stem cell proliferation in microfluidic cell culture arrays." Nat Meth **8**(7): 581-586.
Lee, C.-Y., Y.-H. Lin and G.-B. Lee (2009). "A droplet-based microfluidic system capable of droplet formation and manipulation." Microfluidics and Nanofluidics **6**(5): 599-610.
Lee, H., L. Xu and K. W. Oh (2014). "Droplet-based microfluidic washing module for magnetic particle-based assays." Biomicrofluidics **8**(4): 044113.
Lee, J. and C. J. Kim (2000). "Surface-tension-driven microactuation based on continuous electrowetting." Journal of Microelectromechanical Systems **9**(2): 171-180.
Lee, S. S., A. Abbaspourrad and S.-H. Kim (2014). "Nonspherical Double Emulsions with Multiple Distinct Cores Enveloped by Ultrathin Shells." ACS Applied Materials & Interfaces **6**(2): 1294-1300.
Lee, W., L. M. Walker and S. L. Anna (2009). "Role of geometry and fluid properties in droplet and thread formation processes in planar flow focusing." Physics of Fluids **21**(3): 032103.
Leitch, G. J. and Q. He (2011). "Cryptosporidiosis-an overview." Journal of Biomedical Research **25**(1): 1-16.
Lequin, R. M. (2005). "Enzyme Immunoassay (EIA)/Enzyme-Linked Immunosorbent Assay (ELISA)." Clinical Chemistry **51**(12): 2415-2418.
Leung, K., H. Zahn, T. Leaver, K. M. Konwar, N. W. Hanson, A. P. Pagé, C.-C. Lo, P. S. Chain, S. J. Hallam and C. L. Hansen (2012). "A programmable droplet-based microfluidic device applied to multiparameter analysis of single microbes and microbial communities." Proceedings of the National Academy of Sciences **109**(20): 7665-7670.
Levine, A., O. Zagoory-Sharon, R. Feldman, J. G. Lewis and A. Weller (2007). "Measuring cortisol in human psychobiological studies." Physiology & Behavior **90**(1): 43-53.
Li, D., H. Yu, X. Huang, F. Huang, X. Hu and K. Xu (2007). Prediction of blood glucose using interstitial fluid extracted by ultrasound and vacuum.
Li Jeon, N., H. Baskaran, S. K. W. Dertinger, G. M. Whitesides, L. Van De Water and M. Toner (2002). "Neutrophil chemotaxis in linear and complex gradients of interleukin-8 formed in a microfabricated device." Nat Biotech **20**(8): 826-830.
Li, L., J. Q. Boedicker and R. F. Ismagilov (2007). "Using a Multijunction Microfluidic Device To Inject Substrate into an Array of Preformed Plugs without Cross-Contamination: Comparing Theory and Experiments." Analytical chemistry **79**(7): 2756-2761.
Li, L. and R. F. Ismagilov (2010). "Protein Crystallization Using Microfluidic Technologies Based on Valves, Droplets, and SlipChip." Annual Review of Biophysics **39**(1): 139-158.
Li, X., D. R. Ballerini and W. Shen (2012). "A perspective on paper-based microfluidics: Current status and future trends." Biomicrofluidics **6**(1): 011301.

Liau, A., R. Karnik, A. Majumdar and J. H. D. Cate (2005). "Mixing Crowded Biological Solutions in Milliseconds." Analytical Chemistry **77**(23): 7618-7625.
Lin, B. C. and Y. C. Su (2008). "On-demand liquid-in-liquid droplet metering and fusion utilizing pneumatically actuated membrane valves." Journal of Micromechanics and Microengineering **18**(11): 115005.
Lin, B. C. and S. Y.C. (2008). "On-demand liquid-in-liquid droplet metering and fusion utilizing pneumatically actuated membrane valves." Journal of Micromechanics and Microengineering **18**(11): 115005.
Link, D. R., S. L. Anna, D. A. Weitz and H. A. Stone (2004). "Geometrically Mediated Breakup of Drops in Microfluidic Devices." Physical Review Letters **92**(5): 054503.
Link, D. R., E. Grasland-Mongrain, A. Duri, F. Sarrazin, Z. Cheng, G. Cristobal, M. Marquez and D. A. Weitz (2006). "Electric Control of Droplets in Microfluidic Devices." Angewandte Chemie International Edition **45**(16): 2556-2560.
Lintel, H., C. M. Van De Pol and S. Bouwstra (2018). A PIEZOELECTRIC MICROPUMP BASED ON MICROMACHINING.
Liu, K., H. Ding, Y. Chen and X.-Z. Zhao (2007). "Droplet-based synthetic method using microflow focusing and droplet fusion." Microfluidics and Nanofluidics **3**(2): 239-243.
Lonnroth, P., P. A. Jansson and U. Smith (1987). "A microdialysis method allowing characterization of intercellular water space in humans." Am J Physiol **253**(2 Pt 1): E228-231.
Løvås, K., T. E. Thorsen and E. S. Husebye (2006). "Saliva cortisol measurement: Simple and reliable assessment of the glucocorticoid replacement therapy in Addison's disease." Journal of Endocrinological Investigation **29**(8): 727-731.
Lucchetta, E. M., M. S. Munson and R. F. Ismagilov (2006). "Characterization of the local temperature in space and time around a developing Drosophila embryo in a microfluidic device." Lab on a Chip **6**(2): 185-190.
Maaroufi, Y., C. Heymans, J.-M. De Bruyne, V. Duchateau, H. Rodriguez-Villalobos, M. Aoun and F. Crokaert (2003). "Rapid Detection of Candida albicans in Clinical Blood Samples by Using a TaqMan-Based PCR Assay." Journal of Clinical Microbiology **41**(7): 3293-3298.
Mader, J. K., H. Weinhandl, G. Köhler, J. Plank, G. Bock, S. Korsatko, M. Ratzer, D. Ikeoka, H. Köhler, T. R. Pieber and M. Ellmerer (2010). "Assessment of different techniques for subcutaneous glucose monitoring in Type 1 diabetic patients during 'real-life' glucose excursions." Diabetic Medicine **27**(3): 332-338.
Mahla, E., K. Tiesenhausen, P. Rehak, S. Fruhwald, P. Pürstner and H. Metzler (2000). "Perioperative myocardial cell injury: The relationship between troponin t and cortisol." Journal of Clinical Anesthesia **12**(3): 208-212.
Mamoru, S. and H. Kazuyuki (1977). "A new colorimetric method for determination of serum glucose." Clinica Chimica Acta **75**(3): 387-391.
María Luisa, C., R. Hans Olav, R. B. Daniel, A. C. Paul, M. David and N. B. Charles (2009). "Mixing via thermocapillary generation of flow patterns inside a microfluidic drop." New Journal of Physics **11**(7): 075033.
Marín, A. G., F. Campo-Cortés and J. M. Gordillo (2009). "Generation of micron-sized drops and bubbles through viscous coflows." Colloids and Surfaces A: Physicochemical and Engineering Aspects **344**(1–3): 2-7.
Martinez, A. W., S. T. Phillips, G. M. Whitesides and E. Carrilho (2010). "Diagnostics for the Developing World: Microfluidic Paper-Based Analytical Devices." Analytical Chemistry **82**(1): 3-10.
Martz, T. R., J. G. Connery and K. S. Johnson (2010). "Testing the Honeywell Durafet® for seawater pH applications." Limnology and Oceanography: Methods **8**(5): 172-184.

Matzeu, G., L. Florea and D. Diamond (2015). "Advances in wearable chemical sensor design for monitoring biological fluids." Sensors and Actuators B: Chemical **211**: 403-418.
Mazutis, L., J.-C. Baret and A. D. Griffiths (2009). "A fast and efficient microfluidic system for highly selective one-to-one droplet fusion." Lab on a Chip **9**(18): 2665-2672.
McDonald, J. C., D. C. Duffy, J. R. Anderson, D. T. Chiu, H. Wu, O. J. A. Schueller and G. M. Whitesides (2000). "Fabrication of microfluidic systems in poly(dimethylsiloxane)." ELECTROPHORESIS **21**(1): 27-40.
McEwen, B. S. (2002). "Cortisol, Cushing's Syndrome, and a Shrinking Brain—New Evidence for Reversibility." The Journal of Clinical Endocrinology & Metabolism **87**(5): 1947-1948.
Meyer, D., R. D. Prien, O. Dellwig, D. P. Connelly and D. E. Schulz-Bull (2012). "In situ determination of iron(II) in the anoxic zone of the central Baltic Sea using ferene as spectrophotometric reagent." Marine Chemistry **130-131**: 21-27.
Miller, J. R., S. Koren and G. Sutton (2010). "Assembly Algorithms for Next-Generation Sequencing Data." Genomics **95**(6): 315-327.
Miller, P. R., S. A. Skoog, T. L. Edwards, D. M. Lopez, D. R. Wheeler, D. C. Arango, X. Xiao, S. M. Brozik, J. Wang, R. Polsky and R. J. Narayan (2012). "Multiplexed microneedle-based biosensor array for characterization of metabolic acidosis." Talanta **88**: 739-742.
Miranda, K. M., M. G. Espey and D. A. Wink (2001). "A rapid, simple spectrophotometric method for simultaneous detection of nitrate and nitrite." Nitric Oxide-Biology and Chemistry **5**(1): 62-71.
Miranda, K. M., M. G. Espey and D. A. Wink (2001). "A Rapid, Simple Spectrophotometric Method for Simultaneous Detection of Nitrate and Nitrite." Nitric Oxide **5**(1): 62-71.
Mitchell, J. S., T. E. Lowe and J. R. Ingram (2009). "Rapid ultrasensitive measurement of salivary cortisol using nano-linker chemistry coupled with surface plasmon resonance detection." Analyst **134**(2): 380-386.
Moon, H., S. K. Cho, R. L. Garrell and C.-J. C. Kim (2002). "Low voltage electrowetting-on-dielectric." Journal of Applied Physics **92**(7): 4080-4087.
Moore, J. K., S. C. Doney, J. A. Kleypas, D. M. Glover and I. Y. Fung (2001). "An intermediate complexity marine ecosystem model for the global domain." Deep Sea Research Part II: Topical Studies in Oceanography **49**(1–3): 403-462.
Moore, J. K., S. C. Doney and K. Lindsay (2004). "Upper ocean ecosystem dynamics and iron cycling in a global three-dimensional model." Global Biogeochemical Cycles **18**(4): n/a-n/a.
Morgan, R. M., M. J. Patterson and M. A. Nimmo (2004). "Acute effects of dehydration on sweat composition in men during prolonged exercise in the heat." Acta Physiologica Scandinavica **182**(1): 37-43.
Mukerjee, E. V., S. D. Collins, R. R. Isseroff and R. L. Smith (2004). "Microneedle array for transdermal biological fluid extraction and in situ analysis." Sensors and Actuators A: Physical **114**(2): 267-275.
Musterd, M., V. van Steijn, C. R. Kleijn and M. T. Kreutzer (2015). "Calculating the volume of elongated bubbles and droplets in microchannels from a top view image." RSC Advances **5**(21): 16042-16049.
Nakamura, S. and Y. Ogura (1968). "Mode of Inhibition of Glucose Oxidase by Metal Ions." Journal of Biochemistry **64**(4): 439-447.
Narayan, R. K. (2002). "Clinical Trials in Head Injury." J Neurotrauma. **19**(5): 503-557.
Neff, T., J. Fischer, S. Fehr, O. Baenziger and M. Weiss (2001). "Start-up delays of infusion syringe pumps." Pediatric Anesthesia **11**(5): 561-565.
Neumann, N. F., D. W. Smith and M. Belosevic (2005). "Waterborne disease: an old foe re-emerging?" Journal of Environmental Engineering and Science **4**(3): 155-171.
Neurauter, G., I. Klimant and O. S. Wolfbeis (2000). "Fiber-optic microsensor for high resolution pCO2 sensing in marine environment." Fresenius' Journal of Analytical Chemistry **366**(5): 481-487.

Ng, A. H. C., K. Choi, R. P. Luoma, J. M. Robinson and A. R. Wheeler (2012). "Digital Microfluidic Magnetic Separation for Particle-Based Immunoassays." Analytical Chemistry **84**(20): 8805-8812.
Nguyen, N.-T., T.-H. Ting, Y.-F. Yap, T.-N. Wong, J. C.-K. Chai, W.-L. Ong, J. Zhou, S.-H. Tan and L. Yobas (2007). "Thermally mediated droplet formation in microchannels." Applied Physics Letters **91**(8): 084102.
Nielsen, J. K., C. B. Djurhuus, C. H. Gravholt, A. C. Carus, J. Granild-Jensen, H. Ørskov and J. S. Christiansen (2005). "Continuous Glucose Monitoring in Interstitial Subcutaneous Adipose Tissue and Skeletal Muscle Reflects Excursions in Cerebral Cortex." Diabetes **54**(6): 1635-1639.
Nightingale, A. M., A. D. Beaton and M. C. Mowlem (2015). "Trends in microfluidic systems for in situ chemical analysis of natural waters." Sensors and Actuators B: Chemical **221**: 1398-1405.
Nightingale, A. M., A. D. Beaton and M. C. Mowlem (2015). "Trends in microfluidic systems for in situ chemical analysis of natural waters." Sensors and Actuators B: Chemical **221**(Supplement C): 1398-1405.
Nightingale, A. M. and J. C. de Mello (2010). "Microscale synthesis of quantum dots." Journal of Materials Chemistry **20**(39): 8454-8463.
Nightingale, A. M. and J. C. deMello (2013). "Segmented Flow Reactors for Nanocrystal Synthesis." Advanced Materials **25**(13): 1813-1821.
Nightingale, A. M., G. W. H. Evans, P. Xu, B. J. Kim, S.-u. Hassan and X. Niu (2017). "Phased peristaltic micropumping for continuous sampling and hardcoded droplet generation." Lab on a Chip **17**(6): 1149-1157.
Nightingale, A. M., S.-u. Hassan, G. W. H. Evans, S. M. Coleman and X. Niu (2018). "Nitrate measurement in droplet flow: gas-mediated crosstalk and correction." Lab on a Chip **18**(13): 1903-1913.
Nisisako, T., T. Torii and T. Higuchi (2002). "Droplet formation in a microchannel network." Lab on a Chip **2**(1): 24-26.
Niu, X. (2015). METHODS AND APPARATUS FOR GENERATING DROPLETS.
Niu, X., F. Gielen, J. B. Edel and A. J. deMello (2011). "A microdroplet dilutor for high-throughput screening." Nat Chem **3**(6): 437-442.
Niu, X., S. Gulati, J. B. Edel and A. J. deMello (2008). "Pillar-induced droplet merging in microfluidic circuits." Lab on a Chip **8**(11): 1837-1841.
O'Donnell, C. and N. Efron (2012). "Diabetes and contact lens wear." Clinical and Experimental Optometry **95**(3): 328-337.
Ogilvie, I. R. G., V. J. Sieben, M. C. Mowlem and H. Morgan (2011). "Temporal Optimization of Microfluidic Colorimetric Sensors by Use of Multiplexed Stop-Flow Architecture." Analytical Chemistry **83**(12): 4814-4821.
Okamura, K., H. Hatanaka, H. Kimoto, M. Suzuki, Y. Sohrin, E. Nakayama, T. Gamo and J.-i. Ishibashi (2004). "Development of an <I>in situ</I> manganese analyzer using micro-diaphragm pumps and its application to time-series observations in a hydrothermal field at the Suiyo seamount." GEOCHEMICAL JOURNAL **38**(6): 635-642.
Olson, R. J. and J. B. Justice (1993). "Quantitative microdialysis under transient conditions." Analytical Chemistry **65**(8): 1017-1022.
Ortiz, D., P. Cabrales and J. C. Briceño (2013). "Transport of nitric oxide by perfluorocarbon emulsion." Biotechnology Progress **29**(6): 1565-1572.
Osborn, J. L., B. Lutz, E. Fu, P. Kauffman, D. Y. Stevens and P. Yager (2010). "Microfluidics without pumps: reinventing the T-sensor and H-filter in paper networks." Lab on a chip **10**(20): 2659-2665.
Ottesen, E. A., J. W. Hong, S. R. Quake and J. R. Leadbetter (2006). "Microfluidic Digital PCR Enables Multigene Analysis of Individual Environmental Bacteria." Science **314**(5804): 1464-1467.

Paixão, T. R. L. C. and M. Bertotti (2004). "Development of a breath alcohol sensor using a copper electrode in an alkaline medium." Journal of Electroanalytical Chemistry **571**(1): 101-109.
Pamme, N. (2006). "Magnetism and microfluidics." Lab on a Chip **6**(1): 24-38.
Pantalei, S., E. Zampetti, A. Bearzotti, F. De Cesare and A. Macagnano (2013). "Improving sensing features of a nanocomposite PEDOT:PSS sensor for NO breath monitoring." Sensors and Actuators B: Chemical **179**: 87-94.
Pantel, K., R. H. Brakenhoff and B. Brandt (2008). "Detection, clinical relevance and specific biological properties of disseminating tumour cells." Nat Rev Cancer **8**(5): 329-340.
Park, S.-Y., T.-H. Wu, Y. Chen, M. A. Teitell and P.-Y. Chiou (2011). "High-speed droplet generation on demand driven by pulse laser-induced cavitation." Lab on a Chip **11**(6): 1010-1012.
Patel, S., H. Park, P. Bonato, L. Chan and M. Rodgers (2012). "A review of wearable sensors and systems with application in rehabilitation." Journal of NeuroEngineering and Rehabilitation **9**(1): 1-17.
Patton, C. J., A. E. Fischer, W. H. Campbell and E. R. Campbell (2002). "Corn leaf nitrate reductase - A nontoxic alternative to cadmium for photometric nitrate determinations in water samples by air-segmented continuous-flow analysis." Environmental Science & Technology **36**(4): 729-735.
Peng, S. L., M. Y. Zhang, X. Z. Niu, W. J. Wen, P. Sheng, Z. Y. Liu and J. Shi (2008). "Magnetically responsive elastic microspheres." Applied Physics Letters **92**(1).
Peterson, M. E., R. M. Daniel, M. J. Danson and R. Eisenthal (2007). "The dependence of enzyme activity on temperature: determination and validation of parameters." Biochemical Journal **402**(Pt 2): 331-337.
Petit-Pierre, G., A. Bertsch and P. Renaud (2016). "Neural probe combining microelectrodes and a droplet-based microdialysis collection system for high temporal resolution sampling." Lab Chip **16**(5): 917-924.
Petrounia, I. P. and F. H. Arnold (2000). "Designed evolution of enzymatic properties." Current Opinion in Biotechnology **11**(4): 325-330.
Peyman, S. A., A. Iles and N. Pamme (2008). "Rapid on-chip multi-step (bio)chemical procedures in continuous flow - manoeuvring particles through co-laminar reagent streams." Chemical Communications(10): 1220-1222.
Peyman, S. A., A. Iles and N. Pamme (2009). "Mobile magnetic particles as solid-supports for rapid surface-based bioanalysis in continuous flow." Lab on a Chip **9**(21): 3110-3117.
Phurimsak, C., M. D. Tarn, S. A. Peyman, J. Greenman and N. Pamme (2014). "On-Chip Determination of C-Reactive Protein Using Magnetic Particles in Continuous Flow." Analytical Chemistry **86**(21): 10552-10559.
Piechotta, G., J. Albers and R. Hintsche (2005). "Novel micromachined silicon sensor for continuous glucose monitoring." Biosensors and Bioelectronics **21**(5): 802-808.
Pit, A., M. Duits and F. Mugele (2015). "Droplet Manipulations in Two Phase Flow Microfluidics." Micromachines **6**(12): 1768-1793.
Plant, J. N., K. S. Johnson, J. A. Needoba and L. J. Coletti (2009). "NH4-Digiscan: an in situ and laboratory ammonium analyzer for estuarine, coastal, and shelf waters." Limnology and Oceanography: Methods **7**(2): 144-156.
Plebani, M. and G. Lippi (2010). "Is laboratory medicine a dying profession? Blessed are those who have not seen and yet have believed." Clinical Biochemistry **43**(12): 939-941.
Plebani, M., L. Sciacovelli, A. Aita, A. Padoan and M. L. Chiozza (2014). "Quality indicators to detect pre-analytical errors in laboratory testing." Clinica Chimica Acta **432**: 44-48.
Plock, N. and C. Kloft (2005). "Microdialysis—theoretical background and recent implementation in applied life-sciences." European Journal of Pharmaceutical Sciences **25**(1): 1-24.

Prausnitz, M. R. (2004). "Microneedles for transdermal drug delivery." Advanced Drug Delivery Reviews **56**(5): 581-587.
Price, D. A., G. C. Close and B. A. Fielding (1983). "Age of appearance of circadian rhythm in salivary cortisol values in infancy." Archives of Disease in Childhood **58**(6): 454-456.
Priest, C., S. Herminghaus and R. Seemann (2006). "Controlled electrocoalescence in microfluidics: Targeting a single lamella." Applied Physics Letters **89**(13): 134101.
Provin, C., T. Fukuba, K. Okamura and T. Fujii (2013). "An Integrated Microfluidic System for Manganese Anomaly Detection Based on Chemiluminescence: Description and Practical Use to Discover Hydrothermal Plumes Near the Okinawa Trough." IEEE Journal of Oceanic Engineering **38**(1): 178-185.
Prunty, H., K. Andrews, G. Reddy-Kolanu, P. Quinlan and P. Wood (2004). "Sweat patch cortisol - a new screen for Cushing's syndrome." Endocrine Abstracts **7**: 202.
Raff, H., J. L. Raff and J. W. Findling (1998). "Late-Night Salivary Cortisol as a Screening Test for Cushing's Syndrome1." The Journal of Clinical Endocrinology & Metabolism **83**(8): 2681-2686.
Ramanathan, A., A. R. Nelson, A. P. Sagare and B. V. Zlokovic (2015). "Impaired vascular-mediated clearance of brain amyloid beta in Alzheimer's disease: the role, regulation and restoration of LRP1." Frontiers in Aging Neuroscience **7**: 136.
Rapp, B. E. (2017). Index. Microfluidics: Modelling, Mechanics and Mathematics. B. E. Rapp. Oxford, Elsevier**:** 755-766.
Ren, K., W. Dai, J. Zhou, J. Su and H. Wu (2011). "Whole-Teflon microfluidic chips." Proceedings of the National Academy of Sciences **108**(20): 8162-8166.
Revsbech, N. P. (1989). "An oxygen microsensor with a guard cathode." Limnology and Oceanography **34**(2): 474-478.
Ricci, F., D. Moscone and G. Palleschi (2008). "Ex Vivo Continuous Glucose Monitoring With Microdialysis Technique: The Example of GlucoDay." IEEE Sensors Journal **8**(1): 63-70.
Rogers, M., C. Leong, X. Niu, A. de Mello, K. H. Parker and M. G. Boutelle (2011). "Optimisation of a microfluidic analysis chamber for the placement of microelectrodes." Physical Chemistry Chemical Physics **13**(12): 5298-5303.
Rogers, M. L. and M. G. Boutelle (2013). "Real-time clinical monitoring of biomolecules." Annu Rev Anal Chem (Palo Alto Calif) **6**: 427-453.
Rogers, M. L., D. Feuerstein, C. L. Leong, M. Takagaki, X. Niu, R. Graf and M. G. Boutelle (2013). "Continuous online microdialysis using microfluidic sensors: dynamic neurometabolic changes during spreading depolarization." ACS Chem Neurosci **4**(5): 799-807.
Romero, P. A. and A. R. Abate (2012). "Flow focusing geometry generates droplets through a plug and squeeze mechanism." Lab on a Chip **12**(24): 5130-5132.
Rosenstein, B. J. and G. R. Cutting (1998). "The diagnosis of cystic fibrosis: A consensus statement." The Journal of Pediatrics **132**(4): 589-595.
Rueckert, A. and H. W. Morgan (2007). "Removal of contaminating DNA from polymerase chain reaction using ethidium monoazide." Journal of Microbiological Methods **68**(3): 596-600.
Rushworth, C. M., G. Jones, M. Fischlechner, E. Walton and H. Morgan (2015). "On-chip cavity-enhanced absorption spectroscopy using a white light-emitting diode and polymer mirrors." Lab on a Chip **15**(3): 711-717.
Russell, E., G. Koren, M. Rieder and S. Van Uum (2012). "Hair cortisol as a biological marker of chronic stress: Current status, future directions and unanswered questions." Psychoneuroendocrinology **37**(5): 589-601.
Ryoji, H. (1981). "Direct assay of cortisol in human saliva by solid phase radioimmunoassay and its clinical applications." Clinica Chimica Acta **117**(2): 239-249.

Sachar, E. J., L. Hellman, H. P. Roffwarg, F. S. Halpern, D. K. Fukushima and T. F. Gallagher (1973). "Disrupted 24-hour patterns of cortisol secretion in psychotic depression." Archives of General Psychiatry **28**(1): 19-24.
Sackmann, E. K., A. L. Fulton and D. J. Beebe (2014). "The present and future role of microfluidics in biomedical research." Nature **507**(7491): 181-189.
Sandoz, P. A., A. J. Chung, W. M. Weaver and D. Di Carlo (2014). "Sugar Additives Improve Signal Fidelity for Implementing Two-Phase Resorufin-Based Enzyme Immunoassays." Langmuir **30**(23): 6637-6643.
Schmid, L. and T. Franke (2014). "Acoustic modulation of droplet size in a T-junction." Applied Physics Letters **104**(13): 133501.
Schnetger, B. and C. Lehners (2014). "Determination of nitrate plus nitrite in small volume marine water samples using vanadium(III)chloride as a reduction agent." Marine Chemistry **160**: 91-98.
Schroeder, M. P., A. Gonzalez-Perez and N. Lopez-Bigas (2013). "Visualizing multidimensional cancer genomics data." Genome Medicine **5**(1): 9-9.
Schwartz, J. A., J. V. Vykoukal and P. R. C. Gascoyne (2004). "Droplet-based chemistry on a programmable micro-chip." Lab on a chip **4**(1): 11-17.
Seemann, R., M. Brinkmann, T. Pfohl and S. Herminghaus (2012). "Droplet based microfluidics." Reports on Progress in Physics **75**(1): 016601.
Shi, H., X. Xu, Y. Ding, S. Liu, L. Li and W. Kang (2009). "Determination of cortisol in human blood sera by a new Ag(III) complex–luminol chemiluminescent system." Analytical Biochemistry **387**(2): 178-183.
Shirley, D.-A. T., S. N. Moonah and K. L. Kotloff (2012). "Burden of disease from Cryptosporidiosis." Current opinion in infectious diseases **25**(5): 555-563.
Sieben, V. J., C. F. A. Floquet, I. R. G. Ogilvie, M. C. Mowlem and H. Morgan (2010). "Microfluidic colourimetric chemical analysis system: Application to nitrite detection." Analytical Methods **2**(5): 484-491.
Skafte-Pedersen, P., D. Sabourin, M. Dufva and D. Snakenborg (2009). "Multi-channel peristaltic pump for microfluidic applications featuring monolithic PDMS inlay." Lab on a Chip **9**(20): 3003-3006.
Sleator, R. D., C. Shortall and C. Hill (2008). "Metagenomics." Letters in Applied Microbiology **47**(5): 361-366.
Smith, S. M. and W. W. Vale (2006). "The role of the hypothalamic-pituitary-adrenal axis in neuroendocrine responses to stress." Dialogues in clinical neuroscience **8**(4): 383-395.
Sommer, M. O. A., G. Dantas and G. M. Church (2009). "Functional characterization of the antibiotic resistance reservoir in the human microflora." Science (New York, N.Y.) **325**(5944): 1128-1131.
Song, H., D. L. Chen and R. F. Ismagilov (2006). "Reactions in Droplets in Microfluidic Channels." Angewandte Chemie (International Ed.) **45**(44): 7336-7356.
Song, H. and R. F. Ismagilov (2003). "Millisecond Kinetics on a Microfluidic Chip Using Nanoliters of Reagents." Journal of the American Chemical Society **125**(47): 14613-14619.
Song, H., J. D. Tice and R. F. Ismagilov (2003). "A Microfluidic System for Controlling Reaction Networks in Time." Angewandte Chemie International Edition **42**(7): 768-772.
Soper, S. A., K. Brown, A. Ellington, B. Frazier, G. Garcia-Manero, V. Gau, S. I. Gutman, D. F. Hayes, B. Korte, J. L. Landers, D. Larson, F. Ligler, A. Majumdar, M. Mascini, D. Nolte, Z. Rosenzweig, J. Wang and D. Wilson (2006). "Point-of-care biosensor systems for cancer diagnostics/prognostics." Biosensors and Bioelectronics **21**(10): 1932-1942.
Squires, T. M. and S. R. Quake (2005). "Microfluidics: Fluid physics at the nanoliter scale." Reviews of Modern Physics **77**(3): 977-1026.

Srinivasan, V., V. K. Pamula and R. B. Fair (2004). "Droplet-based microfluidic lab-on-a-chip for glucose detection." Analytica Chimica Acta **507**(1): 145-150.
St-Louis, P. (2000). "Status of point-of-care testing: promise, realities, and possibilities." Clinical Biochemistry **33**(6): 427-440.
St John, A. and C. P. Price (2014). "Existing and Emerging Technologies for Point-of-Care Testing." The Clinical Biochemist Reviews **35**(3): 155-167.
Stahl, M., R. Bouw, A. Jackson and V. Pay (2002). "Human Microdialysis." Current Pharmaceutical Biotechnology **3**(2): 165-178.
Stan, C. A., S. K. Y. Tang and G. M. Whitesides (2009). "Independent Control of Drop Size and Velocity in Microfluidic Flow-Focusing Generators Using Variable Temperature and Flow Rate." Analytical Chemistry **81**(6): 2399-2402.
Statham, P. J., D. P. Connelly, C. R. German, T. Brand, J. O. Overnell, E. Bulukin, N. Millard, S. McPhail, M. Pebody, J. Perrett, P. Stevenson and A. Webb (2005). "Spatially Complex Distribution of Dissolved Manganese in a Fjord as Revealed by High-Resolution in Situ Sensing Using the Autonomous Underwater Vehicle Autosub." Environmental Science & Technology **39**(24): 9440-9445.
Statham, P. J., D. P. Connelly, C. R. German, E. Bulukin, N. Millard, S. McPhail, M. Pebody, J. Perrett, M. Squires, P. Stevenson and A. Webb (2003). "Mapping the 3D Spatial Distribution of Dissolved Manganese in Coastal Waters Using an In Situ Analyser and the Autonomous Underwater Vehicle Autosub." Underwater Technology **25**(3): 129-134.
Stenken, J. A. and A. J. Poschenrieder (2015). "Bioanalytical chemistry of cytokines--a review." Anal Chim Acta **853**: 95-115.
Stone, H. A. (1994). "Dynamics of Drop Deformation and Breakup in Viscous Fluids." Annual Review of Fluid Mechanics **26**(1): 65-102.
Stone, H. A. L., L.G. (1990). "The effects of surfactants on drop deformation and breakup." J. FluidMech. **220**: 161-186.
Strong, A. J., M. Fabricius, M. G. Boutelle, S. J. Hibbins, S. E. Hopwood, R. Jones, M. C. Parkin and M. Lauritzen (2002). "Spreading and synchronous depressions of cortical activity in acutely injured human brain." Stroke **33**(12): 2738-2743.
Sun, K., N. Ramgir and S. Bhansali (2008). "An immunoelectrochemical sensor for salivary cortisol measurement." Sensors and Actuators B: Chemical **133**(2): 533-537.
Swindells, J. F., S. C.F., H. R.C. and G. P.E. (1958). "Viscosities of Sucrose Solutions at various Temperatures Tables of Recalculated Values." United States Department of Commerce National Bureau of Standards.
Tadmor, A. D., E. A. Ottesen, J. R. Leadbetter and R. Phillips (2011). "Probing Individual Environmental Bacteria for Viruses by Using Microfluidic Digital PCR." Science **333**(6038): 58-62.
Takeshita, Y., T. R. Martz, K. S. Johnson and A. G. Dickson (2014). "Characterization of an Ion Sensitive Field Effect Transistor and Chloride Ion Selective Electrodes for pH Measurements in Seawater." Analytical Chemistry **86**(22): 11189-11195.
Talary, M. S., F. Dewarrat, D. Huber and A. Caduff (2007). "In vivo life sign application of dielectric spectroscopy and non-invasive glucose monitoring." Journal of Non-Crystalline Solids **353**(47–51): 4515-4517.
Tan, S.-H., S. M. S. Murshed, N. Nam-Trung, W. Teck Neng and Y. Levent (2008). "Thermally controlled droplet formation in flow focusing geometry: formation regimes and effect of nanoparticle suspension." Journal of Physics D: Applied Physics **41**(16): 165501.
Tan, W.-H. and S. Takeuchi (2006). "Timing controllable electrofusion device for aqueous droplet-based microreactors." Lab on a Chip **6**(6): 757-763.
Tan, Y.-C., V. Cristini and A. P. Lee (2006). "Monodispersed microfluidic droplet generation by shear focusing microfluidic device." Sensors and Actuators B: Chemical **114**(1): 350-356.

Tan, Y.-C., J. S. Fisher, A. I. Lee, V. Cristini and A. P. Lee (2004). "Design of microfluidic channel geometries for the control of droplet volume, chemical concentration, and sorting." Lab on a Chip **4**(4): 292-298.
Tan, Y.-C. and A. P. Lee (2005). "Microfluidic separation of satellite droplets as the basis of a monodispersed micron and submicron emulsification system." Lab on a Chip **5**(10): 1178-1183.
Tarn, M. D., R. F. Fakhrullin, V. N. Paunov and N. Pamme (2013). "Microfluidic device for the rapid coating of magnetic cells with polyelectrolytes." Materials Letters **95**: 182-185.
Teruhisa, U., H. Ryoji, I. Taisuke, S. Tatsuya, M. Fumihiro and S. Tatsuo (1981). "Use of saliva for monitoring unbound free cortisol levels in serum." Clinica Chimica Acta **110**(2): 245-253.
Thakur, R., A. M. Amin and S. Wereley (2015). "On-chip dilution in nanoliter droplets." Analyst **140**(17): 5855-5859.
Thakur, R., Y. Zhang, A. Amin and S. Wereley (2015). "Programmable microfluidic platform for spatiotemporal control over nanoliter droplets." Microfluidics and Nanofluidics **18**(5-6): 1425-1431.
Thorsen, T., R. W. Roberts, F. H. Arnold and S. R. Quake (2001). "Dynamic pattern formation in a vesicle-generating microfluidic device." Phys Rev Lett **86**(18): 4163-4166.
Thouron, D., R. Vuillemin, X. Philippon, A. Lourenço, C. Provost, A. Cruzado and V. Garçon (2003). "An Autonomous Nutrient Analyzer for Oceanic Long-Term in Situ Biogeochemical Monitoring." Analytical Chemistry **75**(11): 2601-2609.
Tice, J. D., A. D. Lyon and R. F. Ismagilov (2004). "Effects of viscosity on droplet formation and mixing in microfluidic channels." Analytica Chimica Acta **507**(1): 73-77.
Tierney, M. J., J. A. Tamada, R. O. Potts, L. Jovanovic and S. Garg (2001). "Clinical evaluation of the GlucoWatch® biographer: a continual, non-invasive glucose monitor for patients with diabetes." Biosensors and Bioelectronics **16**(9–12): 621-629.
Timmer, B., W. Olthuis and A. v. d. Berg (2005). "Ammonia sensors and their applications—a review." Sensors and Actuators B: Chemical **107**(2): 666-677.
Tlili, C., N. V. Myung, V. Shetty and A. Mulchandani (2011). "Label-free, chemiresistor immunosensor for stress biomarker cortisol in saliva." Biosensors and Bioelectronics **26**(11): 4382-4386.
Trinder, P. (1969). "Determination of Glucose in Blood Using Glucose Oxidase with an Alternative Oxygen Acceptor." Annals of Clinical Biochemistry: An international journal of biochemistry in medicine **6**(1): 24-27.
Turnbaugh, P. J. and J. I. Gordon (2008). "An Invitation to the Marriage of Metagenomics and Metabolomics." Cell **134**(5): 708-713.
Utada, A. S., A. Fernandez-Nieves, J. M. Gordillo and D. A. Weitz (2008). "Absolute Instability of a Liquid Jet in a Coflowing Stream." Physical Review Letters **100**(1): 014502.
Utada, A. S., A. Fernandez-Nieves, H. A. Stone and D. A. Weitz (2007). "Dripping to Jetting Transitions in Coflowing Liquid Streams." Physical Review Letters **99**(9): 094502.
Van Caenegem, E., K. Wierckx, T. Fiers, H. Segers, E. Vandersypt, J. Kaufman and G. T'Sjoen (2011). "Salivary cortisol and testosterone: A comparison of salivary sample collection methods in healthy controls." Endocr Abstr **26**.
van Steijn, V., C. R. Kleijn and M. T. Kreutzer (2009). "Flows around Confined Bubbles and Their Importance in Triggering Pinch-Off." Physical Review Letters **103**(21): 214501.
van Steijn, V., C. R. Kleijn and M. T. Kreutzer (2010). "Predictive model for the size of bubbles and droplets created in microfluidic T-junctions." Lab on a Chip **10**(19): 2513-2518.
VanBruggen, M. D., A. C. Hackney, R. G. McMurray and K. S. Ondrak (2011). "The Relationship Between Serum and Salivary Cortisol Levels in Response to Different Intensities of Exercise." International Journal of Sports Physiology and Performance **6**(3): 396-407.

Venugopal, M., S. K. Arya, G. Chornokur and S. Bhansali (2011). "A realtime and continuous assessment of cortisol in ISF using electrochemical impedance spectroscopy." Sensors and Actuators A: Physical **172**(1): 154-160.
Venugopal, M., K. E. Feuvrel, D. Mongin, S. Bambot, M. Faupel, A. Panangadan, A. Talukder and R. Pidva (2008). "Clinical Evaluation of a Novel Interstitial Fluid Sensor System for Remote Continuous Alcohol Monitoring." IEEE Sensors Journal **8**(1): 71-80.
Vining, R. F., R. A. McGinley, J. J. Maksvytis and K. Y. Ho (1983). "Salivary Cortisol: A Better Measure of Adrenal Cortical Function than Serum Cortisol." Annals of Clinical Biochemistry **20**(6): 329-335.
Vuillemin, R., D. Le Roux, P. Dorval, K. Bucas, J. P. Sudreau, M. Hamon, C. Le Gall and P. M. Sarradin (2009). "CHEMINI: A new in situ CHEmical MINIaturized analyzer." Deep Sea Research Part I: Oceanographic Research Papers **56**(8): 1391-1399.
Wagner, O., J. Thiele, M. Weinhart, L. Mazutis, D. A. Weitz, W. T. S. Huck and R. Haag (2016). "Biocompatible fluorinated polyglycerols for droplet microfluidics as an alternative to PEG-based copolymer surfactants." Lab on a Chip **16**(1): 65-69.
Wallin, O., J. Söderberg, B. Van Guelpen, H. Stenlund, K. Grankvist and C. Brulin (2008). "Preanalytical venous blood sampling practices demand improvement — A survey of test-request management, test-tube labelling and information search procedures." Clinica Chimica Acta **391**(1): 91-97.
Wang, J.-H. and G.-B. Lee (2013). "Formation of Tunable, Emulsion Micro-Droplets Utilizing Flow-Focusing Channels and a Normally-Closed Micro-Valve." Micromachines **4**(3): 306.
Wang, J. (2002). "Electrochemical detection for microscale analytical systems: a review." Talanta **56**(2): 223-231.
Wang, J. (2006). "Electrochemical biosensors: Towards point-of-care cancer diagnostics." Biosensors and Bioelectronics **21**(10): 1887-1892.
Wang, J., J. Wang, L. Feng and T. Lin (2015). "Fluid mixing in droplet-based microfluidics with a serpentine microchannel." RSC Advances **5**(126): 104138-104144.
Wang, L., W. Liu, S. Li, T. Liu, X. Yan, Y. Shi, Z. Cheng and C. Chen (2015). "Fast fabrication of microfluidic devices using a low-cost prototyping method." Microsystem Technologies **22**(4): 677-686.
Wang, M., G. T. Roman, K. Schultz, C. Jennings and R. T. Kennedy (2008). "Improved Temporal Resolution for in Vivo Microdialysis by Using Segmented Flow." Analytical Chemistry **80**(14): 5607-5615.
Wang, P. M., M. Cornwell and M. R. Prausnitz (2005). "Minimally Invasive Extraction of Dermal Interstitial Fluid for Glucose Monitoring Using Microneedles." Diabetes Technology & Therapeutics **7**(1): 131-141.
Wang, W., C. Yang and C. M. Li (2009). "Efficient On-Demand Compound Droplet Formation: From Microfluidics to Microdroplets as Miniaturized Laboratories." Small **5**(10): 1149-1152.
Wang, Y., S. L. Wong and R. J. Sawchuk (1993). "Microdialysis Calibration Using Retrodialysis and Zero-Net Flux: Application to a Study of the Distribution of Zidovudine to Rabbit Cerebrospinal Fluid and Thalamus." Pharmaceutical Research **10**(10): 1411-1419.
Weeks, D. A. and K. S. Johnson (1996). "Solenoid Pumps for Flow Injection Analysis." Analytical Chemistry **68**(15): 2717-2719.
Weibel, D. B. and G. M. Whitesides (2006). "Applications of microfluidics in chemical biology." Curr Opin Chem Biol **10**(6): 584-591.
Weinstein, R. L., S. L. Schwartz, R. L. Brazg, J. R. Bugler, T. A. Peyser and G. V. McGarraugh (2007). "Accuracy of the 5-Day FreeStyle Navigator Continuous Glucose Monitoring System." Comparison with frequent laboratory reference measurements **30**(5): 1125-1130.

Westerink, B. H. C., G. Damsma, H. Rollema, J. B. De Vries and A. S. Horn (1987). "Scope and limitations of in vivo brain dialysis: A comparison of its application to various neurotransmitter systems." Life Sciences **41**(15): 1763-1776.
Whitesides, G. M. (2006). "The origins and the future of microfluidics." Nature **442**(7101): 368-373.
Whitesides, G. M. S., A. D. (2001). "Flexible methods for microfluidics." Phys. Today **54**(6): 42-48.
Wijnen, B., E. J. Hunt, G. C. Anzalone and J. M. Pearce (2014). "Open-Source Syringe Pump Library." PLOS ONE **9**(9): e107216.
Windmiller, J. R., N. Zhou, M.-C. Chuang, G. Valdes-Ramirez, P. Santhosh, P. R. Miller, R. Narayan and J. Wang (2011). "Microneedle array-based carbon paste amperometric sensors and biosensors." Analyst **136**(9): 1846-1851.
Wong, H., C. J. Radke and S. Morris (1995). "The motion of long bubbles in polygonal capillaries. Part 2. Drag, fluid pressure and fluid flow." Journal of Fluid Mechanics **292**(-1): 95.
Wong H, R. C., Morris S. (1995). "The motion of long bubbles in polygonal capillaries. Part 1. Thin films." J. Fluid Mech. **292**: 71-94.
Wonsei, R. and H. Toshiro (2010). "Design and fabrication of a screw-driven multi-channel peristaltic pump for portable microfluidic devices." Journal of Micromechanics and Microengineering **20**(8): 085036.
Woodward, A., T. Cosgrove, J. Espidel, P. Jenkins and N. Shaw (2007). "Monodisperse emulsions from a microfluidic device, characterised by diffusion NMR." Soft Matter **3**(5): 627-633.
Woronoff, G., A. El Harrak, E. Mayot, O. Schicke, O. J. Miller, P. Soumillion, A. D. Griffiths and M. Ryckelynck (2011). "New Generation of Amino Coumarin Methyl Sulfonate-Based Fluorogenic Substrates for Amidase Assays in Droplet-Based Microfluidic Applications." Analytical Chemistry **83**(8): 2852-2857.
Woyke, T., A. Sczyrba, J. Lee, C. Rinke, D. Tighe, S. Clingenpeel, R. Malmstrom, R. Stepanauskas and J.-F. Cheng (2011). "Decontamination of MDA Reagents for Single Cell Whole Genome Amplification." PLoS ONE **6**(10): e26161.
Xing, S., J. Jiang and T. Pan (2013). "Interfacial microfluidic transport on micropatterned superhydrophobic textile." Lab on a Chip **13**(10): 1937-1947.
Xu, J. and D. Attinger (2008). "Drop on demand in a microfluidic chip." Journal of Micromechanics and Microengineering **18**(6): 065020.
Xu, J. H., S. W. Li, J. Tan, Y. J. Wang and G. S. Luo (2006). "Preparation of highly monodisperse droplet in a T-junction microfluidic device." AIChE Journal **52**(9): 3005-3010.
Xu, Y., D. L. McArthur, J. R. Alger, M. Etchepare, D. A. Hovda, T. C. Glenn, S. Huang, I. Dinov and P. M. Vespa (2010). "Early nonischemic oxidative metabolic dysfunction leads to chronic brain atrophy in traumatic brain injury." J Cereb Blood Flow Metab **30**(4): 883-894.
Yalow, R. S. and S. A. Berson (1960). "IMMUNOASSAY OF ENDOGENOUS PLASMA INSULIN IN MAN." Journal of Clinical Investigation **39**(7): 1157-1175.
Yang, E. H., S. S. Yang, S. W. Han and S. Y. Kim (1995). "Fabrication and dynamic testing of electrostatic actuators with p+ silicon diaphragms." Sensors and Actuators A: Physical **50**(1): 151-156.
Yang, T., S. Stavrakis and A. deMello (2017). "A High-Sensitivity, Integrated Absorbance and Fluorescence Detection Scheme for Probing Picoliter-Volume Droplets in Segmented Flows." Analytical Chemistry **89**(23): 12880-12887.
Yates, P. J., W. H. Williams, A. Harris, A. Round and R. Jenkins (2006). "An epidemiological study of head injuries in a UK population attending an emergency department." Journal of Neurology, Neurosurgery, and Psychiatry **77**(5): 699-701.
Yazdi, A. A., A. Popma, W. Wong, T. Nguyen, Y. Pan and J. Xu (2016). "3D printing: an emerging tool for novel microfluidics and lab-on-a-chip applications." Microfluidics and Nanofluidics **20**(3).

Yehuda, R., S. L. Halligan and L. M. Bierer (2002). "Cortisol levels in adult offspring of Holocaust survivors: relation to PTSD symptom severity in the parent and child." Psychoneuroendocrinology **27**(1): 171-180.
Yehuda, R., S. L. Halligan and R. Grossman (2001). "Childhood trauma and risk for PTSD: Relationship to intergenerational effects of trauma, parental PTSD, and cortisol excretion." Development and Psychopathology **13**(3): 733-753.
Yobas, L., S. Martens, W.-L. Ong and N. Ranganathan (2006). "High-performance flow-focusing geometry for spontaneous generation of monodispersed droplets." Lab on a Chip **6**(8): 1073-1079.
Yokoyama, W. M., M. Christensen, G. D. Santos and D. Miller (2001). Production of Monoclonal Antibodies. Current Protocols in Immunology, John Wiley & Sons, Inc.
Yong, Z., M. Shin and T. Wang (2013). "Programmable active droplet generation enabled by integrated pneumatic micropumps." Lab on a Chip **13**(2): 267-273.
Yoo, E.-H. and S.-Y. Lee (2010). "Glucose Biosensors: An Overview of Use in Clinical Practice." Sensors (Basel, Switzerland) **10**(5): 4558-4576.
Yool, A., E. E. Popova and T. R. Anderson (2013). "MEDUSA-2.0: an intermediate complexity biogeochemical model of the marine carbon cycle for climate change and ocean acidification studies." Geosci. Model Dev. **6**(5): 1767-1811.
Yucel, M., A. D. Beaton, M. Dengler, M. C. Mowlem, F. Sohl and S. Sommer (2015). "Nitrate and Nitrite Variability at the Seafloor of an Oxygen Minimum Zone Revealed by a Novel Microfluidic In-Situ Chemical Sensor." Plos One **10**(7).
Zagnoni, M. and J. M. Cooper (2009). "On-chip electrocoalescence of microdroplets as a function of voltage, frequency and droplet size." Lab on a Chip **9**(18): 2652-2658.
Zeng, J. and T. Korsmeyer (2004). "Principles of droplet electrohydrodynamics for lab-on-a-chip." Lab on a Chip **4**(4): 265-277.
Zeng, S., B. Li, X. o. Su, J. Qin and B. Lin (2009). "Microvalve-actuated precise control of individual droplets in microfluidic devices." Lab on a Chip **9**(10): 1340-1343.
Zeng, Y., R. Novak, J. Shuga, M. T. Smith and R. A. Mathies (2010). "High-Performance Single Cell Genetic Analysis Using Microfluidic Emulsion Generator Arrays." Analytical chemistry **82**(8): 3183-3190.
Zhang, J., W. Hodge, C. Hutnick and X. Wang (2011). "Noninvasive Diagnostic Devices for Diabetes through Measuring Tear Glucose." Journal of Diabetes Science and Technology **5**(1): 166-172.
Zhou, C., P. Yue and J. J. Feng (2006). "Formation of simple and compound drops in microfluidic devices." Physics of Fluids **18**(9): 092105.
Zhu, Y. and Q. Fang (2013). "Analytical detection techniques for droplet microfluidics—A review." Analytica Chimica Acta **787**: 24-35.
Zhu, Z., G. Jenkins, W. Zhang, M. Zhang, Z. Guan and C. J. Yang (2012). "Single-molecule emulsion PCR in microfluidic droplets." Analytical and Bioanalytical Chemistry **403**(8): 2127-2143.

Appendices

ROBUST DROPLET GENERATION AND SAMPLING WITH MICRO-PERISTALTIC PUMP AND ANTIPHASE PULSED FLOWS

G. W. H. Evans, A. M. Nightingale, S. Hassan, B. J. Kim and X. Niu
Faculty of Engineering and the Environment, University of Southampton, U.K., SO17 1BJ.

ABSTRACT

This paper reports a robust and field deployable droplet sampling and generation method, and its engineering implementation of a 3D printed and highly integrated push-pull micro-peristaltic pump.

KEYWORDS: Droplet Microfluidics, Droplet Generation, Micropump

INTRODUCTION

Droplet microfluidics has emerged as a powerful engineering tool for biochemical assay and analysis using small sample volumes and high throughput [1]. Generation of droplets is a crucial step in any droplet microfluidics system and is typically achieved by pumping aqueous and oil phases continuously into a T-junction or a flow focusing channel geometry. This paper presents that droplet generation can be achieved with anti-phase pulsed flows using a simple, fully integrated push-pull peristaltic pump. The pump design and fabricated device are shown in Fig. 1A. The pump utilizes an anti-phased pulsed droplet generation regime as shown in Fig. 1C, where spatially arranged rotorhead features pump the aqueous and oil phases into a channel in pulses with phase difference defined by the rotorhead features (Anti-phase). Thereby, the discrete phase (typically aqueous) can be 'chopped' into droplets by the immiscible continuous/carrier phase (typically oil) at a T-junction. The velocity profile shown is taken downstream and so never reaches zero as the pulsations are dampened further from the pump.

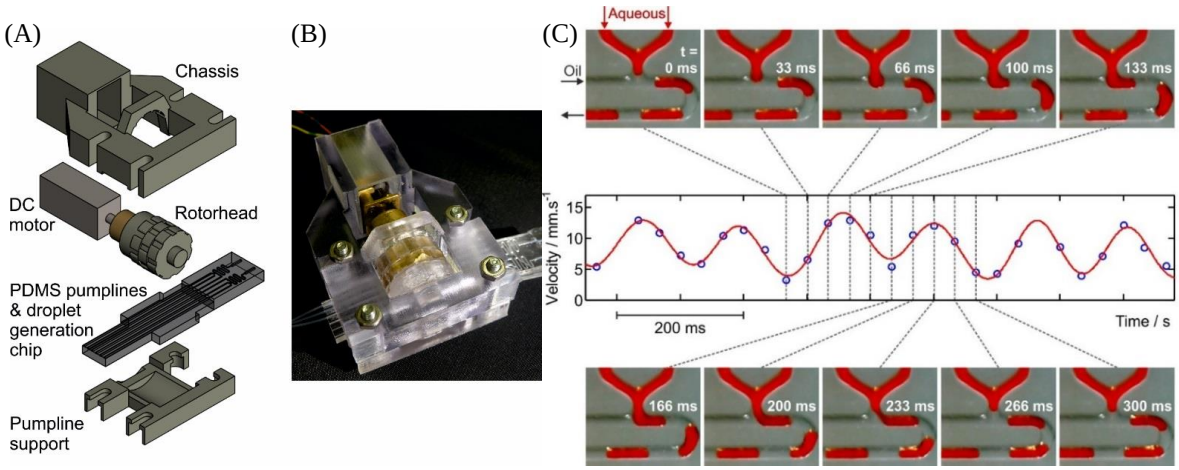

Figure 1: The push-pull peristaltic micropump with integrated microfluidic chip. (A) Exploded schematic of the peristaltic micropump's constituent parts. (B) Photograph of the assembled pump. (C) Pulsed droplet generation regime. Total flow velocity is measured downstream after the T-junction. It shows two distinct peaks in one period of droplet generation due to alternate pumping of the aqueous and oil phases into the T-junction (aqueous t=0-133ms, oil t=166ms-300ms) and the droplet is generated at 266ms.

EXPERIMENTAL

The pump is driven by a single DC motor with a 3D printed (Objet500 Connex3 printer) rotorhead, pumpline support and chassis Fig. 1A&B. A monolithic chip (Fig. 2) was fabricated by soft lithography and sacrificial moulding of PDMS as previously described [2]. Fibre optics are placed inside the 3D printed mould producing raised circular microchannels where channel size corresponds to the outer diameter of the fibre optics. These raised circular microchannels can be easily sealed by the rotorhead of the pump. The droplet generation portion of the chip is produced by a simple PDMS casting procedure where fluidic structures are cast in PDMS from a 3D printed positive mould and then sealed with a layer of half-cured PDMS before being fully cured, similar to previously described methods [3]. These two parts are then joined and further fostered with PDMS to form the monolithic chip.

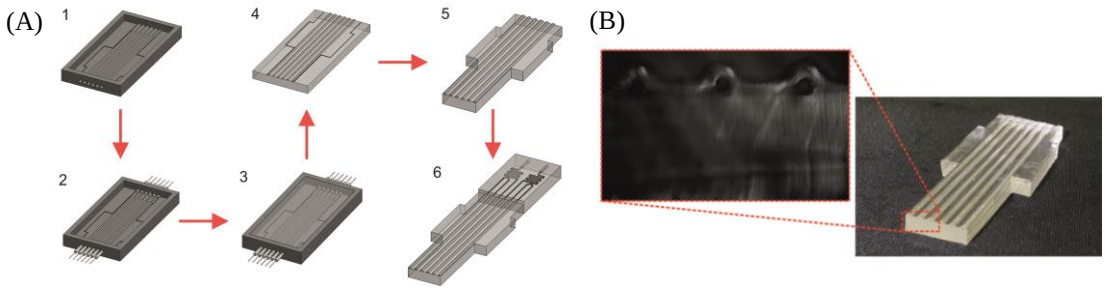

Figure 2. Fabrication flow chart of the monolithic PDMS chip. (A) The process from insertion of sacrificial moulding fibre optics to the 3D printed mould to the bonding of the droplet generation chip (B). Image of the finished PDMS pumplines with cross section.

RESULTS AND DISCUSSION

Once the push-pull peristaltic pump is fully assembled, droplet generation is easily achieved by the rotation of the DC motor and connected rotorhead. In this method, droplet generation rate is defined by the number of features on the rotorhead and the motor speed as shown in Fig. 3A. Droplets generated have a fixed volume reliant on pumping volume (defined by channel size and spacing of the features on the rotorhead) which can easily be designed to suit the desired droplet size as shown in Fig. 3B&C. Importantly, droplet size produced by this pumping regime is not affected by flow conditions (Fig. 3B).

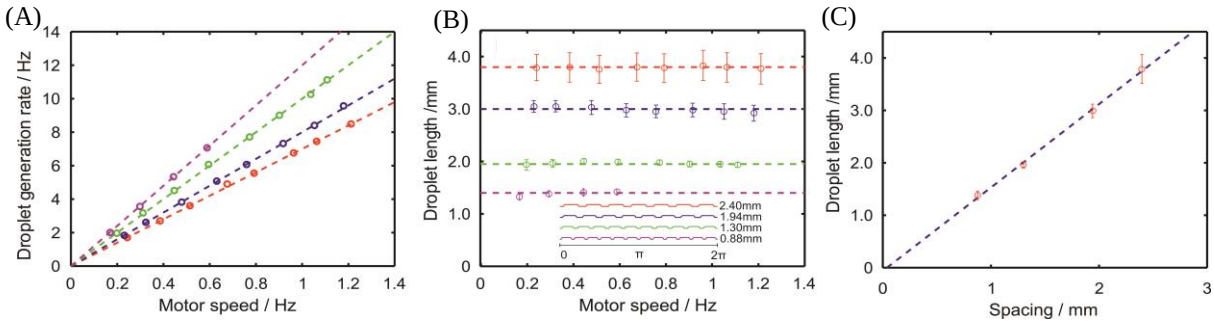

Figure 3. Calibration of the micropump. (Two aqueous channels 245µm diameter and one oil channel 320µm diameter) (A) Droplet generation rate as it relates to motor speed for four rotorheads with differing number of features (B) Droplet length as it relates to motor speed (C) Average droplet length over a number of droplet generation rates as it relates to the spacing on the rotor head.

CONCLUSION

A new miniaturized push-pull pump was designed and tested, which can accurately pump multiple fluid lines and generate droplets with designed and fixed sizes. This system can generate droplets close to the sampling site with reduced Taylor dispersion, no dead volume and no contamination of the sampling site. We envisage this pumping and robust droplet generation method has the potential to be used for the continuous collection of minute liquid samples, performing quantitative and real-time biochemical assays using droplet microfluidics, both in the lab and in point-of-care environments.

ACKNOWLEDGEMENTS

This work was funded by EPSRC grant EP/M012425/1 and IfLS Studentship.

REFERENCES

[1] "Recent Advances in Applications of Droplet Microfluidics" W.L. Chou et al., Micromachines, 2015, 6, 9, 1249-1271

[2] "Multi-channel peristaltic pump for microfluidic applications featuring monolithic PDMS inlay" P. Skafte-Pedersen et al., Lab Chip, 2009, 9, 3003

[3] "Miniaturized tools and devices for bioanalytical applications" M. Chudy et al., Anal. Bioanal. Chem., 2009, 395, 657-668

CONTACT

* Dr. Xize Niu ; phone: +44 (0) 2380592367; Email: X.Niu@soton.ac.uk

GENERATION OF DROPLET SEQUENCES WITH PRE-SPECIFIED COMPOSITIONS USING A "HARDCODED" PERISTALTIC MICROPUMP

A. M. Nightingale, G. W. H. Evans, S. Hassan, B. J. Kim, and X. Niu
Faculty of Engineering and the Environment, University of Southampton, U.K.

ABSTRACT

We report how sequences of droplets with a range of pre-specified compositions can be repeatedly and reproducibly generated using a "hardcoded" 3D-printed peristaltic micropump.

KEYWORDS: Droplets, peristaltic pumping, 3D printing, dilution, titration.

INTRODUCTION

Control of droplet composition is of particular importance in droplet microfluidics, most notably for application in high-throughput assays and screening. Previous methods for generating sequences of droplets with varying composition have focused on either slowly adjusting inlet flow rates over time, [1] or sequential dilution using on-chip trap structures. [2, 3] The former method needs comparably large sample volumes while the latter requires complicated valve control. Our micropump-based method allows for the arbitrary specification of composition within a sequence of droplets by rational design of the pump architecture, and in contrast to previous methods can be performed with minimal (nanolitre) sample volumes and without the need for any extraneous valves or other actuators.

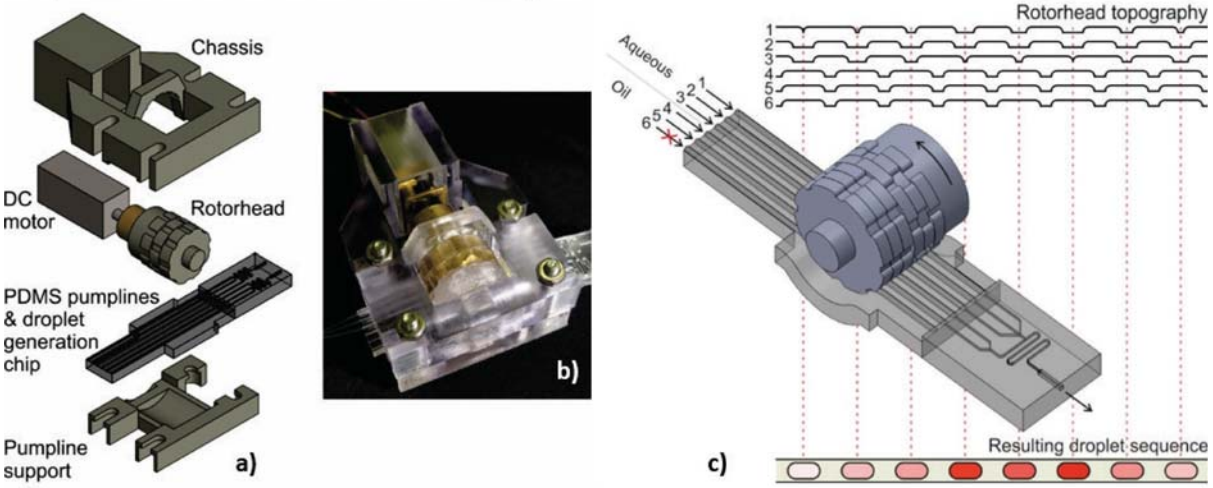

Figure 1: a) A schematic showing the exploded constituent parts of the peristaltic micropump. b) An image of the assembled pump. All parts are 3D-printed except for the DC motor, the PDMS pumplines and adjoining PDMS droplet generation microchip. c) Illustration of a rotorhead with topography suitable for producing sequences of droplets with a range of pre-specified compositions. Shown centre is the rotorhead with a corresponding set of pumplines fed with aqueous (lines 1-3) and oil-based (lines 4-6) fluids. The rotorhead has six different profiles, corresponding to the six pumplines and these are shown top. Shown bottom are the corresponding sequence of droplets that should result if line 1 were fed with a dye solution and the other aqueous lines fed with water.

EXPERIMENTAL

The design of the pump is shown in an exploded schematic in Fig. 1. The supporting structures and the rotorhead (the rotating part that contacts the pumplines to motivate fluid through them) are all 3D printed using an Objet500 Connex3 printer. The pump lines are monolithically molded in PDMS as previously described by Skafte-Pedersen et al. [4]. The exits of the pump lines are immediately connected to a PDMS microchip where droplets are generated at the confluence of aqueous and oil-based fluids at a T-junction. An image of the assembled pump is shown in Fig. 1b). The topography of the rotorhead is crucial to the operation of this system. The rotorhead is composed of six separate profiles, each of which corresponds to a separate fluid line (Fig 1c, top). The aqueous lines (1-3) and the

oil lines (4-6) feature topology that is out-of-phase, meaning the fluids are delivered to the T-junction in phase-separated pulses giving highly robust droplet generation where each feature corresponds to a single segment (oil or droplet) in the resulting flow. Thus by carefully designing the topology of each aqueous profile we can define the final composition of each droplet (Fig 1c, bottom).

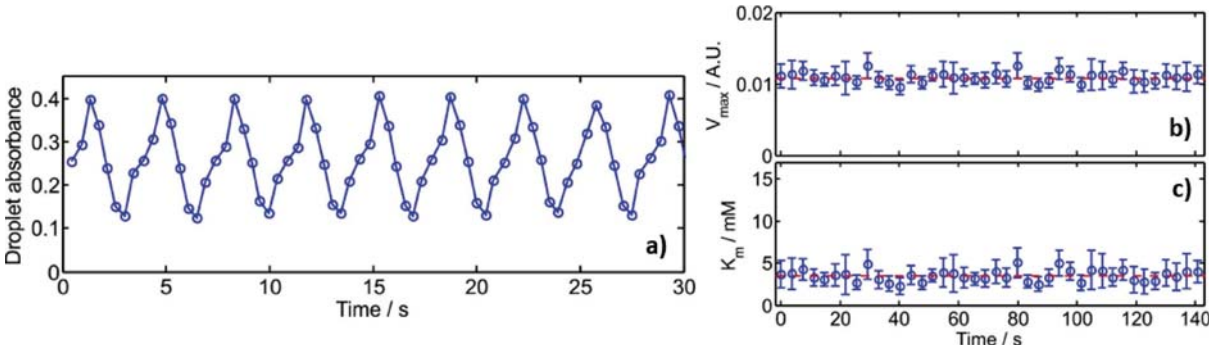

Figure 2: a) The absorbance of sequences of droplets with different concentrations of dye repeatedly generated using the rotor topography shown in Fig 1c). Absorbance was measured using an inline absorbance flow cell downstream of the droplet generation chip. b) Continuous monitoring of the reaction kinetics of an enzymatic reaction. The rotorhead shown in Fig 1c) was used to generate a sequence of droplets composed of a range of glucose concentrations and a constant concentration of Trinder reagent. The progress of the reaction in each droplet was tracked via an inline multidetector absorption flow cell [5] and the results for each sequence of droplets fitted to a Michaelis-Menten model to obtain the kinetic parameters, V_{max} (b) and K_m (c), of the reaction. One pair of K_m and V_{max} values can be obtained from one revolution of the pump.

RESULTS AND DISCUSSION

Successful generation of reproducible repeated sequences of droplets of different concentrations was confirmed using a dye and measuring each droplet downstream using an inline flow cell (Fig. 2a).

As a test application, we used the pump to repeatedly characterise an enzymatic assay. Traditionally, the kinetic parameters of any enzymatic reaction are obtained by laboriously performing the reaction multiple times using different substrate concentrations. Using the hard-coded pump we generated droplets with different substrate concentrations and tracked the reaction in each droplet over time using an inline multidetector absorption flow cell.[5] In this way, we were able to continuously quantify the reaction kinetics (Fig.s 2b and 2c). This high-throughput measurement of the reaction kinetics allows for rapid screening of inhibitors and other important reaction parameters.

CONCLUSION

We have shown how rational design of a peristaltic micropump can deliver highly reproducible repeated sequences of droplets of pre-specified composition. We have demonstrated its utility in continuous measurement of enzyme kinetics, however, we note that the pump should allow rapid execution of any time-consuming dilution- or titration-based assay.

ACKNOWLEDGEMENTS

This research was funded by the EPSRC (EP/M012425/1).

REFERENCES

[1] L. Li et al., “Nanoliter microfluidic hybrid method for simultaneous screening and optimization validated with crystallization of membrane proteins” PNAS, 2006, 103, 51, 19243

[2] X. Niu et al., “A microdroplet dilutor for high-throughput screening” Nat. Chem., 2011, 3, 437

[3] P. M. Korczyk et al., “Microfluidic traps for hard-wired operations on droplets” Lab Chip, 2013, 13, 4096

[4] P. Skafte-Pedersen et al., “Multi-channel peristaltic pump for microfluidic applications featuring monolithic PDMS inlay” Lab Chip, 2009, 9, 3003

[5] S. Hassan et al., “Continuous measurement of enzymatic kinetics in droplet flow for point-of-care monitoring” Analyst, 2016, 141, 3266

CONTACT

* X. Niu; phone: +44 (0) 2380592367; x.niu@southampton.ac.uk

WEARABLE DROPLET-BASED MICROFLUIDIC SENSOR DEVICE FOR CONTINUOUS SAMPLING AND REAL-TIME ANALYSIS

S. Hassan[1], A.M. Nightingale[1], C.L. Leong[1], Y. Zhang[1], G. Evans[1], M.G. Boutelle[2] and X.Z. Niu[1]

[1] Faculty of Engineering and Environment, University of Southampton, UK and
[2] Department of Bioengineering, Imperial College London, UK

ABSTRACT

This paper reports a wearable droplet-microfluidic based continuous chemical sensing device. The device combines microdialysis and droplet microfluidic techniques, can continuously sample from interstitial or other body fluids into nanolitre droplets and perform biochemical assays and measurements in situ and in real-time.

KEYWORDS: Droplet, Wearable, Continuous, Sensor

INTRODUCTION

Continuous measurement of biomolecule/drug concentrations directly from tissue fluid or blood offers the exciting possibility of understanding physiological or pathological processes, recording responses to stimuli and drug metabolism, and even developing new therapies that use biomarker levels to guide treatment in real-time. Microdialysis is a widely used minimal invasive technology, especially in neuroscience, for collecting samples from cerebrospinal fluid, tissue fluids or intravenous blood. Recently, Kennedy's group and others have shown that microdialysis sample (dialysate) can be compartmentalized into droplets with oil [1,2], thereby Taylor dispersion in a long sampling tubing can be avoided, and online derivatization and detection become possible. Here we show a novel push–pull screw-driven micropump that can provide robust and safe microfluidic control, as well as uniform droplet generation and reagent addition. The pump is further integrated with microdialysis probe, home developed optical detector and electronics, forming a self-sustained and wearable microfluidic device for continuous sampling and analysis.

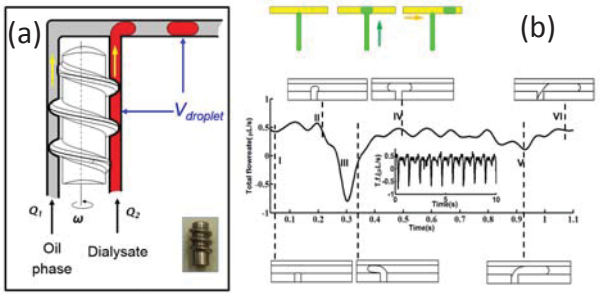

Figure 1: (a) The schematics of the push-pull peristaltic pump and the principle of droplet generation. (b) The detailed calibration on flow rate during droplet generation. The pulsations of the flows facilitate droplet generation (break-up) at the T-junction.

DESIGN AND EXPERIMENT

Fig.1a shows the schematic of the pump design. A homemade metal screw, driven by a DC motor, is used to pump liquids in several tubings surrounding to the screw. The tubings are connected to oil and reagent containers, or microdialysis probe at one end. After pumping, these liquid streams join at a T-junction and droplets are produced there. The screw is a few millimeters long, therefore droplets can be formed very close to the sampling cite (e.g. tissue). This provides minimum Taylor diffusion of samples in the tubing before the compartmentalization. The droplet volume is determined by the pitch of the screw and tubing dimension, not affected by viscosity of the liquid or flow speed. As a biomedical device, the pump was also designed to be safe - as the screw thread effectively prevents back flow, the oil or reagent will not contaminate the sampling cite. The pump head was 3-D printed with PVC tubing installed as pumplines. Droplet generation chip is made of PDMS using standard soft lithography technique.

RESULTS AND DISCUSSION

Fig.1b shows droplet generation and measured flow rate at the T-junction area. Owning to a unique 'chopping' mechanism (anti-phased flows for oil and aqueous), droplet generation in the device is robust. This is clearly shown in Fig. 2a&b, the comparison of droplet generation between the

screw-driven pump and a syringe pumping system. In the former, the total flow rate, droplet size and composition in droplet reached their stable values within sub-seconds once the pump was turned on. While in the syringe pumping system, minutes or longer was required for the flow rate to reach a stabilization. Notably, the composition of droplets in the later shows apparent variations even after 10 minutes. The screw-driven pump was tested to produce droplets from 4 Hz to as slow as one droplet per minute or hour, easily controlled by the rotation of the DC motor. Each pump head could run stably for 2 weeks using standard peristaltic pump tubing (PVC, 0.19mm i.d., Ismatic), with constant droplet generation frequency as shown in Fig 2c.

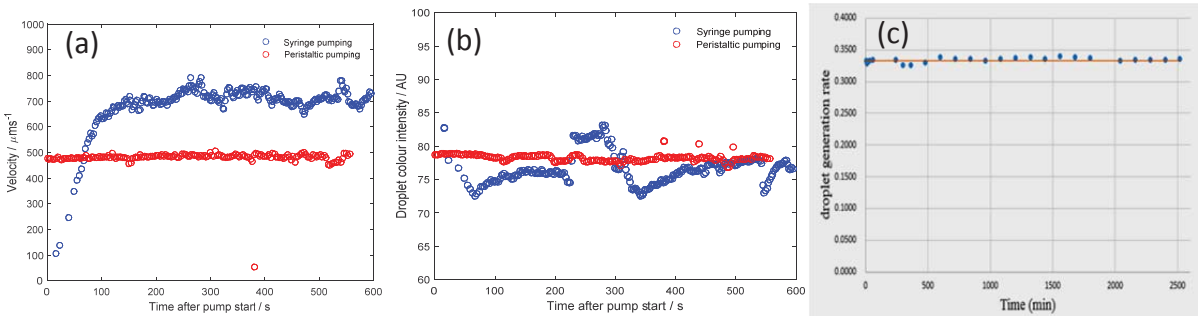

Figure 2: Calibration of droplet generation with the screw-driven pump and its comparison to droplet generation using a syringe pump. (a) Measured total flow velocities after the pump start (b) Concentration of constituent in the droplets generated with the two approaches. (c) Continuous droplet generation from the peristaltic pump (measured by droplets per second) over long-time.

Additional to the pump, the palm sized wearable device (Fig. 3a) is also equipped with an optical sensor array for colorimetric detection of droplets [3], electronic circuit for data acquisition and Bluetooth wireless transmission, SD card and batteries. As an example application, we have tested the sensor in vitro for continuous glucose monitoring at physiological concentrations (Fig.3b) with errors less than 6%, and a sample-to-signal time in less than 2 minutes.

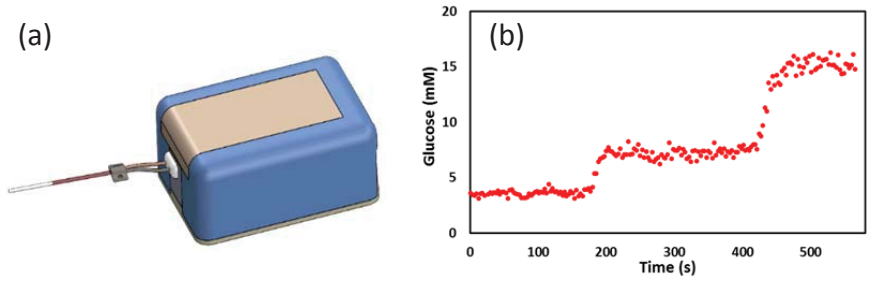

Figure 3 (a)Schematic of the integrated device with a microdialysis probe connected. (b) Glucose concentration in droplets measured via an enzymatic assay [3].

CONCLUSION

A droplet based wearable microfluidic sensor was developed. It differs from the widely studied electrochemical sensors by using droplet microreactors and miniaturization of well-calibrated wet-chemical assays. This technology could find broad applications in disease diagnostics and monitoring, drug development and environmental monitoring.

ACKNOWLEDGEMENTS

This research was funded by the EPSRC (EP/M012425/1).

REFERENCES

[1] Chultz KN, Kennedy RT, Time-resolved microdialysis for in vivo neurochemical measurements and other applications, Annu. Rev. Anal. Chem, 2008, 1, 627–61.

[2] Rogers, M. L., Boutelle, M, G., Clinical Monitoring of Biomolecules. Annu. Rev. Anal. Chem, 2013, 6, 427–53.

[3] Hassan, S., Nightingale, A.M. and Niu, XZ, Analyst, 2016, DOI: 10.1039/C6AN00620E

CONTACT

* Xize Niu; phone: +44 (0) 2380592367; x.niu@soton.ac.uk

Lab on a Chip

PAPER

View Article Online
View Journal | View Issue

Cite this: *Lab Chip*, 2017, **17**, 1149

Phased peristaltic micropumping for continuous sampling and hardcoded droplet generation†

Adrian M. Nightingale,‡[ab] Gareth W. H. Evans,‡[ab] Peixiang Xu,[a] Byung Jae Kim,[a] Sammer-ul Hassan[ab] and Xize Niu*[ab]

Received 3rd December 2016,
Accepted 7th February 2017

DOI: 10.1039/c6lc01479h

rsc.li/loc

Droplet microfluidics has recently emerged as a new engineering tool for biochemical analysis of small sample volumes. Droplet generation is most commonly achieved by introducing aqueous and oil phases into a T-junction or a flow focusing channel geometry. This method produces droplets that are sensitive to changes in flow conditions and fluid composition. Here, we present an alternative approach using a simple peristaltic micropump to deliver the aqueous and oil phases in antiphase pulses resulting in a robust "chopping"-like method of droplet generation. This method offers controllable droplet dynamics, with droplet volumes solely determined by the pump design, and is insensitive to liquid properties and flow rates. Importantly, sequences of droplets with controlled composition can be hardcoded into the pump, allowing chemical operations such as titrations and dilutions to be easily achieved. The push–pull pump is compact and can continuously collect samples, generating droplets close to the sampling site and with short stabilisation time. We envisage that this robust droplet generation method is highly suited for continuous *in situ* sampling and chemical measurement, allowing droplet microfluidics to step out of the lab and into field-deployable applications.

Introduction

The development and uptake of droplet microfluidics, in which sample fluids are broken into – and then manipulated in – a flow of discrete droplets, has seen rapid progress over recent years. This reflects the many advantages offered by droplet flow, including rapid fluid mixing, accurate reaction control and high analytical throughput. Consequently, it has been used to address many wide-ranging challenges in chemistry, biochemistry, microbiology, and medicine.[1–4]

The method by which droplets are generated is fundamentally important to all droplet-based microsystems. As droplets must be produced with tightly pre-defined composition and size distribution, much effort has been expended on studying droplet breakup mechanisms and droplet generation methods. The most common method of droplet generation, so-called "passive" generation, involves flowing two or more streams of immiscible fluids into a microfluidic junction at constant flow rates. As studied by Garstecki *et al.* for T-junction geometry[5] and Weitz and co-workers[6] for flow focusing channels, the formation of droplets in microchannels falls into three distinct regimes: "squeezing", "dripping" and "jetting", each of which has different generation characteristics. The regime is largely determined by the critical capillary number, $C_a = \mu V/\gamma$ (where μ is the viscosity of the dispersed fluid, V is the flow velocity and γ is the interfacial tension determined by the carrier fluid and the dispersed phase). Under typical microfluidic conditions ($C_a < 0.01$), droplets are generated in the squeezing regime and are found to be sensitive to changes in C_a, with droplet sizes shifting in response to changes in the flow rate and interfacial tension.[7] Thus, in addition to the high precision pumping methods necessary for stable flow rates, passive droplet generation requires that fluidic properties should be constant.

To allow droplet generation that can tolerate variable flow conditions, or tune droplet generation dynamics, various "active" approaches have been explored. These either volumetrically control the fluids or control one or more of the three parameters related to C_a. Volumetric control methods such as alternate aspiration of sample and oil,[8] use of slipchips,[9] momentary acoustic pumping[10,11] or parallel chopping[12] offer 'brutal' but robust droplet generation by circumventing the dynamic competition between the viscous and capillary forces of co-flowing fluids. The alternative approach for controlling C_a can be achieved in several ways: by tuning the viscosity *via* local heating using a microheater or laser

[a] *Faculty of Engineering and the Environment, University of Southampton, Southampton, SO17 1BJ UK. E-mail: x.niu@soton.ac.uk*
[b] *Institute for Life Sciences, University of Southampton, Southampton, SO17 1BJ UK*

† Electronic supplementary information (ESI) available: Document with extra experimental data and description of the pump, and three-dimensional models of all 3D-printed pump parts. See DOI: 10.1039/c6lc01479h

‡ These authors contributed equally.

beam,[13–16] tuning the flow rate by using microvalves to change the flow speed or local channel dimensions,[17–21] or tuning the surface tension (most notably in electrowetting on dielectric devices[22–26]). While all active approaches offer robust and tunable droplet generation, they require manual operation or extra pumping, valving or actuation systems. These additional control elements add complexity to the droplet microfluidic system and place additional barriers to its moving out of specialised labs to wider applications – perpetuating the problem of "chip-in-a-lab" microfluidics.

Here, we present a new approach to droplet generation that offers the levels of control and robustness exhibited by active droplet generation methods, but without the need for extraneous equipment as is seen in passive generation. This is achieved by using a miniature peristaltic pump that can deliver the two immiscible phases (*e.g.* oil and aqueous) in anti-phase pulses such that the two phases are pumped into a microfluidic junction alternately. In this way, droplets are produced in a robust manner, with the droplet size determined by the volume delivered in each aqueous pulse and with the generation dynamics insensitive to the total flow rate, viscosity or interfacial tension. Droplet size and composition can be pre-specified in the pump design and, as multiple droplets are produced in a single turn of the motor, droplets can be generated in repeated sequences with the characteristics of each sequence (size and composition) "hardcoded" into the pump. As a proof of principle, we designed and tested a system to perform rapid on-chip dilutions to allow continuous high-throughput measurement of enzymatic kinetics. In addition to the control it offers over droplet generation, the pump allows easy connection between the outer world and the microfluidic chip – enabling quick sampling and rapid subsequent on-demand droplet generation with minimal stabilisation times.

Experimental

Pump fabrication

All components of the pump are shown in Fig. 1 and detailed in the exploded diagram in Fig. S1.† The main pump chassis, rotorhead, pumpline support bed and motor attachment plate were all 3D-printed. Each part was first modelled using CAD software (SolidWorks, Dassault Systemes) and then printed in a "VeroClear" material using an Objet500 Connex3 polyjet printer (Stanford Marsh Ltd). 3D models of the printed part files are included in the ESI† along with additional details on the rotorhead design. A DC motor (Pololu 210:1 Micro Metal Gearmotor) was attached to the chassis *via* the motor attachment plate. The motor was used to drive the rotorhead (16.25 mm in diameter including raised features), which was fixed on a stainless steel square shaft (2 inch length, 3 × 3 mm cross-section, Active Robots Ltd, UK), manually machined at both ends to give a 3 mm circular cross-section to fit the ball bearings (Technobots Ltd, UK). Additionally, a "D" cross-section was machined into one end to enable attachment to the brass shaft coupler (Technobots Ltd, UK) which connected the main shaft to the motor.

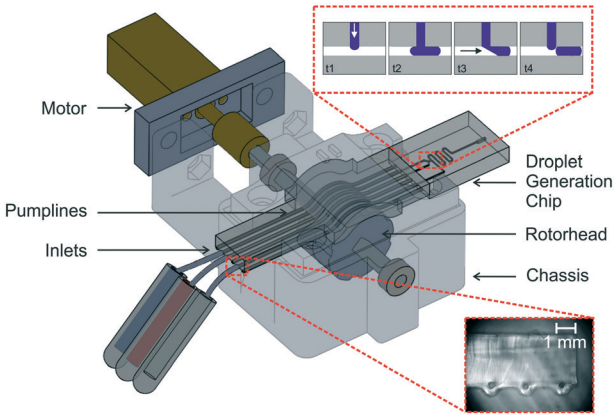

Fig. 1 Schematic showing pump operation. The 3D-printed supporting chassis is shown semi-transparent to highlight the operational parts – motor, axle, rotorhead, PDMS pumpline chip and adjoining droplet generation chip. The top inset shows the method of droplet generation. The bottom inset shows the cross-section of the monolithic pumpline chip.

The PDMS chip which handled all fluids consisted of two parts: the pumplines and a droplet generation chip which were fabricated separately and then joined. The pumplines were monolithically cast as raised structures (see Fig. 1 inset) so that they could be easily and reproducibly deformed by the rotorhead. The procedure is shown schematically in Fig. S2† and is similar to that previously reported by Skafte-Pedersen *et al.*[27] First, a mould was designed using CAD software and 3D-printed in a "VeroClear" material using an Objet500 Connex3 3D printer. The printed mould was dried overnight at 70 °C to drive off any unreacted monomer or solvent and then wiped with a hydrophobic coating (Aquapel, PPG Industries) to ensure easy removal of the PDMS chip after casting. Sacrificial lengths of optic fibres (Thorlabs) were inserted into the 3D-printed mould. These fibres sit within the semi-circular channels at the bottom of the mould to produce the raised channel cross-section as shown in Fig. 1. The outer diameter (OD) of the fibre optics defines the ID of the finished pumpline (typically, a 245 μm diameter fibre was used for aqueous lines and a 320 μm diameter fibre for oil lines). The fibre optics were held in position in the mould using short (~2 mm) lengths of PVC tubing (Gradko International Ltd., 0.5 mm wall, ID chosen depending on the fibre optics used). The use of this soft support around the fibres ensured that they fitted snugly into the mould, leaving no gaps for the PDMS to leak through. Liquid PDMS (Sylgard 184, Farnell Onecall) was poured into the mould and oven-cured at 70 °C overnight. The fibre optics were then removed and the chip was subsequently peeled off from the mould. It was then cut into shapes using guide lines included in the mould. It should be noted that the shape of the PDMS pumpline chip ensured it fitted into a similarly shaped recess in the 3D-printed pumpline support to ensure that the pumplines didn't move during pump operation.

The droplet generation chip was fabricated by standard PDMS casting procedures – moulding in PDMS[28] from a 3D-printed mould and then sealing the channel structure with a layer of half-cured PDMS.[29] The pumpline and droplet generation parts were linked by ~4 mm long PTFE tubing (0.4 mm ID, 0.15 mm wall, Adtech Polymer Engineering Ltd.) and then permanently bonded by sealing the joint with a small amount of liquid PDMS on a hotplate (Fisher Scientific) at 105 °C for approximately 5 minutes. After fabrication, the microfluidic channels were surface-functionalised by manually flowing a small volume of Aquapel followed by flushing with air and drying in an oven at 70 °C for ten minutes in order to render the channels hydrophobic and ensure that the oil phase preferentially wets the channel.

Droplet generation and characterisation

The pump was assembled from its constituent parts. M3 nuts and bolts were used to hold the pump support bed and the motor attachment plate to the chassis. Fluid was brought to the pumplines *via* PTFE tubing (ID 0.3 mm, 0.15 mm wall) inserted into the pumpline channels. The oil used was a low-viscosity fluorocarbon (FC-40, 3M, UK) containing a 1.8% w/w non-ionic tri-block copolymer surfactant synthesised in-house[30] while the aqueous phase varied depending on the experiment. The fluid was pumped by supplying the motor with a constant power supply between 1.5 and 6 V and droplets were generated in the droplet generation chip (channel dimensions: 300 μm width, 450 μm depth). They were then subsequently taken off-chip using PTFE tubing (0.4 mm ID, 0.15 mm wall) inserted into the chip outlet. To characterise the generated droplets, a portable microscope camera (dnt Digimicro Mobile Mikroskop) was used to record either directly at the T-junction of the chip or off-chip within the PTFE tubing. The videos recorded were analysed using Droplet Morphology and Velocimetry (DMV) software[31] and the data were subsequently processed in Matlab. The droplet volume was calculated from the DMV measurements of droplets recorded within tubing of a known cross-sectional area.

Glucose assay

D-Glucose, glucose oxidase (GOx), horseradish peroxidase (HRP), 4-aminoantipyrine (4-AAP) and phenol were purchased from Sigma-Aldrich (Dorset, UK) and used without further purification. Deionised water (18.2 MΩ cm, MilliQ) was used to prepare all the solutions and reagents. 0.1 M phosphate buffered saline (PBS, pH 7.0) was used throughout. The reagent consisted of 6.25 mM 4-AAP, 18.75 mM phenol, 22.5 U mL^{-1} HRP and 45 U mL^{-1} GOx in PBS. The enzymatic reagent was freshly made prior to the experiment and was covered from ambient light. The 15 mM glucose standards were also made using 0.1 M PBS.

Results and discussion

Pump design

The pump is schematically shown in Fig. 1 and as an exploded model and representative image in the ESI† (Fig. S1). Fluid is moved by the interaction of the two main parts – the rotorhead (driven by the motor) and the pumplines. The pumplines are composed of six parallel raised microfluidic channels of circular cross-section (Fig. 1). The rotorhead is composed of a series of raised features which, upon contact with the pump chip, pinch the microfluidic channels so that the fluid can be driven along the channel *via* peristalsis. The rotorhead is 3D-printed, which allows the features on its circumference to be arbitrarily specified depending on the pumping requirements.

As shown in Fig. 1, the pumplines directly adjoin a droplet generation chip based on a T-junction design. The close proximity of the droplet generation chip to the pumplines has two advantages: firstly, any unwanted Taylor dispersion effects from the fluid passing through the pumplines are reduced, meaning that compositions along the generated droplet train will be representative of compositional change over time at the inlet. Secondly, it minimises any smoothing of the pulsatile flow due to compliance of the channel material, an effect which would be detrimental to our proposed approach to droplet generation. The assembled pump is small in size (see the image in Fig. S1†), easily fitting on the palm of the hand, making it suitable for field-deployable analytical monitoring or diagnostic devices.

Characterisation of pumping

The pump's ability to deliver accurate and tunable flow was first determined for individual lines pumping fluid in isolation. The fluid was pumped through pumplines of different diameters (245 μm and 320 μm), at different motor speeds and using different rotorhead designs (varying the spacing between the pronounced features). The instantaneous flow rate was characterised by aspirating the droplets (formed by moving the inlet between fluorous and dyed aqueous fluids), recording their movement downstream and then analysing the video.

As expected for a peristaltic pump, the resulting flow was characteristically pulsatile. In all cases, the flow rate was seen to periodically rise and fall over time (Fig. 2a–c), with each period (peak and trough) corresponding to a single feature on the rotorhead. Fig. 2a and b show data for the flow rate obtained using the same channel diameter (320 μm) and rotorhead spacing (1.7 mm, defined as shown in Fig. 2d inset) but with different motor speeds. As the motor rotation speed doubled from 0.30 Hz (Fig. 2a) to 0.58 Hz (Fig. 2b), the pulse period halved (375 to 175 ms) and both the peak flow rate and the mean flow rate (dashed red line) doubled. It should be noted that in both Fig. 2a and b, the area under each peak (which corresponds to the volume pumped in a single pulse) stayed constant regardless of the motor speed, as each pulse corresponds to the volume in the pumpline

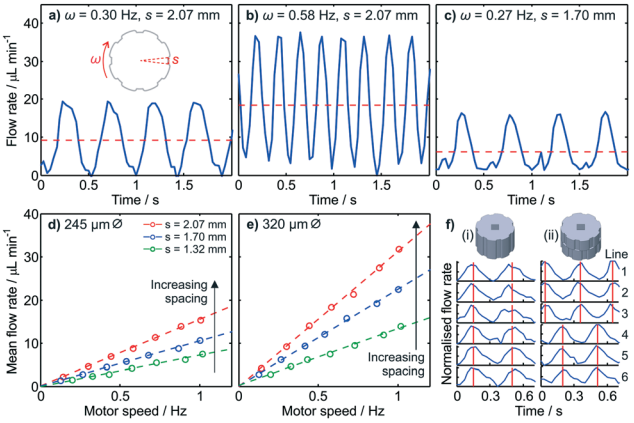

Fig. 2 Characterisation of pumping in individual pumplines. a–c) Volumetric flow rates for differing motor speeds and rotorhead feature spacings. Solid blue lines show transitory flow rates over time while dashed red lines show mean flow rates. d and e) Plots showing how the mean flow rates can be tuned by controlling the feature spacing, motor speed and cross-sectional area. f) Plot showing the relative flow profiles for all six pumplines when using rotorheads with features aligned (i) and features anti-phase offset (ii).

occluded between adjacent features on the pump head. The average flow rate can also be changed by keeping the motor speed constant and changing the volume occluded between features as shown in Fig. 2c, where the space between the features is reduced from 1.70 mm in Fig. 2a to 1.47 mm.

To quantify how the pump could be rationally designed to tune the net flow rate, we measured the flow rate while systematically varying the motor speed for three different rotorhead feature spacings with a constant cross-sectional area, as shown in Fig. 2d. In each case, the pumpline diameter was kept constant at 245 μm. For all rotorheads, increasing the motor speed had the effect of linearly increasing the mean flow rate. The gradient increased with feature spacing due to the increase in the volume delivered in each individual pulse. Fig. 2e further shows that wider channels (diameter 320 μm) allow higher flow rates due to the increased volume delivered in each pulse, with the increase approximately equal to the ratio of the channel cross-sectional areas. Thus, careful design of the pump can tune the flow rate as required, with multiple different design options available (channel cross-section, spacing of the feature, number of spacings and pumping frequency).

The relative position of the rotorhead features for each individual pumpline can determine the relative timing (phase) of pulsing in different pumplines. Fig. 2f shows the flow profiles obtained when using rotorheads with the same topology (*i.e.* the same number and size of features) but with the topology offset around the rotorhead. These rotorheads were used to pump all six pumplines and the resulting downstream flow was analysed simultaneously so as to characterise the phase difference of the pulses. When the features were aligned, as shown in Fig. 2f(i), the obtained flow profiles were in phase. By contrast when the features on the top half of the rotorhead (which comes into contact with lines 1–3) were anti-phase to those on the bottom half (which comes into contact with lines 4–6), the resulting flow profiles in lines 1–3 were in phase, but were exactly anti-phase to those in lines 4–6, as shown in Fig. 2f(ii). The rotorhead can be easily redesigned to deliver any arbitrary phase offset that might be required for each individual line. Importantly, however, the ability to introduce oil and aqueous fluid in alternating pulses into a junction enables robust droplet generation.

Droplet generation using anti-phased oil/aqueous pulses

As shown in the images in Fig. 3, two aqueous streams were merged at a Y-shaped junction and then segmented into droplets by the oil at a T-junction. The relative cross-sectional areas of the pumplines (245 μm ID for aqueous pumplines and 320 μm ID for oil pumplines) gave approximately equal volumetric flows of the different phases, while the spacing between features on the rotorhead was deliberately offset, as shown in Fig. 2f(ii), so that the oil and aqueous flows were delivered in anti-phase pulses to the T-junction where the droplets were produced. The droplet velocity measured after the first bend of the channel shows clear periodicity against time. Each period is composed of two flow pulses as labelled with red and blue dashed lines. A comparison of the video and flow velocity shows that the incursion of the red aqueous stream into the main channel (top images) gave rise to the pulse labelled with red dashed lines, while the following velocity peak (blue dashed lines) corresponds to the oil stream pushing the aqueous incursion downstream (bottom images), breaking it from the main aqueous stream to form a discrete droplet which is then carried downstream. In brief, each droplet was produced firstly by incursion of the aqueous stream into the main channel and then 'chopping' of the aqueous incursion into droplets by the pulse from the oil stream.

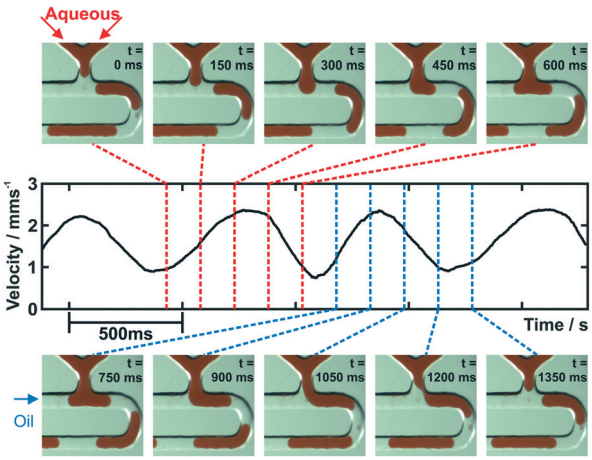

Fig. 3 Correlation of optical images of droplet generation at the T-junction with downstream flow velocity. Incursion of the aqueous phase into the main channel (top images) is associated with a single velocity pulse peak, while its subsequent break-up by the oil flow (bottom images) is associated with the following velocity peak.

This method for droplet generation implies that the volume of each droplet should be solely defined by the volume injected by the corresponding aqueous pulse. To test this, we designed a series of rotorheads where the spacing between features (defined in Fig. 2d inset) was systematically varied, hence varying the volume delivered in each pulse (see Fig. 4). For all rotorhead designs, the droplet generation rate increased linearly with motor speed (Fig. 4a), indicating that each pulse period universally generated a single droplet. A maximum generation rate of approximately 12 Hz was obtained here, however higher rates could be obtained by using rotorheads with more features, a more powerful motor or splitting the droplets downstream.[32]

The droplet size remained constant irrespective of the motor speed (and hence the total flow rate) and droplet generation rate, as shown in Fig. 4b, with a larger rotorhead spacing producing larger droplets (Fig. 4c). The coefficient of variation of droplet volume was between 2 and 5% (as indicated by the error bars in Fig. 4b and c) which compares favourably with those for previously reported droplet generation methods.[33–35] The droplet size was also invariant with aqueous viscosity (see Fig. S3†), which means that the system can be used in the analysis of more viscous biological fluids (*e.g.* blood serum and whole blood), or dealing with liquid samples with varied viscosities over time.

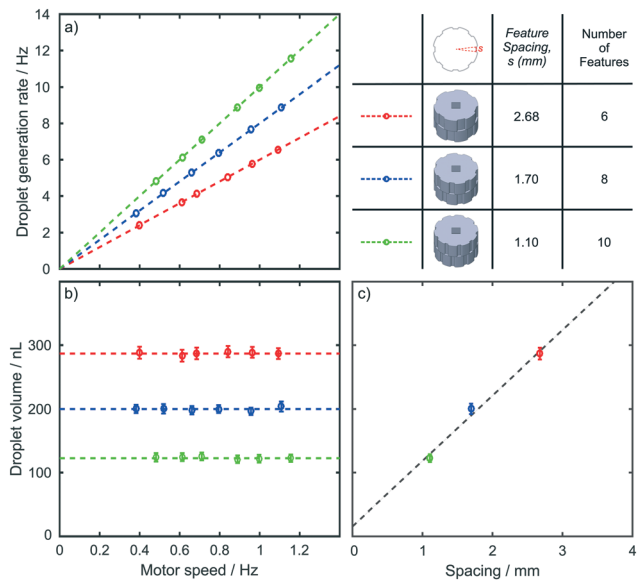

Fig. 4 Droplet generation dynamics for rotorheads with different feature spacings. a) The droplet generation rate increases linearly with motor speed, with the gradient corresponding to the number of features on the rotorhead. b) Droplet volume corresponding to each feature spacing remains constant irrespective of motor speed. Error bars show the standard deviation of droplet volume, typically between 2 and 5%. c) Droplet volume increases linearly with feature spacing. Error bars represent the total standard deviation of droplet volume over different motor speeds.

Comparison of droplet generation with passive generation

Compared with traditional co-flowing droplet generation using syringe pumps, the anti-phase pulsed approach described here offers continuous operation (with no need to stop or refill) within a much smaller total package. More importantly, the short distance and small fluidic volume from the rotorhead to the droplet generation point (approximately 1 cm and 2 μL) mean that the system should achieve stabilised droplet generation much faster than syringe pumping.

To compare the difference in droplet generation dynamics, droplets were first generated using two syringe pumps (PHD 2000, Harvard Apparatus, with 1 mL BD plastic syringes used) pumping fluorous oil and red food dye solution into the same droplet generation chip. The velocity and size of the droplets were measured downstream and then compared to those of droplets generated using the peristaltic pump under the same total flow rate and oil-to-aqueous phase ratio (0.85). At a total flow rate of 80 μL min^{-1}, the syringe pumps took approximately 60 seconds to come up to pressure and deliver a stable flow as shown in Fig. 5a and b. The size of the droplets varied from approximately 60 to 120 nL before stabilising at 71.0 nL. By contrast, the peristaltic pump delivered stable droplet generation from the first droplet produced (in less than 0.5 seconds), also indicating that the pump could be operated in a stop/start fashion or for droplet generation-on-demand applications.

For lower total flow rates of 40 and 20 μL min^{-1}, the stabilisation time required for the syringe pump improved (to a minimum of 25 s at 20 μL min^{-1}, see Fig. 5c) but was consistently much worse than that for the peristaltic device which generated droplets with negligible stabilisation time. Comparing the size of the droplets once stabilised (Fig. 5d),

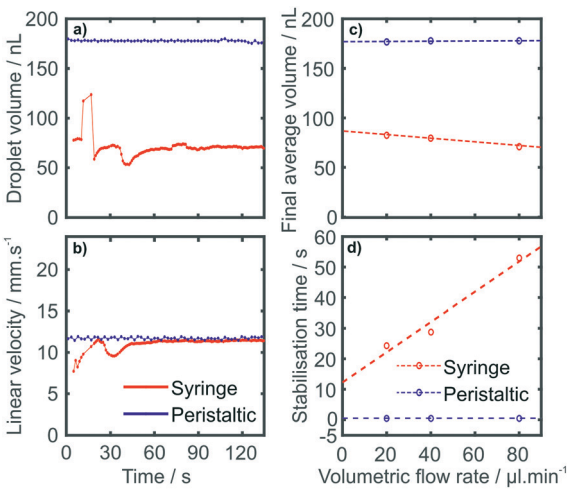

Fig. 5 Comparison of droplet generation *via* anti-phased peristalsis (blue) and syringe-pumped traditional passive co-flow (red). a and b) The variation of droplet volume (a) and droplet linear velocity (b) as a function of time following pump startup is shown. c and d) The time taken for the flow to stabilise and the stabilised droplet volume are recorded respectively as a function of the total volumetric flow rate.

it is notable that the syringe pumps produced droplets 14% smaller at 80 compared to 20 μL min^{-1} (71.0 *versus* 82.5 nL). In contrast, the peristaltic pump gave droplets of equivalent size regardless of the total flow rate – consistent with our previous observation that the droplet size is determined by the physical design of the pump and is independent of the total flow rate (Fig. 4).

"Hard-coding" chemical operations – rapid titrations

In all the experiments described thus far, we used a rotorhead topology comprising multiple identical features around the rotorhead circumference. However, each feature could be designed independently such that they each introduce a different volume of liquid. Thus, if so desired, a single turn of the rotorhead could deliver a sequence of droplets with a range of arbitrarily predetermined sizes, spacings and/or compositions. This ability to automatically generate an array of droplets with different pre-specified properties in a single turn of the rotorhead could be useful in changing the reaction conditions, for example screening reaction[36] or crystallisation conditions,[37] studying mass transfer[38] or performing routine dilutions[39,40] or titrations.[41]

As a proof-of-principle, we designed a rotorhead that generated a dilution series in each turn to allow rapid and continuous measurement of enzyme reaction kinetics. The kinetics of enzyme-based reactions are dependent on the concentration of the substrate (the starting molecule converted by the enzyme), as described by the Michaelis–Menten law, $v_0 = v_{max}[S]/(K_m + [S])$, where v_0 is the initial reaction rate, $[S]$ is the concentration of the substrate, v_{max} is the maximum possible rate (when $[S]$ is in large excess) and K_m is the Michaelis constant representing the value of $[S]$ at which $v_0 = \frac{1}{2} v_{max}$.[42] The values of v_{max} and K_m define the kinetics of the reaction and in benchtop testing are usually determined by running the reaction multiple times, varying $[S]$ in each test and measuring v_0. The measured values of v_0 are then plotted against $[S]$ and fitted with a Michaelis–Menten curve to obtain the values of v_{max} and K_m. As this involves accurate execution and analysis of multiple separate experiments, it can be a time-consuming process – even more so if additional reaction parameters such as temperature or the presence of molecular inhibitors need to be tested.

To continuously measure the Michaelis–Menten kinetics of an enzyme-based assay, we designed the rotorhead and droplet generation chip that could generate a sequence of droplets of constant size but varying composition (see Fig. 6). The chip featured three aqueous inlets which met at a single junction and were then introduced into the oil stream. The three aqueous lines supplied the substrate (line 1), the reagent (line 2) and an additional stream of buffer (line 3). The sizes of the rotorhead features driving the substrate and buffer varied in opposition to each other, ensuring that the volume of the droplets (and thus the final concentration of the reagent) remained constant and producing a sequence of 8 droplets with varied substrate

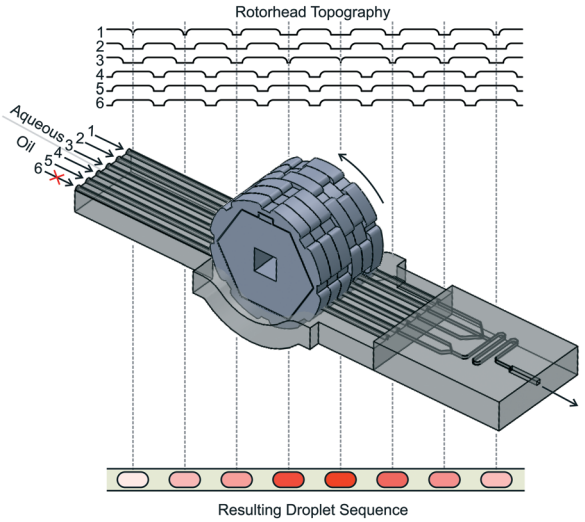

Fig. 6 Schematic of the roller and chip for creating a dilution series of droplets pre-specified by the pumphead design. The topography of the rotorhead's circumference is shown at the top and demonstrates how the aqueous lines (1–3) and oil lines (4–6) are anti-phase, and how lines 1 and 3 vary in opposition to each other to maintain a constant droplet volume. The droplet sequence corresponding to the rotorhead topography is shown at the bottom and qualitatively shows the colour range expected if red dye was supplied to line 1 and water to lines 2 and 3.

concentrations. This droplet sequence was measured downstream using absorption flow cells[43] which could optically measure the progress of the reaction and hence the reaction rates (shown in Fig. S4†).

The system was firstly calibrated to quantify the range and reproducibility of the droplet composition in each sequence by substituting the substrate for a food dye solution. As each droplet passed through the absorption flow cell, it produced a characteristic dip in the signal (Fig. 7a), with the consistent width of each dip indicating a uniform droplet size (confirmed *via* a separate video analysis of the droplet flow, which gave a 4% relative standard deviation). By comparison to a series of blank droplets (obtained by later replacing the dye with water), the light intensity transmitted through each

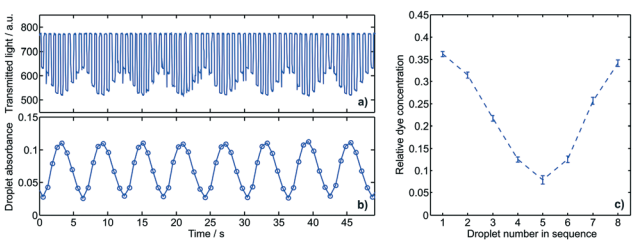

Fig. 7 Calibration of dilution series produced using the "hard-coded" rotorhead and dye. a) Raw signal from the inline absorption flow cell showing characteristic square-wave-like traces as droplets of different compositions pass through the light path. b) Absorbance of the droplets passing through the flow cell against time, calculated from the raw data in (a). c) Mean droplet composition within the dilution sequence, shown relative to the undiluted dye. Error bars show the standard deviation of multiple sequences (n = 12).

droplet could be converted to an absorbance value, as shown in Fig. 7b. The periodic nature of the responses clearly indicates that the system generated droplets with a highly reproducible range of dye concentrations. Fig. 7c shows that the dye content within the droplets varied by a factor of 4.6 (0.079–0.362 relative dye concentration). It is interesting to note that the relative spacings on the rotorhead should theoretically produce relative dye concentrations ranging from 0 to 0.5. The reduced range recorded here is likely due to "carry-over" in the short channel in between the confluence of the aqueous streams and the T-junction where they are broken into droplets. Larger concentration ranges should be possible by minimising the volume in this channel and the interfacial area between the two streams.

Following calibration with food dye, the system was then used to quantify the kinetics of the Trinder assay – a colorimetric glucose assay that uses a reagent based on glucose oxidase.[44] A 15 mM solution of glucose in 0.1 M PBS was supplied to line 1, a premixed reagent (see Experimental for the formulation) was supplied to line 2 and PBS to line 3, while fluorous oil was pumped through lines 4 and 5. Repeated sequences of droplets were generated with glucose concentrations ranging from 1.18 mM to 5.44 mM (as calculated from the calibration data). The absorbance is a direct measure of the assay product, hence the rate of absorbance increase gives the reaction rate (as shown in Fig. S5†). In Fig. 8a, the reaction rates for a single sequence of droplets are plotted against glucose concentration, and fitted with a Michaelis–Menten curve using non-linear regression (R^2 = 0.98), indicating that the reaction followed standard Michaelis–Menten enzyme kinetics, as expected. The K_m value was obtained from the fit, yielding a value of 5.9 mM which is in good agreement with previously reported values (7.63 ± 2.22 mM, 6.47 ± 0.85 mM)[45] for the same assay under the same reaction conditions (pH, temperature).

It should be noted that the Michaelis–Menten curve shown in Fig. 8a was obtained in the time taken to generate a single sequence of droplets (one turn of the motor) and flow them through the multi-detector flow cell, which is less than 60 seconds in total. By contrast, if these values were obtained using standard laboratory procedures, they would involve multiple manual experiments and take a much longer time.

Moreover, as the pump turns continuously and no manual operation is required, it is possible to continuously monitor the kinetics. Fig. 8b shows a sequence of Michaelis–Menten plots (like that shown in Fig. 8a) obtained by continuously generating and measuring sequences of droplets over 6 minutes. K_m values were obtained from each droplet sequence, to allow continuous measurement over the full 6 minutes as shown in Fig. 8c. Continuous measurement such as this would be impossible in bulk experimentation and allows the quantification of reaction kinetics in real time, which could be used to explore the effect of perturbations such as variations in temperature[46] or continuous monitoring of inhibiting species[47] in real time.

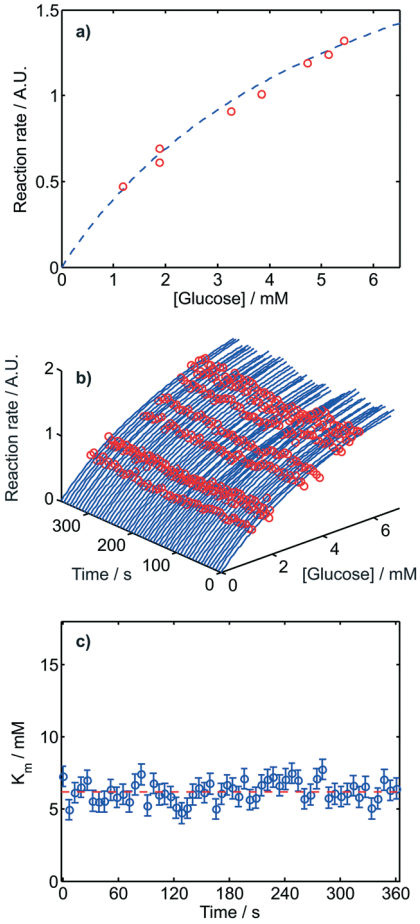

Fig. 8 Continuous analysis of glucose (Trinder) assay kinetics. a) Reaction rates for the different concentrations of glucose produced within a single dilution sequence. The data is fitted with a curve described by the Michaelis–Menten equation. b) Reaction rate measurement and the corresponding Michaelis–Menten fits continuously obtained over a 6 minute period. c) Derived K_m values obtained from the fits shown in (b).

Conclusions

We have demonstrated a new method for droplet generation that produces droplets with robust tunable droplet size and composition, with negligible ramp-up time, and without having to resort to extraneous and bulky actuation systems typically found in active droplet generation methods. Our method exploits the pulsatile flow generated by peristaltic pumping to deliver oil and aqueous fluid to a droplet generation junction. Each aqueous pulse delivers a discrete volume of fluid into the main channel which is subsequently broken into droplets by the ensuing oil pulse. The droplet size and composition are solely defined by the volume delivered in each aqueous pulse and are insensitive to the total flow rate and fluid viscosity, therefore the droplet can be specified by rational design of the pump. By careful control of the contours of the pump rotorhead, sequences of droplets with a range of pre-specified compositions or sizes can be generated, as demonstrated here to generate a dilution series to

continuously measure the reaction kinetics of an enzymatic assay. Moreover, as the pump can drive many channels of fluids and support droplet generation in parallel, it allows complex operations such as multiple sample analysis and multi-step droplet operations (*e.g.* multiple step reactions). While we note that the maximum droplet generation frequency is limited to a few Hz, much less than the kHz achievable with traditional co-flowing passive droplet generation,[48] the droplets could be further divided into daughter droplets *via* splitting junctions if required.[32] Finally, we note that the robustness, simplicity, fast stabilisation and compact nature of our system make it perfect for use in field-deployable devices, for both single time and continuous measurement or monitoring.

Acknowledgements

This work was supported by the Engineering and Physical Sciences Research Council, UK (Grant EP/M012425/1).

References

1 H. Song, D. L. Chen and R. F. Ismagilov, *Angew. Chem., Int. Ed.*, 2006, **45**, 7336–7356.
2 Y. Zhang and H.-R. Jiang, *Anal. Chim. Acta*, 2016, **914**, 7–16.
3 W.-L. Chou, P.-Y. Lee, C.-L. Yang, W.-Y. Huang and Y.-S. Lin, *Micromachines*, 2015, **6**, 1249.
4 N. Shembekar, C. Chaipan, R. Utharala and C. A. Merten, *Lab Chip*, 2016, **16**, 1314–1331.
5 P. Garstecki, M. J. Fuerstman, H. A. Stone and G. M. Whitesides, *Lab Chip*, 2006, **6**, 437–446.
6 A. S. Utada, A. Fernandez-Nieves, H. A. Stone and D. A. Weitz, *Phys. Rev. Lett.*, 2007, **99**, 094502.
7 S. L. Anna, *Annu. Rev. Fluid Mech.*, 2016, **48**, 285–309.
8 F. Gielen, L. van Vliet, B. T. Koprowski, S. R. A. Devenish, M. Fischlechner, J. B. Edel, X. Niu, A. J. deMello and F. Hollfelder, *Anal. Chem.*, 2013, **85**, 4761–4769.
9 W. Du, L. Li, K. P. Nichols and R. Ismagilov, *Lab Chip*, 2009, **9**, 2286–2292.
10 D. J. Collins, T. Alan, K. Helmerson and A. Neild, *Lab Chip*, 2013, **13**, 3225–3231.
11 L. Schmid and T. Franke, *Appl. Phys. Lett.*, 2014, **104**(13), 133501.
12 R. M. Lorenz, G. S. Fiorini, G. D. M. Jeffries, D. S. W. Lim, M. He and D. T. Chiu, *Anal. Chim. Acta*, 2008, **630**, 124–130.
13 N.-T. Nguyen, T.-H. Ting, Y.-F. Yap, T.-N. Wong, J. C.-K. Chai, W.-L. Ong, J. Zhou, S.-H. Tan and L. Yobas, *Appl. Phys. Lett.*, 2007, **91**, 084102.
14 S.-H. Tan, S. M. S. Murshed, N. Nam-Trung, W. Teck Neng and Y. Levent, *J. Phys. D: Appl. Phys.*, 2008, **41**, 165501.
15 C. A. Stan, S. K. Y. Tang and G. M. Whitesides, *Anal. Chem.*, 2009, **81**, 2399–2402.
16 S.-Y. Park, T.-H. Wu, Y. Chen, M. A. Teitell and P.-Y. Chiou, *Lab Chip*, 2011, **11**, 1010–1012.
17 B. C. Lin and Y. C. Su, *J. Micromech. Microeng.*, 2008, **18**, 115005.
18 S. Zeng, B. Li, X. O. Su, J. Qin and B. Lin, *Lab Chip*, 2009, **9**, 1340–1343.
19 W. Lee, L. M. Walker and S. L. Anna, *Phys. Fluids*, 2009, **21**, 032103.
20 K. Leung, H. Zahn, T. Leaver, K. M. Konwar, N. W. Hanson, A. P. Pagé, C.-C. Lo, P. S. Chain, S. J. Hallam and C. L. Hansen, *Proc. Natl. Acad. Sci. U. S. A.*, 2012, **109**, 7665–7670.
21 J. Xu and D. Attinger, *J. Micromech. Microeng.*, 2008, **18**, 065020.
22 A. Pit, M. Duits and F. Mugele, *Micromachines*, 2015, **6**, 1768–1793.
23 T. B. Jones, *Langmuir*, 2002, **18**, 4437–4443.
24 J. Zeng and T. Korsmeyer, *Lab Chip*, 2004, **4**, 265–277.
25 J. Lee and C. J. Kim, *J. Microelectromech. Syst.*, 2000, **9**, 171–180.
26 H. Moon, S. K. Cho, R. L. Garrell and C.-J. C. Kim, *J. Appl. Phys.*, 2002, **92**, 4080–4087.
27 P. Skafte-Pedersen, D. Sabourin, M. Dufva and D. Snakenborg, *Lab Chip*, 2009, **9**, 3003–3006.
28 J. C. McDonald and G. M. Whitesides, *Acc. Chem. Res.*, 2002, **35**, 491–499.
29 M. A. Unger, H.-P. Chou, T. Thorsen, A. Scherer and S. R. Quake, *Science*, 2000, **288**, 113–116.
30 V. Chokkalingam, J. Tel, F. Wimmers, X. Liu, S. Semenov, J. Thiele, C. G. Figdor and W. T. Huck, *Lab Chip*, 2013, **13**, 4740–4744.
31 A. S. Basu, *Lab Chip*, 2013, **13**, 1892–1901.
32 D. R. Link, S. L. Anna, D. A. Weitz and H. A. Stone, *Phys. Rev. Lett.*, 2004, **92**, 054503.
33 S. Y. Jung, S. T. Retterer and C. P. Collier, *Lab Chip*, 2010, **10**, 2688–2694.
34 A. R. Abate, M. Kutsovsky, S. Seiffert, M. Windbergs, L. F. V. Pinto, A. Rotem, A. S. Utada and D. A. Weitz, *Adv. Mater.*, 2011, **23**, 1757–1760.
35 S. H. Tan, S. M. S. Murshed, N. T. Nguyen, T. N. Wong and L. Yobas, *J. Phys. D: Appl. Phys.*, 2008, **41**, 165501.
36 K. Churski, P. Korczyk and P. Garstecki, *Lab Chip*, 2010, **10**, 816–818.
37 L. Li and R. F. Ismagilov, *Annu. Rev. Biophys.*, 2010, **39**, 139–158.
38 Y. Bai, X. He, D. Liu, S. N. Patil, D. Bratton, A. Huebner, F. Hollfelder, C. Abell and W. T. S. Huck, *Lab Chip*, 2010, **10**, 1281–1285.
39 X. Niu, F. Gielen, J. B. Edel and A. J. deMello, *Nat. Chem.*, 2011, **3**, 437–442.
40 R. Thakur, A. M. Amin and S. Wereley, *Analyst*, 2015, **140**, 5855–5859.
41 K. Kawai, M. Fujii and S. Shoji, *Pricise Titration Microfluidic System using Sub-Picoliter Droplet Injection*, 2009.
42 J. M. Berg, J. L. Tymoczko and L. Stryer, in *Biochemistry*, W. H. Freeman & Co Ltd, New York, 5th edn., 2002.
43 S. Hassan, A. M. Nightingale and X. Niu, *Analyst*, 2016, **141**, 3266–3273.
44 P. Trinder, *Ann. Clin. Biochem.*, 1969, **6**, 24–27.

45 K. Karmali, A. Karmali, A. Teixeira and M. J. M. Curto, *Anal. Biochem.*, 2004, **333**, 320–327.
46 M. E. Peterson, R. M. Daniel, M. J. Danson and R. Eisenthal, *Biochem. J.*, 2007, **402**, 331–337.
47 S. Nakamura and Y. Ogura, *J. Biochem.*, 1968, **64**, 439–447.
48 D. Bardin, M. R. Kendall, P. A. Dayton and A. P. Lee, *Biomicrofluidics*, 2013, **7**, 034112.

GENERATION OF "DROPLET TRAINS" FOR CONTINUOUS AND MULTIPLE SAMPLE OR MULTIPLE STEP ASSAYS IN DROPLET MICROFLUIDICS

Gareth W.H. Evans, Adrian M. Nightingale, Sammer-Ul Hassan and Xize Niu*

Faculty of Engineering and the Environment, University of Southampton, Southampton, U.K. SO17 1BJ

ABSTRACT

This paper showcases a hand-held all-in-one integrated device for continuous generation and optical detection/analysis of droplet 'trains' containing up to four different sample/reagent droplets in each train. Combined with an ability to collect one or more samples directly from a sampling site (e.g. bodily fluids), this means the device is capable of performing multiplexed or multiple step assays continuously at the point-of-care.

KEYWORDS: Droplet Microfluidics, Droplet Generation, Micropump

INTRODUCTION

Droplet microfluidics has proven to be a powerful tool for biochemical analysis, offering high throughput with small sample volumes [1]. While it is relatively easy to perform 'mix-and-read' assays in droplets, multiplexed or multiple step reactions have proven more challenging, especially those requiring washing steps including immunoassays such as ELISA (Enzyme linked immune-sorbent assay). To address this issue Ferraro *et al*. have demonstrated generation of droplet trains and moving of magnetic particles between the droplets with magnetic tweezers. This has introduced huge potential for miniaturizing many of the 'gold standard' ELISA assays into droplet microfluidic platforms [2]. However, their approach to droplet generation relies on large instrumentation and complex operation of pumps and valves. Here we present a robust method for continuous generation of droplet trains with pre-specified arbitrary composition in each droplet and no cross talk between the droplets.

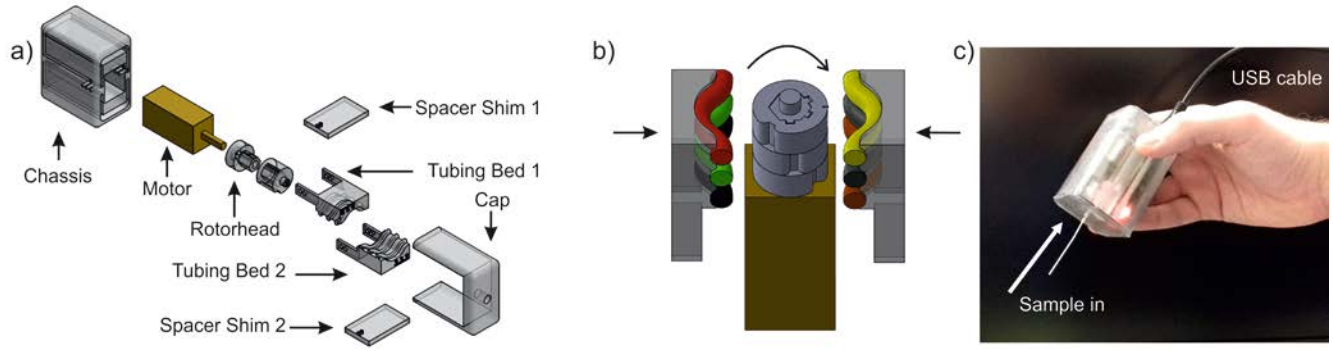

*Figure 1: a) Exploded Schematic of the micropump used in the device b) Schematic showing rotorhead used to generate a four-droplet train in each motor revolution c) Image of the integrated device comprising fluidic conduits, liquid cartridge, optics and electronics (Total footprint 6cm*4cm*4cm).*

EXPERIMENTAL

The method is based on a micro-peristaltic pump for robust sampling and droplet generation, reported by our group earlier this year, which uses temporally-distinct pulses of oil/aqueous phases for robust droplet generation. [3] The fluid pulses originate from a 3D-printed pump shown in Fig. 1a. The rotorhead of the pump (Fig 1b) is designed to deliver fluids in six separate pulses to an attached PDMS droplet generation chip. In the chip six parallel T-Junction tributaries (four aqueous and two oil) feed into a shared main channel (Fig. 2a). The pump, microfluidic chip, optical flow cell and accompanying electronics required for continuous monitoring of chemistry can fit in a single handheld unit (Fig 1c).

RESULTS AND DISCUSSION

The micro-peristaltic pump produces one droplet train per revolution of the rotorhead. The four droplets in the train exhibit no cross-talk in droplet composition, with the aqueous tributary streams never contacting generated droplets. Variation of droplet volume is consistently low approximately 2 % relative standard deviation across the entire droplet population as shown in Fig. 2d.

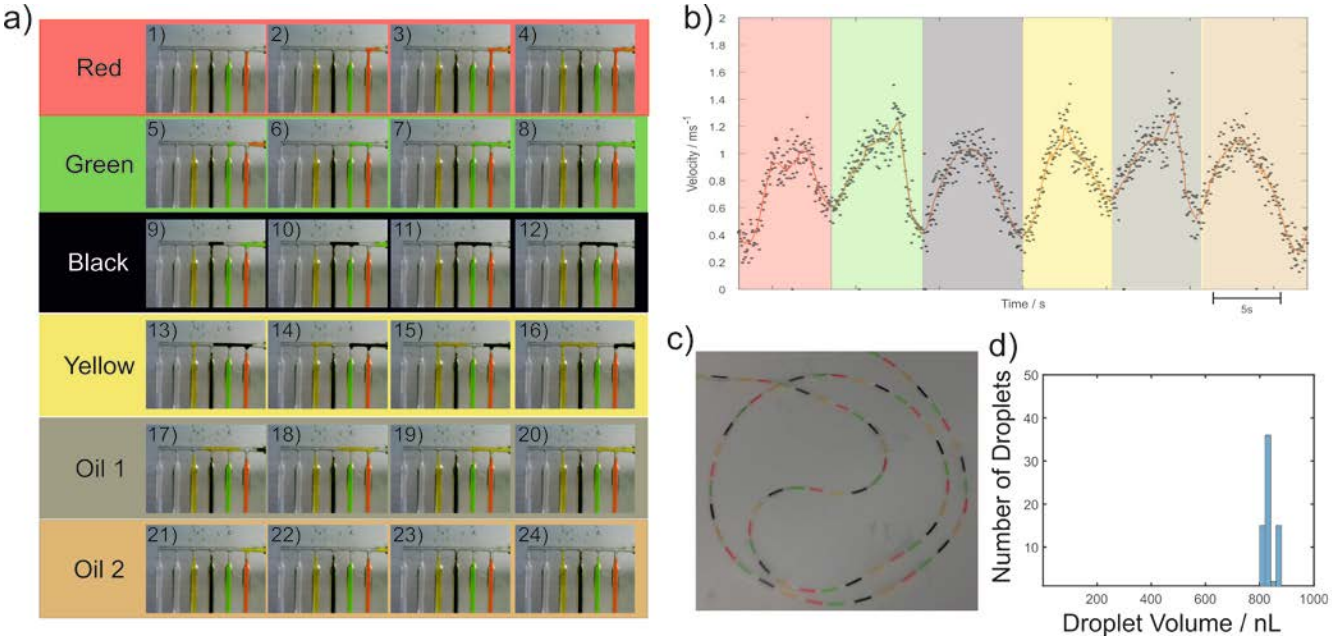

Figure 2: a) Generation of a single 4-droplet train in a single turn of the pump motor. b) The total flow velocity, measured downstream of the droplet generation chip, during a single turn of the pump motor. Six distinct peaks are seen in one due to the incursion of the four aqueous and two oil pulses. c) Image of the continuously generated droplet trains with zero cross talk d) 2% Relative standard deviation across the entire droplet population (mean volume 834nL).

The device can run for multiple days with low power consumption (0.05W) with negligible drift in droplet dynamics (size, speed, composition *etc*.). In the device, we have also integrated an optical flow cell [4] for absorption detection of the droplets and electronics for data logging. The complete sensor device has a total footprint of 6cm*4cm*4cm and supports microUSB or Bluetooth data transmission.

CONCLUSION

This method of droplet train generation shows potential for carrying out multiplexed and multi-step assays continuously and at the point of care. This method can be integrated with technologies such as magnetic tweezers into the all in one device for the continuous measurement of low concentration protein biomarkers that can change rapidly and over prolonged periods of time.

ACKNOWLEDGEMENTS

This work was funded by EPSRC EP/M012425/1 and a University of Southampton Institute for Life Sciences studentship.

REFERENCES

[1] "Recent Advances in Applications of Droplet Microfluidics" WL.Chou et al., *Micromachines*, 6, 9, 1249-1271. (2015)

[2] "Microfluidic platform combining droplets and magnetic tweezers: application to HER2 expression in cancer diagnosis" D. Ferraro et al., *Scientific Reports*, 6, 25540 (2016)

[3] "Phased peristaltic micropumping for continuous sampling and hardcoded droplet generation" A.M. Nightingale, G.W.H. Evans, P. Xu, B.J. Kim, S. Hassan, X. Niu, *Lab on a Chip*, 17, 6 (2017)

[4] "Continuous measurement of enzymatic kinetics in droplet flow for point-of-care monitoring" S. Hassan et. al, *Analyst*, 141, 11 (2016)

CONTACT

* Dr. Xize Niu ; phone: +44 (0) 2380592367; Email: X.Niu@soton.ac.uk

A DROP IN THE OCEAN: MONITORING OF WATER CHEMISTRY USING DROPLET MICROFLUIDICS

Gareth W.H. Evans, Adrian M. Nightingale, Sammer-Ul Hassan and Xize Niu *
Faculty of Engineering and the Environment, University of Southampton, UK

ABSTRACT

This paper reports a novel droplet microfluidic based chemical sensor device capable of monitoring water chemistry in rivers, lakes and oceans. The device features small footprint, low reagent and energy consumption, and can provide high frequency and accurate measurement with continuous internal calibrations.

KEYWORDS: Droplet Microfluidics, Sensor, Analytical Chemistry, Optical Detection, Nitrate, Nutrient

INTRODUCTION

Measurement of aqueous nutrients such as nitrate and phosphate are important for determining the health of aquatic ecosystems and studying biogeochemical changes. Traditional manual sampling and laboratory analysis is logistically challenging and costly. *In situ* measurement using small and low power analytical devices obviates the need for sample transport, allowing for larger and more temporally detailed datasets. Current state of the art *in situ* microfluidic analyzers are all based on continuous (single-phase) microfluidics [1]. Here we present the first sensor platform for in-situ monitoring of water chemistry based on field-deployable droplet microfluidics. Shifting to a droplet-flow regime greatly improves the temporal resolution, fluid and power economy and also allows continuous calibration. The sensor device makes use of our recently developed micro peristaltic pump that can sample and robustly generate droplet flows using anti-phased peristaltic micropumping. [2].

EXPERIMENTAL

Fig. 1a shows a schematic of the sensor fluidics. The 3D printed peristaltic pump and microfluidic chip produce a pair of droplets from four temporally-separated pulsations at two parallel T-junctions during each rotation of the pump. Each pair of droplets consists of a) a sample mixed with an analyte-specific reagent and b) a standard solution with reagent (for inline calibration). The reagent reacts with the analyte of interest to generate a measurable colour which is quantified using integrated optical flow cells [3]. The flow cell can also measure droplet length and flow rate. Using the standard droplets and the oil segments, the device can provide continuous internal calibration for quality assurance.

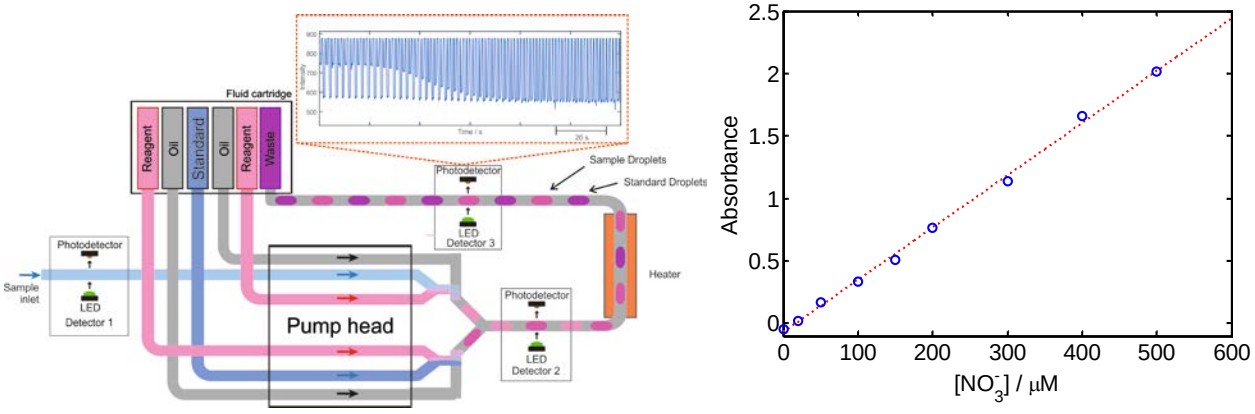

Figure 1: a) Schematic of the sensor fluidics. Shown top are example raw flow-cell data relating to sample and standard droplets. (In the period shown, sample droplets change intensity due to changing incoming sample concentration, but standard droplets remain constant). b) Pre-deployment calibration of absorbance values with changing nitrate concentration.

RESULTS AND DISCUSSION

We demonstrated the sensor platform in measuring nitrate; one of the most important macronutrient in natural waters, which forms the base of many ecosystems. A colorimetric assay based on a modified Griess reagent [4] was

first optimized for droplet microfluidics and incorporated into the device. Fig. 1b shows calibration data showing how the device can accurately measure nitrate in a linear range up to 500 μM, with a limit of detection of 10 μM for a 0.4 mm optical path length.

The device was deployed in a tidal river (River Itchen, Southampton, UK), measuring once every 10 seconds. Fig. 3 shows the variation of nitrate concentration over 24 hours (> 8000 measurements) from an on-going test. This data is consistent with the change between nitrate-rich freshwater and nitrate-poor seawater, with short term peaks observed at low tide when fresh water dominates.

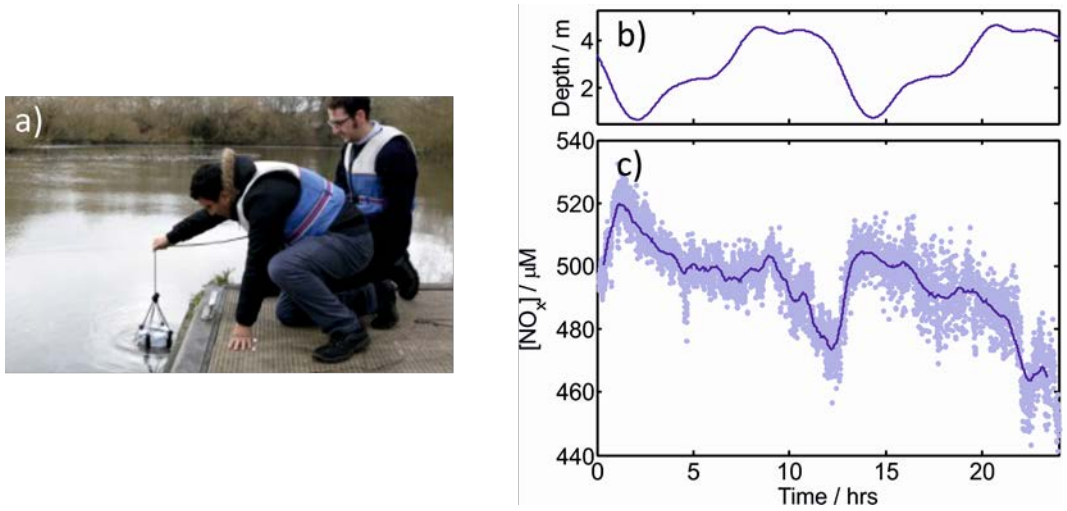

Figure 2: a) Image of deployment, on a tidal section of the River Itchen, where the sensor was deployed for 24 hours. b) How the tide level varied during the deployment, correlated with c) the measured nitrate level over the same period. The data is both shown as raw measurements (dots) and smoothed data (line), and is seen to vary with tide level.

CONCLUSION

We envisage this sensor device could be deployed as a platform technology for the measurement of a variety of chemical species. It can be deployed in arrays or be carried by autonomous vehicles, to form the next generation of water sensors providing chemical data with high temporal/spatial resolution.

ACKNOWLEDGEMENTS

This research was funded by the Engineering and Physical Sciences Research Council UK (EP/M012425/1) and the Natural Environment Research Council UK (NE/P004016/1).

REFERENCES

[1] "Trends in microfluidic systems for in situ chemical analysis of natural waters" A. M. Nightingale et. al, *Sensors and Actuators B: Chemical.*, 221, 1398, (2015)

[2] "Phased peristaltic micropumping for continuous sampling and hardcoded droplet generation," A. M. Nightingale et. al, *Lab on a Chip*, 17, 6, (2017)

[3] "Continuous measurement of enzymatic kinetics in droplet flow for point-of-care monitoring" S. Hassan et al, *Analyst*, 141, 11 (2016)

[4] Automated determination of nitrate plus nitrite in aqueous samples with flow injection analysis using vanadium (III) chloride as reductant," S. Wang et. al, *Talanta*, 146, 744, (2016)

CONTACT

* Dr. Xize Niu; phone: +44-238-059-2367; x.niu@soton.ac.uk

Droplet Microfluidics for the Continuous Chemical Sensing of Cortisol

Gareth W.H. Evans*, Wahida T. Bhuiyan*, Sammer Ul Hassan*, Susan Pang (LGC)** and Xize Niu*

*Faculty of Engineering and the Environment & Institute for Life Sciences, University of Southampton

**Health Science and Innovation, LGC Group

1. INTRODUCTION

Here we present early data for a droplet microfluidics based system currently in development for continuously measuring cortisol, utilising small volumes (nl) of both sample and reagent per measurement.

Why Droplet Microfluidics?

- Droplet microfluidics has proven to be a powerful tool for biochemical analysis offering high temporal resolution and throughput with small sample volumes. This system will apply these same benefits to continuous monitoring.

Why Measure Cortisol continuously?

- Cortisol is a stress related steroid hormone secreted in a 24 hr cycle (highest 30 minutes after awakening and progressively lower by night).
- Cortisol is an important biomarker indicating body condition and training effects athletes and abnormal variation of cortisol levels is strongly linked to a variety of diseases such as Cushing's syndrome and Addison's disease.
- Due to interferrents and low quantities of cortisol in the sample, cortisol measurement is carried out in the lab using ELISA with single sample. This fails to provide a representative picture of cortisol in a patient and unable to capture short term events or characterise circadian cycles.

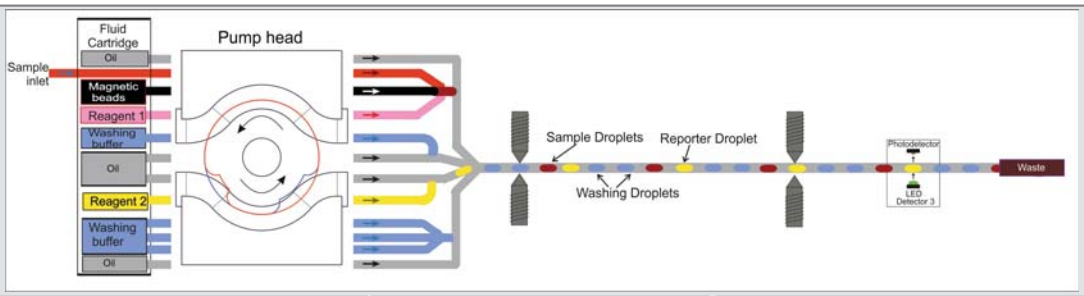

2. ROBUST DROPLET TRAIN GENERATION

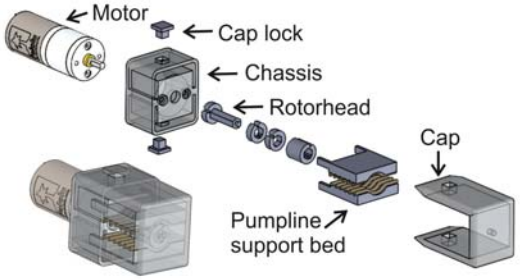

This system utilises a peristaltic micropump [1] for all liquid handling including droplet generation via a pulsed regime which unlike 'traditional' co-flowing pressure driven systems:

- Require no preloading of sample into a syringe,
- Require no 'ramping up' period,
- Droplet size is flow rate invariant,
- Droplet size does not change with viscosity or interfacial tension of fluids.
- Droplet size is not affected by the ratio between oil to sample.
- Droplet size and composition can be "Hard coded" into the design.

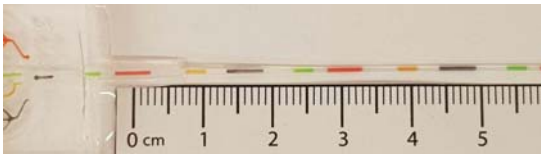

3. MAGNETIC TWEEZERS

The magnetic tweezers in the device comprises ferrite cores wrapped in copper wire in 3D printed housing

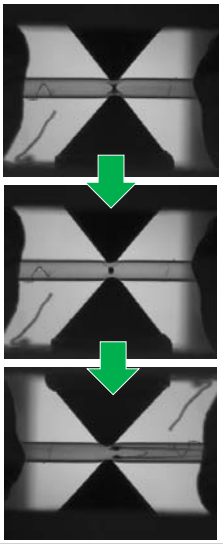

4. CORTISOL ASSAY AND OPTICAL DETECTION

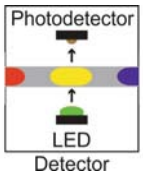

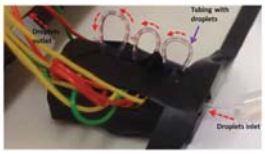

The final detection of the luminescence signal is carried out by an inline optical flow cell [2].
The cortisol sensing platform makes use of a heterogeneous competitive chemiluminescence assay.

The various steps of this assay are held within the droplets and the passage of the magnetic beads between them facilitates the reaction.

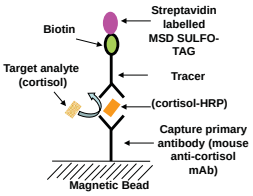

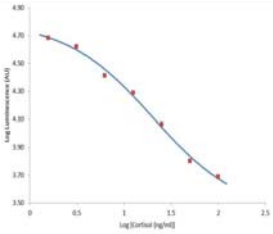

Example concentration-dependent standard curve for cortisol. Adequate recovery of total cortisol can be achieved when <350ng/ml.

6. CONCLUSIONS AND FUTURE WORK

A mini peristaltic pump was designed to continuously collect sample and robustly produce trains of droplets. Droplets can be generated close to the sampling site with reduced Taylor dispersion, and no contamination of the sampling site. Our magnetic tweezers are capable of facilitating the transfer of magnetic beads between droplets to carry out complex assays The droplet based heterogeneous competitive chemiluminescence assay for cortisol has performed well in early tests.

In the future

We are currently developing this platform into an all-in-one prototype ready for clinical testing, capable of performing this assay continuously over long periods with high analytical throughput and accuracy. This prototype will include all aspects discussed here and also custom electronics for data logging and microUSB or Bluetooth for data transmission and be capable of running for multiple days with low power consumption and negligible signal drift. This platform will also be tailored to perform other complex assays for a wide variety of biochemical markers, metabolites and other analytes of interest.

Corresponding author

*Dr. Xize Niu
X.Niu@soton.ac.uk

[1] "Phased peristaltic micropumping for continuous sampling and hardcoded droplet generation" A.M. Nightingale, G.W.H. Evans, P. Xu, B.J. Kim, S. Hassan, X. Niu, Lab on a Chip, 17, 6 (2017)
[2] "Continuous measurement of enzymatic kinetics in droplet flow for point-of-care monitoring" S. Hassan et. al, Analyst, 141, 11 (2016)

EPSRC Pioneering research and skills

Lab on a Chip

PAPER

View Article Online
View Journal | View Issue

Cite this: *Lab Chip*, 2018, **18**, 1903

Nitrate measurement in droplet flow: gas-mediated crosstalk and correction†

Adrian M. Nightingale, [ab] Sammer-ul Hassan, [ab] Gareth W. H. Evans, [ab] Sharon M. Coleman[a] and Xize Niu *[ab]

Received 24th January 2018,
Accepted 1st June 2018

DOI: 10.1039/c8lc00092a

rsc.li/loc

In droplet microfluidics, droplets have traditionally been considered discrete self-contained reaction chambers, however recent work has shown that dissolved solutes can transfer into the oil phase and migrate into neighbouring droplets under certain conditions. The majority of reports on such inter-droplet "crosstalk" have focused on surfactant-driven mechanisms, such as transport within micelles. While trialling a droplet-based system for quantifying nitrate in water, we encountered crosstalk driven by a very different mechanism: conversion of the analyte to a gaseous intermediate which subsequently diffused between droplets. Importantly we found that the crosstalk occurred predictably, could be experimentally quantified, and measurements rationally post-corrected. This showed that droplet microfluidic systems susceptible to crosstalk such as this can nonetheless be used for quantitative analysis.

Introduction

Droplet microfluidics is a powerful tool for analytical science that has been exploited in a wide range of applications such as (bio)chemical assaying,[1] single-cell testing,[2] DNA analysis and drug screening.[3] Aqueous samples and reagents are carried as discrete droplets within an immiscible oil, removing dispersion effects, surface interactions at channel walls, and increasing measurement throughput. Droplets have traditionally been thought of as self-contained reaction chambers, however recent research has shown solutes can leave droplets under routine conditions, travelling into the oil phase[4,5] and on into neighbouring droplets.[6,7] For applications such as materials production,[8–11] inter-droplet migration of molecules is not problematic as all droplets have identical compositions. However for analytical applications and other applications where droplet composition will change, crosstalk leads to sample contamination and can severely compromise the reliability of a given procedure.[4]

Molecules can leave droplets *via* several different mechanisms. The simplest route involves hydrophobic molecules partitioning into the oil phase.[12–14] The widespread use of perfluorinated oils in microfluidics, however, makes this mechanism relatively uncommon as most non-fluorinated molecules display negligible solubility in perfluorinated oils.[15,16] The most commonly reported mechanism is the movement of molecules through the oil phase within micelles, generated by surfactants included to stabilise the droplet-oil interface.[17] The dynamics of this process, reviewed in more detail elsewhere,[18] can be controlled by tuning parameters such as the composition of the droplet,[5,6,17,19] the choice and concentration of surfactant,[6,19] and the hydrophobicity of the migrating species.[4,7] In addition to forming micelles, surfactants can also drive droplet leakage by direct chemical bonding and extraction of droplet contents. Surfactants that have carboxylate groups within their hydrophilic moiety can form strong hydrogen bonds with amines[16] rendering amine-containing molecules oil-soluble and allowing them to partition into the oil phase.[20,21]

A less common mechanism, which bypasses the requirement for the surfactant, is diffusion through the oil as a gas. This has been previously reported by Kreutz *et al.* who designed it into a droplet-based system for catalyst screening.[22] There they tested new catalysts by pairing catalyst-containing droplets with neighbouring "indicator" droplets within polytetrafluoroethylene (PTFE) tubing. Methane and oxygen were introduced through the tubing walls and diffused into the catalyst-containing droplets where they reacted to form methanol. On heating, methanol vapour then diffused through the oil to the neighbouring indicator droplets where they reacted with a reagent to produce a coloured product – thus reporting successful catalytic activity. This report is, to the best of our knowledge, the only previous description of solutes leaving a droplet *via* a gas.

Here we describe an instance of gas-based inter-droplet crosstalk that was unexpectedly encountered whilst

[a] *Faculty of Engineering and the Environment, University of Southampton, Southampton, SO17 1BJ, UK. E-mail: x.niu@soton.ac.uk*
[b] *Institute for Life Sciences, University of Southampton, Southampton, SO17 1BJ, UK*

† Electronic supplementary information (ESI) available. See DOI: 10.1039/c8lc00092a

measuring nitrate in water samples. Nitrate is a key nutrient in natural waters (rivers, lakes, oceans *etc.*) and must be monitored in rivers susceptible to anthropogenic pollution to give early warning of algal blooms and eutrophication.[23] There are numerous reports of field-deployable microfluidic analysers based on continuous-microfluidics,[24,25] however, droplet-based systems could offer several advantages,[25] most notably reducing carryover and the accompanying need to flush the system between samples. This would, in principle, increase power efficiency and reduce the amount of fluid used in each measurement from millilitres to microlitres.

With a long-term goal of producing a field-deployable droplet-based system for *in situ* nitrate analysis, we first aimed to demonstrate the use of a standard laboratory colorimetric assay (the Griess reaction)[26] in droplet flow. Here we describe how the assay was implemented, how analyte was found to migrate between droplets, and how the underlying cause was determined to be its conversion into an intermediary gas which could diffuse between droplets. We demonstrate that under fixed reaction conditions, the gas-mediated crosstalk can be counteracted by using an arithmetic method which corrects crosstalk-compromised measurements to give reliable readings that can be used for quantitative measurement of nitrate in droplets, irrespective of crosstalk.

Results

A droplet microfluidic system was designed for nitrate measurement, as shown in Fig. 1a, with a key feature being the generation of alternating droplets of sample and a standard. Interspersing standard droplets between sample droplets allows continuous calibration of the sample measurement, an approach that has been successfully demonstrated in (low-throughput) continuous-phase microfluidic analysers.[27,28] The system operated by drawing a sample into the system using a peristaltic pump and delivering it into a polydimethylsiloxane (PDMS) microfluidic chip where it met a stream of reagent (1 : 1 volumetric ratio) at a Y-shaped junction. The reagent was a variant of the well-documented Griess reagent, a mixture of sulfanilamide and *N*-naphthyl-ethylenediamine (NEDD),[26] which featured an additional reducing agent, vanadium(III) chloride.[29–31] When heated, the vanadium reduces nitrate (NO_3^-) to nitrite (NO_2^-) which then reacts with the standard Griess reagent to produce a coloured diazonium product. After the sample and reagent met, they co-flowed into a T-junction to meet a fluorous oil (Fluorinert FC-40, with 1.8 wt% non-ionic triblock co-polymer surfactant) which broke the co-flow into droplets (which we will refer to as "sample" droplets). While fluorous capillary tubing and T-connectors could have been feasibly used for droplet generation, we used a microfluidic chip here as it offered advantages in space-saving and the ability to tailor fluid paths as required. The pump and chip were designed such that droplets of a nitrate standard mixed with reagent ("standard" droplets) were also produced in alternation with the sample droplets.

Droplet generation was achieved using the "anti-phase pulsed flow" method we previously reported[32] which takes advantage of the pulsatile nature of peristaltic pumping. A custom-built peristaltic pump delivered the oil and aqueous

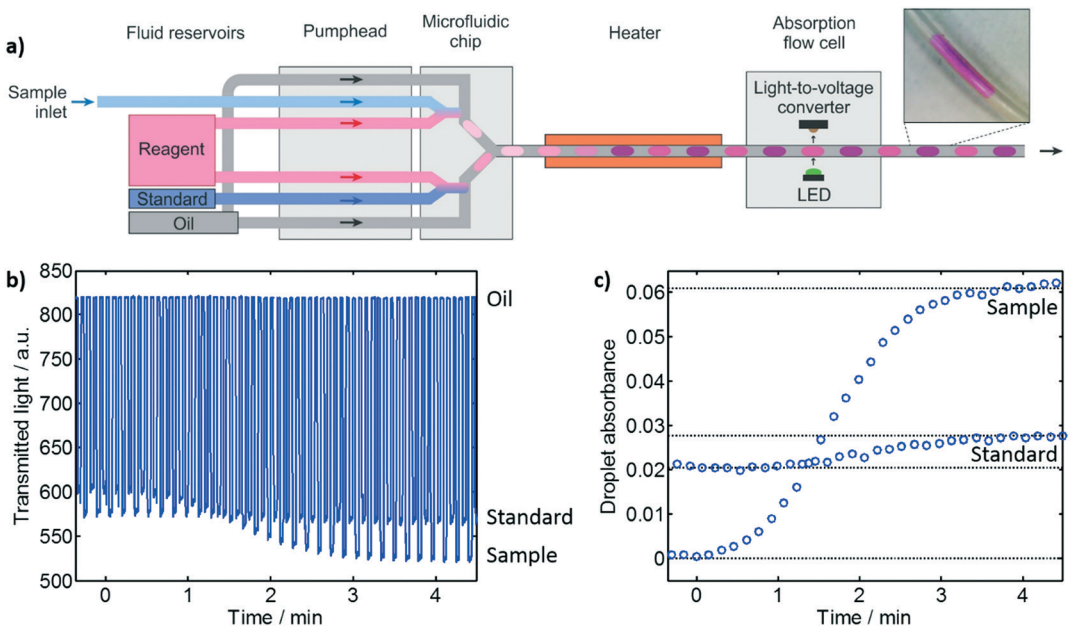

Fig. 1 a) Schematic of the experimental setup for measuring nitrate in droplets. The pumphead and microfluidic chip generate alternating droplets of sample and reagent, and standard and reagent which then travel downstream through a heater to accelerate reaction and an absorption flow cell to quantify the generated colour. A photograph of an example droplet in PTFE tubing (500 μm inner diameter) is shown top right. b) Raw data from the flow cell where the standard is held constant at 100 μM NO_3^- while the incoming sample changes from 0 to 200 μM NO_3^-. c) Conversion of the raw data shown in (b) into droplet absorbance.

phases into the T-junction in alternating, temporally separate pulses. Droplets were thus generated by a robust "chopping" mechanism, with their volume solely determined by the volume of the corresponding aqueous pulses, independent of fluid composition and total flow rate.[32] In this way the size of each droplet and, crucially, the precise timing of its generation can be hard-coded into the pump design. This allows the generation of repeated sequences of droplets with different compositions.[32] Here the system produced alternating droplets of sample and standard, each of which were monodisperse and had an identical average volume of 1.47 μL (see Fig. S1†).

After generation, the droplets exited the chip into PTFE tubing (500 μm inner diameter) which passed through an electrical heater (50 °C, 8 minutes residence time) to accelerate the reduction of nitrate to nitrite by the vanadium (which is much slower than the subsequent Griess reaction which can complete in seconds at room temperature[29–31]). The reagent was in excess such that the quantity of product, and hence the colour of the droplet, was directly proportional to the initial quantity of nitrate. It should be noted that the assay will also account for any nitrite in the sample, however nitrite concentrations are typically orders of magnitude lower than nitrate in oxygenated waters.[27] The droplet colour was quantified downstream using an absorption flow cell fabricated in-house.[33,34] Fig. 1b shows typical raw data from the flow cell. The signal, representing the light transmitted through the fluidic channel, remains high while clear oil segments pass through the light path but drops when the coloured droplets pass through and absorb light.

This system was designed such that sample could be continuously drawn in and measured while the standard can be used to quantify and compensate for any drift in the system such as degradation of the reagent. In Fig. 1b, for example, the sample was swapped from 0 to 200 μM nitrate while the standard was kept constant at 100 μM. The sample response increased as the change to higher nitrate concentration gave increased reaction product and thus stronger light absorbance, while the standard response remained seemingly flat. On closer inspection, however, the standard did not remain exactly constant as expected. This is more obvious when the raw data is converted to absorbance (relative to blank droplets of reagent and ultrapure water) as shown in Fig. 1c. As the absorbance of the sample increased from 0 to ~0.06, the standard droplet absorbance is clearly seen to shift in sympathy from 0.021 to 0.028. Inter-droplet crosstalk such as this was repeatedly and consistently observed, with the standard's absorbance typically changing by ~12% of the change in the sample absorbance.

As most reports of droplet crosstalk have been driven by surfactant-related mechanisms,[18] we began to address the crosstalk problem here by reducing the surfactant content. As the droplet generation method used here is independent of interfacial tension,[32] and the droplets travelled through the PTFE tubing evenly spaced, we found that the surfactant concentration could be reduced to zero without compromising the droplet flow. This had no effect on the crosstalk, however, with standard droplet absorption values changing by approximately 12% of the change in sample absorption as before (see for example Fig. S2†). Likewise, changing the oil to an alternative (non-fluorous) silicone oil was found to offer no improvement (see Fig. S3†). These observations suggested that crosstalk was not occurring *via* the surfactant-dependent mechanisms commonly reported.[18]

To remove any possibility that the crosstalk could be due to wetting of the walls within the PDMS microfluidic chip, a major failure mode for droplet microfluidics,[35] we temporarily changed the method of droplet generation to manual aspiration of droplets. Oil and aqueous segments were aspirated using a standard commercial peristaltic pump (Ismatec ISM597D) to individually draw discrete volumes of fluid into PTFE tubing, segment-by-segment (Fig. 2a). The aqueous segments naturally form droplets upon entering the tubing without interdroplet cross-contamination[36,37] due to the preferential wetting of the PTFE walls by the fluorous oil. Following droplet aspiration, the tubing was attached to the PTFE tubing passing through the heater and absorption flow cell, and the pump flow reversed to push the droplets through (Fig. 2b).

Assuming that cross-contamination *via* channel walls was not a contributing cause, we also needed to identify which solute was moving between droplets. To ascertain the migrating species, the content of the aspirated droplets was alternated between a) sample (either 400 μM nitrate, 400 μM nitrite or a blank) and b) reagent. With the reagent separated from the nitrate and nitrite, we would not expect colour development in the absence of crosstalk. If nitrate or nitrite were migrating we would expect colour development in the reagent droplets, while if the reagent were migrating colour development would occur in the sample droplets. Fig. 2c shows the absorbance of alternating droplets of sample and reagent (using water droplets as the absorbance blank), with the composition of the sample droplets varying between nitrate, nitrite and ultrapure water (5 droplets of each aspirated in turn). When the sample droplets contained only water they exhibited zero absorbance, as expected, while their associated reagent droplets showed an absorbance of 0.015 corresponding to the native colour of the reagent (a pale blue colour due to the presence of vanadium ions). Similar results were obtained when the sample was swapped to nitrate, indicating that neither the nitrate nor reagent was migrating. When the sample was swapped to nitrite, however, the absorbance of the reagent droplets increased to 0.025, indicating that some nitrite had left the sample droplets, migrated to the reagent droplets and reacted to form the coloured product. When the experiment was repeated but omitting the heating step by flowing the droplets straight through the flow cell, (Fig. 2d) no change in the reagent droplet absorbance was observed indicating elevated temperatures were required for droplet migration. Moreover, this demonstrated that the crosstalk was occurring specifically in the heated section of PTFE and not, for example, within the PDMS chip. The specificity of the crosstalk problem to nitrite was confirmed by

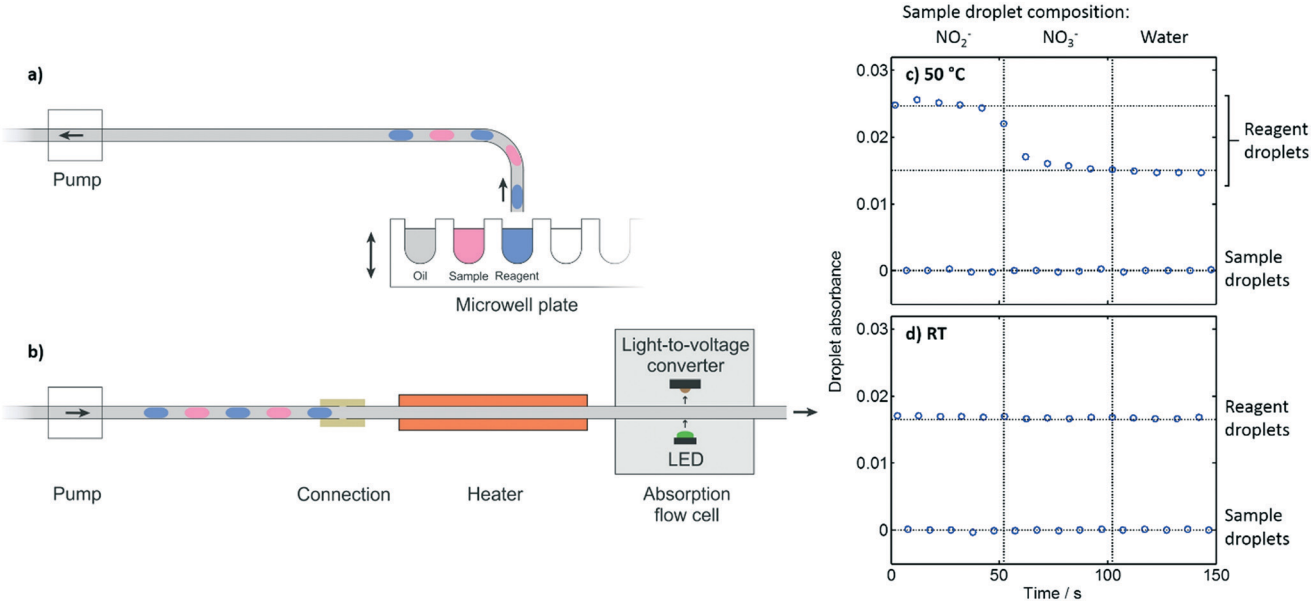

Fig. 2 a) Schematic showing how alternating droplets of reagent and sample were generated by manual aspiration and then b) flowed through the heater and flow cell. c & d) Absorbance of alternating droplets of sample and reagent generated by manual aspiration. The sample composition was changed from nitrite (NO_2^-) to nitrate (NO_3^-) to water. The experiment was conducted both with (c) and without (d) heating.

implementing a similar mix-and-read assay for phosphate (PO_4^{3-}, an analogous anionic analyte important for water quality) using the same aspirated-droplet experimental setup. No colour development was observed in the reagent droplets (Fig. S4†), indicating no droplet crosstalk when measuring phosphate.

It was interesting to note that the crosstalk only occurred for nitrite and not nitrate or phosphate. Each is a negatively charged ion of similar size, hence we might expect to observe similar behaviour. This suggested that the crosstalk might not be due to the nitrite itself but that it underwent a chemical change to a more labile species. To test this theory we devised a simple experiment to ascertain whether changing the pH of the nitrite-containing droplet could affect the crosstalk. As pH can have a profound effect on aqueous reaction dynamics, if the nitrite was undergoing a chemical transformation it would likely be affected by a change in pH. Nitrite solutions at acidic, basic and neutral pH were crudely

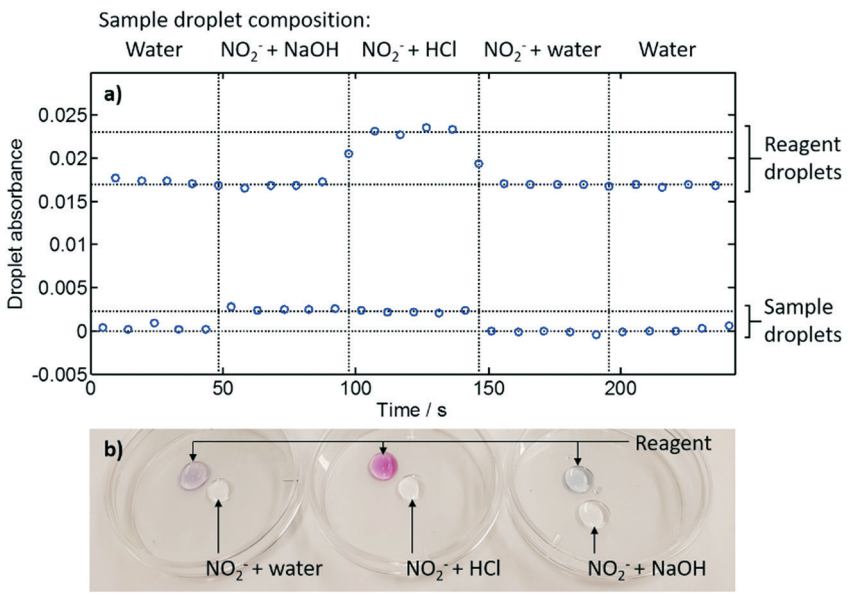

Fig. 3 a) Absorbance of alternating droplets of sample and reagent generated by manual aspiration. The sample composition was changed from water, to basic nitrite (NO_2^- + NaOH), to acidified nitrite (NO_2^- + HCl), to neutral nitrite (NO_2^- + water) and then water. b) Photographic image of droplets of nitrite solutions and reagent placed in covered petri dishes in the absence of oil. The image was taken ~20 minutes after the droplets were deposited.

formulated by mixing 400 μM nitrite at a 1 : 1 volumetric ratio with 1 M HCl, 1 M NaOH and ultrapure water respectively. They were then aspirated into droplets, alternating with reagent droplets as before (Fig. 2a), and flowed immediately through the flow cell without heating. The water and neutral nitrite sample droplets showed no absorbance (Fig. 3a) while the sample droplets containing NaOH or HCl both showed small apparent increases in absorbance (~0.002) attributable to the change in refractive index caused by the high concentration of acid/base (see Fig. S5†). Again, the baseline for the reagent droplets (0.017) was higher than the sample droplets due to the native colour of the reagent. No increase in absorbance was seen in reagent droplets neighbouring neutral nitrite (nitrite + water) droplets, (consistent with Fig. 2d) or in those neighbouring the basic nitrite droplets. However the reagent neighbouring the acidic droplets showed a marked increase to 0.023 indicating colour development due to nitrite migration from the sample droplets.

The enhanced crosstalk at low pH pointed to the root cause of the droplet crosstalk. Under acidic conditions nitrite reversibly decomposes to nitrate and nitric oxide:[38,39]

$$3NO_2^- \rightleftharpoons NO_3^- + 2NO$$

Nitric oxide is a gas and will be able to diffuse out of droplets through the oil to neighbouring droplets where it can undergo reaction to regenerate nitrite, either by the reverse reaction or by reaction with dissolved oxygen.[40] This gas-based crosstalk mechanism was confirmed by placing 0.5 ml droplets of nitrite solution into covered petri dishes, alongside droplets of Griess reagent (Fig. 3b). This was carried out with acidified, basic and neutral nitrite solutions (as for Fig. 3a) and in contrast to previous experiments was carried out in the absence of any oil. Care was taken to ensure that while the droplets were placed close to each other (a gap of ~3 mm), they did not physically contact each other. No colour was initially observed apart from the native pale blue colour of the reagent droplets. After being left covered for 20 minutes at room temperature a strong deep purple colour developed in the reagent neighbouring the acidified nitrite solution (Fig. 3b, centre) with the colour strongest on the side of the droplet adjacent to the nitrite solution – consistent with the generation of nitric oxide and its diffusion across the air gap into the reagent. The purple colour was absent in the reagent neighbouring the basic nitrite solution (Fig. 3b, right) while the reagent neighbouring the neutral nitrite solution (Fig. 3b, left) exhibited a very pale purple colour, consistent with the generation of a limited quantity of nitric oxide. The droplets remained static throughout, with a clear airgap between the nitrite and reagent droplets meaning that the analyte could have only reached the reagent by travelling across the air gap as a gas.

This mechanism is consistent with previous observations of crosstalk within the original experimental setup (Fig. 1a). Griess reagent is inherently acidic, with pH typically less than 3,[41] hence nitric oxide will be generated within each droplet as soon as the nitrate has been reduced to nitrite. The nitric oxide will then be able to diffuse through the droplet/oil barrier aided by the enhanced solubility of nitric oxide in fluorocarbon oils over water.[42] This is a competitive process however, as shown in Fig. 4a which illustrates the various reaction, diffusion, and convection processes occurring within the system. Following nitric oxide generation there will be an ensuing competition between the chemical reactions that can remove nitric oxide (regenerating nitrite and then converting to the diazonium dye) and transport of nitric oxide from the droplet. This competition determines how much nitric oxide leaves the droplet and thus the extent of the crosstalk. As the crosstalk was observed to be more pronounced at higher temperatures (Fig. 2c and d) it seems likely that the increased generation of nitric oxide[39] and raised diffusivity expected at higher temperature prevails over the increased Griess reaction rate[30,31] and encourages loss of nitric oxide from the droplet. In the oil phase the nitric oxide will be transported within each segment *via* convection[43,44] and will have opportunity to diffuse into the neighbouring droplet. The lower gas diffusion coefficients of PTFE relative to FC40 oil (*e.g.* oxygen diffusion coefficients 2.8×10^{-7} cm^2 s^{-1} at 25 °C for PTFE[45] *versus* 5.7×10^{-5} cm^2 s^{-1} at 37 °C for a similar low-viscosity fluorocarbon oil[22]) ensures negligible nitric oxide is lost through the tubing walls. The nitric oxide that enters the oil will, in time, re-enter a droplet, at which point it can be converted back into nitrite and then on into the coloured diazo product (see Fig. 4a). If the nitric oxide re-enters the droplet it was generated from, there is no perceived crosstalk, however if it enters a neighbouring droplet then extra diazonium dye is generated and crosstalk arises. As a finite quantity of nitric oxide is produced, we would expect the concentration within the oil to ultimately return to zero. This is confirmed by reproducing the experiment shown in Fig. 2c using different quantities of oil (see Fig. S6†). The same level of crosstalk was observed, indicating that no nitric oxide is retained within the oil at the point of measurement.

We then looked to calibrate the inter-droplet crosstalk and ascertain whether it might be possible to mathematically correct for it in our original experimental setup. This was done by measuring the absorption of both sample and standard droplets (Fig. 4b and c respectively) whilst running through different concentrations of nitrate in the sample droplets (0–600 μM) with the standard set at 0 μM, 200 μM, and 600 μM nitrate. When ultrapure water (blank) was used as the standard, the sample absorbance (Fig. 4b, red triangles) increased linearly with nitrate concentration with the *y*-intercept at the origin as expected. In the absence of crosstalk we would expect the corresponding standard droplets (Fig. 4c, red triangles) to be constant, however the absorbance increased with sample concentration, with the linear trend indicating that the crosstalk was a fixed proportion of the sample droplet concentration.

As the standard was increased to 200 μM (blue squares) and 600 μM (green circles) the absorbance of the standard

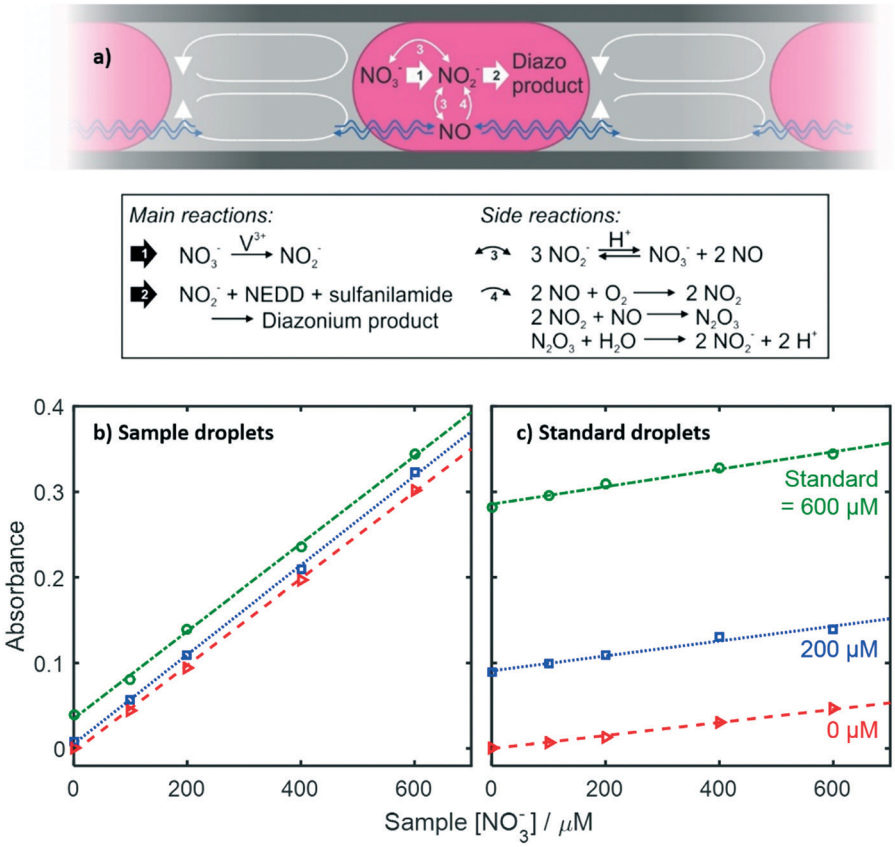

Fig. 4 a) Schematic illustrating the processes occurring within each droplet in the original experimental setup (Fig. 1a). b) Absorbance of sample droplets within a flow of alternating sample and standard droplets (Fig. 1a). The droplets were measured with the introduction of different sample concentrations (0–600 μM, *x*-axis) and standard concentrations (0 μM, red triangles; 200 μM, blue squares; 600 μM, green circles). c) Absorbance of standard droplets measured at the same time.

droplets increased, as expected (Fig. 4c). So too, however, did the corresponding sample droplets (Fig. 4b) – consistent with crosstalk from the standard droplets into the neighbouring sample droplets. It is important to note that while the standard concentrations changed, the gradients of the lines of best fit for both the sample and standard droplets (*i.e.* the change in absorbance with respect to sample droplet concentration) remained constant. This indicates that the amount of nitric oxide transferring from the sample droplets into the standard droplets depended only on the concentration within the source (sample) droplet and was not affected by the concentration within the destination (standard) droplet.

The observations that the magnitude of the crosstalk is a fixed proportion of the source droplet, and that it is independent of the destination droplet concentration suggested that we could derive an expression to correct for the crosstalk. Previous mathematical descriptions of surfactant driven crosstalk have used diffusion-based models,[6,46] however the empirical model we developed means that minimal prior knowledge of the mechanistic process of the crosstalk and its associated kinetics was required.

We first defined crosstalk as the ratio of the amount of analyte that transfers to neighbouring droplets relative to that which remains in the source droplet (henceforth referred to as the crosstalk ratio, α). This ratio is defined by the quantities found in the droplets *after* crosstalk has occurred, and as such can be experimentally determined. The crosstalk ratio can be measured in two different ways: if one of the droplets is a blank, it is simply given by the ratio of measured concentration in the two droplet populations. For the data shown in Fig. 4b and c, for example, it would be given by the ratio of the standard absorbance (Fig. 4c, red triangles) to sample absorbance (Fig. 4b, red triangles) for the same sample concentration (*e.g.* when the sample was 600 μM, α = 0.046/0.302 = 0.15). This method is dependent on one droplet having zero analyte concentration before crosstalk. When both droplets initially contain analyte, an alternative method must be used. In this case the crosstalk ratio can be measured experimentally if one droplet population (sample or standard) is kept constant while the analyte concentration in the other is varied. This assumes that the constant population would not vary for the duration of the measurements in the absence of crosstalk. In the data shown in Fig. 4, for example, the crosstalk ratio is given by the ratio of the gradients of the lines of best fit for the standard (Fig. 4c) and sample (Fig. 4b) absorbances (*e.g.* when the standard was 200 μM, $\alpha = 8.723 \times 10^{-5}\ \mu M^{-1}/5.224 \times 10^{-4}\ \mu M^{-1} = 0.17$). This second method requires multiple measurements and as such is likely

to be more accurate than the first as experimental errors will be reduced by averaging. Given the gas-mediated crosstalk mechanism, the crosstalk ratio will change with reaction temperature, however for fixed reaction conditions we would expect it to remain constant and we note anecdotally that this was found to be the case.

Using the crosstalk ratio we can derive an expression for the absorbance we would expect if there were no crosstalk (*i.e.* a corrected absorbance) based on the measured absorbance of the two sets of droplets:

$$A_{\mathrm{a,corrected}} = \left(\frac{1+\alpha}{1-\alpha^2}\right)\left(A_{\mathrm{a}} - \alpha A_{\mathrm{b}}\right) \quad (1)$$

where A_{a} is the measured absorbance of droplet "a" (sample or standard), A_{b} is the measured absorbance of the neighbouring droplets, "b" (standard or sample) and α is the crosstalk ratio as described earlier. The full derivation is given in the ESI.† The equation is derived assuming that the residence time is long enough that no nitric oxide remains at the point of measurement, having been converted to first nitrite and then diazonium dye within the droplets (see Fig. 4a). Our system, which featured a residence time of 8 minutes in the heated section and approximately one minute from the heater to the flow cell, was found to be sufficient (see Fig. S6†) without requiring further optimisation. If $\alpha = 0$, (*i.e.* there is no crosstalk) eqn (1) simply reduces to $A_{\mathrm{a,corrected}} = A_{\mathrm{a}}$, as we might expect, while if α is very large (in the practically unfeasible case that almost all analyte transfers to neighbouring droplets) it reduces to $A_{\mathrm{a,corrected}} = A_{\mathrm{b}}$. In practice we would expect $0 \leq \alpha \leq 1$, in which case the equation accounts for the partial migration of analyte from the droplet, while also accounting for any incoming analyte that originated from the neighbouring droplets.

Applying eqn (1) to the data shown in Fig. 4b and c gives the combined set of corrected data shown in Fig. 5a. Again the data obtained using standard concentrations of 0, 200 and 600 μM are shown as red triangles, blue squares and green circles respectively. The absorbance of the standards are constant with respect to the sample concentration, while the sample responses all overlay each other irrespective of the concentration standard with a shared y-intercept at the origin. Importantly, this is the behaviour we would expect in the absence of crosstalk.

As a further test of the mathematical correction, we measured five river water samples and quantified their concentration using two separate methods: firstly using a calibration curve determined by running standards through the sample inlet before testing (calibrations shown in Fig. S7†). Secondly by using an inline calibration which uses the absorbance of the inline standard droplets:

$$\left[\mathrm{NO_3^-}\right]_{\mathrm{sample}} = \frac{A_{\mathrm{sample}}}{A_{\mathrm{standard}}} \cdot \left[\mathrm{NO_3^-}\right]_{\mathrm{standard}} \quad (2)$$

where $[NO_3^-]_{sample}$ is the measured sample concentration, $[NO_3^-]_{standard}$ is the known concentration of the standard (320 μM in this case) and A_x is the absorbance of the droplet (sample or standard). In the absence of crosstalk absorbances can be used as measured,[27,47] but corrected absorbances (as determined by eqn (1)) will be required with crosstalk. This second method in effect performs a new single-point calibration for each individual sample and can compensate for calibration drift.[27,28,47] While unnecessary for laboratory-based testing, inline calibration is critical for field-deployable microfluidic chemical analysers where aging reagents and/or changing ambient conditions can shift the calibration. This method relies on the fidelity of the inline standard droplets and as such is particularly vulnerable to crosstalk.

The five river samples were taken at different positions along the tidal River Itchen in Southampton (Fig. 5b) during a ninety minute period at high tide. During this sampling

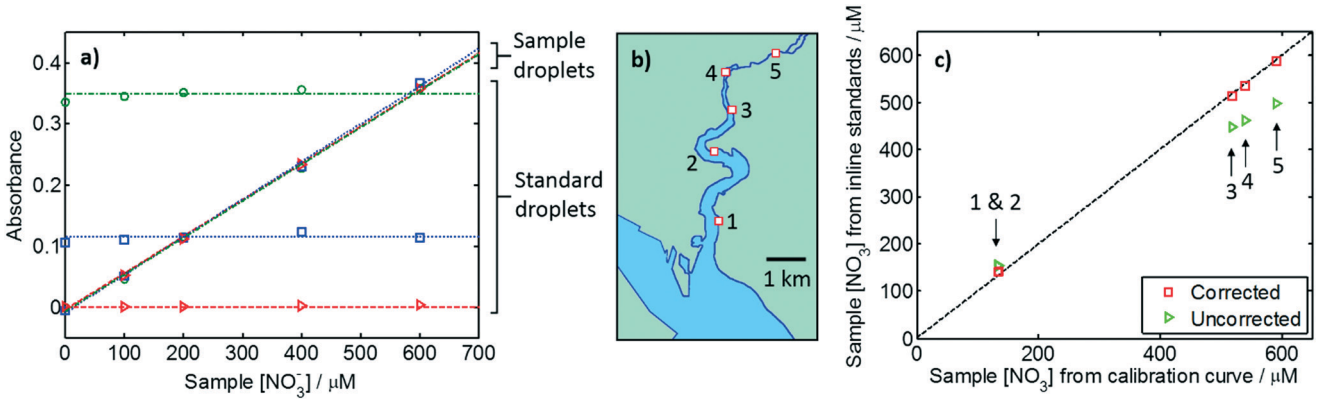

Fig. 5 a) Data from Fig. 4b and c with absorbance corrected using eqn (1). The red triangles, blue squares and green circles correspond to standard droplets of nitrate concentrations of 0, 200 and 600 μM respectively. b) Positions where water samples were taken on the tidal river Itchen in Southampton. c) Quantification of the nitrate content of the river samples measured in droplet flow. Nitrate concentrations were calculated using a calibration curve (*x*-axis) and using inline standard droplets (*y*-axis). Values were calculated using data which was either corrected (red squares) or uncorrected (green triangles) for crosstalk using eqn (1).

period the tidal height did not change appreciably (see Fig. S8†) so that any measured differences in nitrate concentration is attributable to the relative sampling locations, not tidal variation. River water typically has nutrient levels two orders of magnitude higher than surface seawater[27] so we would expect to see a range of nitrate concentrations in the samples, with lower concentrations in the downstream samples.

Fig. 5c shows the concentrations as quantified using the two methods, with the value obtained from the calibration curve (method one) on the *x*-axis and the value obtained from inline calibration (method two) on the *y*-axis. Both methods give the same expected qualitative trend with the freshwater-rich upstream samples having higher concentrations of nitrate. Locations 1 and 2 had identical nitrate concentrations and there was a distinct step-change between location 2 and 3, indicating poor mixing between the influx of seawater from Southampton Water and the river flow. There were notable discrepancies between the absolute values obtained from the two methods when using uncorrected absorbance values (green triangles) however. Where the sample concentration was higher than the standard, inline calibration gave anomalously low values. This is due to crosstalk decreasing the measured sample concentration while increasing the standard concentration – decreasing the concentration as calculated using eqn (2). For the same reason inline calibration gave slightly high values when the sample concentration was lower than the standard, due to crosstalk raising the sample concentration and decreasing the standard. Using corrected values (red squares) removed this problem, however, resulting in concentrations that perfectly matched the values obtained using the calibration curve as we would expect in the absence of crosstalk.

Discussion and conclusion

The crosstalk found in this droplet-based assay resulted from the conversion of nitrite to gaseous nitric oxide at low pH. Such a transfer of analyte *via* a gaseous intermediate species is in contrast with most previously reported mechanisms concerning direct partitioning or surfactant-driven mechanisms.[18] An obvious way to eliminate the crosstalk would have been to conduct the assay at elevated pH, however this was not an option as the Griess reagent requires low pH to render its constituent reactants soluble.[26] We could have tried removing the heating step and thus reducing the diffusion rate of the nitric oxide, however the vanadium-based reduction step is slow (several hours at room temperature[31]) hence, if conducted at room temperature, much longer channels would be required with high accompanying backpressures. Alternative nitrate assays exist, but these either use highly caustic[48] or unstable reagents.[49,50] These methods weren't required however, as we showed that an arithmetic method can be used to correct for the crosstalk. We note that while mathematical methods have previously been used to model and describe crosstalk in droplet microfluidics,[46] this is, to the best of our knowledge, the first case where they have been used to accurately correct for crosstalk in experimental data.

It is interesting to note that loss of analyte *via* nitric oxide has not been previously highlighted in reports of nitrate analysis using the Griess assay.[26,31] Given the low pH intrinsic to the Griess assay, the generation of nitric oxide must also be present, however it is likely that the higher surface area to volume ratios and juxtaposition of droplets of different concentrations contributed to its prevalence in this study. This highlights, however, the suitability of droplet flow for transferring solutes between droplets *via* gas intermediates, which could be exploited in assays where it is favourable to convert constituents to gases. One such example is in ammonium assays, where the analyte can be extracted as gaseous ammonia to remove it from potential interferences, as demonstrated by Sraj *et al.*[51] Another example is in alkalinity measurements using the "single-point" method,[52] where gaseous CO_2 needs to be removed from an acidified sample before the alkalinity can be gauged *via* the final sample pH. We anticipate that these kinds of measurements, which currently still rely on continuous fluidics, might benefit from the high throughput and low fluid use in droplet flows as demonstrated here.

In summary we have shown novel droplet fluidics that can continuously measure nitrate in water, with each measurement only requiring sub-microlitre sample and reagent. Inline calibration was achieved by interspersing sample droplets with standard droplets. Interestingly we found that the standard Griess assay generated notable inter-droplet crosstalk due to the generation of gaseous nitric oxide which then diffused between droplets, in contrast to the majority of previous reports of crosstalk which are surfactant-driven. An arithmetic method was developed which corrected for crosstalk, giving the concentrations we would expect in the absence of crosstalk.

Experimental

Chemicals

Hydrochloric acid (37%), sulfuric acid (95–98%), tin(II) chloride (98%), glycerol (≥99%), potassium nitrate (≥99%), vanadium(III) chloride (97.0%), sulphanilamide (≥99.0%), *N*-(1-napthyl)ethylenediamine dihydrochloride (NEDD, >98%), sodium nitrite (99.0%), potassium phosphate monobasic (99.0%) and silicone oil (Dow Corning 200, 50 cSt at 25 °C) were obtained from Sigma Aldrich, UK. Ammonium molybdate tetrahydrate (99%) was obtained from Alfa Aesar, UK. Unless otherwise stated, water was ultrapure grade (18.2 MΩ, Barnstead EASYpure RODI). Fluorinert FC40 oil was obtained from Acota Ltd, UK. The tri-block co-polymer surfactant (perfluorinated polyether/polyethylene glycol/perfluorinated polyether) was synthesised in-house using the previously reported protocol.[53]

Nitrate assay reagent formulation

The modified Griess reagent was formulated by first weighing out 2.5 g of vanadium(III) chloride and adding to a 250 ml

volumetric flask along with 50 ml of ultrapure water to form a dark brown solution. 15 ml of concentrated (37%) hydrochloric acid was added which caused the solution to turn a dark turquoise colour. 1.25 g of sulfanilamide and 0.125 g of NEDD was added, dissolved and the solution finally made up to the volumetric mark using ultrapure water.

Phosphate assay reagent formulation

A 2.5 wt% solution of ammonium molybdate in 3 M concentrated sulfuric acid was formed by dissolving 6.125 g of ammonium molybdate in approximately 200 ml of water in a 250 ml volumetric flask. 40 ml concentrated sulfuric acid was added and then the solution made up to the volumetric mark. A 2.5 wt% solution of tin chloride in glycerol was formulated by dissolving 2.5 g of tin(II) chloride in 100 ml glycerol in a volumetric flask. Before the assay was performed the reagent was made by mixing 2 drops (approximately 100 μL) of the tin chloride solution in 2 ml of ammonium molybdate solution, and then used immediately.

Nitrate, nitrite and phosphate standards

A 100 mM stock solution of potassium nitrate was made by dissolving 2.528 g of potassium nitrate in ultrapure water in a 250 ml volumetric flask. A 100 mM stock solution of sodium nitrite was made by dissolving 1.725 g of sodium nitrite in ultrapure water in a 250 ml volumetric flask. A 10 mM stock solution of potassium phosphate was made by dissolving 0.136 g potassium phosphate monobasic in ultrapure water in a 100 ml volumetric flask. All stock solutions were further diluted as required for each specific experiment.

Microfluidic chip

PDMS microfluidic chips were replica moulded from a 3D-printed master. The master was designed in 3D CAD software (SolidWorks, Dassault Systemes) and printed in "VeroClear" material using an Objet500 Connex3 polyjet printer (Stanford Marsh Ltd). The channel design had nominal channel dimensions of 600 μm height for all channels, with a main channel of 200 μm width and inlets of 100 μm width (as shown schematically in Fig. S9a†). Limitations in printing resolution and feature shrinkage with post-treatment resulted in final channels with a Gaussian profile and dimensions of 590/350 μm height/full-width-half-maximum for the 200 μm nominal-width channels and 480/320 μm for the 100 μm nominal-width channels. The entry/exit points featured enlarged channels (660 μm nominal width and 550 μm nominal height) so that tubing could be later inserted. After printing, the mould was baked overnight at 65 °C to remove any uncured precursor materials and then treated with a non-stick coating by wiping with a lint free wipe dipped in "Aquapel" (PPG Industries). PDMS was added to the mould (Sylgard 184, 10 : 1 ratio of elastomer to curing agent) and baked at 65 °C for a minimum of one hour. After removal from the mould, the chips were cut to shape and then sealed to a flat piece of PDMS using the "half-cure" method.[54–56] To allow reliable droplet generation, the channels were treated to ensure preferential wetted by the fluorous oil. This was done by filling the channels with Aquapel (PPG Industries) using a syringe and blunt dispensing needle, waiting for approximately 5 minutes, and then flushing the channels with air. The chips were then left overnight in an oven at 70 °C. PTFE tubing (inner diameter, ID, 500 μm; outer diameter, OD, 700 μm; Adtech Polymer Engineering, UK) was inserted into the inlet/outlet sections and then fixed in place by placing the chip and tubing on a hotplate at 110 °C and applying uncured PDMS to the join. An image of a finished chip is shown in Fig. S9b.†

In-house pump and droplet generation

Fluid was pumped using a peristaltic pump built in-house which has previously been described in detail elsewhere.[32] Briefly, it operated using a DC motor (Pololu 1000 : 1 Micro Metal Gearmotor) which turned a 3D-printed rotor contacting a microfluidic channel. The patterning of features on the rotor determined the timing and magnitude of the fluidic pulses induced in the channel. The main pump chassis and the rotor were 3D printed in "VeroClear" material using an Objet500 Connex3 polyjet printer (Stanford Marsh Ltd). Six fluidic lines were used, with the pump outlets connected to the microfluidic chip, as indicated in Fig. S9a,† using PTFE tubing (ID 500 μm, OD 700 μm). Droplets were generated by the previously described "anti-phased peristaltic pumping" method,[32] whereby oil and aqueous phases are injected alternately. To achieve the alternating sample/standard droplets, the rotor was designed to pump the fluids in the order: 1. sample and reagent (lines 2 and 3 in Fig. S9a†); 2. oil (line 1); 3. standard and reagent (lines 4 and 5); 4. oil (line 6). The motor was run at 1.5 V, which produced a total flowrate of 22 μL min^{-1}.

Flow cell

Droplet absorbance was measured using an inline spectrophotometric flow cell which has been previously reported in detail elsewhere.[33] Briefly, black polymethylmethacrylate (PMMA) was micromilled with two channels: one to hold a short length of PTFE tubing (ID 500 μm, OD 700 μm, Adtech Polymer Engineering, UK) and another to define a light path to directly transect the tubing. An LED (Cree CLM4B-GKW-CWBYA693, Farnell Onecall, for the nitrate assay; Avago HSMH-A100-N00J1, RS, for the phosphate assay) and light-to-voltage converter (TSL257, Texas Advance Optical Solutions, UK) were positioned at either end of the light path using a 3D-printed support (polylactic acid, printed on an Ultimaker 2 fused deposition modelling printer). The LED was powered by a benchtop power supply (Tenma 72-7245) operating on constant current mode while the light-to-voltage converter was powered from a microcontroller (Arduino Nano) which also continuously measured the signal voltage and passed it back to a benchtop computer running Labview 2012 (National Instruments) which processed and saved the data.

Heater

The heater was fabricated in-house by winding 120 cm of PTFE tubing (500 μm ID, 700 μm OD) around a 1 cm length of copper tubing. 3D-printed end-pieces (polylactic acid, Ultimaker 2) were attached to each end of the tube to help keep the PTFE tubing in place. A resistive polyimide thin film heater (Watlow Kapton K05711980AL-L 1/2″ × 1.1/8″) was placed on the inside surface of the tubing and a digital thermometer (Maxim DS18b20) was placed in the centre of the tubing. The whole assembly was wrapped in an approximately 3 cm-thick blanket of cotton wool. The heater was powered by a 9 V battery *via* a metal oxide semiconductor field emission transistor (MOSFET, Vishay TO-220AB) controlled by the same microcontroller used to transfer the flow cell data. The microcontroller was programmed with custom pulse width modulation (PWM) code to control the power supplied to the heater and maintain its temperature (as determined by the digital thermometer) at 50 °C.

Aspirating droplets

Droplets were aspirated using a commercial peristaltic pump (Ismatec ISM597D) fitted with PVC tubing (250 μm ID, 2 mm OD). A 30 cm length of PTFE tubing (500 μm ID, 700 μm OD) was attached to the "pull" end of the PVC tubing and all tubing first flushed with FC40 oil. The pump was then set to pump a specific volume (0.95 μL at a flow rate of 5 μL min^{-1}) at the push of a button. Droplets were aspirated by placing the mouth of the tubing into a reservoir of aqueous fluid, activating the pump, waiting for it to pump the set volume, then moving the tubing mouth to an oil reservoir, activating the pump and waiting for it to pump the set volume. This procedure, which produced a single discrete droplet, was repeated until the desired droplet train was produced. The mouth of the PTFE tubing was then attached to the same heater and flow cell used for the standard setup (Fig. 1a), the pump direction reversed and flowed through at a rate of 20 μL min^{-1}.

River water sampling protocol

The sampling protocol was developed with literature recommendations for good sampling and storage practice.[26] Prior to sampling, five 60 ml Nalgene bottles (VWR, UK) were cleaned by first soaking in a solution of 2% detergent (Decon 90) for 24 hours, rinsing with ultrapure water, then soaking in 10 vol% solution of concentrated hydrochloric acid, rinsing with ultrapure water and then drying. For each sample collection, a 10 ml plastic disposable syringe (Normject luer-lock, Henke Sans Wolf) was rinsed with river water 3 times. The syringe was then used to rinse a syringe filter (Millipore Millex GP, 0.22 μm pore polyethersulfone membrane) with 5 ml of river water. A sample bottle was rinsed 3 times with ~2.5 ml of filtered river water and then filled with filtered river water taken from immediately under the surface at the riverbank. All samples were obtained on 7th June, 2017 between 1138 and 1304 (British Summer Time) at the locations specified in Fig. 5b and then immediately frozen for later analysis.

Conflicts of interest

There are no conflicts of interest.

Acknowledgements

We thank the funding from the Engineering and Physical Sciences Research Council UK (EP/M012425/1) and the Natural Environment Research Council UK (NE/P004016/1).

References

1 E. Y. Basova and F. Foret, *Analyst*, 2015, **140**, 22–38.
2 E. Brouzes, M. Medkova, N. Savenelli, D. Marran, M. Twardowski, J. B. Hutchison, J. M. Rothberg, D. R. Link, N. Perrimon and M. L. Samuels, *Proc. Natl. Acad. Sci. U. S. A.*, 2009, **106**, 14195–14200.
3 M. Courtney, X. M. Chen, S. Chan, T. Mohamed, P. P. N. Rao and C. L. Ren, *Anal. Chem.*, 2017, **89**, 910–915.
4 J. W. Janiesch, M. Weiss, G. Kannenberg, J. Hannabuss, T. Surrey, I. Platzman and J. P. Spatz, *Anal. Chem.*, 2015, **87**, 2063–2067.
5 P. A. Sandoz, A. J. Chung, W. M. Weaver and D. Di Carlo, *Langmuir*, 2014, **30**, 6637–6643.
6 P. Gruner, B. Riechers, B. Semin, J. Lim, A. Johnston, K. Short and J. C. Baret, *Nat. Commun.*, 2016, **7**, 10392.
7 G. Woronoff, A. El Harrak, E. Mayot, O. Schicke, O. J. Miller, P. Soumillion, A. D. Griffiths and M. Ryckelynck, *Anal. Chem.*, 2011, **83**, 2852–2857.
8 C. A. Serra and Z. Q. Chang, *Chem. Eng. Technol.*, 2008, **31**, 1099–1115.
9 J. T. Wang, J. Wang and J. J. Han, *Small*, 2011, **7**, 1728–1754.
10 A. M. Nightingale, J. H. Bannock, S. H. Krishnadasan, F. T. F. O'Mahony, S. A. Haque, J. Sloan, C. Drury, R. McIntyre and J. C. deMello, *J. Mater. Chem. A*, 2013, **1**, 4067–4076.
11 W. K. Wong, S. K. Yap, Y. C. Lim, S. A. Khan, F. Pelletier and E. C. Corbos, *React. Chem. Eng.*, 2017, **2**, 636–641.
12 H. Chen, Q. Fang, X. F. Yin and Z. L. Fang, *Lab Chip*, 2005, **5**, 719–725.
13 F. Courtois, L. F. Olguin, G. Whyte, A. B. Theberge, W. T. S. Huck, F. Hollfelder and C. Abell, *Anal. Chem.*, 2009, **81**, 3008–3016.
14 P. Mary, V. Studer and P. Tabeling, *Anal. Chem.*, 2008, **80**, 2680–2687.
15 A. Studer, S. Hadida, R. Ferritto, S. Y. Kim, P. Jeger, P. Wipf and D. P. Curran, *Science*, 1997, **275**, 823–826.
16 K. L. O'Neal and S. G. Weber, *J. Phys. Chem. B*, 2009, **113**, 149–158.
17 Y. Skhiri, P. Gruner, B. Semin, Q. Brosseau, D. Pekin, L. Mazutis, V. Goust, F. Kleinschmidt, A. El Harrak, J. B. Hutchison, E. Mayot, J. F. Bartolo, A. D. Griffiths, V. Taly and J. C. Baret, *Soft Matter*, 2012, **8**, 10618–10627.

18 P. Gruner, B. Riechers, L. A. C. Orellana, Q. Brosseau, F. Maes, T. Beneyton, D. Pekin and J. C. Baret, *Curr. Opin. Colloid Interface Sci.*, 2015, **20**, 183–191.
19 G. Caldero, M. J. GarciaCelma, C. Solans, M. Plaza and R. Pons, *Langmuir*, 1997, **13**, 385–390.
20 K. L. O'Neal, S. Geib and S. G. Weber, *Anal. Chem.*, 2007, **79**, 3117–3125.
21 C. Palomo, J. M. Aizpurua, I. Loinaz, M. J. Fernandez-Berridi and L. Irusta, *Org. Lett.*, 2001, **3**, 2361–2364.
22 J. E. Kreutz, A. Shukhaev, W. B. Du, S. Druskin, O. Daugulis and R. F. Ismagilov, *J. Am. Chem. Soc.*, 2010, **132**, 3128–3132.
23 T. P. Burt, N. J. K. Howden, F. Worrall and M. J. Whelan, *J. Environ. Monit.*, 2010, **12**, 71–79.
24 U. Bende-Michl and P. B. Hairsine, *J. Environ. Monit.*, 2010, **12**, 127–134.
25 A. M. Nightingale, A. D. Beaton and M. C. Mowlem, *Sens. Actuators, B*, 2015, **221**, 1398–1405.
26 K. Grasshoff, K. Kremling and M. Ehrhardt, *Methods of Seawater Analysis*, Wiley-VCH, 1999.
27 A. D. Beaton, C. L. Cardwell, R. S. Thomas, V. J. Sieben, F. E. Legiret, E. M. Waugh, P. J. Statham, M. C. Mowlem and H. Morgan, *Environ. Sci. Technol.*, 2012, **46**, 9548–9556.
28 G. S. Clinton-Bailey, M. M. Grand, A. D. Beaton, A. M. Nightingale, D. R. Owsianka, G. J. Slavikt, D. P. Connelly, C. L. Cardwell and M. C. Mowlem, *Environ. Sci. Technol.*, 2017, **51**, 9989–9995.
29 E. Garcia-Robledo, A. Corzo and S. Papaspyrou, *Mar. Chem.*, 2014, **162**, 30–36.
30 K. M. Miranda, M. G. Espey and D. A. Wink, *Nitric Oxide*, 2001, **5**, 62–71.
31 B. Schnetger and C. Lehners, *Mar. Chem.*, 2014, **160**, 91–98.
32 A. M. Nightingale, G. W. H. Evans, P. X. Xu, B. J. Kim, H. Sammer-ul and X. Z. Niu, *Lab Chip*, 2017, **17**, 1149–1157.
33 S. U. Hassan, A. M. Nightingale and X. Z. Niu, *Micromachines*, 2017, **8**, 58.
34 S. U. Hassan, A. M. Nightingale and X. Z. Niu, *Analyst*, 2016, **141**, 3266–3273.
35 A. P. Debon, R. C. R. Wootton and K. S. Elvira, *Biomicrofluidics*, 2015, **9**, 024119.
36 F. Gielen, L. van Vliet, B. T. Koprowski, S. R. A. Devenish, M. Fischlechner, J. B. Edel, X. Niu, A. J. deMello and F. Hollfelder, *Anal. Chem.*, 2013, **85**, 4761–4769.
37 J. Wu, M. Zhang, X. Li and W. Wen, *Anal. Chem.*, 2012, **84**, 9689–9693.
38 N. N. Greenwood and A. Earnshaw, *Chemistry of the Elements*, Oxford, 1997.
39 H. H. Sisler, in *Comprehensive Inorganic Chemistry*, ed. M. C. Sneed and R. C. Brasted, D. Van Nostrand Company Inc., 1956, vol. 5.
40 E. M. Hetrick and M. H. Schoenfisch, *Annu. Rev. Anal. Chem.*, 2009, **2**, 409–433.
41 D. Giustarini, R. Rossi, A. Milzani and I. Dalle-Donne, in *Nitric Oxide, Part F: Oxidative and Nitrosative Stress in Redox Regulation of Cell Signaling*, ed. E. Cadenas and L. Packer, 2008, vol. 440, pp. 361–380.
42 D. Ortiz, P. Cabrales and J. C. Briceno, *Biotechnol. Prog.*, 2013, **29**, 1565–1572.
43 M. T. Kreutzer, A. Gunther and K. F. Jensen, *Anal. Chem.*, 2008, **80**, 1558–1567.
44 A. Günther, M. Jhunjhunwala, M. Thalmann, M. A. Schmidt and K. F. Jensen, *Langmuir*, 2005, **21**, 1547–1555.
45 N. T. S. Evans and T. H. Quinton, *Respir. Physiol.*, 1978, **35**, 89–99.
46 Y. Chen, A. Wijaya Gani and S. K. Y. Tang, *Lab Chip*, 2012, **12**, 5093–5103.
47 M. Yucel, A. D. Beaton, M. Dengler, M. C. Mowlem, F. Sohl and S. Sommer, *PLoS One*, 2015, **10**, e0132785.
48 D. Cogan, J. Cleary, T. Phelan, E. McNamara, M. Bowkett and D. Diamond, *Anal. Methods*, 2013, **5**, 4798–4804.
49 C. J. Patton, A. E. Fischer, W. H. Campbell and E. R. Campbell, *Environ. Sci. Technol.*, 2002, **36**, 729–735.
50 W. H. Campbell, P. F. Song and G. G. Barbier, *Environ. Chem. Lett.*, 2006, **4**, 69–73.
51 L. O. Sraj, M. Almeida, S. E. Swearer, S. D. Kolev and I. D. McKelvie, *TrAC, Trends Anal. Chem.*, 2014, **59**, 83–92.
52 Q. Li, F. Wang, Z. A. Wang, D. Yuan, M. Dai, J. Chen, J. Dai and K. A. Hoering, *Environ. Sci. Technol.*, 2013, **47**, 11139–11146.
53 V. Chokkalingam, J. Tel, F. Wimmers, X. Liu, S. Semenov, J. Thiele, C. G. Figdor and W. T. S. Huck, *Lab Chip*, 2013, **13**, 4740–4744.
54 J. S. Go and S. Shoji, *Sens. Actuators, A*, 2004, **114**, 438–444.
55 M. A. Eddings, M. A. Johnson and B. K. Gale, *J. Micromech. Microeng.*, 2008, **18**, 067001.
56 S. L. Peng, M. Y. Zhang, X. Z. Niu, W. J. Wen, P. Sheng, Z. Y. Liu and J. Shi, *Appl. Phys. Lett.*, 2008, **92**, 012108.

ISBN 978-1-9996465-0-9

BioMedEng18

Droplet microfluidics for continuous chemical sensing of cortisol

Gareth Evans[1], Wahida Bhuiyan[1], Sammer-Ul Hassan[2], Brett Warren[2] Sharon Coleman[2] and Xize Niu[1]*

[1] *Faculty of Engineering and the Environment, University of Southampton, Southampton, U.K. SO17 1BJ*

[2] *SouthWestSensor Limited, 2 Venture Road, Chilworth, Southampton, U.K. SO16 7NP*

Introduction

Droplet microfluidics has proven to be a powerful tool for bio-chemical analysis using small sample volumes [1]. Many 'mix-and-read' assays have been demonstrated in droplets however, multiple step reactions are more challenging. In 2016, Ferraro *et al.* demonstrated a method with obvious potential for integrating many 'gold standard' ELISA assays for biochemical analysis into droplet microfluidic platforms [2]. However, their approach relies on large instrumentation and complex operation of pumps and valves for droplet generation, not suitable for field applications.

Methods

Here we show a new point-of-care monitoring technique performing heterogeneous assays continuously in micro droplets. Our small and low power system makes use of droplet microfluidics, magnetic beads and optical detection. We have chosen to demonstrate a competitive assay for cortisol (a stress related steroid hormone), however this platform may be tailored for a wide variety of target analytes. Our all-in one integrated device shown in Fig.1a contains a peristaltic micropump and microfluidic chip for continuously generating repeated sequences of droplets by our group's novel pulsed method [3], automated magnetic traps for transferring magnetic beads between droplets to carry out assay steps and a miniaturized in-line spectrophotometer for the final measurement [4].

Results & Discussion

Figure 1b shows an example (50ng/ml) of the raw readout (light intensity) data from the miniaturized inline spectrophotometer used for final detection and Fig1c. shows a promising early calibration of the assay carried out in droplets with expected trend.

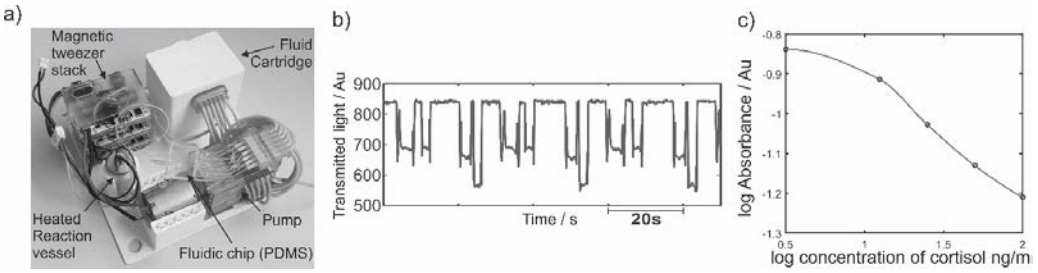

Figure 1a) Photograph of the device b) Example raw data from inline spectrophotometer (50ng/ml) c) Early calibration data of Cortisol assay

Conclusion

Our device can collect samples directly from the sampling site (e.g. body fluids), making it possible to perform complex assays continuously at the point-of-care. The continuous nature of this method combined with the small-footprint of the experimental setup promises to revolutionize chemical monitoring in the medical field and offers exciting research opportunities for studying the biochemistry of short term events and long-term trends.

References

1. WL.Chou et al., Micromachines, 6, 9, 1249-1271. (2015)
2. D. Ferraro et al., Scientific Reports, 6, 25540 (2016)
3. A.M. Nightingale et al, Lab on a Chip, 17, 6 (2017)
4. S. Hassan et. al, Analyst, 141, 11 (2016)

Acknowledgments

We thank the EPSRC for funding this work (EP/M012425/1). * Further contact: x.niu@soton.ac.uk

BioMedEng18

C.H.A.D.: CONTINUOUS HETEROGENOUS ASSAY IN DROPLETS FOR THE MEASUREMENT OF CORTISOL

Gareth Evans[1], Wahida Bhuiyan[1], Sammer-Ul Hassan[2], Brett Warren[2], Sharon Coleman[2] and Xize Niu[1, 2*]

[1] Faculty of Engineering and the Environment, University of Southampton, Southampton, U.K. SO17 1BJ
[2] SouthWestSensor Limited, 2 Venture Road, Chilworth, Southampton, U.K. SO16 7NP

ABSTRACT

This paper showcases a new method for performing heterogeneous assays continuously utilizing droplet microfluidics suitable for point-of-care monitoring.

KEYWORDS: Droplet Microfluidics, Immunoassay

INTRODUCTION

Droplet microfluidics has proven to be a powerful tool for high throughput bio-chemical analysis using small sample volumes [1]. Many groups have shown a wide variety of 'mix-and-read' assays in droplets. However, multiplexed and multiple step reactions are more challenging, especially those like ELISA (enzyme-linked immune sorbent assay) which require washing steps. Ferraro *et al.* have demonstrated the generation of droplet trains and movement of magnetic particles between droplets using magnetic tweezers. This has introduced huge potential for miniaturizing many of the 'gold standard' ELISA assays for biochemical analysis into droplet microfluidic platforms [2]. However, their approach relies on large instrumentation and complex operation of pumps and valves for droplet generation not suitable for field applications. While this platform could be tailored for a wide variety of target analytes, here we have chosen to demonstrate a competitive assay for cortisol, a stress related steroid hormone relevant to a wide variety of disease states (assay schematic shown in Fig. 1).

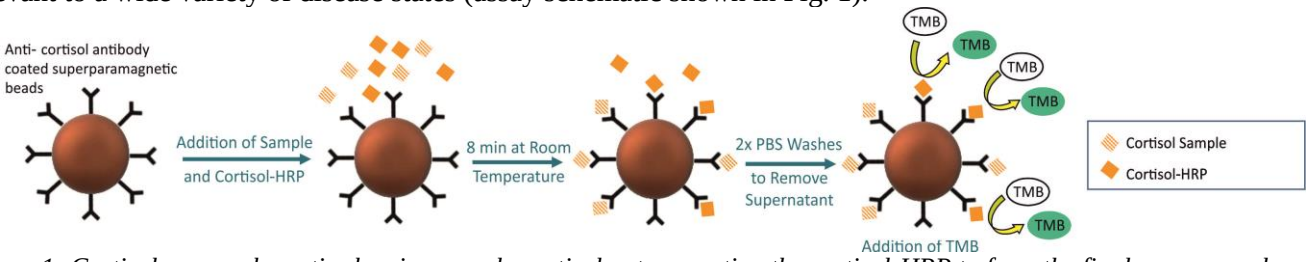

Figure 1: Cortisol assay schematic showing sample cortisol out-competing the cortisol-HRP to form the final assay complex.

EXPERIMENTAL

Our device makes use of a pulsed method of droplet generation for continuous production of droplet trains facilitated by a peristaltic micropump previously reported by our group [3]. Droplet composition can be arbitrarily 'hardcoded' into the design with no cross talk between droplets. The rotorhead of the pump delivers fluids in eight separate pulsations to the PDMS chip that features four parallel T-junctions for droplet generation. After generation, the droplets flow through a branched junction in turn and on into the shared main channel, as shown in Fig. 2.

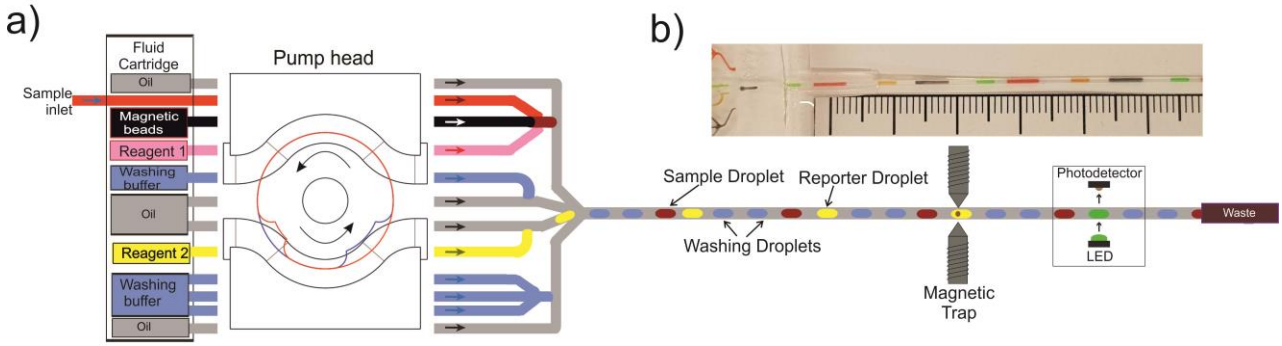

Figure 2: a) Schematic of fluidic structure used to generate the 4 droplet sequence b) Photograph of the microfluidic chip and droplet sequence (food dye)

Figure 3 shows the automated magnetic bead trap featuring two 'light gates' (spectrophotometers) which are used to determine when to activate the trap and when to re-disperse the beads into a new droplet. Also shown here is an example of how effective this method is at purifying the magnetic beads, removing them from a highly concentrated droplet of rose bengal dye. Early tests of the cortisol assay performed in droplets have proven this method to be very promising.

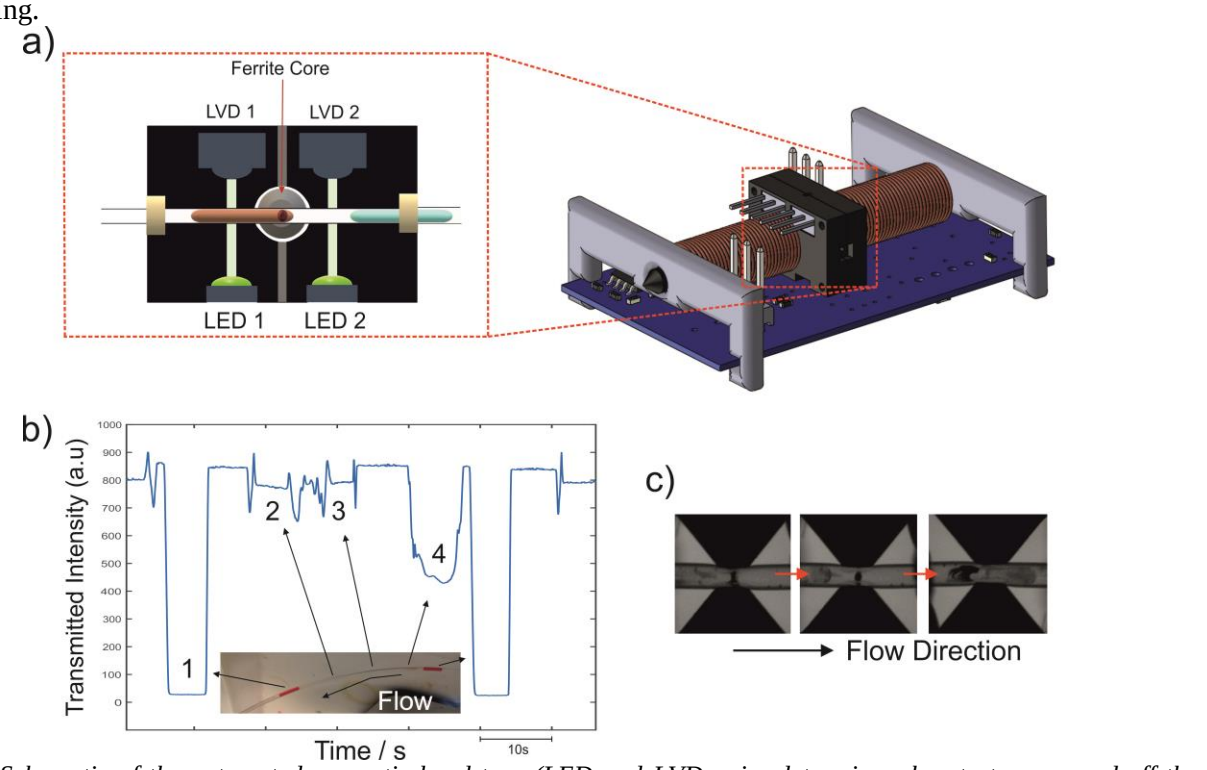

Figure 3: a) Schematic of the automated magnetic bead trap (LED and LVD pairs determine when to turn on and off the magnetic field). b) Example transmittance trace from the spectrophotometer showing the magnetic beads post drag wash through 2 washing steps after removal from a droplet of rose Bengal dye. (Inset Photograph of this sequence.) c) Images of the magnetic bead trap in operation

RESULTS AND DISCUSSION

The all-in one integrated device shown in Fig. 4a contains a peristaltic micropump and microfluidic chip for continuously generating droplet 'trains' (repeated sequences of droplets), automated magnetic traps for passing magnetic beads between droplets to carry out assay steps and a miniaturized in-line spectrophotometer for the final measurement [4]. Example raw readout (light intensity) data from the miniaturized inline spectrophotometer used for final detection can be seen in fig. 4b. Figure 4c shows an early calibration and example (50ng/ml).

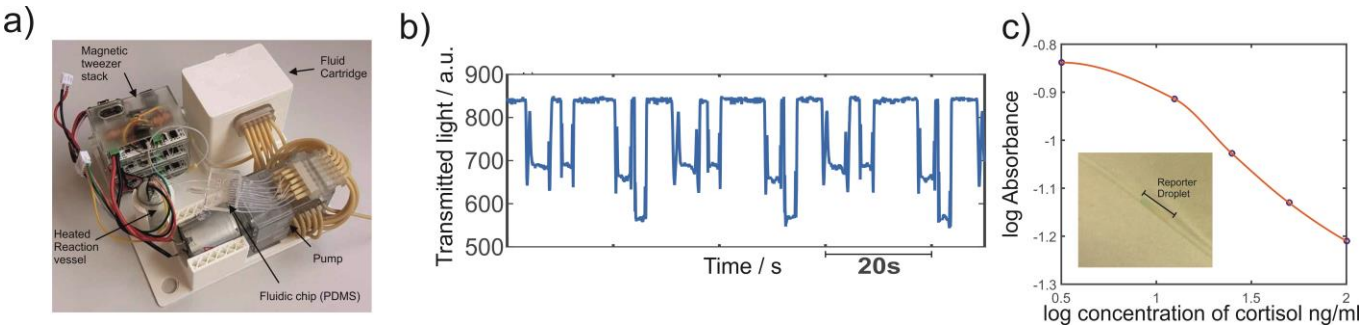

Figure 4a: Photograph of the fully integrated platform including micro-peristaltic droplet generation system, all required liquids (FC40 oil and reagents) for a long term run, heated reaction vessel and 3 automated magnetic tweezers. b) Example raw data readout from mini spectrophotometer reading (50ng/ml) with the reporter droplet colour leading to lower intensity c) Calibration curve of absorbance of various cortisol samples (inset example of colour developing in the reporter droplet)

CONCLUSION

This device can collect samples directly from the sampling site (e.g. bodily fluids), making it possible to perform complex assays continuously at the point-of-care. The continuous nature of this method, combined with the small-footprint of the experimental setup promises to revolutionize chemical monitoring in the medical and environmental fields as well as offering exciting new research opportunities for studying the biochemistry of events both short term and trends over long periods of time.

ACKNOWLEDGEMENTS

This work was funded by EPSRC EP/M012425/1 and University of Southampton Institute for Life Sciences studentship to Gareth Evans.

REFERENCES

[1] WL.Chou et al., Micromachines, 6, 9, 1249-1271. (2015)
[2] D. Ferraro et al., Scientific Reports, 6, 25540 (2016)
[3] A.M. Nightingale, G.W.H. Evans, P. Xu, B.J. Kim, S. Hassan, X. Niu, Lab on a Chip, 17, 6 (2017)
[4] S. Hassan et. al, Analyst, 141, 11 (2016)

CONTACT

* Dr. Xize Niu ; phone: +44 (0) 2380592367; Email: X.Niu@soton.ac.uk

Additional technical drawings of first chip based peristaltic micropump
All measurements in millimetres

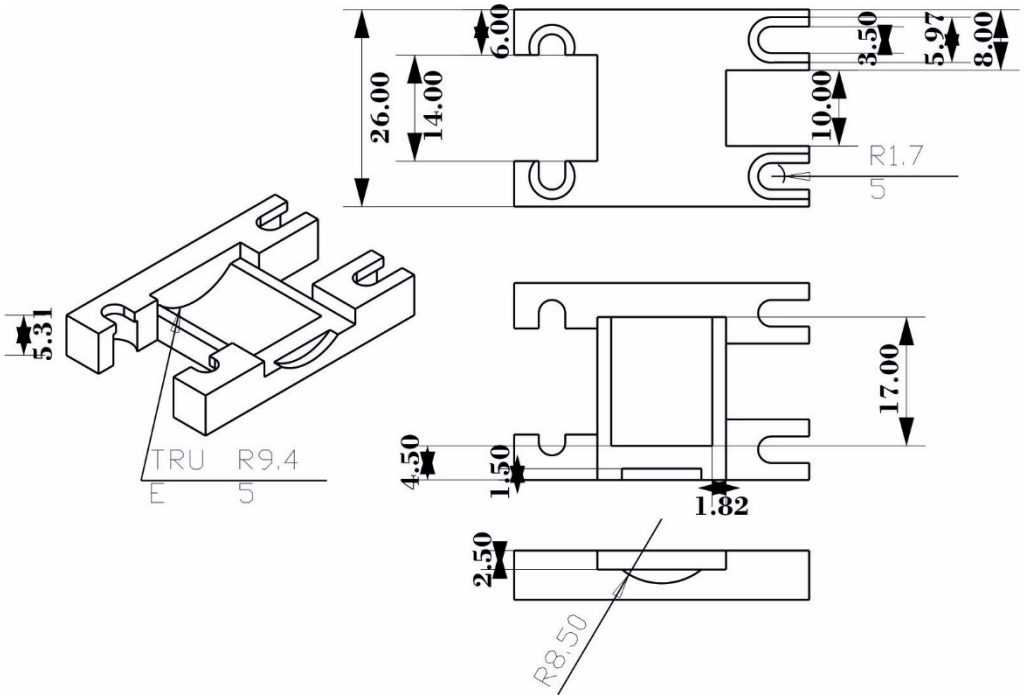

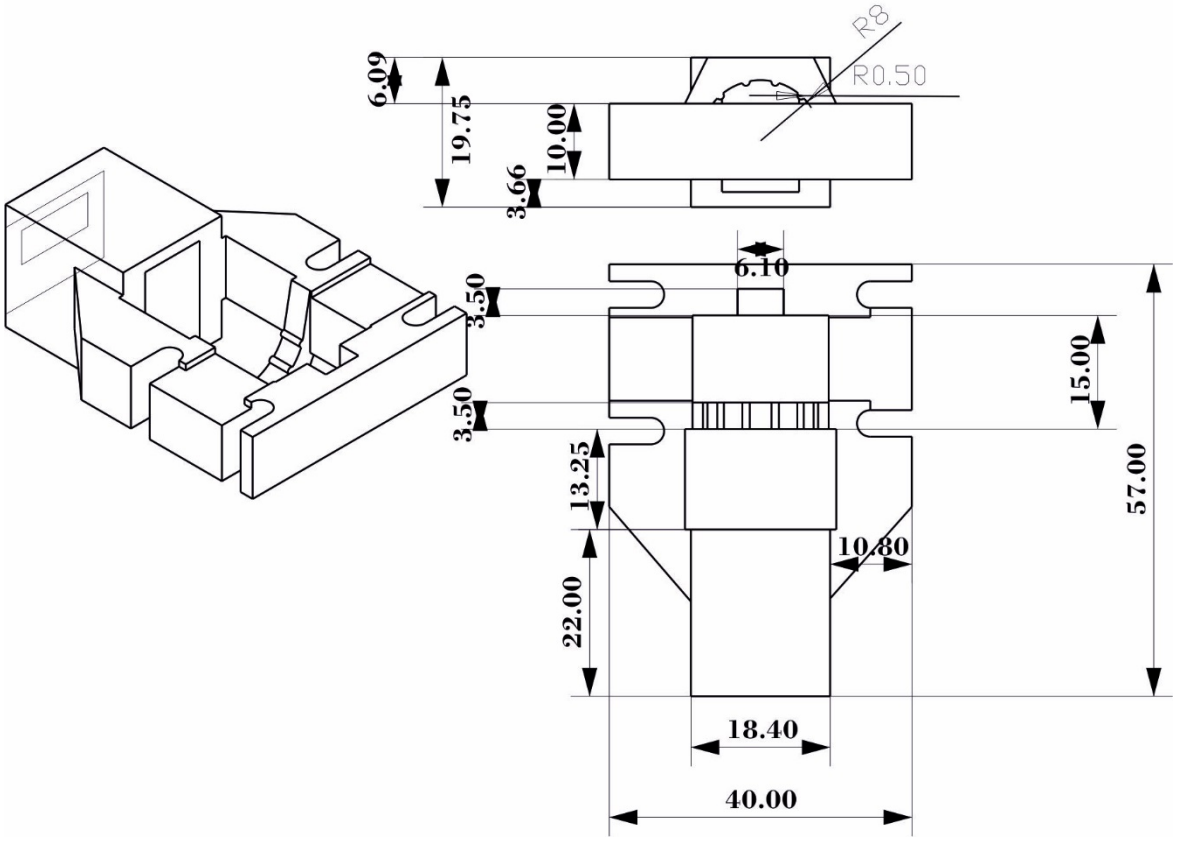

Additional technical drawings of first chip based peristaltic micropump
All measurements in millimetres

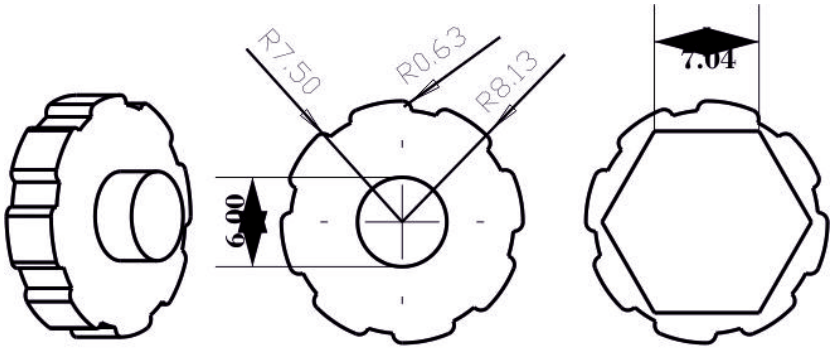

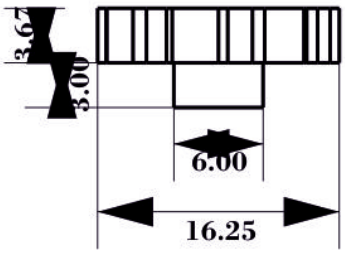

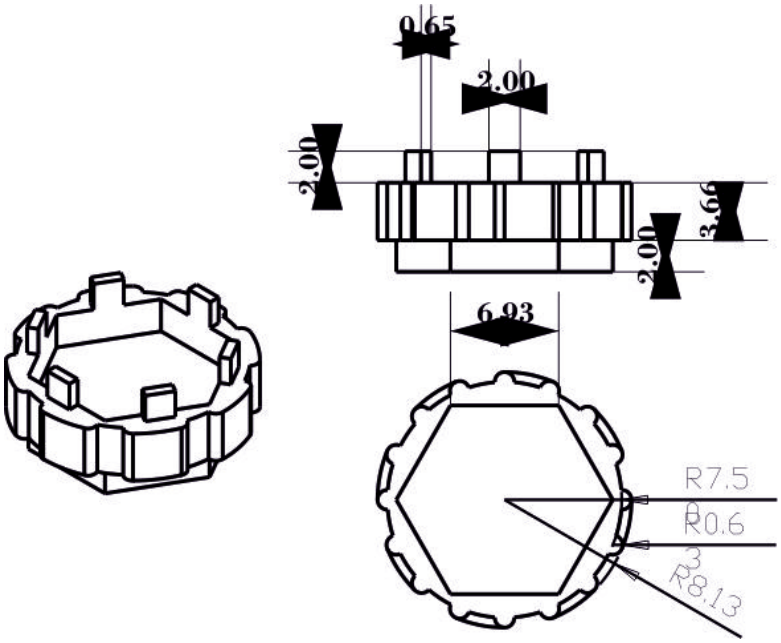

Additional technical drawings of first chip based peristaltic micropump
All measurements in millimetres

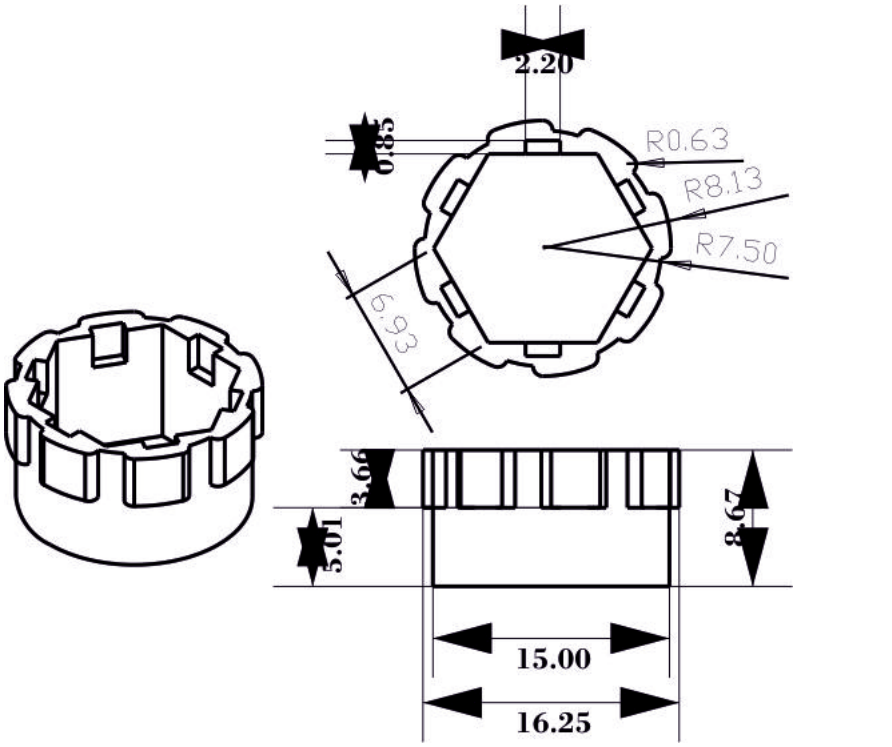

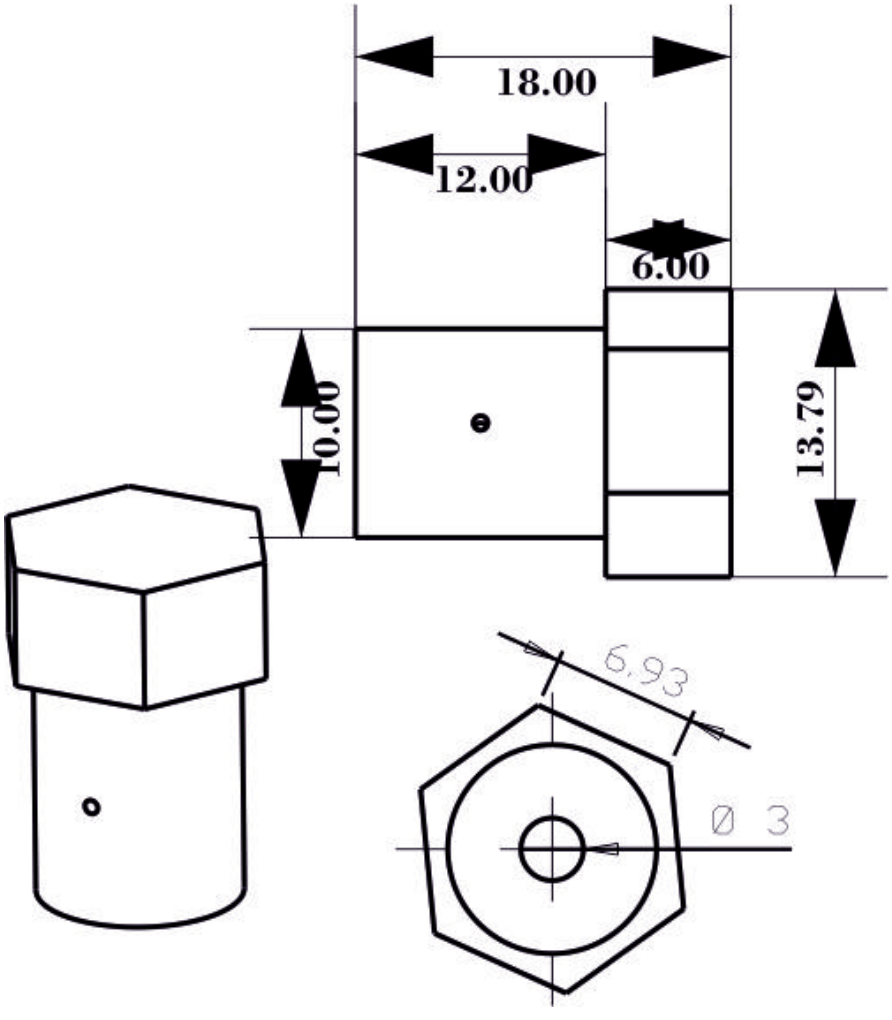

Additional technical drawings of optimised chip based peristaltic micropump
All measurements in millimetres

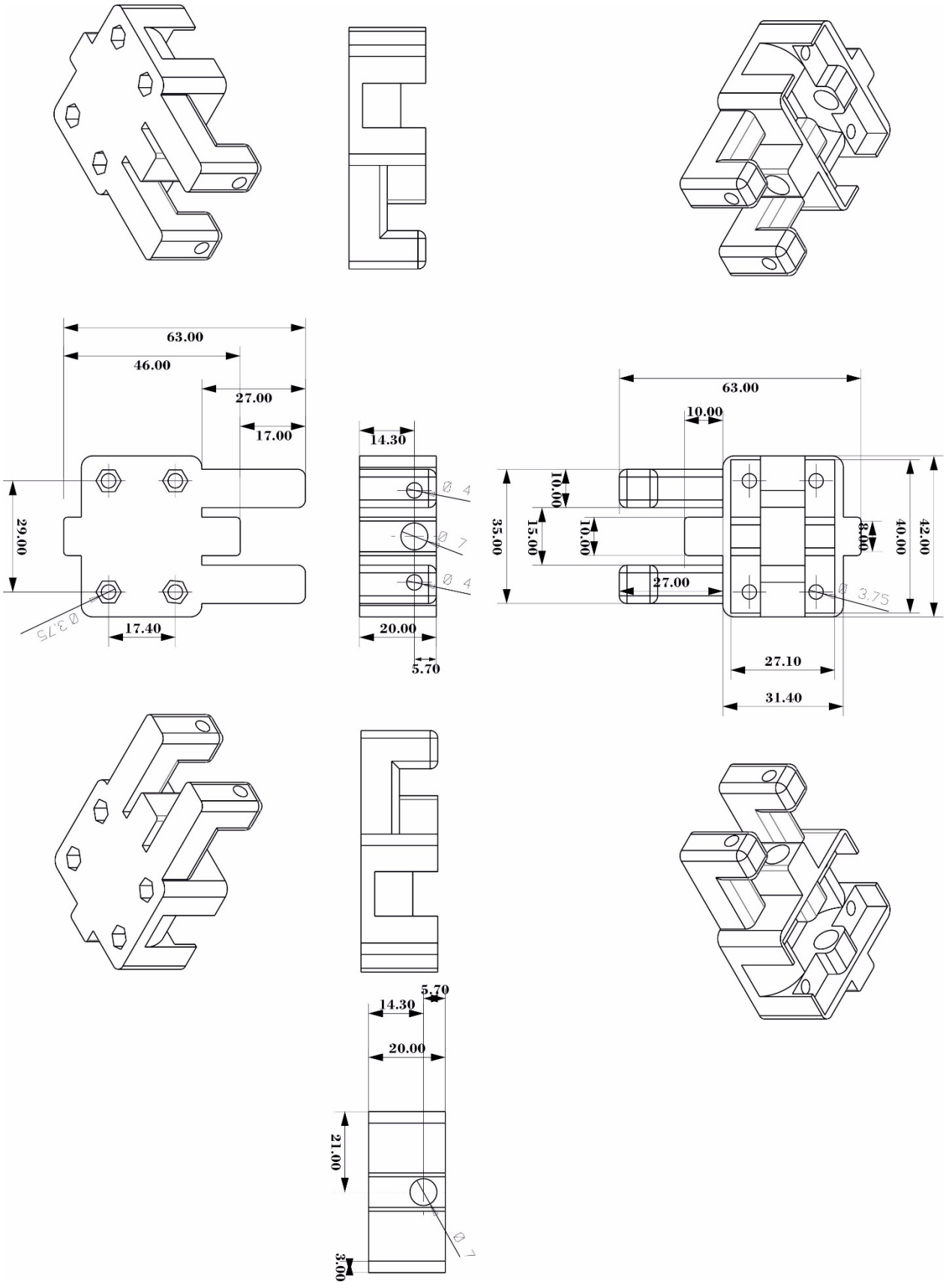

Additional technical drawings of optimised chip based peristaltic micropump
All measurements in millimetres

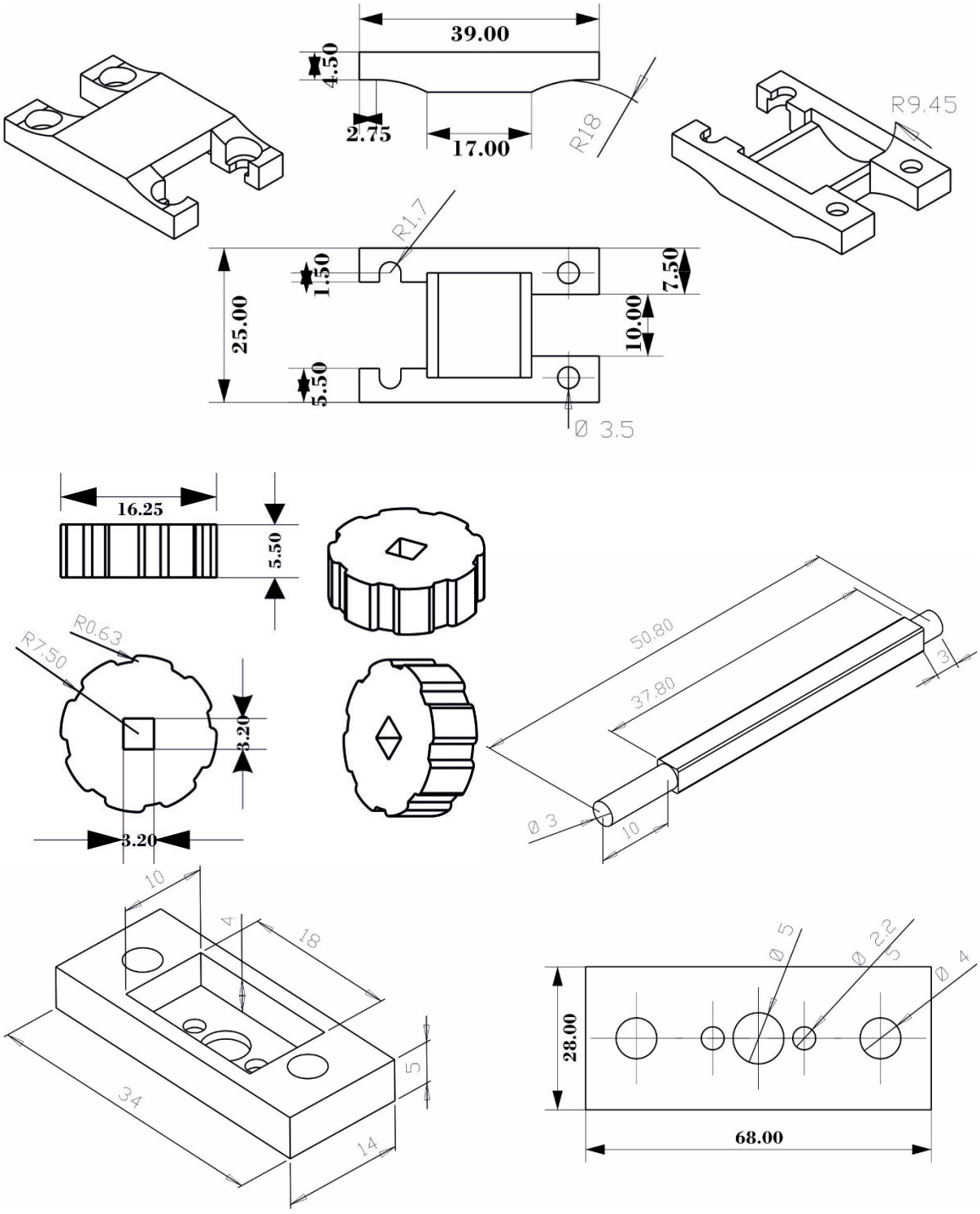

Additional technical drawings of optimised chip based peristaltic micropump
All measurements in millimetres

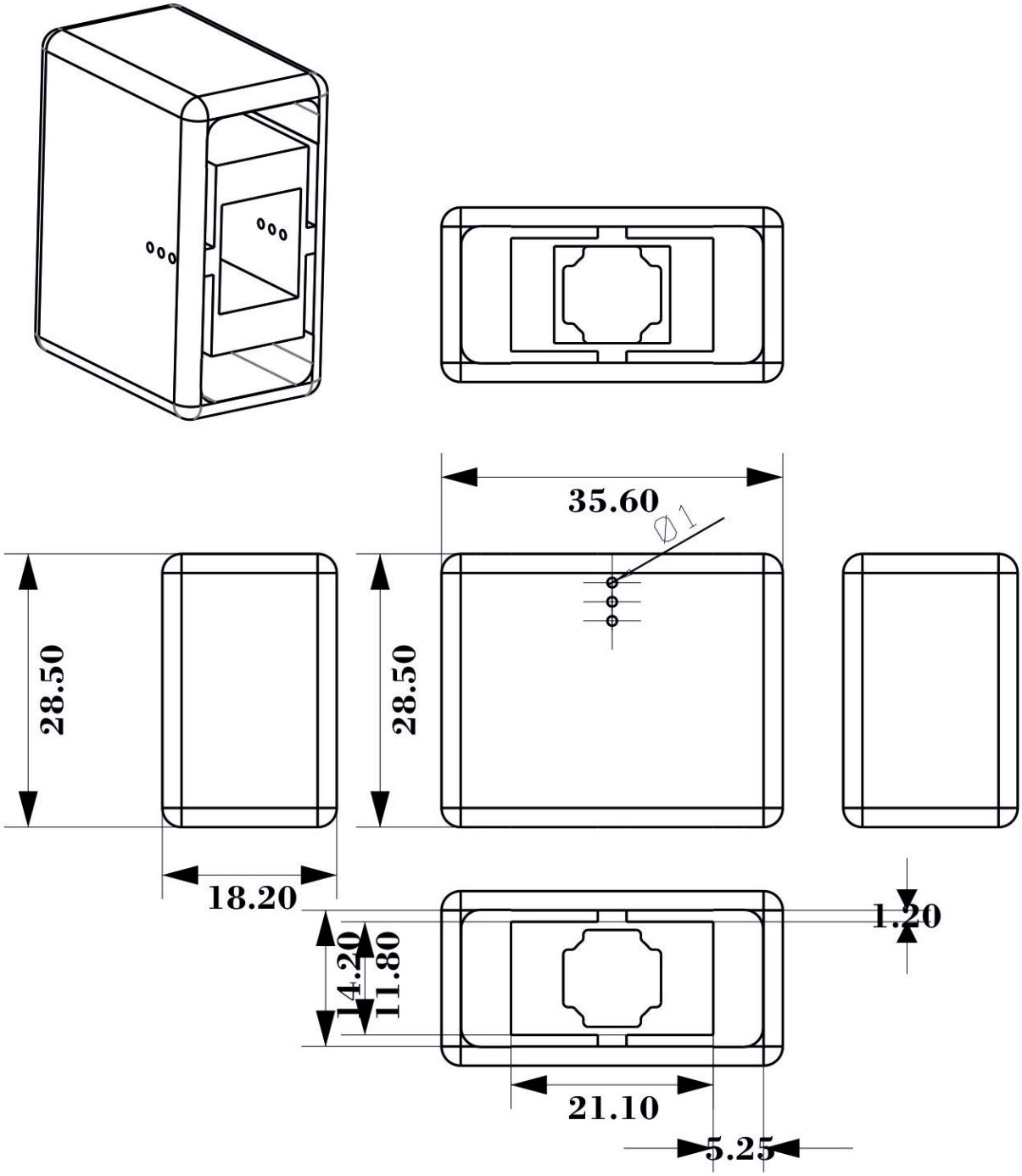

Additional technical drawings of optimised chip based peristaltic micropump
All measurements in millimetres

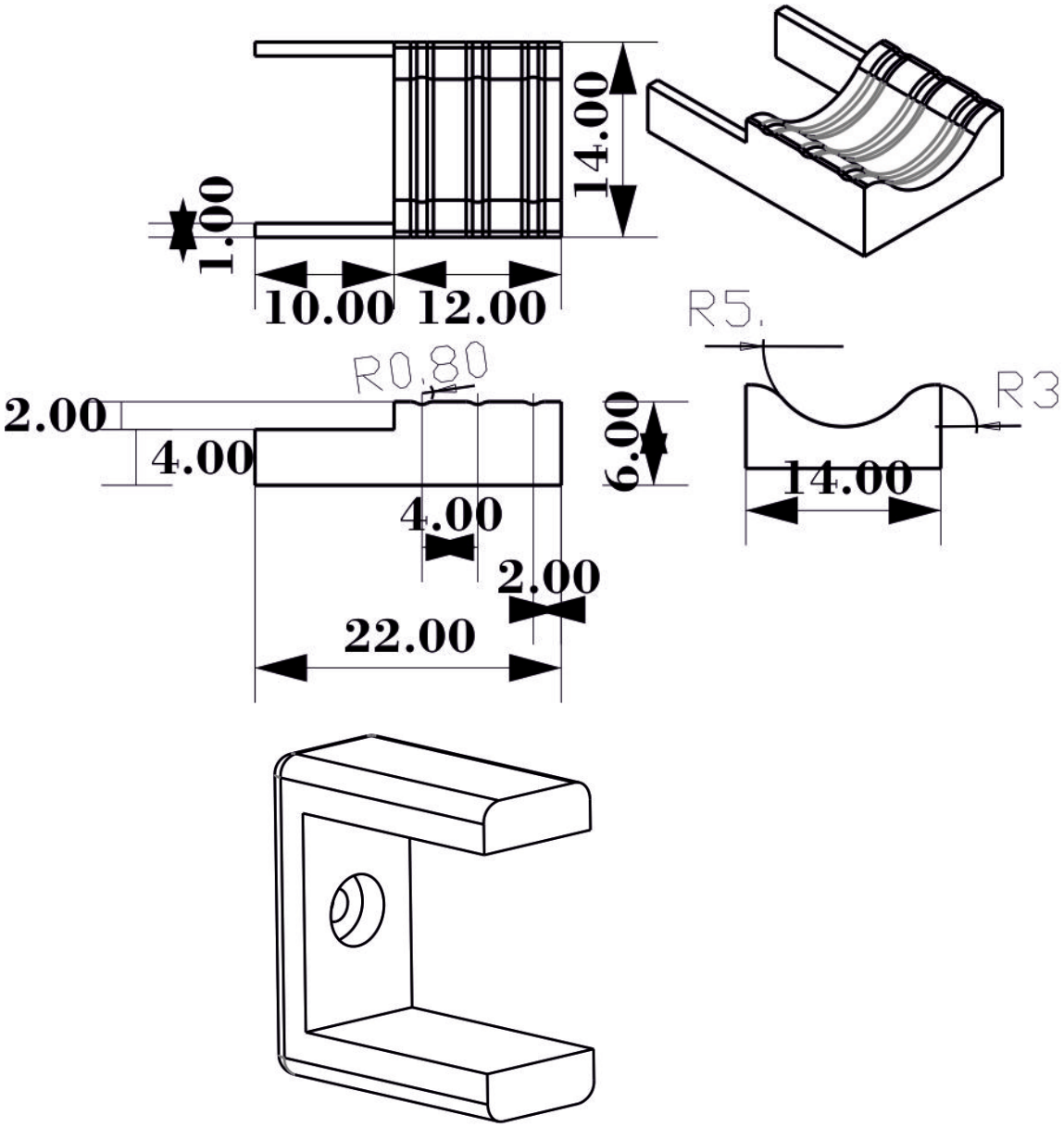

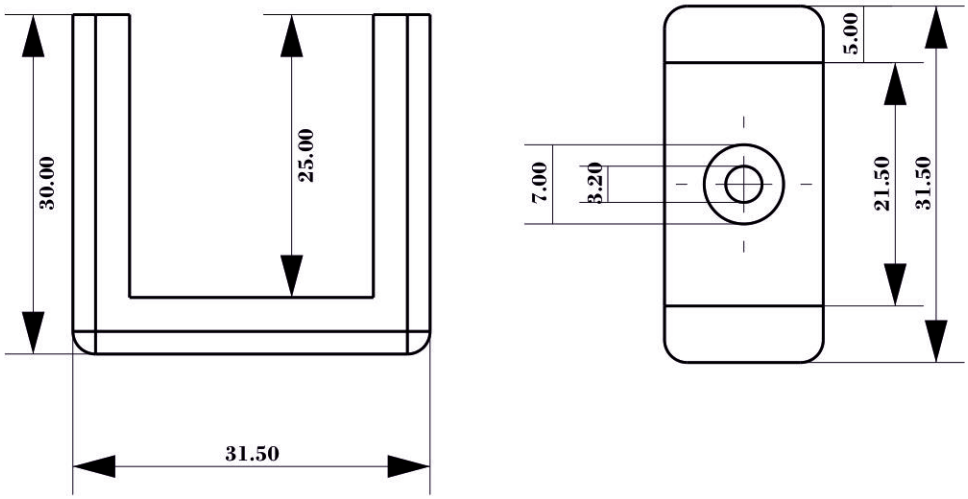

Additional technical drawings of optimised chip based peristaltic micropump
All measurements in millimetres

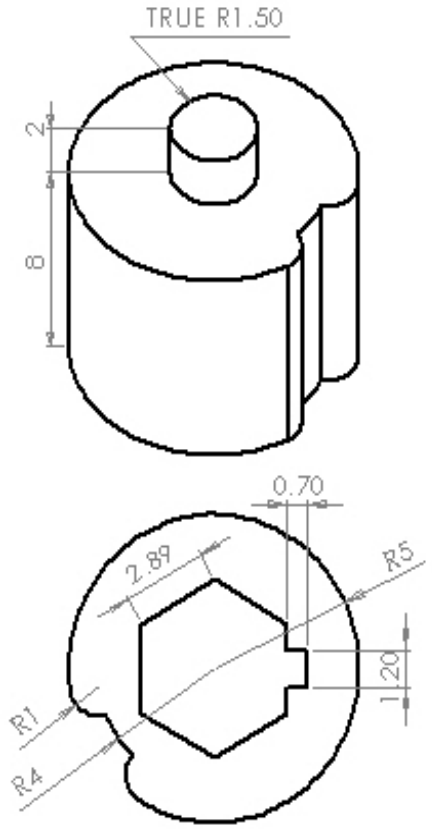

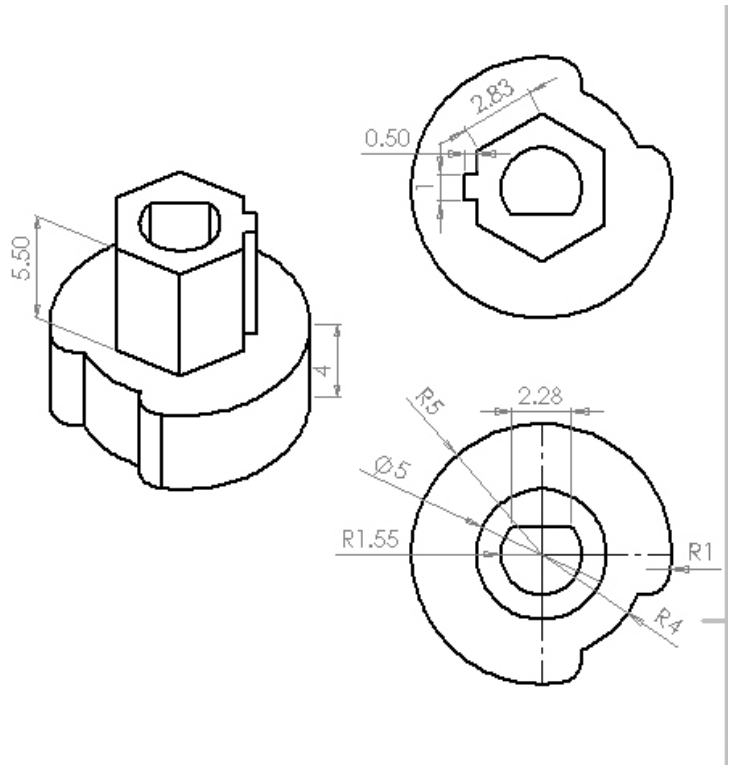

Additional technical drawings of Droplet train generating peristaltic micropump
All measurements in millimetres

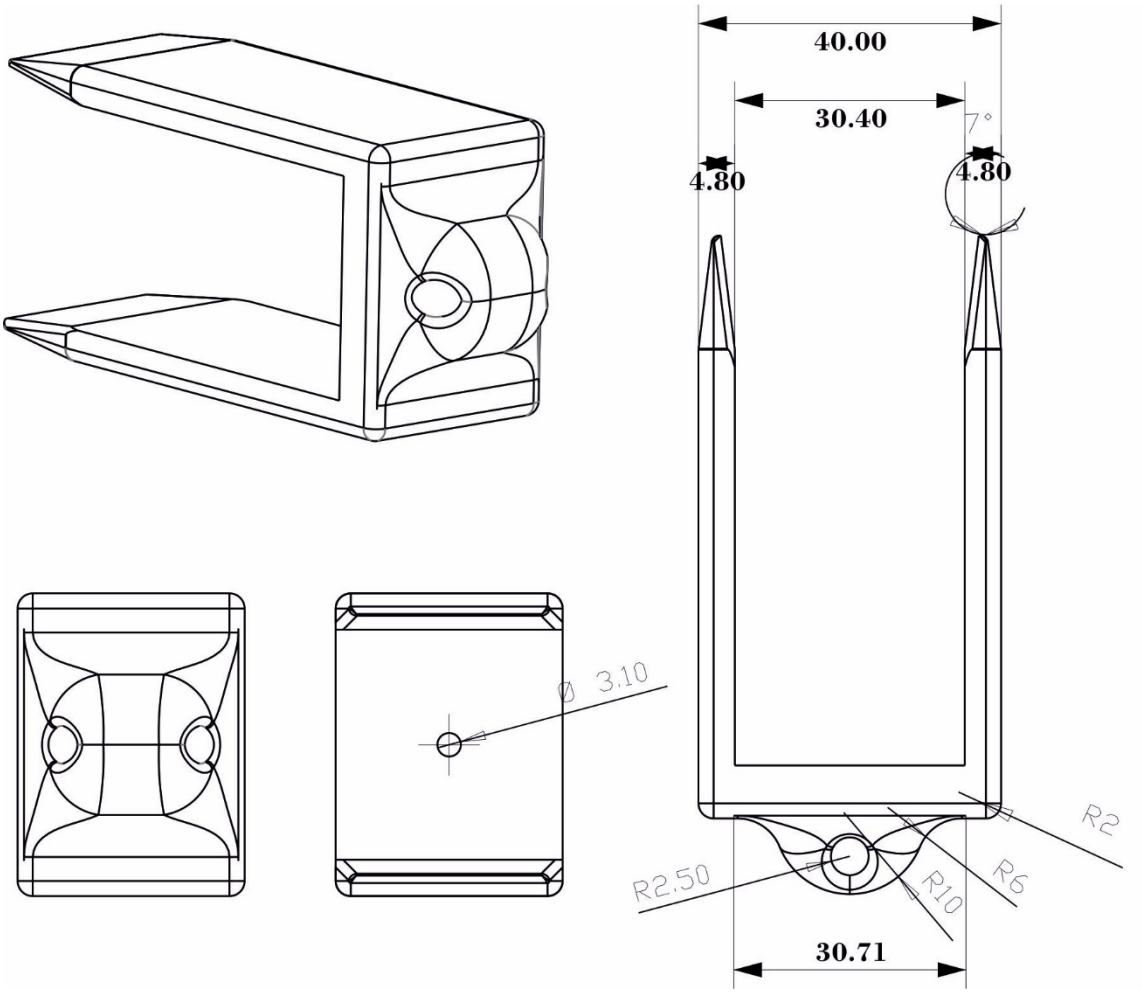

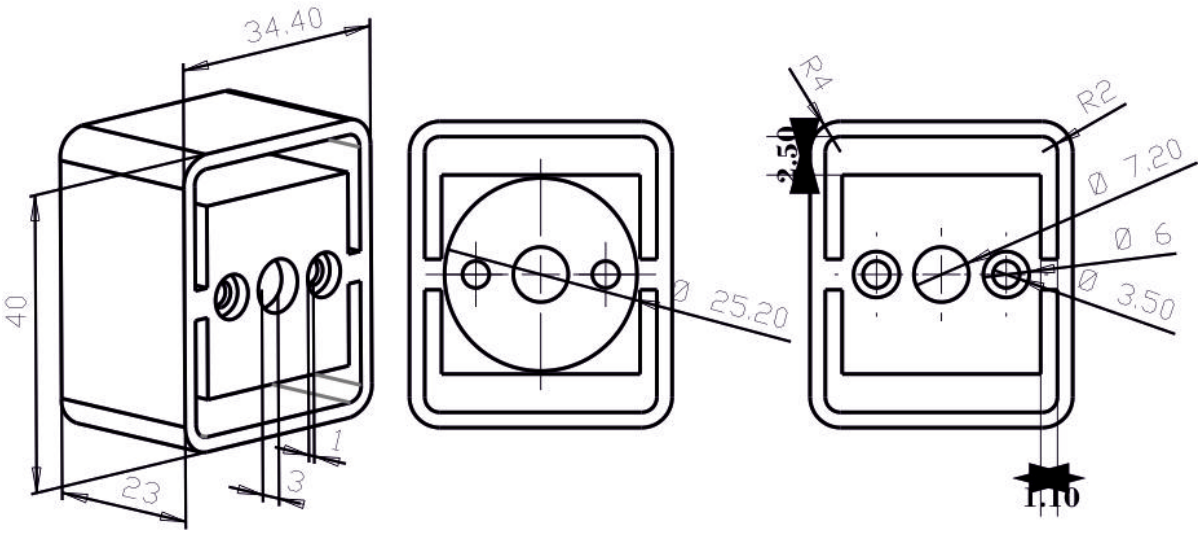

Additional technical drawings of Droplet train generating peristaltic micropump
All measurements in millimetres